"GAS ADSORPTION STUDIES AND MICROCALORIMETRY ON SOME IRON OXIDES."

by

David John Bloomfield.

A Thesis submitted in partial fulfilment of the requirements for the Degree of Doctor of Philosophy in the University of London.

The Bourne Laboratory,
Royal Holloway College.

1983.

Abstract.

A volumetric gas adsorption apparatus was built and calibrated with two surface area standards. The nitrogen adsorption and desorption isotherms were determined for five iron oxides and the specific surface area was calculated. Four of the oxides were found to be mesoporous. α_s-plots were constructed using the non-porous sample (α-haematite) as the reference. An attempt was made to measure the effectiveness of an organic pretreatment on two of the porous samples by comparing their surface areas and pore size distributions before and after treatment.

A commercial flow microcalorimeter was used to investigate the adsorption and desorption of 1-butanol and 1,2-epoxybutane on one of the porous samples ('A') and haematite. For haematite the adsorption of both 1-butanol and 1,2-epoxybutane were reversible. The surface area of both samples estimated from microcalorimetry were smaller than their measured specific surface areas, probably because of water precoverage. The heat of 1-butanol adsorption on sample 'A' was a function of concentration, the number of previous adsorption-desorption cycles and the volume of solvent passed over the surface prior to the adsorption. The adsorption of 1,2-epoxybutane on sample 'A' was substantially irreversible. Dilution effects became important for both samples for concentrations above ca. 1·0 wt.%.

A speculative water vapour adsorption experiment was performed using the microcalorimeter. Comparisons were made of

the water adsorption-desorption properties of all the samples. The observed effects could not be simply explained. The heats and rates of water adsorption and desorption increased with increasing sample temperature.

To My Parents,
and Gillian.

Acknowledgements.

I wish to extend my thanks to:

Dr. P.J. Gardner for suggesting this project and for his continued help and guidance throughout the course of the work;

Professor T. Edmonds for many helpful discussions and much advice;

The late Professor T.G. Bonner and Professor K.G. Singer for their support;

The technicians of the Bourne Laboratory;

The financial support of an S.R.C. Studentship;

and my many friends and colleagues for their help and 'charity', especially: Jane Bignall, Howard Hill, David Netherton, Michael Stephens and Ray and Hazel Ward; and, indeed, my family.

CONTENTS.

		Page No.
CHAPTER I. : INTRODUCTION.		
1-1.	General Introduction:	16.
1-2.	General Theories and Principles of Adsorption:	18.
1-2-1	Introduction:	18.
1-2-2	Types of Surface:	19.
1-2-3	Surface Conventions:	20.
1-2-4	Surface Thermodynamic Quantities:	21.
1-2-5	The Gibbs Adsorption Equation:	22.
1-2-6	The Two-Dimensional Perfect Gas:	23.
1-2-7	The Langmuir Adsorption Isotherm:	25.
1-2-8	Forces between Particles:	25.
1-2-9	Enthalpies of Adsorption:	28.
1-2-10	The Description of Real Solid Surfaces:	29.
1-2-11	The Surfaces of Metal Oxides:	31.
Figures for Chapter I.:		33-36.
CHAPTER II. : PHYSICAL ADSORPTION OF GASES.		
II-1.	Introduction : The Classification of Isotherms;	37.
II-2.	The BET Equation:	38.
II-3.	Criticisms of the BET model:	41.
II-4.	The Choice of Adsorbate:	43.
II-5.	Other Models for Adsorption:	44.
II-6.	Adsorption on Porous Solids:	46.
II-7.	Adsorption Isotherms : Type IV.:	47.
II-8.	Equilibrium in the Hysteresis Loop:	49.
II-9.	The Kelvin Equation:	50.
II-10.	Mesopore Analysis:	52.
II-11.	The Estimation of the Adsorbed Film Thickness:	53.
II-12.	The Method Piecre[55] for Estimating Pore Size Distributions:	55.
II-13.	The Modelless Method of Pore Analysis:	57.
II-14.	"t" and "α_s" Plots:	58.
Figures for Chapter II.		60-65.

CONTENTS. (Cont.).

CHAPTER III. : THE SOLID-LIQUID INTERFACE.

III-1. Introduction: 66.

III-2. Adsorption from Binary Liquid Mixtures: 67.

III-3. Liquid Adsorption Models: 68.

III-4. Surface Orientation as a Function of Concentration: 70.

III-5. The Estimation of Surface Areas from Solution Adsorption: 71.

III-6. Surface Areas from Microcalorimetry: 73.

Figure for Chapter III. 75.

CHAPTER IV. : SOME ASPECTS OF IRON OXIDE SURFACE CHEMISTRY.

IV-1. Introduction: 76.

IV-2. The Iron Oxide / Water Interface: 77.

IV-3. Adsorption on Iron Oxide Surfaces: 86.

Figures for Chapter IV.: 91.

CHAPTER V. : EXPERIMENTAL.

V-1. Gas Adsorption Apparatus:

V-1-1. Introduction: 92.

V-1-2. The Gas Burette: 95.

V-1-3. The Manometer: 95.

V-1-4. The Pressure Measurement: 96.

V-1-5. The Thermostat: 97.

V-1-6. The Adsorption Bulbs, Gas Storage System, Outgassing Unit and Vapour Pressure Thermometer: 100.

(Cont.)

CONTENTS (Cont.).

		Page No.
CHAPTER V. (Cont.).		
V-2.	Gas Adsorption Procedure.	
V-2-1.	Free Space Calibration:	101.
V-2-2.	Treatment of Results:	103.
V-2-3.	A Consideration of Possible Corrections:	104.
V-2-4.	Calculation of the Free Space:	106.
V-2-5.	Dead Space Calibration and Adsorption:	107.
V-2-6.	Calculation of Dead Space and Amount Adsorbed:	111.
V-3.	Microcalorimetry.	
V-3-1.	Introduction and Principles:	112.
V-3-1.	The Liquid Adsorption Experiment:	118.
V-3-3.	The Water Vapour Adsorption Experiment:	119.
V-4.	Materials.	121.
Figures for Chapter V.:		124-135.
CHAPTER VI. : The Vacuum Adsorption Experiments.		
VI-1.	Results.	
VI-1-1.	The Free Space Calibration:	136.
VI-1-2.	Standardisation of the Vacuum Apparatus:	136.
VI-1-3.	The Adsorbent Ferric Oxide A.:	138.
VI-1-4.	The Maleic Anhydride Treated Ferric Oxide A.:	141.
VI-1-5.	The Absorbent Ferric Oxide B.:	143.
VI-1-6.	The Maleic Anhydride Treated Ferric Oxide B.:	144.
VI-1-7.	The Absorbent α-Goethite:	145.
VI-1-8.	The Absorbent β-Goethite:	145.
VI-1-9.	The Absorbent α-Haematite:	146.
VI-2.	Discussion.	
VI-2-1.	Apparatus Standardisation:	146.
VI-2-2.	α_s-Plots:	146.
VI-2-3.	Ferric Oxide A and β-Geothite:	147.
VI-2-4.	Ferric Oxide B and α-Goethite:	149.
VI-2-5.	The Maleic Anhydride Treated Ferric Oxide A. :	151.

Contents. (Cont.)

Page No.

Chapter VI. (Cont.).

VI-2. Discussion. (Cont.).

VI-2-6. The Maleic Anhydride Treated Ferric Oxide B.: 154.

Figures for Chapter VI.: 156-180

CHAPTER VII : THE LIQUID ADSORPTION EXPERIMENTS.

VII-1. Results. 181.

VII-1-1. The Adsorption of Butanol on α-Haematite: 181.

VII-1-2. The Adsorption of 1,2 Epoxybutane on α-Haematite: 182.

VII-1-3. The Adsorption of Butanol on Ferric Oxide A.: 183.

VII-1-4. The Adsorption of 1,2-Epoxybutane on Ferric Oxide A: 185.

VII-2. Discussion.

VII-2-1. Butanol Adsorption on α-Haematite: 185.

VII-2-2. 1,2 Epoxybutane Adsorption on α -Haematite: 188.

VII-2-3. Butanol Adsorption on Ferric Oxide A.: 190.

VII-2-4. 1,2 Epoxybutane Adsorption on Ferric Oxide A.: 196.

Figures for Chapter VII. 199-210.

CHAPTER VIII. : THE WATER VAPOUR ADSORPTION EXPERIMENT.

VIII-1. Results: 211.

VIII-1-1. The Calibration Experiment: 211.

VIII-1-2. Water Adsorption on Ferric Oxides A and B: 213.

VIII-1-3. Water Adsorption on α & β Goethite: 214.

VIII-2. Discussion: 215.

VIII-2-1. The Calibration Experiment: 215.

VIII-2-2. Water Adsorption on Ferric Oxide A.: 218.

VIII-2-3. Comparison between the Iron Oxides: 221.

Figures for Chapter VIII.: 222-229.

CHAPTER IX. : SUMMARY AND CONCLUSION: 230.

Contents. (Cont.)

	Page No.
Statement of 'Key to Tables':	235.
Tables. :	236 - 266.
References. :	268 -280.

Chapter I.

Introduction.

I-1. General Introduction.

The use of adhesive bonding of metals is becoming increasingly important industrially. However, the durability of adhesive joints is preventing the full potential of the new technology being realised. When adhesive joints are exposed to weathering tests in which water is present, the mechanical properties of the joints often deteriorate rapidly[1].

This work stems from observations[2] of the loss of shear strength of steel lap joints bonded with epoxy resins and subjected to weathering in an aqueous environment. Experiments have shown that different proportions of hardener present in the resin have a marked effect on joint strength. Excess hardener, usually a polyfunctional amine, is detrimental to joint strength, and is thought to migrate towards the substrate adhesive interface during curing. The amine groups create a hydrophilic layer at the interface which is a favourable situation for the ingress of water resulting in a loss of strength. The locus of failure of steel lap joints exposed to moist and dry weathering tests is different. In moist environments, failure always occurs at the interface[1,2,3] rather than in the adhesive layer. It is clear that water is extremely damaging in the interfacial region. Water may reach the interface by diffusion through the resin or direct transport along the interface.

This work was carried out in support of a research program designed to elucidate the factors involved in joint failure induced by the presence of water. It is anticipated that an understanding of the mechanism of water

induced joint failure could result in the development of techniques that reduce the damaging effects of water. The experimental approach is thermodynamic rather than surface analytical.

To simulate the surface of real and therefore corroded steel plate various iron oxides and oxyhydroxides have been used in a powdered form.

The objective of this work has been to characterise the surface of these "oxides" and attempt preliminary studies of the adsorption of some model components of epoxy resins. The interaction of water vapour with the model steel surface has also been studied. A commercial flow microcalorimeter was used for both the liquid and water vapour adsorption studies. Eley and Rudham[4] have discussed the validity of a microcalorimetric approach to the problem.

A vacuum volumetric gas adsorption apparatus capable of measuring nitrogen adsorption/desorption isotherms was built. Specific surface areas and pore size distributions extracted from the nitrogen isotherms were also used to characterise the iron oxides.

Ionic polymers have a great potential for technological application.[5] If they could be incorporated into the oxide film on a steel plate the resultant surface could provide a good bonding substrate for subsequent application of adhesive. The reduction in polarity of the interfacial region might also reduce the ingress of water. It is possible that uniform adsorption of a carboxylic acid anhydride on a steel plate might have a similar effect. This film could form with the simultaneous removal of physically

adsorbed water from the oxide surface. Preliminary work in this laboratory based on this hypothesis has been tested using the vacuum apparatus.

I-2. General Theories and Principles of Adsorption.

I-2-1 Introduction.

An interface is usually defined as the boundary region between two adjacent bulk phases. When one of these phases is a gas or a vapour the term surface is used.

Often solid and liquid surfaces are treated differently because of the different experimental techniques used to characterise them. The general relationships and properties which in principle may be applied to any interface, solid-liquid, solid-gas, liquid-liquid or liquid-vapour, will now be summarised.

Adsorption is the partitioning of a chemical species between a bulk phase and an interface. Adsorption is distinct from absorption, although the two processes can occur simultaneously. There are two limiting types of adsorption, chemical and physical, depending on the forces involved. Van der Waals forces are associated with physical adsorption, or physisorption. The formation of a chemical bond between a surface and an adsorbed particle gives rise to chemical adsorption or chemisorption.

Physical adsorption is characterised by low exothermic heats of adsorption ($\lesssim 20\ kJ\ mol^{-1}$ of adsorbate) of the same order of magnitude as the heat of liquefaction, is non-specific, reversible and has no activation energy.

The formation of a physically adsorbed layer is similar to the condensation of a vapour to a liquid, with the adsorbed layer tending to behave like a two-dimensional liquid. Physical adsorption only occurs to an appreciable extent at temperatures and pressures near those required for liquefaction. In contrast, the heat of chemisorption is high (80-400 $kJ\,mol^{-1}$ of adsorbate) and of the same order of magnitude as covalent bonds. The adsorption is specific, often requires an activation energy, and is irreversible, requiring high temperatures to initiate desorption. Chemisorption is complete once a monolayer is formed, whereas physical adsorption is characterised by the formation of multilayers. A chemical species may chemisorb on a surface to form a monolayer and then further adsorb by means of the physical process to form a multilayer bound to the monolayer. The adsorption of water on metal oxides is a classic example of this phenomenon.

I-2-2 Types of Surface.

Considering only adsorbent-adsorbate interactions it is possible to define two types of surfaces on a submicroscopic but not molecular level. Homogeneous surfaces are energetically uniform with a heat of adsorption independent of surface coverage. Heterogeneous surfaces are energetically non-uniform with heats of adsorption dependent on surface coverage. Liquid surfaces are homogeneous because of their inherent fluidity, while solid surfaces tend to be heterogeneous because of the lack of surface motion.

On a molecular level, the surface structure

has a potential associated with it that varies periodically with the structure as shown in Figure I.1. V(b) is the energy of the bulk phase, ΔV, is the depth of the potential well and ΔaV is the energy of adsorption. An adsorbed molecule will possess some thermal energy E and as a consequence will vibrate about the minimum of the potential well. If ΔV is much larger than E then the adsorbed species will spend most of their time on the surface near to the minima of the potential well, and are said to be localised. When ΔV and E are comparable or ΔV is less than E, the molecules may move over the surface, becoming non-localised.

In reality there are often no sharp distinctions between types of adsorption, types of surface and degree of surface mobility, although for reasons of theoretical simplicity the limiting cases outlined above are often retained.

I-2-3 Surface Conventions.

There are two major conventions for the thermodynamic treatment of a surface, one due to Gibbs[6] and the other to van der Waals and Bakker, as discussed by Guggenheim[7].

Gibbs defined the interface as a plane pp' with no volume or thickness (Figure I-2a) separating two bulk phases α and β. The bulk phases are pure up to the planes AA' and BB' in α and β respectively. Adsorption is measured by the extra amount of component x in between AA' and BB' by virtue of the presence of the interface.

The other approach, which is equivalent but conceptually simpler, considers the interface as a separate phase P, as in Figure I-2b with a finite thickness between

the two adjacent bulk phases α and β . All changes in properties between the bulk phases occur in the surface phase P between AA' and BB'. This approach is physically more realistic than the Gibbs method, although the choice between a particular model is simply a matter of convenience.

I-2-4 Surface Thermodynamic Quantities.

The thermodynamic functions commonly used for bulk phases, U the internal energy, A the Helmholtz free energy, G the Gibbs free energy and S the entropy, may all be adapted for use in the examination of surfaces.

For a closed system, with no interface, at equilibrium an infinitesimal change is reversible and the first law of thermodynamics states that:

$$dU = dq + dw \qquad \text{(I-1)}$$

where dq is the heat change corresponding to an amount of work dw. It is known that for an isothermal change (in an ideal gas) the internal energy remains constant, so that $dw = -pdV$, where p and V are the pressure and volume of the system respectively. Also, from the second law of thermodynamics $dq = TdS$ where T and S are the temperature and entropy respectively, if the system contains an interface, in addition to the $p\Delta V$ work, work may be done altering the area of the interface, so:

$$dw = -pdV + \gamma da$$

where γ is the surface tension and a the area of the interface. It follows that for a closed system:

$$dU = TdS - pdV + \gamma da \qquad \text{(I-2)}$$

and if the composition is variable:

$$dU = TdS - pdV + \gamma da + \sum_i \mu_i dn_i \qquad \text{(I-3)}$$

where μ_i is the chemical potential of component i and n_i the number of moles of i.

Similar equations may be written for dA and dG. Either convention for the surface is applicable. Representing any of the functions U, A or G by F, then for a system containing two bulk phases α and β separated by an interface:

$$F(\text{system}) = F_{(\alpha)} + F_{(\beta)} + F_{(\text{interface})} \qquad \text{(I-4)}$$

The choice of surface convention becomes important when considering the surface alone. If the Gibbs convention is chosen, the volume of the surface is zero.

I-2-5 The Gibbs Adsorption Equation.

The Gibbs adsorption equation relates the surface concentration to the surface tension and the bulk fugacity or activity of an adsorbate. In liquid-liquid and liquid-vapour systems, where the surface tension is directly measurable, the Gibbs equation may be used to determine a surface concentration. Conversely, for systems where the surface tension cannot be measured directly, the Gibbs equation can be used to calculate the lowering of the surface tension γ, when adsorption occurs. The spreading pressure, a two dimensional pressure exerted by the adsorbed molecules in the plane of the surface, defined by $\Pi = \gamma^{\circ}$(no adsorption) $- \gamma$(adsorption) may therefore be calculated. The Gibbs equation may be derived, using either of the surface conventions[8], it is

$$-d\gamma = \sum_i \tau_i d\mu_i \qquad \text{(I-5)}$$

where $\tau_i = n_i/a$ is the surface concentration of component i.

The Gibbs equation finds application in the study of gas-solid systems, and in the interconversion of

surface equations of state and adsorption isotherms.

An adsorption isotherm relates a bulk pressure or concentration of an adsorbate to the surface concentration, at constant temperature:

$$P = Kf(\tau) \qquad (I\text{-}6)$$

where P is the pressure, K is a proportionality constant and $f(\tau)$ is some function of the surface concentration. A surface equation of state connects the spreading pressure to the surface concentration:

$$\Pi = \gamma^{\circ} - \gamma = RTf'(\tau) \qquad (I\text{-}7)$$

where R and T have their usual meaning and $f'(\tau)$ is another function of the surface concentration. Thus the Gibbs equation can be used to relate the lateral adsorbate interactions described by the equation of state to the normal interactions between the adsorbent and adsorbate described by the isotherm, since both equations contain a surface concentration expression.

I-2-6 The Two Dimensional Perfect Gas.

The fundamental principle of surface chemistry is that bulk measurements of pressure or concentration before and after reaction with a surface can yield information concerning the surface. Neglecting the surface heterogeneity and the lateral interactions of adsorbed species, it is possible to derive an ideal equation of state based on a perfect two-dimensional gas (an ideal non-localised monolayer). Following the method of Fowler and Guggenheim[9], the partition function $Z(1)$ for an adsorbed particle may be written:

$$Z(1) = Z(\text{TRANSLATIONAL})\ Z(\text{VIBRATIONAL})\ Z(\text{ROTATIONAL}) \qquad (I\text{-}8)$$

and related to the partition function of a monolayer of N

indistinguishable non-interacting particles by the expression:

$$Z\ (\text{MONOLAYER}) = \frac{1}{N!}\ Z(1)^N \qquad \text{(I-9)}$$

The Helmholtz free energy A(M) and the spreading pressure $\Pi(M)$ of the monolayer are related to the monolayer partition function Z(M) by:

$$A(M) = -KT\ .\ \ln Z(M) \qquad \text{(I-10)}$$

$$\Pi(M) = -\left(\frac{\delta\ A(M)}{\delta\ a}\right)_{T,V,N} \qquad \text{(I-11)}$$

Application of Stirling's approximation followed by differentiation with respect to a, the interfacial area, yields the surface equation of state:

$$\Pi a = NKT \qquad \text{(I-12)}$$

where K is the Boltzmann constant.

The chemical potential of the monolayer may be obtained by differentiation of the monolayer Helmholtz free energy with respect to $N\left[\left(\frac{\delta A}{\delta N}\right)_{T,V,a}\right]$. For equilibrium the chemical potential of the adsorbate on the surface and in the bulk must be the same. By comparison of the chemical potential for a perfect gas (Fowler and Guggenheim[9]) with that of the adsorbed species the adsorption isotherm is obtained:

$$P = KN \qquad \text{(I-13)}$$

where P is the bulk pressure, N the number of adsorbed particles and K a constant containing a number of molecular parameters and a potential term for the adsorbent-adsorbate interaction. Equation I-13 states that for ideal phases the amount adsorbed is directly related to the bulk pressure.

By suitable adjustment of the particle

partition function, deviations from ideality may be accounted for by including terms for the size of the particles and their lateral interactions. The adsorption isotherm becomes dependent on coverage and describes two dimensional monolayer condensation[10]. This phenomenon is observed experimentally for adsorption on solids and liquids.

I-2-7 The Langmuir Adsorption Isotherm.

The first quantitative theory of the adsorption of gases on solids was given by Langmuir[11] using a kinetic approach considering the rate of condensation and evaporation of particles on a surface. The derivation assumes an ideal localised monolayer and results in the well known equation:

$$bp = \theta/(1-\theta) \qquad (I\text{-}14)$$

where θ is the fraction of the surface covered at the pressure p and b is the ratio of the rate constants for adsorption and desorption. The statistical derivation[9] yields the constant in terms of the molecular parameters. The model, although more useful for the description of chemisorption, is important because extensions of it form the basis for the derivation of isotherms describing the multilayer character of the physical adsorption of gases on solids. The most important of these is that developed by Brunaeur, Emmett and Teller[12], and is to be discussed later.

I-2-8. Forces Between Particles.

It is well-established that the resultant force between any pair of isolated particles is simply the difference

between the attractive and repulsive forces. These forces F, may be represented as gradients of potential U, since $\underline{F} = -\text{grad } U$.

For forces with no radial symmetry:

$$F = -\frac{\partial U(r)}{\partial r} \qquad \text{(I-15)}$$

where r is a distance. The potential between two isolated particles may be written as:

$$U = \frac{A}{d^n} - \frac{B}{d^m} \qquad \text{(I-16)}$$

A and B are constants, d is the distance of separation and m and n are the powers by which the attractive and potential terms vary. The repulsive term (A/d^n) is not well understood and may have n values between 9 and 12. The attractive term is better understood and may have any one of a variety of m values or a combination. The interaction of two ions corresponds to $m = 1$. Ion-permanent dipoles and permanent dipole-permanent dipole interactions correspond to $m = 2$ and $m = 3$ respectively. $m = 4$ corresponds to an ion-induced dipole interaction. Dipole-induced dipole and 'London' dispersion interactions both correspond to $m = 6$. Permanent dipole-quadrupole interactions and quadrupole-quadrupole interactions correspond to $m = 8$ and $m = 10$ respectively. The situation is further complicated because the interaction of macroscopic bodies is the result of the combination of all possible interactions. It is not simply the sum of pair wise interactions since multibody interactions are also present. The phenomenon of retardation may reduce the range of the London forces in a multibody system,[13] m increasing to 7.

The forces of physical adsorption can be considered as having two major components, a non-specific contribution always present irrespective of the system and a specific

component dependent on the particular properties of the system, ie. charge and shape. By definition, the forces have a short range and are weak.

The non-specific interactions include the London force[14,15] and a short range repulsion. The London forces are the primary cause of attraction between neutral particles and arise from the rapid, random movement of the electron cloud of one particle polarising the electron cloud of a neighbouring particle. The transient attraction is between the instantaneous dipole and the induced dipole and not between the instantaneous dipoles since these do not have time to align and will repel as often as they attract. In addition there are induced dipole-quadrupole and quadrupole-quadrupole interactions, so that strictly the attraction potential function should contain m = 6, 8 and 10 terms. The repulsive forces have a short range and are strong, resulting from the compression of two electron clouds in the absence of chemical reaction. The total potential between two isolated atoms is to a good approximation characterised by a (12 : 6) potential:

$$U(d) = \frac{A}{d^{12}} - \frac{B}{d^{6}} \qquad \text{(I-17)}$$

the potential curve for which is plotted in figure I-3. The specific interactions are important when the adsorbent or the adsorbate or both are ionic or polar. Kiselev[16] and Barrer[17] have discussed these interactions. They are important when the adsorbent is a metal oxide, has exposed surface ions and reactive surface hydroxyl groups and the adsorbate is ionic or polar. In general, for the adsorption of polar species on a polar surface, the total energy of interaction ϕ is the sum of the non-specific interactions $\phi(NS)$ and the various

specffic interactions $\phi(S)$ as appropriate:

$$\phi = \phi(N.S.) + \phi(S) \qquad (I\text{-}18)$$

where $\phi(N.S.)$ is the sum of a dispersion term and a repulsion term and $\phi(S)$ contains a small polarisation term $\phi(p)$ and possibly a field-dipole term $\Phi(F\mu)$, and a field-gradient-quadrupole term $\Phi(\dot{F}Q)$:

$$\phi(S) = \phi(P) + \Phi(F\mu) + \Phi(\dot{F}Q) \qquad (I\text{-}19)$$

The field-dipole term is important for the adsorption of species with a permanent dipole moment (e.g. H_2O), while the field-gradient quadrupole term is significant for molecules with a permanent quadrupole (e.g. N_2).

The above discussion has assumed adsorption on plane surfaces. When adsorption on non-planar, porous surfaces is considered, the potential at a distance d from the surface will vary with position over the surface. In particular, the overlap of the potential associated with opposing walls in a pore will enhance the net potential, thus increasing the probability of adsorption (the other factors being equal) compared to a plane surface. When the walls become sufficiently close ($\lesssim 2nm$) the phenomenon of 'micropore filling' occurs and the heat of physisorption becomes significantly larger than that for adsorption on a similar but non-porous surface[18].

I-2-9 Enthalpies of Adsorption.

Physical adsorption is spontaneous which rqquires that ΔG, the Gibbs free energy change of the system, is negative. It is reasonable to assume that the entropy of an adsorbent does not change significantly on adsorption. The entropy of the adsorbate must decrease during adsorption

because of the restriction in movement on the surface compared with the free phase. Hence, the total entropy change ΔS, accompanying adsorption must be negative; so, from the equation:

$$\Delta G = \Delta H - T\Delta S \qquad \text{(I-20)}$$

the enthalpy of adsorption ΔH, must also be negative. Equation I-20 is written in terms of integral quantities, so ΔH is the integral enthalpy (or heat) of adsorption. If the addition of n moles of adsorbate to a surface releases an amount of heat Q the integral heat is[19]:

$$\Delta H = q(i) = Q/n \qquad \text{(I-21)}$$

A differential heat is defined by:

$$\bar{\Delta}H = q(d) = \left(\frac{\partial Q}{\partial n}\right)_{T,V} \qquad \text{(I-22)}$$

The isoteric heat (enthalpy) of adsorption q(st) or $-\bar{\Delta}H'$ is related to the differential heat by:

$$q(st) = q(d) + RT = -\bar{\Delta}H' \qquad \text{(I-23)}$$

and may be calculated from isotherms measured at different temperatures.

I-2-10 The Description of Real Solid Surfaces.

A perfect bulk crystal is a practically unattainable state and a perfectly ideal surface is equally removed from reality; a perfect crystal could not grow. There are a number of readily identifiable deviations from perfect crystals and hence perfect crystal surfaces[13].

Lattice defects may be of the Schottky or Frenkel type. The former may be considered as an ideal

lattice disturbed by simple vacancies in the lattice positions and the latter is the result of the movement of ions (usually cations since these are smaller) to interstitial positions leaving behind lattice vacancies. At the surface, both these effects are relatively easy, and the distinction between them becomes blurred because there is effectively a row of empty lattice sites above the surface into which a displaced ion may move.

Non-stoichiometry is a common phenomenon, especially among the metallic oxides. Four non-stoichiometric types of defect may be identified[20] and the presence of any of them near to or at the surface would drastically alter the surface energy.

The addition of a foreign ion to a lattice always creates a degree of disorder irrespective of the charge of the ion, because of differences in size and polarisability. If the foreign ion valency is different from that of the ions in the host lattice it is possible that the impurity ion may maintain its own valency state at the expense of the crystal, resulting in lattice vacancies.

Dislocations may be considered as the result of a sliding of a plane of lattice positions leaving a non-uniform three dimensional system of lattice planes. The most common forms of dislocations are the edge and screw dislocations. They arise during the processes of nucleation crystal growth and flocculation (if the crystal was precipitated from solution).

The real microscopic world is not flat; a degree of surface roughness exists and in the limit results in the phenomenon of porosity. A point or an edge will always have a surface energy that is different from that of the plane surface. In addition, many freshly-made materials undergo a weathering

process when exposed to a particular environment. Typically, oxide gels precipitated from an aqueous solution change their adsorption properties with time.

I-2-11 The Surfaces of Metal Oxides.

It is well established that metals exposed to dry air rapidly develop an oxidised surface film with a thickness in the range 1-10nm. If moisture is present, the oxide film reacts to form a hydroxyl monolayer which then further adsorbs molecular water. The adsorption of oxygen and the initial hydroxylation both proceed by a dissociative chemisorption mechanism that often involves the overcoming of an activation energy before true chemisorption occurs[13]. The adsorption of a molecule X_2 may be considered first as a physical adsorption, followed by increasing molecular strain in the adsorbate resulting in bond cleavage and then true chemisorption of the dissociated species. The potential energy curves representing this situation are sketched in figure I-4. ΔE is the activation energy and ΔD the dissociation energy of X_2. The curve $S + X_2$ traces the potential as the molecule X_2 approaches the surface S and the curve $S + X + X$ denotes the potential of S and the dissociated species $X + X$. The large potential well U(c) represents the formation of two S - X bonds, the smaller potential well corresponds to the initial physical adsorption. Hence as X_2 approaches the surface it is initially attracted by the long range surface forces and can dissociate at D and chemisorb by following the $S + X + X$ curve. When ΔE is a significant fraction of ΔD the reaction will tend to be slow at low temperatures, as in the hydroxylation of many metal oxides, even though it is

thermodynamically favoured.

The extent of molecular water adsorption on the hydroxyl layer depends on the relative humidity of the atmosphere and is physical in nature. An ice-like structure bound by Hydrogen bonds is found to exist on the hydroxyl layer. As the depth of the adsorbed water film increases so the rigidity decreases and the outer layers become more mobile. Additionally, a state of dynamic equilibrium exists between the outer physically adsorbed layers and the bulk environment. It is well known that the proton of a surface hydroxyl may exchange with gaseous deuterium[21]. Surface mobility is not confined to adsorbed species, although it may become significant at temperatures near a solid's melting point; when a scratched silver surface is heated the scratches fill up as the melting point is approached.[22]

FIG. I.1.

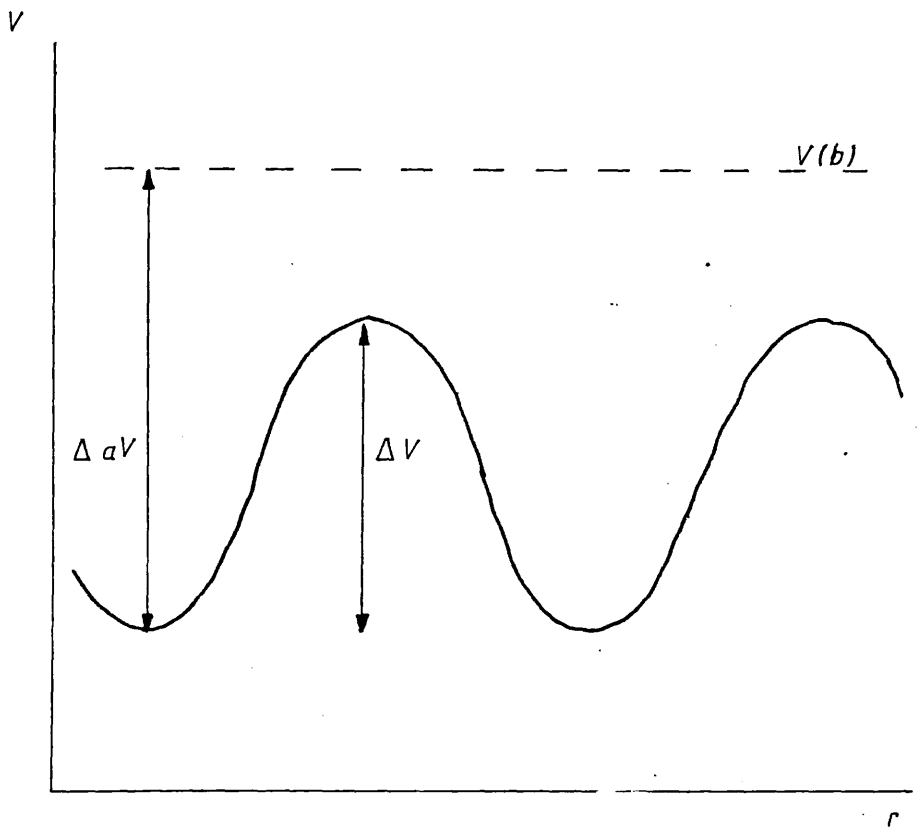

The Variation of Potential V

with distance along an ideal surface.

FIG. I.2a.

THE GIBBS DIVIDING PLANE.

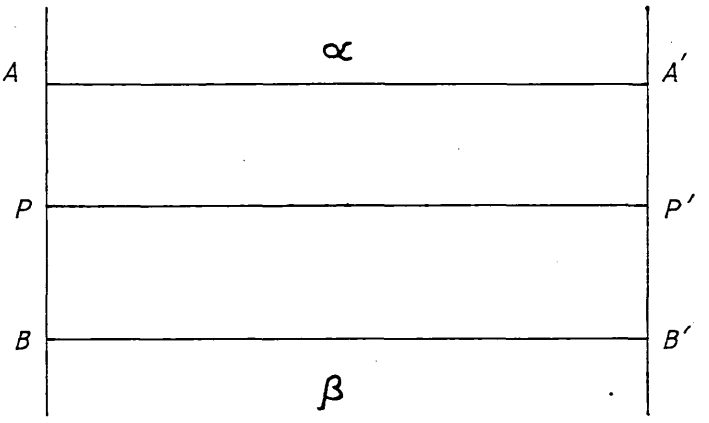

*FIG.*I.2b.

THE INTERFACIAL PHASE CONVENTION

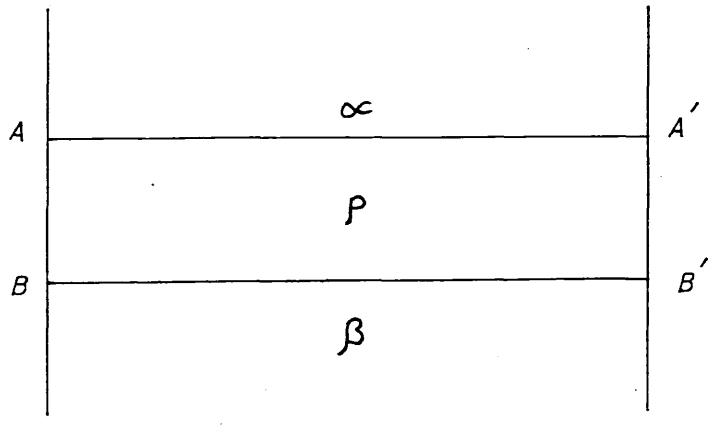

FIG. I-3.

THE 12 : 6 POTENTIAL CURVE.

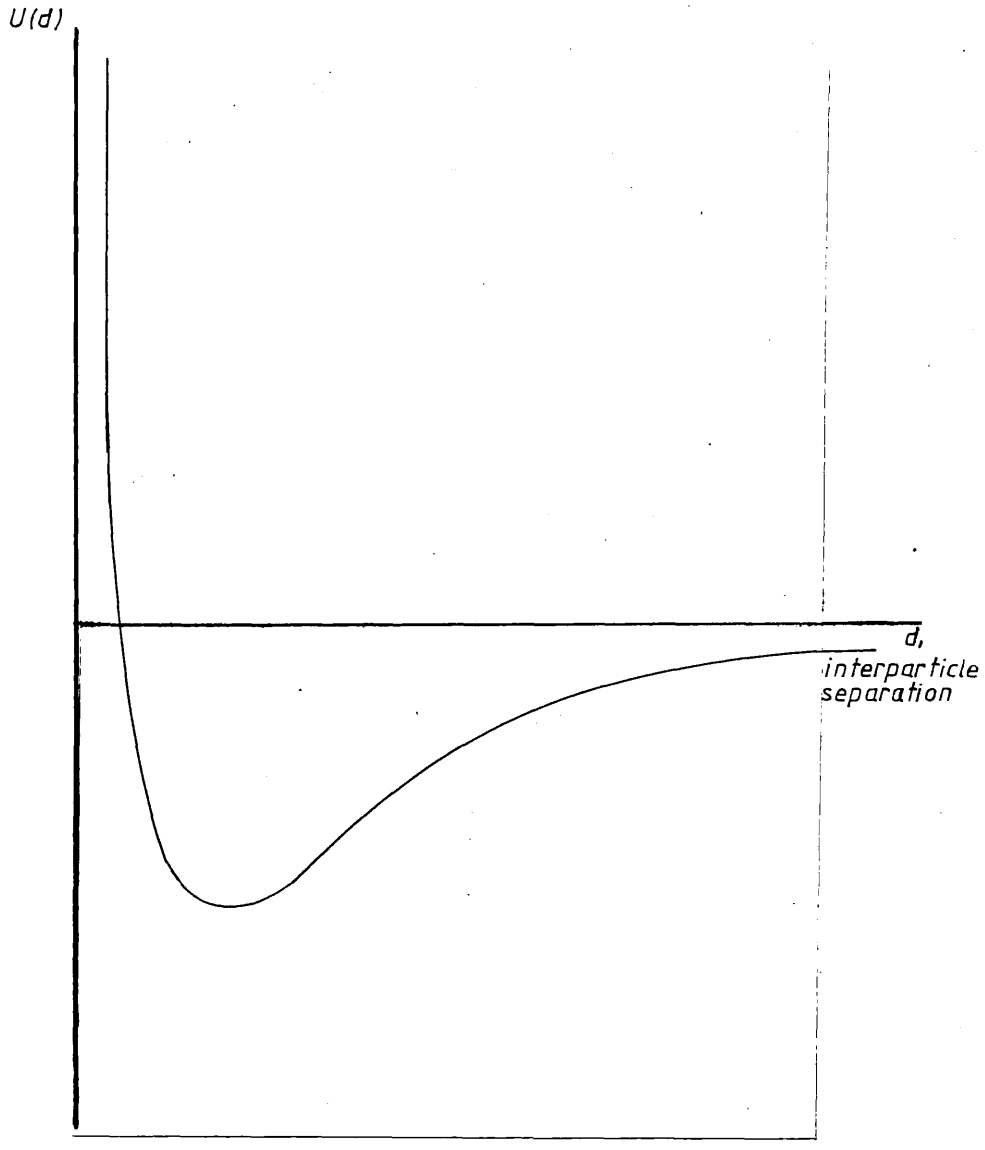

FIG. **I.4.**

The Chemisorption Process

Involving an Activation Barrier.

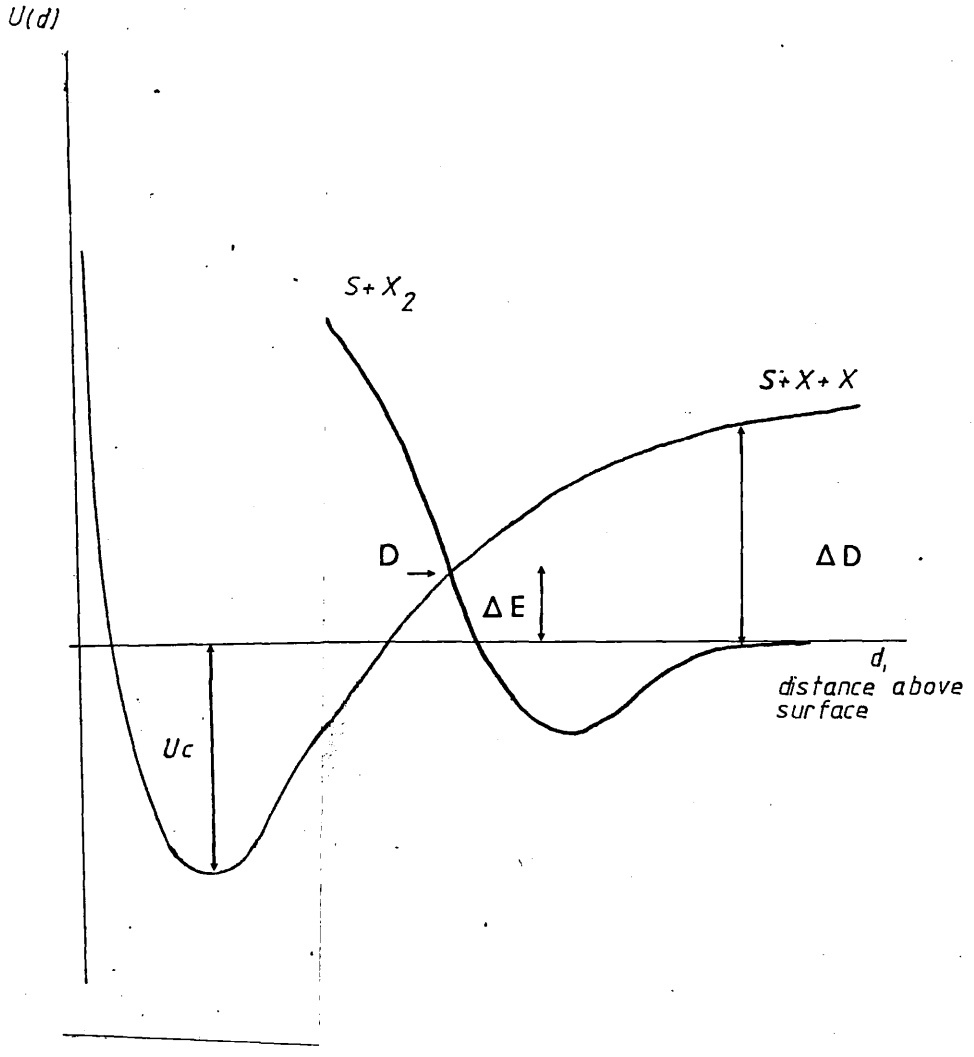

CHAPTER II.

Physical Adsorption of Gases.

II-1 Introduction - The Classification of Isotherms.

To interpret the vast array of accumulated data for the adsorption of gases and vapours on solids many different models have been advanced[19, 23]. Often these models have similar mathematical forms and can therefore be made to fit a variety of experimental data[24]. To test a particular model it is desirable to obtain data at a number of different temperatures. Many models are complex, containing numerous variable parameters, making their practical application difficult. Consequently some of the simpler models, based on rather inadequate assumptions, have found extensive use. The BET model, used for the estimation of specific surface areas is an example. Physical adsorption proceeds by the formation of multilayers on a surface, eventually resulting in the establishment of a condensed adsorbate phase. The initial part of any isotherm, corresponding to low relative pressures, is thus largely dependent on adsorbate-adsorbent interactions, while the latter part depends more on adsorbate-adsorbate interactions. Dollimore, Spooner and Turner[25] have discussed experimental isotherms in terms of low and high pressure behaviour although the traditional description of Brunauer, Deming, Deming and Teller (BDDT)[26], with the addition of hysteresis loops where appropriate, is commonly used. The characteristic curves are shown in Figure II-1 as types I to V with the addition of type VI, a step-wise isotherm describing the adsorption of noble gases on homogeneous surfaces.

The type I isotherm is traditionally described

in terms of Langmuir-like monolayer adsorption although Gregg and Sing[27] have advanced the view that type I isotherms are indicative of micropore filling. The type II isotherm corresponds to multilayer adsorption on non-porous powders, the inflexion being taken as the completion of the monolayer (the Point B). The BET model is most successful in describing type II isotherms. The relatively rare type III isotherms appear to be characterised by a low heat of adsorption which is less than the heat of liquefaction. As adsorption proceeds adsorbate-adsorbate interactions become of increasing importance, and the Point B (associated with an adsorbent-adsorbate interaction) is difficult to define. The type IV and V isotherms reflect capillary condensation in porous powders and show the characteristic hysteresis loop (the adsorption and the desorption pathways are different). Type IV isotherms are the more common, the knee corresponds to the completion of the monolayer and the hysteresis loop is associated with pores in the radius range 20–500Å .

II-2 The BET Equation.

Brunauer, Emmett and Teller[12] advanced the first model of multilayer physical adsorption as an extension of Langmuir's monolayer model. The original derivation was based on kinetic arguments of the rates of adsorption and desorption. The assumptions involved may be summarised:

1. The surface consists of a plane of equivalent adsorption sites;
2. At certain pressures particles may adsorb on a site and may also adsorb on top of an occupied site to form a number of layers in a 'stack';

3. There are no lateral adsorbate-adsorbate interactions;
4. The heat of adsorption for all layers except the first is the same and equal to the heat of liquefaction of the liquid adsorbate;
5. A particle covered by another cannot evaporate;
6. At equilibrium the number of particles evaporating from a layer is equal to the number condensing on the layer below;
7. At saturation the number of layers becomes infinite.

The treatment yields the BET equation:

$$\frac{P}{(P_o - P)} \frac{1}{V} = \frac{1}{V_m C} + \frac{(C-1)}{V_m C} \frac{P}{P_o} \qquad \text{(II-1)}$$

where P is the equilibrium pressure of adsorbate, P_o the saturation vapour pressure at the temperature of adsorption, V is the volume of gas adsorbed at pressure P, V_m is the volume of gas required to form a monolayer and C is a constant. It is possible to derive the BET equation by statistical methods which do not assume any particular kinetic mechanism and yield the constant in terms of molecular parameters. The monolayer volume need not necessarily correspond to an actual real monolayer; it simply denotes the number of particles required for a statistical monolayer. In the original derivation, the constant C expresses the relative residence times of particles in a given layer. To a first approximation C is related to the difference between the heat of liquefaction L, and the heat of adsorption E of the first layer.

$$E - L \simeq RT \ln C \qquad \text{(II-2)}$$

where R is the gas constant, and T the temperature. Generally

a high C ($C \gg 1$) value suggests a large heat of adsorption and adsorption in the first layer is preferred. The first layer is therefore substantially complete before higher layers are formed and a type II isotherm with the characteristic 'knee' results. Many isotherms fit the BET equation in the region in which the knee occurs, in the relative pressure range 0.05 to 0.30. Although the knee is associated with the completion of the monolayer ($v/v_m = 1$) the statistical nature of the phenomenon ensures that the monolayer will almost certainly not be complete. However, the smaller the difference between the point $V/V_m = 1$ and the completion of the monolayer in reality, the higher C is, and the more distinct the knee becomes. This is the basis of the Point B method for surface area determination. By inspection of the isotherm an approximate monolayer capacity may be obtained by identification of the Point B (the high pressure end of the knee at the point at which the curve becomes linear), and equating this to $\frac{V}{V_m} = 1$.

The BET equation in the form above, equation II-1, predicts a straight line when $P/(P_o-P).V$ is plotted against P/P_o with a gradient of $C-1/V_mC$ and intercept $1/V_mC$. Thus, for an isotherm which fits the BET equation in the requisite pressure range, V_m and C may be obtained. If the cross sectional area σ, of the adsorbate on the surface is known, the specific surface area S_w of the adsorbent can be calculated since

$$S_w = V_m \sigma N/V_o W \qquad (II-3)$$

where N is Avogadro's number, V_o is the ideal gas volume and W the weight of the adsorbent.

The surface areas of some porous materials may

be estimated with caution. Strictly the model is only valid for plane surfaces although most hysteresis loops associated with capillary condensation close at relative pressures above 0.3. However, if microporosity is present and hysteresis is found to occur in the BET region the validity of the approach must be severely doubted.[27].

For the evaluation of a surface area, the BET model strictly requires the use of the cross sectional area of an adsorption site rather than the area occupied by an adsorbed particle. The former quantity is unknown, and 'absolute' surface areas are therefore unobtainable. This defect in no way diminishes the usefulness of the BET model for the assessment and comparison of 'BET surface areas'.

Small C values ($c \simeq 1$) indicate a low heat of adsorption and are associated with type III isotherms. Some negative C values have been obtained [28].

II-3 Criticisms of the BET Model.

Many authors have examined closely the assumptions of the BET model[25,27]. Brunauer[29] has acknowledged that for 'real' systems the assumptions of equivalent adsorption sites and lack of lateral interactions are incorrect, but pointed out that for coverages approaching the completion of the monolayer they are self compensating. The most energetic sites of an energetically heterogeneous surface will be covered first, so that the overall adsorption potential decreases with increasing coverage. Conversely, lateral interaction between adsorbed species will increase with increasing coverage. The result is that the adsorption energy E often remains approximately constant up to monolayer coverage as in Figure II-2 and C is hence constant.

A major criticism concerns the assumption that the heat of adsorption for the second and higher layers is the same and equal to the heat of liquefaction. The polarising affect of a surface decreases uniformly with distance from the surface so that the heat of adsorption for the n^{th} layer will be greater than for the $(n + 1)$th layer. Only far from the surface will the polarising power become negligible, and the heat of adsorption of succeeding layers be nearly constant and equal to the heat of liquefaction. When the assumptions concerning the heat of adsorption of the first layer E, and the heat of adsorption of subsequent layers L, break down C will vary with coverage, since equation II-2 may be written:

$$C \simeq \exp\left[(E - L)/RT\right] \qquad \text{(II-4)}$$

Dollimore et al[25] review the constancy of C and Lowell[30] has derived an equation relating the fraction of surface covered θim, by i layers at the point $V = V_m$ to c:

$$\theta im = C\left[\frac{C^{\frac{1}{2}} - 1}{C - 1}\right]^{i + 1} \qquad \text{(II-5)}$$

The assumption of non-interacting stacks of adsorbed particles and the consequent lack of mobility is clearly incompatible with the assumption of a phase above the first layer exhibiting liquid-like interactions.

The kinetic deriviation produces a third constant, 'q' that is removed by setting it equal to P_o. This should occur at saturation and so as $P \longrightarrow P_o$, $V \longrightarrow \infty$. This does not always occur and can never occur for a porous material.

Hence the range of relative pressure for which the BET model is applicable corresponds to the low pressure

region before extensive multilayer formation has occurred, typically for P/P_o between 0.05 and 0.30. Often the range of applicability is much less[28]. To overcome the deficiencies of the BET model many modifications have been suggested, for example by Anderson[31], Brunauer[32], Hüttig[33], Dole[34], Halsey[35], Ferguson and Barrer[36] and Theimer[37]. Often, as in the case of the further equations of Brunauer[32] the number of variable parameters increases, so reducing the usefulness of the equations. The Frenkel-Halsey-Hill (FHH)[10,35,38,39,40] approach treats the adsorbed layer as a slab of liquid similar to the bulk liquid and is complementary to the BET theory. The FHH model works best for coverages and pressures above those for which the BET model breaks down .

Despite the many criticisms of the BET model and the attempts to improve it, the basic model is the most extensively used method for determining surface areas.

II-4 The Choice of Adsorbate.

It is essential for the estimation of surface areas that an adsorbate gives a well defined knee in a type II or possibly a type IV isotherm. The effective area of the adsorbate must be known and should remain constant for a number of adsorbents. This requirement dictates the use of small molecules with known surface orientation. The stacking must also be known, again favouring the use of small molecules. The gas or vapour should be well characterised so that deviation from ideality can be accounted for in the calculation of the amount adsorbed. Many adsorbates have been used[41] the most common being the inert gases, nitrogen and water vapour. Where only the

surface area is sought rather than additional chemical information concerning the surface, nitrogen is the standard adsorbate. Nitrogen gives type II isotherms with many adsorbents; it is approximately ideal, and the deviations from ideality are well-documented[42]. The uncertainty in the calculation of the nitrogen cross-sectional area is small, and the generally accepted value is 16.2$\mathring{A}^2$ at -195.8$\mathring{C}$. A practical consideration is the question of the rate of attainment of equilibrium. For nitrogen on many plane surfaces this is virtually instantaneous and is almost certainly completed within about ten minutes. If narrow pores are present so that the adsorption within the pores becomes activated, it may, however, take weeks to achieve equilibrium.

II-5 Other Models for Adsorption.

In addition to the BET type descriptions of multilayer adsorption there are two other broad approaches, those based on the equation of state of the adsorbed film and those based on a consideration of adsorbate particles moving in a potential field close to the surface.[43] The most important of the former class are those isotherms derived from two-dimensional equations of state. The ideal gas law equation of state gives a Henry's law isotherm; corrections may be applied for non-ideality in the form of Van der Waals' equations of state or by the application of virial equations. A number of isotherms exist which are related to the original potential theory of adsorption advanced by Polanyi[44]. The space above a surface is assumed to consist of a network of equipotential planes so that a cross-section contains a number of equipotential contours above the surface as in Figure II-3. The adsorption potential E

is a maximum at the surface and decreases with distance from the surface. Successive potential planes enclose a volume of space V which increase with distance from the surface as E decreases, so:

$$E = f(V) \qquad \text{(II-6)}$$

It is assumed E is independent of temperature. The curve represented by equation II-6 is the 'characteristic curve' for a given system. As the treatment is thermodynamic it is open to less criticism than the BET model. For multilayer adsorption, condensation to a thin, negligibly compressed, liquid film is assumed. The work done, per mole E, compressing an ideal gas at constant temperature from the pressure of the bulk $P_{(o)}$ to the vapour pressure of the liquid P(L) is:

$$E = RT \ln (P(L)/ P_{(o)}) \qquad \text{(II-7)}$$

Corrections may be applied to account for the work done in creating a liquid gas interface and for the compressibility of the adsorbed phase. Dubinin[18,45 a-c] and others have applied the potential theory to adsorption on porous surfaces, particularly adsorption in micropores. The Frenkel-Halsey-Hill slab theory is one of a number of modifications to the original potential theory. The potential is assumed to vary with the distance from the surface. For a plane solid and a 'slab' of adsorbed liquid, the principal adsorbent-adsorbate interaction involves dispersive forces so, at a distance x from the surface:

$$E(x) = E(o) / (a + x)^3 \qquad \text{(II-8)}$$

where a is a constant. The derived adsorption isotherm becomes:

$$(V / V(m))^n = A / \ln (P_o / P), \text{ with } A = E_o / (x^n_{(m)} . RT) \qquad \text{(II-9)}$$

where x(m) is the film thickness at the monolayer point, V and V(m) are film volumes and the power n lies between two and three for many nitrogen isotherms.

There is no one model that completely describes all the features of multilayer physical adsorption. Treatments of a two dimensional phase are only adequate in the submonolayer region. The potential model is more realistic and arguably has a sounder basis than the BET type models. There are two major problems to surmount. The first of these is that the theory of liquids is incomplete so that the problems of a thin liquid film held in a potential field are hardly likely to be solved before advances occur in the understanding of the bulk liquid. The second effect is that of surface heterogeneity which is present unless great care has been exercised in the preparation of the surface. An experimentally observed isotherm is the result of adsorptions on all the different surface sites. Thus, in addition to the pressure dependence a site energy distribution function is required to describe the isotherm.

II-6 Adsorption on Porous Solids.

Generally, adsorbates above their critical temperatures do not give multilayer type isotherms and porous and non-porous surfaces behave similarly provided the pore sizes are significantly greater than the size of the particular adsorbate. Below the critical temperature multilayer adsorption occurs and the effects of porosity become apparent. Within a pore the thickness of the adsorbed layers is limited. In addition, the overlap of the potential fields of the opposing walls enhances the adsorption potential and can increase the amount adsorbed at a given relative pressure compared to a plane surface. Once filled with adsorbate, pores show a reluctance to empty. The phenomena of capillary condensation and adsorption hysteresis characterise adsorption in porous materials. Pore

sizes are classified according to their width as in Table II-1, using the 1972 International Union of Pure and Applied Chemistry classification.

The type IV isotherm results when an adsorbent possess mesopores and has the same adsorbent-adsorbate interactions as those responsible for type II isotherms. The type V isotherm is rare and difficult to interpret. It results from similar interactions to those determining type III isotherms. If an adsorbent is entirely microporous a type I isotherm is obtained experimentally and if mesopores are also present, the effects of microporosity are revealed as small low pressure hysteresis loops additional to the main condensation loop. Only the type IV isotherm and hence the properties of mesoporous adsorbents will be discussed here.

II-7 Adsorption Isotherms, Type IV.

A type IV isotherm is shown schematically in Figure II-4. The low pressure region ABC is analogous to monolayer formation in type II isotherms; between B and C the monolayer is completed. In the absence of microporosity the adsorption is reversible, so that the adsorption and desorption curves are identical. Multilayers begin to form above C on the branch CDE. At E the pores are filled with adsorbate in a liquid like phase and any further adsorption occurs on the exterior surfaces only, resulting in the branch EFG. Condensation in large pores or between particles may cause the isotherm to turn sharply upwards to H at some point F along EFG, approaching P_o asymptotically. Above E the adsorption is reversible, thus the adsorption and desorption curves are identical. Desorption occurs primarily from the exterior surfaces

up to the point E. Thereafter the branch EIC is followed. At any point along the hysteresis loop the quantity of adsorbate on the surface is greater for the desorption branch than for the adsorption branch. Along EIC, material is not initially lost from the interior of pores, but rather from the shrinkage of the liquid like menisci covering the various pore entrances. Thus the desorption along EIC starts slowly. At some point after E a particular meniscus will become unstable. Any further small reduction in pressure then causes the meniscus to collapse and a substantial volume of the liquid within the pore evaporates rapidly, leaving a thin film of adsorbate on the pore walls. If the desorption process is commenced before all the pores are full, then the loop J will be traced from the adsorption to the desorption branches of the isotherm.

Within the hysteresis loop, the adsorption process depends on the potential field within a pore, and hence on the size and shape of the pore. However, the initial desorption process is controlled by the behaviour of the liquid meniscus in the potential field of the pore entrance. Clearly the mechanisms for adsorption and desorption between C and E are different.

de Boer[46] has further classified isotherms exhibiting hysteresis, the three most important ones are shown in Figure II-5. The type A loop has traditionally been associated with capillary condensation in open-ended tubular pores. A cylindrical meniscus forms during the adsorption process so that the desorption process, which occurs through evaporation of a hemispherical meniscus, takes place at a lower relative pressure. The type B loop was considered to be associated with slit-shaped pores. During adsorption a meniscus does not form until high relative pressures are reached. Desorption is controlled by evaporation

of a cyndrical meniscus. The type E loop associated with many oxide adsorbents is associated with condensation in 'ink bottle' type pores. The initial flat part of the desorption loop results from evaporation of small menisci. This is followed by the emptying of the entire pore at the relative pressure at which the narrow meniscus collapsed. Since the pore filled at a pressure corresponding to the widest part of the pore there is a large disparity between two branches of the isotherm. The relation between pore and meniscus shapes is not fully understood.

On a macroscopic scale liquid surfaces are described by the Laplace and Kelvin equations. The former equation relates the pressure drop across a curved surface to the principal radii of curvature and the surface tension and finds application in the evaluation of surface tension by capillary rise methods. The Kelvin equation which relates vapour pressure to surface curvature, is important in the context of the estimation of mesopore sizes from gas physical adsorption data.

II-8 Equilibrium in the Hysteresis Loop.

The existence of adsorption hysteresis poses problems in the application of equations such as the Kelvin equation, which are based on the general principle of thermodynamic reversibility. If pore emptying is considered as a catastrophic event occurring at some critical pressure in the 'ink-bottle' hypothesis, it is doubtful if reversible thermodynamic equations can be applied. In general, the work of expansion and compression in "piston and cylinder" experiments are functions of the path. Therefore, on moving through a hysteresis cycle, the possibility exists that the net change in work will not be zero. An irreversible process

must therefore be involved. Applying this argument to adsorption hysteresis results in the conclusion that Second Law equations become suspect when applied to hysteresis[43,47].

Opinion varies as to whether to use the adsorption or desorption branches for calculations of pore size distributions[27,43,48,49,50]. If the molar free energy change for the condensation and evaporation of a quantity of liquid in a pore can be represented by:

$$\Delta G = RT \ln (P/P_o) \qquad \text{(II-10)}$$

then the desorption loop corresponds to the more stable situation. In general, unless 'ink-bottle' type pores have been identified the literature tends to suggest the use of the desorption branch for assessments of pore sizes. Irrespective of which branch of the isotherm is chosen for analysis, the mathematical treatment is in principle the same.

II-9 The Kelvin Equation.

The Kelvin equation describes the relationship between the vapour pressure over a curved surface and the radius of curvature. It is usually written in the form:

$$\ln \frac{P}{P_o} = \frac{-2\gamma V(m)\cos\theta}{RT\,R(K)} \qquad \text{(II-11)}$$

where P/P_o is the relative pressure at which condensation occurs in a pore of radius R(K); γ is the surface tension; V(m) is the molar volume, θ is the contact angle and R and T have their usual meanings. For θ between 0° and 90° the right hand side of this equation remains negative so that P is less than P_o. Hence liquid should condense in a pore at some pressure less than

the saturated vapour pressure. Unfortunately, contact angles between liquids and capillary walls are unknown. Equation II-11 is commonly approximated:

$$R(K) \simeq \frac{-2\,\gamma\,V(m)}{RT\,\ln(P_o/P)} \qquad \text{(II-12)}$$

with θ equal to zero. R(K) will therefore be high by a factor $1/\cos\theta$ although the error is small for quite large values of θ ($\cos 20 = 0.94$). Gregg and Sing[27] discuss the implications of this assumption and draw attention to the constancy of θ throughout the isotherm. In the form II-12, a hemispherical meniscus in cylindrical pores is assumed.

The applicability of the Kelvin equation to adsorption phenomena requires that the concepts of a liquid meniscus with the associated surface tension remain valid. This immediately precludes the investigation of micropores where the concept of a liquid meniscus ceases to be meaningful. Condensation in macropores occurs at high relative pressures where P and P_o are nearly the same. Hence the Kelvin equation finds most use in the mesopore range. However, questions concerning the applicability of bulk surface tension, molar volume, pressure and temperature to the interior of the pores remain unanswered. An article by Everett, Haynes and McElroy[51] concludes by noting the lack of experimental verification of the Kelvin equation It is well known that for small r the surface tension itself becomes a function of curvature. This effect does not become apparent until the curvature is comparable to molecular dimensions[52,53].

In reality most porous solids have a distribution of pore sizes and in addition a variety of irregular shapes. Unless the shape of an isotherm or preferably an independent method (e.g. electron microscopy) suggest some predominant pore structure, it is common to assume cylindrical pores and use the Kelvin equation in the form II-12. Corrections may be applied if the pore shape is known.

II-10 Mesopore Analysis.

The volume of all pores is calculated as a function of the pore radius and is plotted as in Figure II-6a. The pore size distribution is simply the derivative of this curve, $dV(r) / dr$ as in Figure II-6b. The calculation is complicated by the fact that for a given pressure change, the change in the amount of material adsorbed on the surface has two components. Considering the desorption process, when bulk liquid has evaporated from a pore it leaves a film of adsorbed material on the pore walls. A further reduction in pressure will cause this film thickness to decrease. Simultaneously, capillary evaporation will occur from smaller pores that did not lose their capillary condensed material in the previous desorption step. The apparent area and volume of pores will increase with multilayer diminution. The average thickness of the film may be estimated from the isotherm of the adsorbate on a non-porous reference material or from some composite isotherm. The true pore radius R(p) is simply the sum of the Kelvin radius R(K) and the film thickness t (Figure II-7):

$$R(p) = R(K) + t. \qquad \text{(II-13)}$$

Wheeler[54] considered adsorption in a matrix of cylindrical pores and obtained the equation:

$$V(p) - V(a) = \int_{r_p}^{\infty} (r(p) - t)^2 L(r)\, dr \qquad \text{(II-14)}$$

where V(p) is the total pore volume, V(a) is the volume of all pores with radii less than r(p), t is the thickness of the adsorbed film and L(r) is the distribution function. The distribution function may be given a particular mathematical form or may be obtained by numerical integration. The latter procedure is usually adopted and was used in this work.

A number of methods of pore analysis have been proposed, most are based on some assumptions of pore shape. The method of Pierce [55] as modified by Orr and Dalla Valle[56] in respect to the calculation of the film thickness, and discussed by Gregg and Sing[27], was used in this study. This procedure utilises Wheeler's[54] ideas that condensation and evaporation occur in cylindrical pores when some critical pressure is obtained. Barrett, Joyner and Halenda[57] also use this idea. Schull[58], Oulton[59], Innes[60] and Cranston and Inkley[50] have proposed various schemes all assuming certain pore shapes.

Brunauer[49,61] and co-workers have developed a "modelless method" for determining the pore size distribution in which no specific pore shape is assumed. This method gives results that are comparable to those based on the Kelvin equation and which assume certain pore shapes[49].

II-11 The Estimation of the Adsorbed Film Thickness.

The statistical thickness t of an adsorbed film

is required to evaluate the true pore radius R(p), see Figure II-7. In the mesopore range the BET equation cannot be applied to determine the multilayer thickness. There are two alternative approaches used to overcome this problem. In the first method, the adsorption isotherm is remeasured on a chemically similar, non-porous reference material. It is assumed that at any pressure the multilayer thickness evaluated for the plane surface is identical to the film thickness inside a pore. t is given by the equation:

$$t = (x/x(m))\sigma = n\sigma \qquad \text{(II-15)}$$

where x is the amount adsorbed at any pressure, x(m) is the monolayer capacity evaluated by the BET method and σ is the 'average' thickness of one layer. n is then simply the number of layers adsorbed. σ is usually less than one molecular diameter as a result of the stacking of the particles on the surface. For nitrogen the value of σ is 3.54Å which is less than the molecular diameter. Each nitrogen molecule rests in the hollow formed by three of the molecules in the hexagonal close packed layer below.

The alternative approach is based on the fact that for many non-porous adsorbents, when x/x(m) is plotted against p/p(o) all the data can be approximately described by a 'common' type[55,58,62] II isotherm. This curve is closely described by the Halsey equation[35], which for nitrogen may be written:

$$t = \sigma \left(\frac{5}{\ln P_o/P} \right)^{1/3} \qquad \text{(II-16)}$$

The agreement between the Halsey plot and experimental data is best at high relative pressures.

II-12 The Method of Pierce[55] For Estimating Pore Size Distributions.

As stated above, the method of Pierce, with certain modifications, was used to estimate pore sizes in this work. The procedure is illustrated with reference to Table II-2.

In columns 1 and 2 are the relative pressure and the amount adsorbed read directly from the isotherm. For each relative pressure, the Kelvin radius R_k is calculated in column 3 and the film thickness t, evaluated from the Halsey equation in column 4. Simple addition yields the true pore radius R_p in column 5. The mean pore radii $\bar{R}_k$ and $\bar{R}_p$ and diminution in film thickness Δt are calculated for each pressure decrement in columns 6,7 and 8 respectively. The total volume desorbed ΔV in column 9 for each successive pressure is obtained from column 2. This volume consists of material desorbed from the capillary condensed liquid in filled pores and from the film on the walls of previously emptied pores. The amount evaporated from the film ΔV_f is calculated from the area present before desorption and the estimated decrease in film thickness Δt, and written in column 10. It has to be assumed that all the pores are full at the highest relative pressure for which data are available. Thus the term ΔV_f is zero for the first pressure decrement, because no desorption can occur from pore walls. When a relative pressure of less than unity is used as the starting point, the error introduced by this assumption is small provided the difference between the initial pressure

and unity is itself small. For a relative pressure of 0.99, the Kelvin radius is about 950Å, and the internal area of a cylindrical pore will be negligible compared to its volume. The volume of capillary condensed material ΔV_K, in column 11 is the difference between the total volume desorbed and the component desorbed from the pore walls. However, ΔV_K is the volume of the inner cylinder in Figure II-7 and is related to the true pore volume ΔV_P in column 12 by the equation:

$$\Delta V_P = \left(\frac{\bar{R}_p}{R_k}\right)^2 \Delta V_K \qquad \text{(II-17)}$$

The internal pore area revealed by each successive pore desorption, ΔS_p is obtained from the equation:

$$\Delta S_p = 31.2 \frac{\Delta V_p}{\bar{R}_p} \qquad \text{(II-18)}$$

which is derived from the volume to area ratio of $\frac{r}{2}$ for a cylinder. ΔS_p is tabulated in column 13 and the cumulative area required for the calculation of ΔV_f is given in column 14. The calculation is terminated either when a relative pressure of about 0.3 is reached or when the amount desorbed from the film becomes equal to, or greater than, the total amount desorbed. The former case reflects the questionable validity of the Kelvin equation when applied to narrow pores and the latter case is a consequence of the inadequacies of the analysis coupled with the probable presence of micropores. Column 15 is the conversion of the gaseous pore volume to a liquid volume. A plot of $\Delta V_p^{Liq}/\Delta R_p$ against $\bar{R}_p$ gives the

pore size distribution (Figure II-6b).

It is assumed that the total surface area of a porous solid is associated with its mesopores. No account is taken of any contribution from either plane surfaces or micropores. If the BET area of a solid is comparable to the cumulative area as calculated above, then the solid must be essentially mesoporous with no plane surfaces. The presence of micropores is suggested if the BET area is much greater than the cumulative area.

The Kelvin procedure and variants of it, find use because of their simplicity rather than their absolute accuracy. There are three major criticisms of the approach[27]; the validity of the Kelvin equation itself, the estimation of the adsorbed film and the assumption of cylindrical pores. The concept of an adsorbed film thickness is purely formal; in reality the thickness will vary randomly. Hence equation II-13 becomes questionable, especially when the film thickness is large compared to the effective pore diameter. In general, the assumption of cylindrical pores will only be fortuitously correct.

II-13 The Modelless Method of Pore Analysis.

To circumvent assumptions of pore shape, Brunauer and co-workers[49,61] have developed a method independent of pore shape, using the thermodynamic relationship of Kiselev[63]:

$$\gamma dA = -\Delta\mu \, dn. \qquad \text{(II-19)}$$

$\Delta\mu$ is the change in chemical potential (equal to $RT.\ln p/p_o$) when dn moles condense in a capillary causing an area dA of

pore wall to be covered. Y is the surface tension. Integration over the limits of condensation, gives the total mesopore area.

$$A = \frac{RT}{\gamma} \cdot \int \ln (P_o / P)\, dn \qquad \text{(II-20)}$$

Brunauer defined a hydraulic pore radius R (h)

$$R(h) = V / A. \qquad \text{(II-21)}$$

where V is the volume of a set of pores with a surface area A. Starting from the relative pressure of one, successive small desorption steps allow the calculation of the volume of pores emptied by the change in n and their area by equation II-20. Substitution into II-21 yields the hydraulic radius. A plot of $\Delta V / \Delta R(h)$ versus R(h) gives a core size distribution. Corrections for the decrease in film thickness may be applied although these become progressively more complicated for each successive step.

II-14 't' and 'α_s' Plots.

A method useful in the assessment of porosity is to compare an experimental isotherm with one obtained on a non-porous reference material. The "t-plot" method of Lippens and de Boer[64] is used to analyse nitrogen adsorption isotherms. The amount adsorbed is plotted against the thickness, t, of the film on the reference material for each pressure. The thickness is proportional to $x / x(m)$, where x is the amount adsorbed at the particular pressure and x(m) is the monolayer capacity. Any difference

between multilayer formation on the plane surface and on the subject material is therefore apparent as a deviation from linearity in the "t-plot". The major disadvantage of this method is that it is dependent on the evaluation of the monolayer capacity by the BET method and is thus sensitive to the choice of the reference material.

The " α(s)-method" of Sing[65,66] uses a reduced isotherm that is independent of estimates of BET monolayer capacities. 't' is replaced by $\alpha(s) = x/x(s)$ where $x(s)$ is the amount adsorbed at some standard relative pressure on the non-porous reference material. $\alpha(s)$ is often set equal to one at a relative pressure of 0.4, since micropore phenomena and monolayer formation occur below this pressure and capillary condensation occurs above it. With reference to Figure II-8 the linear plot indicates that the unknown material has a surface similar to that of the non-porous reference. The upward deviation is interpreted as adsorption additional to planar multilayer formation indicative of capillary condensation. The plot with a downward deviation at low pressures suggests the presence of micropores. In this case, the use of the initial slope as an estimate of the surface area becomes questionable, contrary to the first two cases.

FIG. II.1

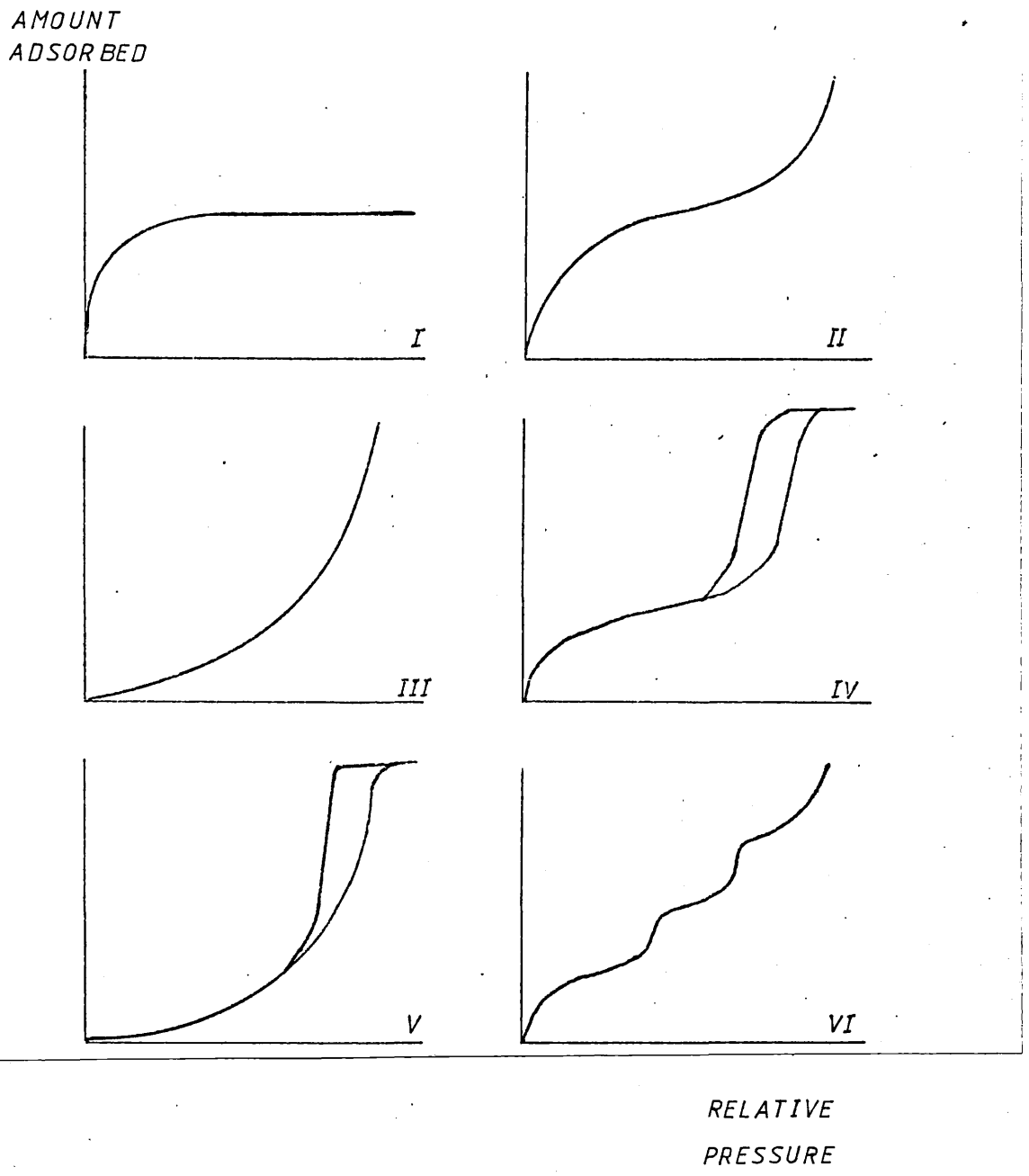

The BDDT Classification of Isotherms.

FIG. **II.2**

Variation of adsorption potential with coverage.

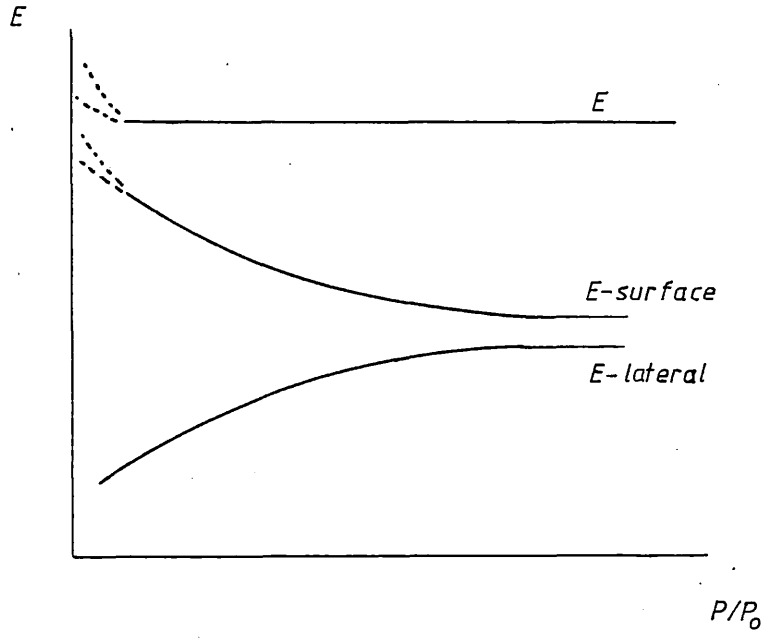

FIG. **II.3**

Potential planes above a surface as used in the Potential Theory of Adsorption.

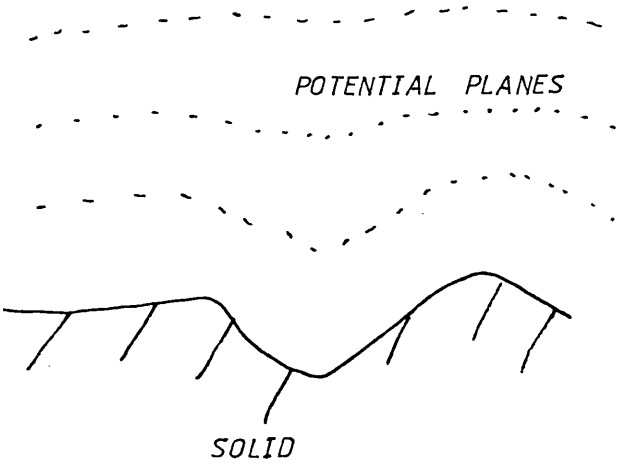

FIG. II.4

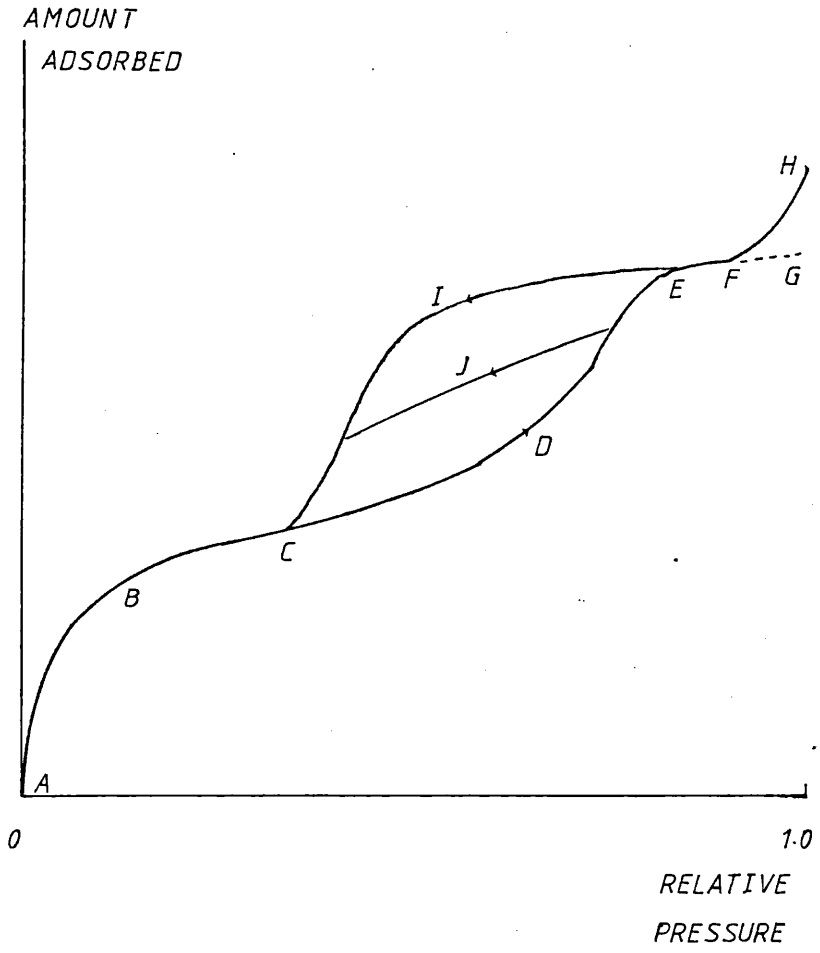

An idealised Type IV Adsorption Isotherm.

FIG. II.5

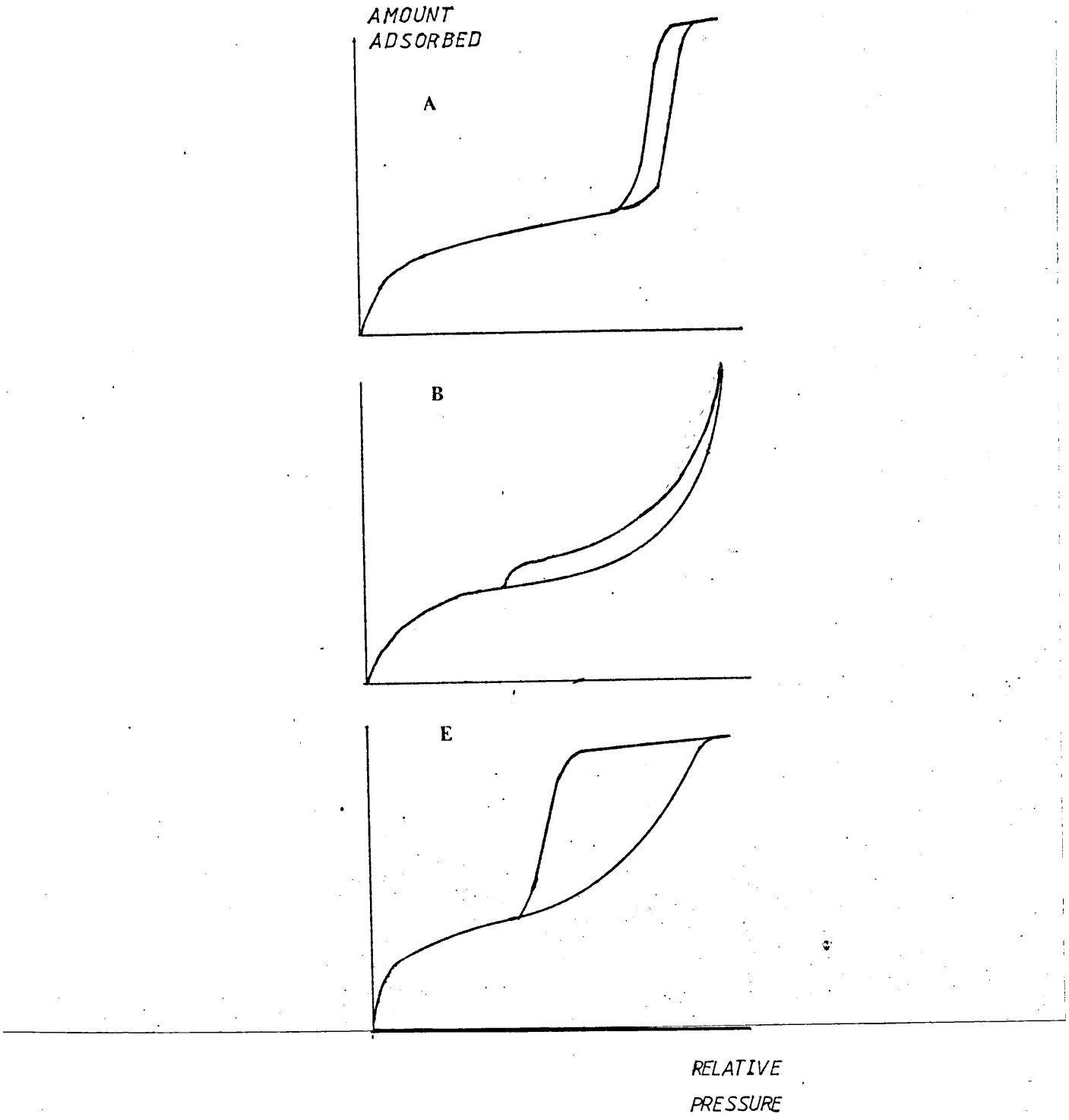

De Boer Isotherms.

FIG. II.6a.

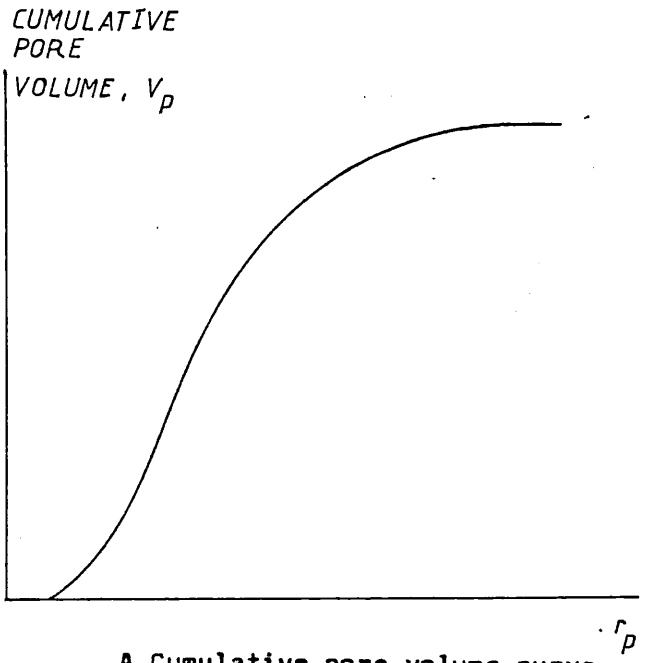

A Cumulative pore volume curve.

Fig. II.6b.

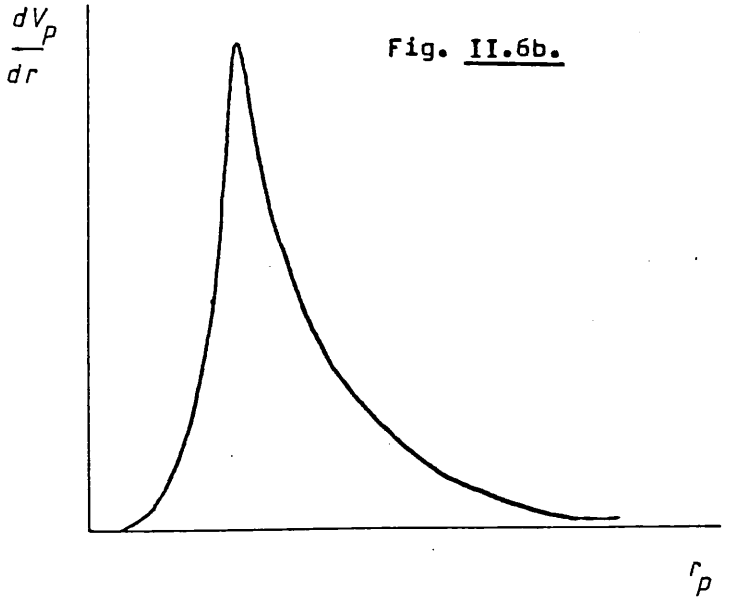

A pore size distribution curve.

FIG. II.7

The idealised interior of a pore.

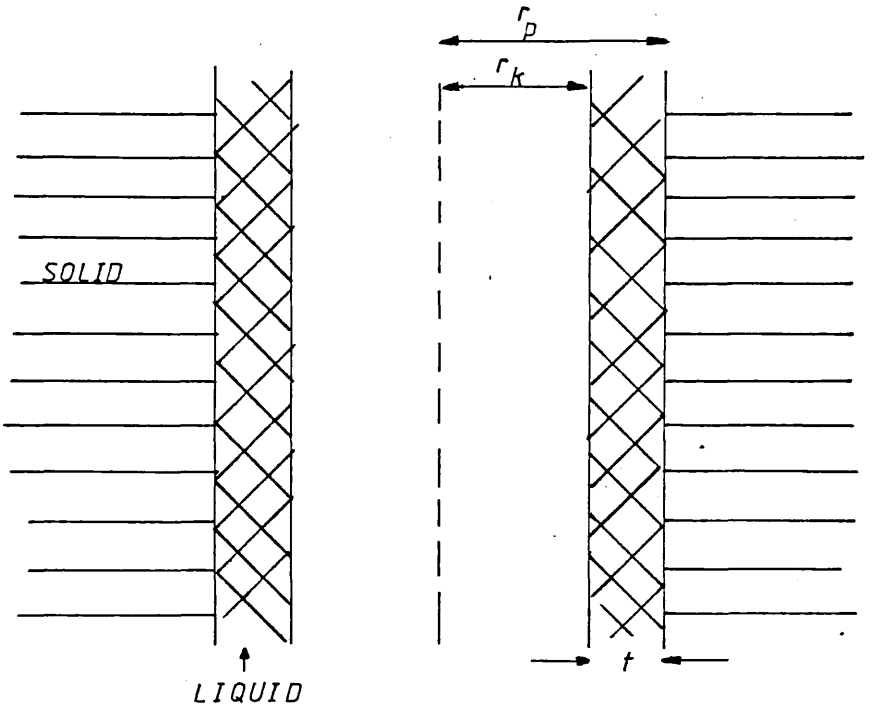

$$r_p = r_k + t$$

FIG. II.8

The α_s- plot.

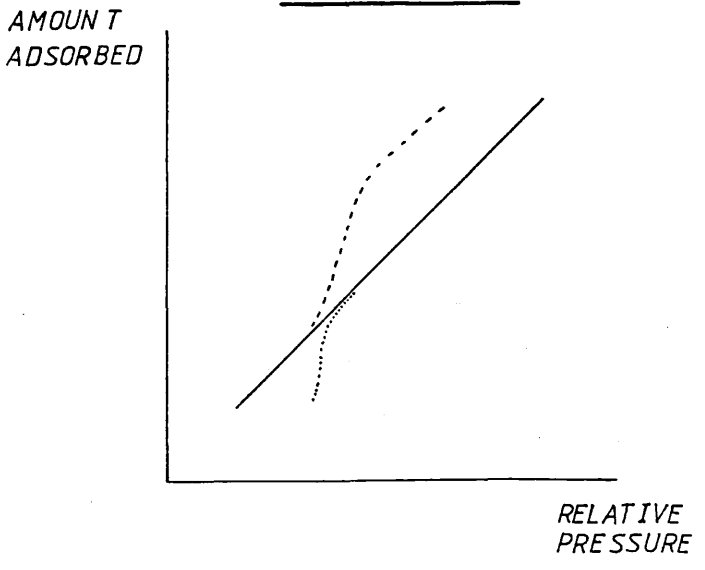

CHAPTER III

The Solid-Liquid Interface.

III-1 Introduction.

The same fundamental principles of adsorption apply equally to the gas-solid and liquid-solid interfaces. However, the liquid-solid interface is complicated because the lateral interactions of the liquid adsorbate cannot be ignored. Everett[67] has pointed out that the understanding of the behaviour of liquids under the influence of the potential associated with a solid surface is unlikely to proceed in advance of the understanding of the liquid state itself. Although progress has been made for the case of adsorption of a pure liquid, most important practical situations involve multicomponent liquids[68,69]. The components may be miscible over the entire concentration range, or the solution may be so dilute that the adsorption of the component in excess does not significantly alter the bulk composition. As discussed by Everett[68] and Kipling[70], most early work was concerned with adsorption from dilute solution. This led to the interpretation of the experimental data in an analogous manner to that employed for gas adsorption.

Irrespective of the composition of a multicomponent non-electrolyte solution, one or more of the components will adsorb onto a solid immersed in the solution. The problem is thus one of preferential adsorption. For the immersion of a solid into a binary system both components will compete for adsorption sites at the interface. A change in the bulk fluid composition will cause the composition of the interface to change. Specific excess or composite isotherms are used to represent the adsorption.

III-2 Adsorption from Binary Liquid Mixtures.

It can be shown[71] that the composite isotherm for the adsorption of the components 1, and 2 of a binary solution over an insoluble adsorbent of mass m, is;

$$\frac{n_o \cdot \Delta x_1}{M} = n_1^s x_2 - n_2^s x_1 \qquad \text{(III-1)}$$

where n_o is the total number of moles of 1 and 2 present before adsorption $\left(n_o = n_{o(1)} + n_{o(2)}\right)$, n_i^s is the number of moles of component i on unit mass of the solid at equilibrium and Δx_1 is the difference in mole fraction of component 1 before and after adsorption. $n_o \Delta x_1 / M$ can be obtained experimentally and a plot of this against x_1 yields the composite isotherm. The measured quantity, the "apparent adsorption", is not the number of moles of component 1 adsorbed but a relative measure of the change in concentration of component 1 on the surface as the composition of the bulk changes. Schay[72] has classified 5 types of composite isotherms for adsorption at the liquid-solid interface, see Figure III-1. Since the apparent adsorption is only a relative quantity, it is possible to obtain a negative value. If $n_o \Delta x_1 / M$ is negative, component 1 is negatively adsorbed $(x_{o1} < x_1)$ and the adsorption process depletes the amount of 1 in the surface phase.

If the solution is sufficiently dilute, such that x_2 and x_1 are effectively unity and zero respectively, equation III-1 reduces to:

$$\frac{n_o}{m} \Delta x_1 \simeq n_1^s \qquad \text{(III-2)}$$

Provided that $n_2^s x_1$ is very small, $n_o \Delta x_1 / M$ represents the actual adsorption of 1. Adsorption from dilute solutions is often characterised by Langmuir type isotherms suggesting the formation of monolayers.

III-3 Liquid Adsorption Models.

There are two approaches[69] to the physical adsorption of non-electrolytes on solid surfaces. The earlier approach considers adsorption in terms of monolayer coverage with little interfacial structure above this layer. The second approach resembles the multilayer theory for the physical adsorption of gases and vapours on solids. The interface is supposed to consist of a series of layers each successive layer bound less strongly to the surface than the layer beneath it. This assumes an adsorbent-adsorbate interaction that decreases slowly with distance from the surface, whereas the monolayer model requires a short range interaction. Both models have found some experimental support[68].

A basic concept used directly or indirectly in most descriptions of the solid/liquid interface is that of an adsorbed phase. This is subjected to the potential field of the adsorbent, has a uniform composition and is in equilibrium with the bulk liquid.

Equations derived from a monolayer model are known[52] to be thermodynamically inconsistent in that the predicted variation of interfacial free energy (i.e. surface tension) with adsorption does not agree with the Gibbs adsorption

isotherm. Nevertheless, in cases where the bulk solutions do not deviate greatly from ideality a monolayer model often fits the experimental data. Ash, Bown and Everett[73] for example, have found that the adsorption systems (benzene + cyclohexane)/ Graphon, (benzene +n-heptane)/ Graphon and (cyclohexane + n-heptane)/Graphon, can be described by a monolayer model. For similar systems, however, the monolayer model breaks down, for example, for the systems[74] (benzene + ethanol)/Graphon and (n-heptane + ethanol)/Graphon, the adsorbed phase extends to three or four layers at the maximum of the surface excess isotherm.

The monolayer model runs into semantic difficulties if the components of a binary mixture are vastly different in size. If one of the molecules consists of a chain of segments each segment being about the size of the other molecular entity then the definition of a monolayer becomes blurred. On the other hand, any multilayer model must take account of all possible orientations of large molecules. It appears from the above, even for relatively simple systems, that small deviations from ideality in the liquid-phase cause the monolayer model to fail.

Multilayer models are often derived on the basis of a lattice model[68] in which it is supposed the system consists of a number of planes each of N adsorption sites, stacked sequentially above each other, starting from the surface. Everett[68] has noted that none of the models are yet capable of explaining all the observed facts.

There are two other approaches. A number of attempts have been made to apply the Polanyi[44] potential

theory of adsorption of gases by solids to liquid-solid systems[75]. Barat[76] has also applied the significant structure theory of liquids[77] to adsorption from solution. In this theory different molecules are characterised by their local environment. The analysis is based on calculating the rates of adsorption and desorption. This is described in terms of the 'gas-like' and 'solid-like' molecules in the liquid and adsorbed phases respectively, and the activation energies involved for the desorption of these two kinds of species from the surface.

III-4 Surface Orientation as a Function of Concentration.

A long chain molecule adsorbed on a surface has a number of possible different orientations available to it. Intuitively, it is reasonable that changes in the composition of the surrounding environment could influence the preferred orientation. The concept of a concentration dependent orientation is especially important when attempts are made to obtain adsorbent surface areas from concentration isotherms[68].

Ash, Everett and Findenegg[78] have used computer simulation methods to study (monomer + trimer/tetramer) -substrate adsorption systems. For the case of a flexible homogeneous tetramer, wholly in the first adsorbed layer, it was assumed that four adsorption sites were occupied. The occupancy of four adsorption sites per molecule at high concentrations does not represent the situation of highest entropy for the layer. To increase the entropy, segments of any horizontally adsorbed tetramers desorb. The increase in potential energy accompanying the desorption of a segment

is counter-balanced by the increase in entropy. Thus orientations with fewer segments attached to the surface tend to be favoured as the concentration increases. This effect was found to be more pronounced if the tetramer contained a terminal segment active in the adsorption process. Consequences of this effect are that the layer thickness and the area occupied on the surface per adsorbate molecule are not constant.

III-5 The Estimation of Surface Areas from Solution Adsorption.

Kipling[70] and Schay[79] have discussed early methods of estimating surface areas from solution. Liquid-solid isotherms may in principle be used to determine surface areas in an analogous fashion to that applied to gas-solid isotherms. The fact that a particular solution isotherm fits a model originally designed to describe gas adsorption cannot be taken as evidence that the same adsorption mechanism is operating in both cases. In particular, Everett[68] has pointed out that Langmuir type isotherms, frequently encountered in studies of adsorption from dilute solution, do not necessarily mean that limiting monolayer coverage has been achieved. The plateau could simply be the maximum of the surface excess isotherm.

It is essential that one component of a binary mixture is preferentially adsorbed, to give a uniform monolayer, before estimation of surface areas can be made. For this reason binary solutions of dissimilar molecules are often used. Additionally, the molecules are chosen so that the surface orientation of the preferentially adsorbed species is known, thereby minimising

the uncertainty in the occupied area. The orientation of a particular adsorbate may depend on the solvent and the nature of the adsorbent in addition to the concentration. As the adsorbates used are often larger than those commonly utilised in gas adsorption measurements the accessibility of the surface must be considered. It is also essential to ensure thermodynamic equilibrium has been obtained before making an experimental measurement. The rate of attainment of equilibrium may be slow for large molecules such as polymers. These problems are further compounded when the adsorbent is porous.

The estimation of surface areas by solution techniques is hence more susceptible to experimental contamination and error and theoretical criticism than gas adsorption methods. However, the apparatus required is often less sophisticated and easier to use since a high-vacuum system is not required. Concentration changes may be followed by optical methods[67,68,69,70]. Dye adsorption has therefore been extensively applied to the estimation of surface areas. Harkins and Jura[80] developed a method based on immersion calorimetry which has been recently modified by Partyka, Rouquerol and Rouquerol[81]. Wedler[82] has reviewed the role of calorimetry in assessing surface phenomena, but concentrated mainly on gaseous adsorption. A microcalorimetric method for estimating surface areas has been developed by Groszek[83,84,85,86].

Comparisons between surface areas obtained by gas and solution methods should take account of the different surface treatments, and therefore the different surfaces presented to the adsorbate molecules.

III-6 Surface Areas From Microcalorimetry.

Groszek[83-86] has established in a series of papers that flow microcalorimetry may be used to evaluate the specific surface areas of polar metal oxides. Other workers have confirmed the technique as reliable and capable of giving results comparable to those obtained from nitrogen adsorption measurements[87-95].

It was found that normal alcohols in normal heptane solutions adsorb preferentially, and at some critical concentrations cover the surface with a film of vertically orientated molecules. In particular, normal butanol in dilute (0.2 wt.%) normal heptane solution, when passed over a number of surfaces previously saturated with heptane adsorbs to form a close-packed physically adsorbed monolayer. The integral heat of preferential adsorption for monolayer formation $\Delta\bar{H}$, was found to be approximately constant for a number of different oxide surfaces. If the specific surface area S_w of some reference surface is known by an independent technique, then the constant E in the equation:

$$S_w = E\Delta\bar{H} \qquad \text{(III-3)}$$

may be evaluated by measuring the integral heat evolved on the formation of a butanol monolayer. Subsequently the areas of surfaces similar to the standard may be obtained by measuring the integral heat of butanol monolayer formation on them and inserting this quantity and the constant E back into equation III-3. The low concentrations used make corrections for heats of dilution insignificant, and these may be neglected.

The flow-microcalorimetric technique for estimating surface areas is quick and easy to use and obviates the necessity of measuring a complete isotherm. One practical disadvantage is

that the passage of large volumes of solvent over the adsorbent while thermal equilibrium is being established, prior to the adsorption of butanol, may poison the surface. Certain surface groups may desorb into the solvent stream or contaminants in the solvent may adsorb into the surface. Unless great care has been exercised in the preparation of the heptane trace quantities of water will almost certainly be present. Collins, McEwan and Heal[96] and Heal and McEwan[97] have shown that extreme care must be exercised in surface pretreatment as relatively small variations in the amount of preadsorbed water have a dramatic effect on the heat of adsorption. The technique does not give absolute areas, since it is necessarily dependent on the surface area of the standard. The assumption of a common constant E for a group of similar materials assumes that they are chemically equivalent per unit area of surface, and that differences between them arise only from differences in the specific surface area.

Groszek's original work[83-86] was primarily concerned with samples of low surface area ($\lesssim 20 m^2 g^{-1}$) which showed no sign of porosity. Extension of the method to include porous solids has not been discussed in the literature. In general, many of the difficulties involved would be expected to be analogous to those encountered when applying gas adsorption methods to porous solids. The stacking and orientation of molecules adsorbed within pores need not necessarily be the same as those on a plane surface. Also the heats of adsorption and desorption may be enhanced in porous materials and the rate of attainment of equilibrium decreased, compared to the non-porous materials. Micropore phenomena are likely to be especially important. The surface areas of porous materials determined by the microcalorimetric method should therefore be treated with caution, and the standard surface ideally, should be porous and have a similar pore size distribution to the unknown.

FIG. **III.1.**

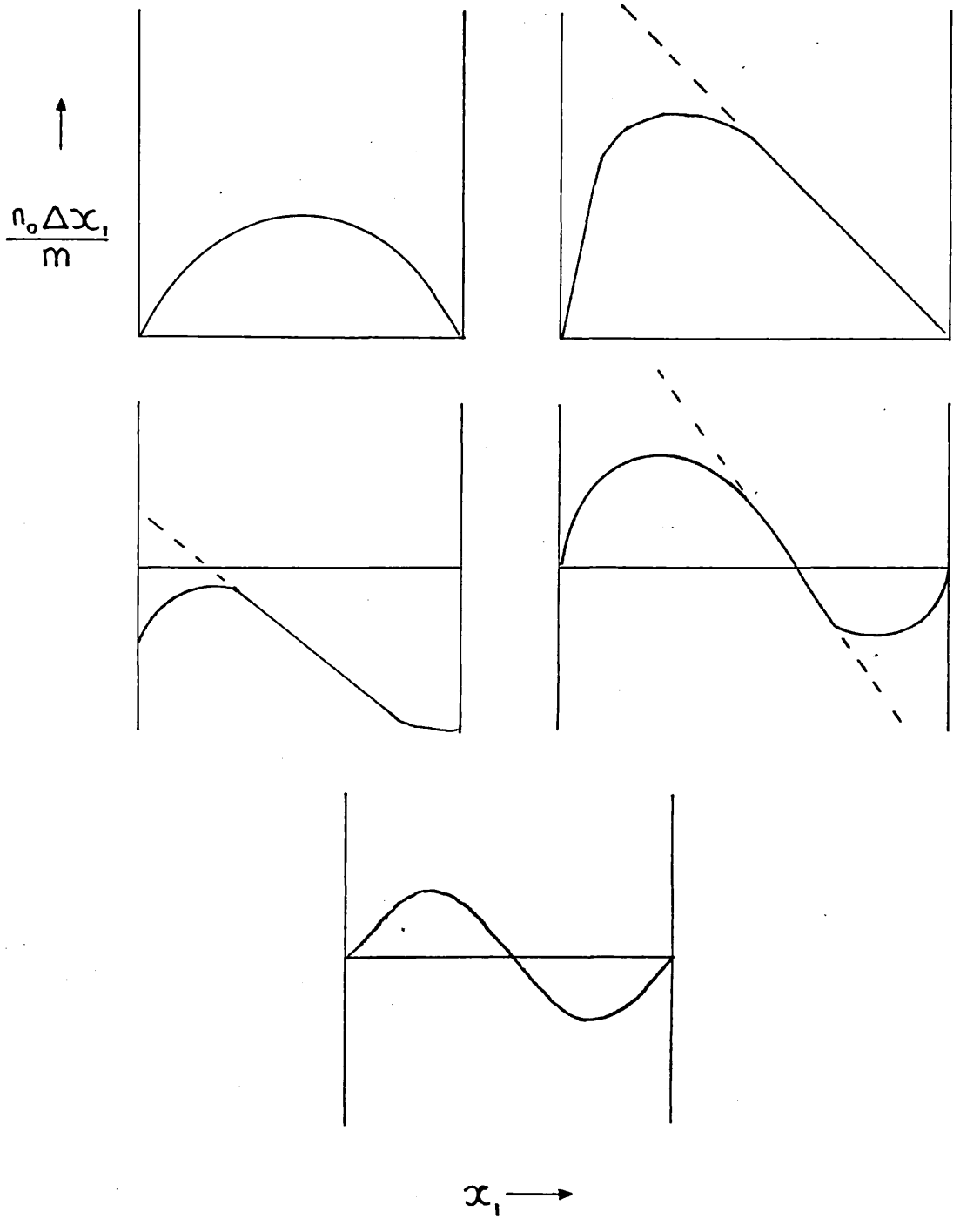

Schay's Composite Isotherms.

CHAPTER IV.

Some Aspects of Iron Oxide Surface Chemistry.

IV-1 Introduction.

The surface of pure iron is oxidised by exposure to dry air. If the resulting oxide film is in turn exposed to moisture, adsorption of water to give a hydroxylated surface occurs. Both processes are of the dissociative chemisorption type described previously. However, the corrosion of iron, and hence many common steels subjected to either atmospheric weathering or immersion in an aqueous medium is more complicated. Typically a range of oxides and oxyhydroxides, often poorly crystallised or amorphous, are formed. The exact composition of the corroded surface depends on the starting material and the weathering conditions[98,99]. X-ray diffraction studies have shown that haematite, α-Fe_2O_3 and its hydrated form, goethite, α-FeO.OH, are often major constituents of rust formed by exposure of iron to oxygen, water and atmospheric pollutants[100,101,102]. Haematite and goethite have been used as model constituents of iron rust in several studies[103,104].

There exist a number of well-known iron oxides, oxyhydroxides and hydroxides. They all tend to be non-stiochiometric[105,106]. Three iron oxides are known, with ideal compositions FeO, Fe_2O_3 and Fe_3O_4. FeO is always iron-deficient and has a rock-salt type structure. At low temperatures FeO decomposes to iron and Fe_3O_4. There are two well-known phases of Fe_2O_3, haematite

or α-Fe_2O_3 with a corrundum structure, and γ-Fe_2O_3 with a spinel like structure deficient in Fe^{III}. A β-phase of Fe_2O_3 is the subject of continuing work[107]. The γ-oxide is readily inter-convertible with Fe_3O_4 which is a mixed Fe^{II}-Fe^{III} oxide and has the inverse spinel structure. The oxygen anions form a cubic close-packed array within which the Fe^{II} ions occupy octahedral interstices and the Fe^{III} occupy both tetrahedral and octahedral interstices. Iron hydroxides, "$Fe(OH)_2$" or "$Fe(OH)_3$" are precipitated from aqueous Fe^{III} solutions and exist as gels or sols. These reogranise on heating with the loss of water to produce various oxyhydroxides of which at least 4 phases are known[105,106,108]. Goethite (α-FeO.OH) and lepidocrocite (γ-FeO.OH) occur naturally. A "δ" phase is known, and also a "β" phase has been reported which requires the presence of an anion to stabilise it. Baneyeva and Bendeliani[109] have reported a new oxyhydroxide phase, ϵ-FeO.OH, stable at high pressures.

IV-2. The Iron Oxide/Water Interface.

The chemistry of the "iron oxide-water" system is complex and the subject of continuing study. Early work by Foster[110] and Rao[111] established the presence of complicated pore structures in ferric oxide gels. The composition and ageing conditions of the gels were shown to be important in determining the surface properties. Rao and Nayer[112] measured water adsorption isotherms on ferric oxide gels. They found that application of an electric discharge to the system only had an effect when the system was in a state corresponding to some point on the desorption isotherm causing the desoprtion isotherm to move to the adsorption curve. The authors considered

their results to indicate the presence of "metastable" water adsorbed in the pores in the gel.

Recently Saraswat et al[113] have investigated ferric oxide gels produced by precipitation from ferric chloride solutions. They found that the gels consisted of protoferrihydrite which has a hexagonally close packed structure similar to that of haematite with a unit cell of approximately $Fe_5HO_8.4H_2O$. Towe and Bradley[114] and Chukhrov et al[115,116] also found certain gels consisted of protoferrihydrite. Van de Giessen[117] considered the gels as either $FeO.OHnH_2O$ or $Fe_2O_3nH_2O$. Ageing of protoferrihydrite solutions produces various intermediate, partial phases of haematite and finally haematite itself after heating above 400°C [113,114,116,117]. Mackenzie and Berggren[118] have found α-, β -, and γ-FeO.OH and α-Fe_2O_3 as primary constituents of the gels. According to Dousma, Van den Haven and de Bruyn[119], the presence of CL^- favours the formation of β-FeO.OH. Saraswat et al[113] found no evidence of any form of oxyhydroxide in their gels, nor in the compounds produced by ageing or heat treatments. Kaufman and Hazel[120] showed that the products depend critically on the concentrations of the initial solutions and on the subsequent ageing conditions. The thermal dehydration of ferric oxide gels provides a standard technique for the synthesis of α-, β -, γ- and δ- oxyhydroxides, despite the difference of opinion concerning the nature of the gel. The further dehydration of these yield information concerning the surface structure of both the oxyhydroxides and the final product which is always haematite provided the temperature is

high enough. Butler and Isen[108] discuss the thermal transformation:

$$FeO.OH \xrightarrow{\Delta} \alpha\text{-}Fe_2O_3$$

and note that the dry heating in air always gives haematite irrespective of the starting phase. When heated in water, the decomposition of all phases to haematite proceeds via geothite as an intermediate and is complete at a much lower temperature than the dry decomposition. Wefers[121,122] found that γ-FeO.OH.(aq) was unstable with respect to α-FeO.OH(aq) at temperatures above 25 °C, and noted discrepancies in the literature for the temperature at which the transformation is complete. Tanaka[123] followed the decomposition of ferric oxide gels by differential thermal analysis. An endothermic change prior to the exothermic decomposition of the gel to haematite was attributed to the loss of adsorbed water. Ishikawa and Inouye[124] observed differences between the β- and the α- and γ-oxyhydroxides during the thermal decomposition to haematite. For all phases, as the temperature of outgassing was increased, and hence the propertion of haematite present increased, so the monolayer capacity for water adsorption and the heat of immersion in water decreased until the conversion to haematite was complete. The heat of immersion then increased with further outgassing. β-FeO.OH showed much higher values than the other phases, and this was attributed to the presence of small pores able to lose water, thereby increasing the surface area available.for reaction. Using electron microscopy, gas adsorption and X-ray diffraction techniques, Gallagher[125] confirmed earlier work and found small pores with a mean diameter of 28.4 Å in his sample of β-FeO.OH. The subcrystal structure consisted of tubes externally square with a circular channel running the length of the subcrystal. These channels are different from the smaller tunnels inherent in the hollandite structure of β - FeO.OH which contain Cl^- ions after precipitation from ferric chloride solutions. In the unwashed state the formula

which is approximately $FeO_{1-\frac{1}{4}}(OH)_{1+\frac{1}{4}} \cdot \frac{1}{4}Cl$, which, on extreme washing with water, becomes $FeO.OH.\frac{1}{4}(H_2O)$. Drying yields FeO.OH. Naono and Fujiwara[126] have observed micropore formation in the thermal decomposition of acicular micro-crystals of goethite to haematitie. This transformation corresponds to the topotactic reaction.[127]

$$\alpha\text{-FeO.OH}\ (100)\ [001] \longrightarrow \alpha Fe_2O_3\ (000\bar{1})\ [10\bar{1}0]$$

An increase in the BET nitrogen surface area was found for outgassing temperatures up to 300 °C. More vigorous outgassing caused the area to decrease. The loss of water from α-FeO.OH up to 100 °C was associated with loss of adsorbed material. Between 200-300 °C a rapid weight loss was found as the decomposition to α-Fe_2O_3 occurred. These results were explained in terms of the initial formation of micropores and their subsequent destruction, as macropores formed at higher temperatures.

Bylholder and Richardson[128] in an infra-red study of haematite found that water chemisorbs on a sample dehydroxylated by outgassing at high temperatures. They postulated that chemisorption involves the dissociation of water to form OH^-, which adsorbs onto a surface Fe^{III} ion, and H^+ which reacts with a surface O^{2-} to form another hydroxyl group. On this layer of hydroxyls, water, retaining the H-O-H configuration, can physically adsorb. The physically adsorbed water was easily removed by evacuation at 25 °C. The labelling experiment of Berube, Onoda and de Bruyn[129] supported the observations of Blyholder. Haematite was labelled by storage under tritiated water for over a month and then subjected to Blyholder's outgassing regime. The tritiated surface was then allowed to exchange with tritium free water. The measured exchange agreed with the amount expected if all the physically adsorbed water

was removed by evacuation at 25 °C, and the surface was populated by chemisorbed OT groups. The water adsorption studies of Asher, Goodman and Gregg[130] on various dehydroxylated haematite samples showed that hydroxylation is a reversible process. Outgassing at 800 °C was found to completely dehydroxylate the surface. Zettlemoyer and McCafferty[103] used heat of immersion studies of haematite in water to confirm the reversibility of the hydration process. They gave further support to the view that room temperature outgassing is sufficient to remove all physically adsorbed water. Morimoto, Nagao and Tokuda[131,132] used water adsorption studies to further support these ideas, and advanced a tentative adsorption mechanism supporting that of Blyholder and Richardson.[128]

McCafferty and Zettlemoyer, in a series of papers, used dielectric methods[133,134] and adsorption thermodynamics[135] to show that the first physically bound water layer on haematite is immobile, each water molecule being doubly hydrogen bonded to the underlying hydroxyls. Succeeding layers are mobile, the molecules bound together by single hydrogen bonds. The hydrogen bonded matrix above the first layer was shown to have an ice-like structure for the next few layers, gradually becoming more liquid like as the distance from the surface increased. These ideas clarified the earlier suggestions of Healey, Chessick and Fraioli[136], and were further consolidated by McCafferty and Zettlemoyer[137] when these authors presented their unified view of the water-haematite interface. The situation is illustrated in Figure IV-1.

The number of hydroxyl groups per unit area has been evaluated for haematite and lies between 5-10 OH/100$\AA^2$ [132,137,138] Boehm[139] has shown that the hydroxyls on metal oxides may be amphoteric

in character. Zettlemoyer and McCafferty[140] discussed the properties of water adsorbed on oxide surfaces and classified the hydroxyls on haematite as "soft" because they are easily removed and regained compared to the "hard" hydroxyls on silica. They also discuss one of the major concerns of powder surface chemistry, that of lack of reproducibility. They stressed the difficulty of ensuring that a particular powder sample is representative of the bulk powder. The dependence of a particular observation on the heterogeneity, degree of surface crystallinity, porosity, particle size, purity and past history of a sample, was noted.

The early infra-red studies of adsorbed water on iron oxides[128,131,141] were extended by Rochester and Topham in detailed investigations of the surface hydroxyls on haematite[142] and goethite[143]. Eleven absorption bands in the infra-red spectra of haematite discs were assigned to the OH-stretching vibrations of surface hydroxyl groups. The relative intensities of these maxima depended on the composition of the gel from which the sample was prepared. Physically adsorbed water was desorbed from the surface of haematite by evacuation at ambient temperatures, a result consistent with general opinion. However, it was found that high temperature treatment of haematite in vacuum caused progressive dehydroxylation and decomposition to magnetite, thereby casting doubt on the interpretation of some earlier work[128,144]. Heat treatment in oxygen had two effects. Surface dehydroxylation occurred and was found to be reversible by chemisorption at room temperature. Extensive heating caused irreversible sintering, and thus a decrease in the number of hydroxyls per unit weight. Variations in the relative proportions of different types of hydroxyls were observed at

high temperatures. Some of the different types of hydroxyls, as identified by their positions on the various crystallographic faces were discussed in relation to the measured spectra.

Morimoto, Yokota and Nagao[145] adsorbed water on dehydroxylated haematite and magnetite. They then removed the phsycially bound water and readsorbed more water onto the hydroxylated surfaces. Differences between the two isotherms were attributed to differences in the initial state of hydroxylation. However, the initial rate of chemisorption was very slow and this hindered the interpretation, as the isotherms tended to diverge at high relative pressures. A slow rate of rehydroxylation has also been observed for the immersion of dehydroxylated alumina in water [146]. At ambient temperatures the evolution of heat continued for several hours. The total heat effect was resolved into a large immediate heat change and a much smaller change with a half life of 51 min. It was also shown[145] that the isotherms for the hydroxylated surfaces of different iron oxides were similar from which it was concluded that the surface characteristics of a compound are largely determined by the hydroxyl covering. The importance of hydroxyl coverage in determining the surface properties of metal oxides has been recorded for many systems[147,148,149].

Partyka, Rouquerol and Rouquerol[81] measured the heat of immersion of a number of metal oxide powders in water and found that between one and two physically adsorbed water layers were sufficient to "screen" the oxide surface from the adsorbate. These results disagreed from the earlier work of Harkins and Jura[80] who found that up to five layers

of water were required to "screen" the surface. However, these authors used severe outgassing conditions likely to create a reactive polar surface. Partyka and co-workers also suggested that the analysis of Harkins and Jura was defective concerning the assumption that the numbers of molecules in each layer is the same.

Jurinak[150] compared the water adsorption properties of haematite and goethite, and found that the goethite-water system was more complicated. The surface acidity of goethite was shown to be greater than that of haematite, and attributed to the proton in the α-FeO.OH structure. Rossi[151] found the heat of immersion of goethite to be about 15% higher than that of haematite. The results of Gast, Landa and Meyer[152] in their comparison of the adsorption of water on geothite and amorphous hydrated ferric oxide further illustrate the differences between the surfaces of haematite and goethite. Like haematite, the amorphous material lost its physically adsorbed water by outgassing at 25°C. Goethite under the same conditions retained about a monolayer which exchanged with D_2O. Integral entropies of water adsorption were calculated and compared with the data of McCafferty and Zettlemoyer[135]. These showed that the first physically adsorbed layer on the amorphous material and the second on goethite were immobile, suggesting strong hydrogen bonding in the latter surface.

Gast[152] and co-workers observed a tenfold reduction in surface area as their amorphous material crystallised to goethite. The dependence of surface area on outgassing temperature is well known[28]. Hagane[153] and Kusano, Nelander

and Wädso[154] have investigated this effect in relation to iron oxides. Kusano and co-workers showed that for haematite there was no simple relation between the decrease in both surface area and heat of immersion of water as the outgassing temperature was increased above 300°C. The variation of surface properties with temperature is complicated by the fact that heat treatment can alter a surface irreversibly. The state of the surface must be known throughout the temperature range of an experiment before the results can be properly interpreted, as pointed out by Rochester et al[142].

The existence of Lewis Acid sites on the surface of goethite has been shown[155] and of at least two types of surface hydroxyl[155,156]. Russell, Parfitt, Fraser and Farmer[156], considered the [100] face of goethite crystals to be predominant and assigned infra-red absorption bands entirely in terms of this face, considered to contain three physically different hydroxyl groups. However, Rochester and Topham[143], in an infra-red study of the systems D_2O / α -FeO.OH and H_2O / α -FeO.OD, pointed out that the [100] face is incompletely represented by only three physically different hydroxyl sites. A total of five surface sites, either occupied by OH^- or O_2^- or unoccupied and considered as anion vacancies, were used to interpret the data. Two different model surfaces were found to fit the data equally well. It was also suggested that the exposed face with the highest surface area need not necessarily be the primary factor in determining the infra-red spectra. The [010] face with three surface sites, each occupied by hydroxyl groups, was also found to explain the spectra. A full analysis of all possible faces and distributions of surface sites on the faces was not attempted. Paterson and Swaffield[157] found

evidence from D.S.C. thermograms of hydroxylated goethite of three types of hydroxyl.

IV-3 Adsorption on Iron Oxide Surfaces.

Most studies of the adsorption of organic molecules on iron odixe surfaces involve preferential adsorption. The species of interest is introduced to the surface in solution so that at least two different molecules compete for adsorption sites. The exceptions involve studies of the adsorption of vapours.

The adsorption of alcohols and mono carboxylic acids in dilute heptane solutions on iron oxides has been extensively studied by microcalorimetry. Groszeck[83-86], in a series of papers, adsorbed n-alcohols on metal oxides, and showed that the adsorption was often physical in nature, and therefore easily reversible. A method of estimating surface areas by butanol adsorption was discussed, and found to give results comparable to those of gas adsorption techniques. A 0.2%, by weight, butanol solution was found to form a close packed monolayer on the surface. Long chain n-alcohols and carboxylic acids formed films, not necessarily close packed, composed of vertically orientated molecules on several iron oxides. The orientation was found to be dependent on concentration, solvent and the nature of the substrate. The stability of the films as estimated by integral heats of preferential adsorption was greater for γ-Fe_2O_3 than for α-Fe_2O_3 and Fe_3O_4. Ground iron behaved differently to the oxide surfaces, indicating the importance of surface pretreatment. It was tentatively suggested that under certain conditions carboxylic acids might displace adsorbed water. Templer[87,88] further stressed the importance of surface pretreatment

and the possibilities of poisoning the surface in flow microcalorimetric experiments on polar oxides.

Allen and Patel[89,90,91], also using microcalorimetry, suggested that the oreintation of long chain fatty acid molecules is different from that of long chain alcohols on haematite. A carboxylic acid group was thought to rest on a hydroxylated surface with the first six methylene group forming a loop above the surface. A seventh methylene group then rested on the surface with subsequent groups lying above the surface extending into the liquid. The hydroxyl group of an alcohol also lies on the surface. However, the carbon chain forms a spiral above the surface, each revolution containing six methylene units. Carboxylic acids have also been shown to be in part irreversibly adsorbed[91,97]. Husbands et al[158] have shown that the adsorption of stearic acid on ferric oxide heated to 140 °C for several hours prior to the experiment, is more complicated than the adsorption of butanol. The acid was in part irreversibly adsorbed. It was found that stearic acid displaced preadsorbed water which the solvent, normal heptane, did not. This effect was not observed for butanol, the adsorption of which was exactly reversible. Heal and McEwan[97] and Jaycock[159] also found evidence for the slow desorption of preadsorbed water in the presence of carboxylic acids. Heal and McEwan[97], however, also observed this effect, characterised by a slow endotherm immediately after the initial exotherm, for the adsorption of butanol on haematite. A similar effect has been observed in this laboratory[160]. Husbands and coworkers[158] and Jaycock[92] find no evidence of slow water desorption, initiated by the adsorption of butanol. The generally agreed

lack of reversibility in the adsorption of carboxylic acids may be due to chemisorption or may only be an apparent effect if the desorption is so slow that it is never completely observed.

Rahman[94] and Rahman and Gosh[93] have discussed the adsorption of stearic acid on powder oxides, and again found some irreversibility. They tentatively suggested that the area occupied per molecule is different on porous and non-porous solids. Using microcalorimetry, it was found that the molecules lie neither parallel to a ferric oxide surface nor perpendicular to it.

Collins, McEwan and Heal[96] found that the adsorption of butanol on their rust samples was very sensitive to the preadsorbed water coverage. Heal and McEwan[97] studied the effect of water in the solvent, and preadsorbed on various iron oxides in their microcalorimetry work. Heats of adsorption were again found to be sensitive to the amount of preadsorbed water present. Haematite and goethite behaved similarly to butanol adsorption and its variations with water precoverage. Generally, an increasing surface water content is associated with a decreasing heat of adsorption of butanol. The converse was also true.

It is well known that the corrosion of iron is retarded by rust inhibitors containing carboxylic acid groups in conjunction with alcohol, carbonyl or olefin double bonds[161]. It has also been established that dicarboxylic acids are better rust inhibitors than monocarboxylic acids[162,163]. This suggests that multiple functional group species are more strongly adsorbed than mono functional species. Hingston, Posner and Quirk[164] have discussed the adsorption of mono and bidentate species. They found that those species such as phosphate capable

of forming two bonds with the surface in a bridged complex were more likely to be irreversibly adsorbed than mono dentate such as F^- or OH^-. Kavangh, Posner and Quirk[165] have shown that increasing substitution of chlorine in the phenyl ring of phenoxyacetic acids increases the amount adsorbed on goethite. The adsorption is, however, reversible[166].

Raghavan and Fuerstenau[167] found that aqueous octlyhydroxamic acid (R-CO-NH.OH) adsorbs to form a hydroxamate complex on ferric oxide.

Pope, Matijevic and Patel[168] adsorbed aqueous carboxylic acid derivatives of pyridine on haematite. Minor structural changes in both the adsorbent and adsorbate were observed to have major effects in determining the amount adsorbed.

Lucas, Vandervell and Waugh[169] have adsorbed maleic anhydride on a mixed oxide (V_2O_5 - MoO_3) catalyst. The adsorption mechanism was shown to be complex. An activation energy was involved, and the adsorbed species was very strongly bound to the surface.

Parfitt and co-workers[170,171,172], in a series of papers, found that dicarboxylic acids tend to be irreversibly adsorbed on iron oxides. The adsorption of aqueous carboxylic acids involved the formation of adsorbed carboxylate groups. Oxalic acid and benzoic acid adsorbed as the oxalate and benzoate ions on geothite. Benzoate was weakly bound whereas oxalate, which can theoretically bind in a bidentate structure, was strongly adsorbed. The mechanism of adsorption was shown to involve singly coordinated surface hydroxyl groups[172]. Surface hydroxyls shared between two or three

cations were thought to be relatively inert. However, in situ techniques were not used. The adsorbent was separated from the adsorbate liquid and then examined by infra-red spectroscopy. Rochester and Topham investigated the adsorption of organic vapours on haematite[173] and goethite[174] by in situ infra-red techniques. The two surfaces were found to be similar, although subtle differences were observed. Pyridine adsorbed weakly on both surfaces. Acetic acid adsorbed chemically and physically on both surfaces. Carbondioxide, however, chemisorbed on goethite, whereas it was only weakly adsorbed on haematite. The reactivities of the various surface hydroxyl groups were distinguished and found to be dependent on the method of preparation of the sample.

Buckland, Rochester and Topham[104] studied the adsorption of carboxylic acids on haematite and goethite in situ at the solid/liquid interface by a novel infra-red technique. Carbon tetrachloride solutions were used. Chemical and physical adsorption was observed to occur on both surfaces. Chemisorption predominated and that led to adsorbed carboxylate species in a chelating bidentate configuration:

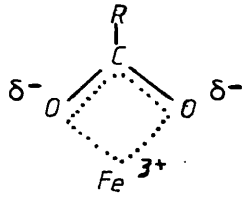

The ratio of carboxylic acid to carboxylate groups was greater for geothite than for haematite. Jurinak has shown the surface of goethite to be more acidic than that of haematite.[150]

FIG. IV-1

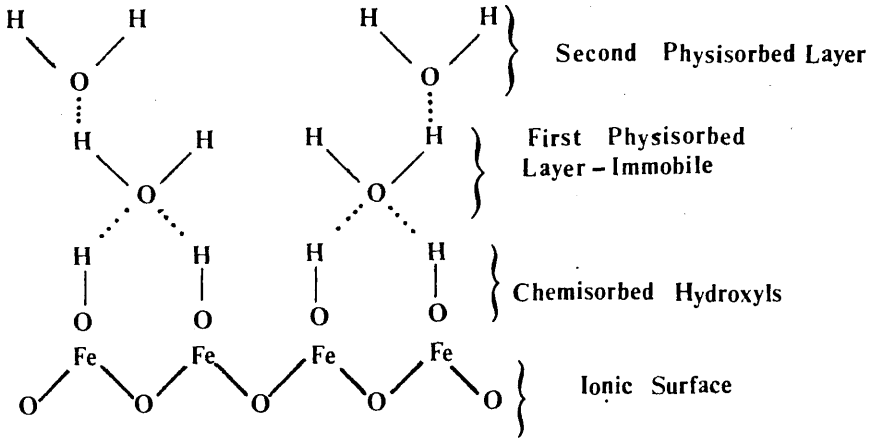

The Water Haematite Interface.

CHAPTER V.

Experimental.

V-1. Gas Adsorption Apparatus.

V-1-1 Introduction.

The determination of adsorption-desorption isotherms by nitrogen gas adsorptions is a well-established technique. Many types of apparatus have been described[56,175,176]. For this work a conventional volumetric apparatus, originally described by Emmett[177], but incorporating minor modifications, was used.

Figure V-1 shows the adsorption apparatus. The adsorption bulb A, gas burette B, manometer C, and mercury reservoirs D, were blown in pyrex glass. They were connected by short lengths of 2mm bore capillary tubing to minimise the internal volume while retaining reasonable pumping speeds. The adsorption bulb was connected to the system by a ball and socket joint E employing a Viton 'O' ring (J. Young Scientific Glassware Ltd., U.K.). The configuration of the taps F,G,H,I,J and K enabled the adsorption bulb to be pumped independently of the burette and manometer, thus reducing the risk of entrained powder being deposited in these components. The taps F,G,H,I and J were of the grease-free 'Rotaflo' type (Corning Ltd., U.K.) and H,I and J were connected via wide bore (ca. 10mm) tubing to the rest of the vacuum system. The gas storage system had an outlet between taps H and I. Tap K, a 3mm bore greased tap, was introduced to enable fine powders to be gradually pumped down without entrainment, using a static vacuum by successively reducing the pressure between K and F with F closed, then closing K and slowly opening F.

Rough vacuum and pressure for both the manometer and burette were provided by a Boreas oil-less pump (Brook Compton Parkinson Motors, U.K.). Control was through a needle valve L, taps M and N (Matheson. Co. Inc., U.S.A.), and Hoffmann clips O and O′, on a length of semi-pressure tubing which could be connected to either the positive or negative outlets of the pump, which was provided with a pressure release valve. Greased 8mm bore taps P and Q separated the burette and manometer respectively from each of their mercury reservoirs.

The entire adsorption apparatus was secured to a wall and the components enclosed within the dotted line in Figure V-1 were enclosed in a large thermostatted box.

Provision was made for the adsorption bulb to be either heated, or thermostatted in a liquid nitrogen bath. The temperature of the bath was measured by an oxygen vapour pressure thermometer R and the liquid nitrogen level was maintained by an automatic topping-up device, S being the sensor and T the pump outlet.

Prior to its introduction into the system the mercury was washed in dilute nitric acid and then in distilled water. It was then double-distilled under a reduced nitrogen atmosphere before loading.

The complete vacuum system is shown in Figure V-2. Two mercury diffusion pumps (Jencons Scientific Ltd.) P, P′ backed by a single rotary pump (Edwards High Vacuum Ltd.) evacuated the system. Pressure was measured by a Pirani (Edwards High Vacuum Ltd.) gauge between pump P and the gas storage system, and by a Penning (Edwards High Vacuum Ltd.)

ionisation gauge situated close to pump P'. Pump P'' was situated as close as possible to the adsorption system to decrease both ultimate pressure and its rate of attainment. Liquid nitrogen traps were positioned on the high vacuum side of each pump. Taps were situated such that each component of the system could be evacuated by either diffusion pump. Pressures of the order of 10^{-6}mmHg were regularly recorded.

The volume of the burette was determined by mercury filling and weighing before the apparatus was assembled. The free space volume, the volume between the reference position in the manometer, the top bulb of the burette and the closed taps G and H (Figure V-1), was calibrated with helium, as will be described later. Before each experiment, the dead space, the volume above the sample in the adsorption bulb up to the closed taps F and G, was also determined by a helium calibration. To measure adsorption on a suitably treated sample, gas was admitted to the burette via tap H with tap G closed. As the volume of the system was known, a measurement of the pressure and temperature allowed the number of moles admitted to be calculated by use of the ideal gas equation. Tap G was opened, and the bulb immersed in liquid nitrogen causing adsorption to occur. The pressure and temperatures were remeasured. The number of moles adsorbed could then be calculated, being directly proportional to the pressure difference. By raising the mercury in the burette further adsorption points were obtained. Additional aliquots of adsorbate could be introduced to the system by closing tap G, remeasuring

the temperature and pressure, and then admitting further gas via tap H and proceeding as above.

V-1-2 The Gas Burette

The gas burette was kindly provided by Prof. T. Edmonds of British Petroleum Ltd. It consisted of six bulbs with a total volume of about 123cm^3, joined by short lengths of 2mm bore capillary tubing on which were etched the reference marks. The bulbs were contained in an outer glass jacket. The mercury height was controlled by use of the tap P at the bottom of the burette in conjunction with the rough vacuum-pressure line.

The volumes of the bulbs were determined prior to assembly of the apparatus. First, the internal surfaces were washed with aqua regia, followed by copious quantities of distilled water and allowed to dry in a stream of nitrogen. Water, thermostatted at about 27 °C, was passed through the jacket. The mercury was raised to the top reference mark and allowed to equilibrate for one hour before drainage between successive reference levels into weighing bottles. The mean temperature was recorded for the emptying of each bulb. From the weight and density of mercury at the measured temperature the volume was calculated. The volumes are given in Table V-1. The figures in the last column are the cumulative volumes used in the calculations. Corresponding calibration volumes supplied by B.P. Ltd at 22.2 °C are also given for comparison.

V-1-3 The Manometer.

The manometer arms were made of precision bore

glass tubing (Jencons Scientific Ltd.) with an internal diameter of 15.00 ± 0.01mm, chosen for its straightness, uniformity of bore and freedom from optical imperfections. The diameter represents a compromise between the capillary depression which decreases with increasing diameter and the meniscus covolume which increases with increasing diameter.

The short arm was 18cm long. Two platinium electrodes U and V in Figure V-1, connected to an external circuit (Figure V-3) enabled the mercury to be raised to a constant height. Both electrodes were inserted through side arms, each filled with mercury. This arrangement was adopted as the only means of ensuring a leak free metal-glass joint. The upper electrode was inserted at the junction of the capillary and manometer tubing to minimise the volume above the intended mercury meniscus position. Electrical contact was indicated by a pilot light and an audible signal. When measuring the free space volume (see later) the short arm could be set to better than ± 0.002cm.

The manometer was 1m in length, and the whole was set vertical in the thermostated box. The mercury was controlled by a similar system to that of the burette. A 2mm constriction in the tube above Q (see Figure V-1) provided additional control when levelling the mercury.

V-1-4 Pressure Measurement.

To measure the elevation of the crown of a mercury meniscus, light that behaves as parallel light with respect to vertical displacement and variation in zenith angle, and as diffuse light with respect to lateral displacement and variation in azithmuthal angle, must be directed from behind the manometer into the cathetometer's telescope[178].

To achieve this, each arm of the manometer was illum-

-inated by a lighting unit consisting of a 2W bulb, in the focal plane of a plano convex cylindrical lens. The width of the beams were reduced by slits. The unit for the short arm was fixed behind the top of the short arm pointing directly into the telescope. The lighting unit for the long arm was attached to a plate which could be moved up and down on an aluminium bar placed behind the long arm, via a length of cord (Figure V-4).

Frontal illumination was used to measure the elevation of the bottom of the meniscus in each arm. A small battery driven lamp attached to the cathetometer was used for this purpose.

A cathetometer (Precision Tool Instrument Co. Ltd), with a brass bar calibrated at 20 °C was used to measure the mercury heights. A vernier enabled the heights to be recorded to 0.001cm. Under optimum conditions, the makers stated that the error in a single height measurement should not exceed 0.004cm. The cathetometer was mounted on a pillar made up of breeze blocks, itself supported on several alternate layers of cork and lead sheet. The telescope was equidistant from the manometer tubes, 60cm away.

The perspex front of the thermostatted box did not cause any significant optical distortion. The heights of certain fixed points were measured with and without the perspex in place, and no difference was noticed.

It was found that the heights of a column of mercury could be recorded to better than 0.002cm during the free space calibration.

V-1-5 The Thermostat.

That part of the apparatus within the dotted line in Figure V-1 was thermostatted in an air bath at 27 °C. The interior laboratory wall, to which the entire apparatus was

secured, formed the back of a box the sides of which were hardboard secured to a wooden frame. The front consisted of two large detachable pieces of 1/8" thick perspex. Two small doors were cut into one of these through which the apparatus could be manipulated. The lid, also removable, was made out of hardboard. Wherever possible, large sheets of polystyrene were glued to the hardboard to provide thermal insulation. The box measured approximately 70 x 70 x 225cm.

Temperature control was provided by a mercury contact thermometer (Electric Thermometer Co. Ltd., U.K.) A, see Figure V-5., and a Sunvic control unit B, operating two heaters. These consisted of blackened 60W and 200W light bulbs C and D respectively. The air was circulated by a 6" diameter mains driven, five bladed fan E, taken from an old refrigeration unit. The fan was placed high in the box behind the manometer. The light bulbs were also positioned above and behind the adsorption apparatus. The thermometers F,G and H were in the same vertical plane as the main adsorption components.

Temperature gradients of less than 0.3 °C and 0.4 °C existed across the width (at half height) and the height of the box respectively. The temperatures were measured by mercury in glass thermometers calibrated against a National Physical Laboratory standardised thermometer. Thermometer F was graduated in 0.02 °C divisions, and thermometers G and H were graduated every 0.1 °C. The temperature of the box could be held at 27 °C over a wide range of room temperatures. The short term cyclical temperature variations caused by the switching of the control system were dependent on room temperature and on whether

the adsorption bulb was being thermostatted in liquid nitrogen. Temperature fluctuations were always much less than 0.4 °C, and usually less than 0.2 °C even for thermometer F. Thermometer H often only altered by 0.05 °C during a temperature cycle. The range of the thermometer was noted during a temperature cycle. The mean (corrected) temperatures T(F), T(G) and T(H) of a cycle were used in the following manner to average out minor temperature gradients:

1) Temperature of burette (T(GB)) = $\frac{1}{2}\left[T(F) + T(G)\right]$ V-1.

2) Temperature of manometer (T(M)) = T(H) V-2.

3) Temperature of free space (T(FS)),

$$T(FS) = \frac{1}{2}\left[T(GB) + T(M)\right] \qquad V\text{-}3.$$

Providing the ambient temperature was greater than 20 °c, leaving the front doors open for periods up to five minutes did not cause significant temperature variations in the box.

The adsorption bulb (C in Figure V-6) was immersed in a narrow necked Dewar filled with liquid nitrogen so that the sample was at least 5cm below the surface[28]. Maintenance of temperature stability in the air bath required that the liquid level be kept about 3cm below the top of the Dewar, see Figure V-6. To reduce evaporation, the top of the Dewar was covered with Kao wool (Morganite Ceramic Fibres Ltd.) A. The temperature was determined by an oxygen vapour pressure thermometer B situated next to the bulb C. A thermistor D, detected when the liquid level dropped and caused a heater E, a short length of resistance wire, to switch on in a partially sealed reservoir of liquid nitrogen outside the air bath. Liquid nitrogen was then forced under slight pressure along a short well-lagged

glass tube F, into the coolant bath. The reservoir consisted of a litre Dewar sealed inside an aluminium cylinder H. The lid was permanently fixed to the side of the air bath. Two steel rods, I and J, bolted to the lid and threaded at the lower end, enabled a metal bar, K, to be screwed tightly to the base of the container. Thus the Dewar, G, could be removed to be refilled. Two screws, L and M, in the lid acted as control valves which could be adjusted easily.

The control circuit diagram for this device is shown in Figure V-7.

V-1-6 The Adsorption Bulbs, Gas Storage System, Outgassing Unit and Vapour Pressure Thermometer.

The adsorption bulbs were blown from 2mm capillary tubing and joined to the adsorption system by a 2mm ball and socket joint, used to give some mechanical flexibility. The bulbs were individually blown to suit the requirements of a particular sample. Figure V-8 shows a typical bulb. The volume was minimised, and the stem was about 10cm long. Sample sufficient to give a total area of about $50m^2$ was used . To stop powder entrainment during evacuation and outgassing, it was found necessary to fill the bulbs to no more than half full for the iron oxide experiments.

The gas storage system shown in Figure V-9 consisted of a $3dm^3$ bulb for nitrogen and a $2dm^3$ bulb for helium, and a simple manometer. The system was pumped down for at least 24 hours to an ultimate vacuum of less than 10^{-4}mmHg prior to filling the storage bulbs. The appropriate gas was passed down a length of PVC tubing through a greased three-way tap and then into an oil

bubbler. When the PVC tube was thought to be effectively flushed, after about an hour, the flow rate was reduced and gas slowly admitted to the evacuated system.

The outgassing unit consisted of two hemicylindrical 200W heaters (type 50201, Lindberg heating unit, A.R. Horwell Ltd.) supported on a ceramic block as in Figure V-10. Power was supplied by a Variac transformer and the unit was lagged with Kao wool. A mercury-in-glass thermometer was attached close to the adsorption bulb which was centrally positioned inside the heating unit. The open top was also lagged with Kao wool.

The vapour pressure thermometer (*S* in Figure V-1) was a simple mercury manometer consisting of a 'U'-tube mounted in front of a metre metal rule. Both arms had an internal diameter of 5mm. One arm was connected to the pumping system and the other was filled with oxygen. The sealed end of the oxygen arm was situated close to the bottom of the adsorption bulb. Oxygen was supplied through a Rotoflo tap. The arm was filled and then evacuated with oxygen several times before the final loading. The rule was read to the nearest 0.25mm using a hand lens.

V-2. Gas Adsorption Procedure.

V-2-1 Free Space Calibration.

After ensuring that the apparatus was vacuum-tight the free space volume had to be determined using helium.

The system was pumped down for 24 hours to an ultimate vacuum of at least 5×10^{-5} mmHg., and 12 hrs. prior to the run the thermostatting system was switched on. During pumping mercury was accurately set at a reference mark in the burette and

approximately set in the short arm of the manometer. Tap G (Figure V-1) was shut and then helium was admitted to the free space volume through tap H which was then closed. A pressure of about 10cm of gas was added. After the manometer was finely adjusted five minutes were allowed to elapse after closing the doors to the air bath before the various readings were made:

1) The room temperature was measured to the nearest 0.5°C using a mercury-in-glass thermometer attached to the cathetometer.

2) The illuminating system was switched on and the cathetometer was set to the top of the meniscus in the short arm. After levelling, the cross-wires of the telescope were set to the crown of the meniscus and the reading noted. The cross-wires were then readjusted and the height noted again. Readings were continued until a height consistent to ± 0.002cm was obtained.

3) The telescope was relevelled at the bottom of the meniscus in the short arm and readings taken until a consistent height was obtained.

4) The telescope was set to the top of the meniscus in the long arm and the illuminating unit adjusted so that the light just passed over the crown. The height was then recorded as in (2).

5) Reading (3) was repeated for the long arm.

6) Readings (2) to (5) were repeated in the reverse order. This process was continued until consistent heights were obtained.

7) Immediately after the final height measurement was recorded the temperatures of the three thermometers in the air bath were noted for a temperature cycle. Finally the room

temperature was noted again.

The mercury was then set to the next reference level in the gas burette, the manometer readjusted and readings (1) to (7) repeated. The means of the recorded heights were used in the calculations.

V-2-2 Treatment of Results.

The difference in height (h) between the mercury crowns in the long and short arms of the manometer is related to the uncorrected pressure (P) by the equation:

$$P = h.\rho.g \qquad \text{V-4.}$$

where ρ is the density of mercury at the temperature of the manometer and g is the local accleration due to gravity [179]. To reduce the pressure to standard conditions four corrections were made, a scale correction and three mercury corrections.

The height h was recorded at some mean temperature T(R)/°C. However, the scale of the brass bar of the cathetometer was calibrated at 20°C.; this temperature difference was corrected as follows:

$$h' = h\left[1 + \alpha(T(R) - 20)\right] \qquad \text{V-5.}$$

where h' is the corrected height and α the mean foefficient of linear expansion of brass from 20°C to T(R)°C ($\alpha = 18.4 \times 10^{-6}\,°C^{-1}$) [180].

The corrected pressure P(c) (cm of mercury) is then given by:

$$P(c) = (h' + \delta_l - \delta_s)\left[\frac{1}{1 + \alpha_{Hg}T_{Hg}}\right]\frac{g_l}{g_s} \qquad \text{V-6.}$$

where δ_l and δ_s are the capillary depressions in the long and short arms of the manometer respectively; T(Hg), the temperature of the mercury, α_{Hg} , the mean coefficient of the cubical expansion of mercury from 0°C to T(Hg)/ °C (181.8×10^{-6} $^{o}C^{-1}$)[180]; g_l and g_s , the local and standard acceleration due to gravity respectively ($g_s = 980.665 cms^{-2}$). Corrections for the compressibility and vapour pressure of mercury were neglected[179].

The capillary depression was read from the tables of Blaisdell[181]. These tables give the parameter H_o , the reduced capillary depression, in terms of the reduced manometer radius X, and the reduced meniscus height Y. Thus,

$$H_o = \frac{h_o}{a} \; ; \; X = \frac{x}{a} \; ; \; Y = \frac{y}{a} \qquad V\text{-}7.$$

where h_o is the true capillary depression, x and y are the radius of the manometer and meniscus height respectively, and a is the capillary constant. This constant is given by the formula:

$$a = \left[\frac{2\gamma}{(\rho Hg - \rho_{air}) g_l} \right]^{\frac{1}{2}} \qquad V\text{-}8.$$

in which γ is the surface tension of Hg , ρ_{Hg} and ρ_{air} the densities of mercury and air and g_l the local acceleration due to gravity. From the densities at 27 °C, the surface tension of a mercury-vacuum interface at 25 °C and the local gravity,[180] 'a' was found to be 0.262cm.

The local gravity which varies with latitude and elevation, was found from tables[180] to be 981.15 cm^{2}

V-2-3 A Consideration of Possible Corrections.

The meniscus covolume in the short arm of the

manometer varies with the meniscus height. Therefore, for accurate work, a correction for the excess meniscus covolume relative to a standard height should be applied. Kistemaker[182] gives the meniscus volume as a function of manometer radius and meniscus height. It was found, by application of these tables to typical experimental data, that the covolume correction was insignificant. It was therefore not applied.

Helium at 300K and nitrogen at 300K and 77K were both assumed to be ideal[42]. The volume (V) of nitrogen held at liquid nitrogen temperatures was never more than $5cm^3$, and often half this value. Using the equation of Emmett and Brunauer[183] to correct for the nonideality of nitrogen, the corrected volume V' is given by:

$$V' = V\left(1 + \frac{\alpha P}{760}\right) \qquad \text{V-9.}$$

where α is 6.6×10^{-5}, and the pressure P is in mmHg. With V equal to 5 cm^3 and P equal to 760mmHg, a value of $5.0003cm^3$ is obtained for V'.

It was considered that the primary factors limiting the precision were the ability to maintain a constant height of liquid hydrogen in the coolant bath and the constancy of the temperature of all parts of the air bath. It was estimated that corrections for non-ideality would only become important if temperature gradients were reduced by an order of magnitude. A similar argument is relevant to the meniscus covolume correction.

Thermal transpiration[184] may occur if two parts of a system containing a gas are held at different temperatures. For temperatures T_1 and T_2, the associated pressures P_1 and P_2 are

related by:

$$\frac{P_1}{P_2} = \left(\frac{T_1}{T_2}\right)^{\frac{1}{2}} \qquad \text{V-10.}$$

For the effects of thermal transpiration to be observed, the mean free path λ of the gas molecules must be large compared to their container's diameter. Using the well-known result from the kinetic theory of gas:

$$\lambda = \frac{7.3T}{P\Pi r_o^2} \times 10^{-20} \qquad \text{V-11.}$$

where r_o is a collision diameter between molecules, and for helium and nitrogen is about 3Å [184], the mean free path is several orders of magnitude smaller than the dimensions of the apparatus for pressures in the range 1-76 mmHg.

V-2-4 Calculation of the Free Space.

The volumes of the gas burette V(GB) and the volume of the free space V(FS) were fitted to an equation of the form:

$$P(c)\sum_i\left(\frac{V(i)}{T(i)}\right) = nR \qquad \text{V-12.}$$

Written explicitly:

$$\frac{Pc\ V(GB)}{T(GB)} + \frac{Pc\ V(FS)}{T(FS)} = nR \qquad \text{V-13.}$$

where T(GB) and T(FS) are the temperatures of the gas burette and free space respectively; R is the gas constant and n the number of moles in the gas phase. For each reference level in the gas burette, equations of the form V-13 were solved, and a mean value of V(FS) found.

V-2-5 Dead Space Calibration and Adsorption.

For each sample there was a further volume that had to be measured before the nitrogen adsorption could be commenced. This volume, the dead space volume (V(T)) was the volume above the sample in the adsorption bulb and the volume of tubing up to the taps F and G (Figure V-1). During an adsorption run the dead space consisted of the sum of a volume (V(S)) at the temperature of the air bath, and a volume (V(N)) at the temperature of the liquid nitrogen bath.

A sample was attached to the adsorption system and evacuated initially by use of a static vacuum using taps F and K, with the rest of the system isolated. The sample was then pumped directly, and the rest of the system evacuated. When a vacuum of about 10^{-4}mmHg was attained, the outgassing furnace was placed in position and switched on. The air bath thermostatting was also switched on. After the requisite length of time, the outgassing furnace was switched off and withdrawn. The tap G was closed and helium admitted via tap H to the burette; H was shut and the pressure and temperatures measured as before. These measurements allowed the number of moles of helium admitted to be calculated, since the free space volume was known. Taps F and K were then closed, and tap G opened a fixed amount. The final position of the PTFE stem of G was carefully adjusted between two marks on the glass wall of the tap. The manometer was

was reset and the pressure and temperatures measured, thus giving an estimate of the total dead space volume. The liquid nitrogen bath was raised to a position surrounding the adsorption bulb and the nitrogen pump switched on. Kao wool was placed over the top of the liquid nitrogen bath. The liquid level was periodically checked visually while the nitrogen topping up system was adjusted, to establish that the level was constant and that the metering system on the control unit was functioning correctly. At least twenty minutes were allowed to elapse once the liquid level was set before the pressure and temperatures were measured again. The oxygen vapour pressure thermometer was read to the nearest 0.25mm, and from this vapour pressure of oxygen, the temperature of liquid nitrogen was obtained from a graph of variation of saturated vapour pressure with temperature[185]. These last measurements enabled the volume at the temperature of the liquid nitrogen to be calculated. By subtraction from the total space volume that volume at the temperature of the air bath was found.

The liquid nitrogen bath was removed, the helium was pumped off, and the system was pumped down to a pressure of ca. 10^{-5} mmHg.

To measure adsorption, tap G was shut, nitrogen gas admitted to the gas burette, and the number of moles determined as before. Taps F and K were then shut, and tap G opened by the fixed amount. The adsorption bulb was thermostatted in liquid nitrogen and the various pressure and temperature measurements made as above. Further adsorption points were simply obtained by raising the mercury in the burette to the next reference level

and repeating the measuring sequence. Addition of more nitrogen was achieved by shutting tap G, measuring pressure and temperature, and then dosing over the nitrogen through tap H. The number of moles of nitrogen was then measured. Subtraction of the number of moles present after the tap G was shut and before the addition, yielded the actual number of moles added. Tap G was reopened and the adsorption experiment continued.

To desorb, the reverse of the adsorption procedure was followed. Starting from a high relative pressure and the gas burette full of mercury, the mercury was successively lowered to each reference level causing desorption to occur. To remove nitrogen from the adsorption system tap G was shut, the number of moles determined and gas removed through tap H. It was usually appropriate to raise the mercury to the top reference level during this operation. When the desired amount of nitrogen was removed, the burette and manometer were accurately set and the number of moles present determined, from which the amount pumped out was calculated. Tap G was opened and the desorption continued.

At the end of the experiment, the coolant bath was slowly removed and the adsorption bulb was allowed to warm under a reduced pressure of nitrogen, Once the ambient temperature was reached, the bulb was filled with nitrogen to atmospheric pressure and removed from the adsorption system. It was immediately stoppered and the weight recorded.

The detailed procedure described above,often took ten or more minutes to complete. It was found that for relative pressures above about 0.3 this time was longer than that for

which the mercury height in the short arm could be held exactly constant. This was because of the inability to maintain an exactly constant level of liquid coolant around the adsorption bulb and the porosity of most of the adsorbents. Porous adsorbents are generally slow to equilibrate, so when the short arm of the manometer was initially set, the mercury moved slowly up or down as equilibrium was established. The mercury level was readjusted, thereby disturbing the position of equilibrium, and again drifted up and down after it was set. The process was repeated with ever decreasing movements above and below the reference electrode. Superimposed on this behaviour were the effects of the minor fluctuations in the coolant level. Once it was established that the movements of the mercury in the short arm arose from the variations in the coolant level only, i.e. were cyclic, the pressure was measured using an abbreviated procedure. The height of the crown and meniscus height of the mercury in the long arm of the manometer were measured when the audible alarm indicated that the mercury in the short arm was set at the correct height. Thus the height of the mercury crown and the meniscus height in the short arm were assumed. When tap G was shut the normal procedure was followed. The average of all the mercury heights in the short arm measured by the full procedure for relative pressures below 0.3 was used as the assumed height when the abbreviated procedure was followed.

The short arm of the manometer had to be set accurately to ensure the volume of the free space was constant. This is an inherent problem of mercury manometry when used in conjunction

with a constant volume apparatus.

V-2-6 Calculation of Dead Space and Amount Adsorbed.

With tap G shut, the number of moles of helium (n) used to determine the dead space volume V(T) was measured. The tap G was opened and the relevant measurements made (Chapter V-2-5). Then V(T) was obtained from:

$$\frac{P(c)V(GB)}{T(GB)} + \frac{P(c)V(FS)}{T(FS)} + \frac{P(c)V(T)}{T(FS)} = nR \qquad V\text{-}14.$$

The temperature of the dead space was assumed to be the same as that of the free space, even when the nitrogen coolant was present. The volume (V(N)) of the dead space at the temperature of the liquid nitrogen was found from the equation:

$$\frac{P(c)V(GB)}{T(GB)} + \frac{P(c)V(FS)}{T(FS)} + \frac{P(c)\{V(T)-V(N)\}}{T(FS)} + \frac{P(c)V(N)}{T(N)} = nR. \qquad V\text{-}15.$$

The amounts adsorbed were calculated using the same principles as above. The initial number of moles of nitrogen n(N) was measured with tap G closed, as before. When the tap G was opened, the number of moles present in the gas phase after adsorption had occurred (n') was measured and calculated from:

$$\frac{P(c)V(GB)}{T(GB)} + \frac{P(c)V(FS)}{T(FS)} + \frac{P(c)V(B)}{T(FS)} + \frac{P(c)V(N)}{T(N)} = n'R. \qquad V\text{-}16$$

The number of moles adsorbed n(a) was given by the difference, $(n(N) - n')$, and was expressed as a volume at standard temperature and pressure:

$$V(a)\left[76cm,\ 273.15K\right] = n(a)\,\frac{R\ 273.15}{76.0} \qquad V\text{-}17.$$

where n(a) refers to P(C) and T(N).

V-3. Microcalorimetry.

V-3-1 Introduction and Principles.

The use of calorimetry as an ivestigative tool is well-established[82]. It is, however, only recently that the availability of sensitive commercial microcalorimeters has permitted the ready exploration of interfacial phenomena[83,84]. In this work, the calorimetry was carried out using an LKB Sorption Microcalorimeter 2107-030 in conjunction with an LKB 2107-210 air thermostat and an LKB 2107-310 control unit. The output from the calorimeter was amplified using a Keithley Instruments 1508 microvolt-ammeter unit and displayed on a Philips PM8000 chart recorder.

The main components of the Microcalorimeter are a heat sink containing two reaction sites each with its own set of heat detectors and heat exchangers and a calibration heater: the whole contained in an insulated box placed inside the air thermostat. One reaction site was for a batch mode, the other for a flow mode of operation. Only the latter was used in this work, and hence only this will be described.

The flow sorption cell consists (Figure V-11) of a stainless steel cylinder with a volume of about 0.5 cm^3, Teflon filters at either end and two Teflon stoppers. Each stopper consisted of 18c gold inserts, Viton 'O' ring seals and a Teflon body. A teflon plug could be fitted into the cell to reduce the volume. The cell A (Figure V-12)fits into a metal block B containing 24c gold, 1.0mm bore heat exchanges C. The metal block is sandwiched between a pair of thermopiles E and an aluminium heat sink D (assumed infinite). Calibration heaters F, of known resistance, are fitted to the mounting block.

The microcalorimeter operates on the heat leakage principle[194], and measures a rate of heat flow. If heat is generated in the cell (an exothermic reaction), the heat flows from the cell to the heat sink. The opposite heat flow occurs if the heat is absorbed by the cell (an endothermic reaction). In each case the heat flow creates a temperature difference across the thermopiles and an electromotive force (e.m.f.) proportional to the temperature difference is generated. The e.m.f. is compared with that from the unused batch reaction site and any e.m.f. common to both sites is balanced out. The output is then amplified and fed to the recorder system. Any experimentally determined heat change is proportional to the area beneath the e.m.f-time curve (see below) and may be calibrated, using an integral heater, through which a known current may be passed for a known time. The e.m.f-time calibration profile is matched as closely as possible to the reaction profile by the current and the time for which it flows.

The flow cell may be used for saturation or injection type experiments. In the former, a fluid solvent (liquid or gas) is continuously pumped through the cell until a stable base line is obtained on the chart recorder. The solvent flow is then interchanged with the flow of the solution of interest by means of a multi-way tap. When the solvent-solution interface percolates through the cell, reaction proceeds; heat is generated until the adsorbent becomes saturated and the evolution of heat ceases. An adsorption peak is recorded. Alternatively, the solution of interest may be introduced by direct injection into the solvent stream. A "heat" pulse is again recorded. In general, continuous

flow saturation methods have the advantage of being more sensitive, but the disadvantage of requiring large fluid volumes and longer analysis times, compared with the injection technique. In this work, the saturation method was employed.

An idealised thermogram showing the completely reversible physical adsorption of an adsorbate on a solid surface is shown in Figure V-13. Initially, solvent flows through the cell until at 'X' the flows of solvent and solution are interchanged. A short time later, an exothermic signal I, results from the physical adsorption process. The calibration heaters are switched on once the adsorption is complete, for a known time, and with a known current. An exothermic calibration peak II results. On interchanging the solvent and solution once more, an endothermic desorption signal III is obtained. The signals I and III are of equal magnitude and opposite sign.

Experimentally, peak areas were determined using a planimeter read to ±1% for large areas. However, the position of the base line introduced an additional uncertainty in the area, possibly ±4%. Hence the overall precision was about ±5% in the estimation of peak areas.

In a heat flow calorimeter, the thermal e.m.f E is proportional to the heat flow across thermopiles Q

$$\dot{Q} = \epsilon E \qquad \text{V-18.}$$

$$Q = \epsilon \int E dt \qquad \text{V-19.}$$

physically, the integral is the area A under the e.m.f-time trace,

$$Q = \epsilon A \qquad \text{V-20.}$$

where ϵ is a proportionality constant determined by the calibration procedure:

$$Q(cal) = I^2 R \cdot t = \epsilon A(cal) \qquad V\text{-}21.$$

where I is the calibration current in amps. R the resistance of the calibration heater in ohms, t is the calibration time in seconds, and A(cal.) the area under the calibration curve (in arbitrary units). It was assumed that the thermal characteristics of the apparatus were such that a single calibration experiment could be used to determine both exothermic and endothermic heat changes.

In the flow mode, a fluid may be pumped upwards or downwards through the adsorbent in the cell. The upwards mode was chosen since this reduces the risk of clogging the filters and achieves a more"stable suspension"[194]. than the downward flow mode. The motion of a fluid over a presumably less tightly-packed powdered sample should give rise to a smaller frictional heating effect, and hence improve the quality of the trace base line. There have been reports of 'channeling' using the upward flow mode. To prevent a syphoning effect and improve the flow characteristics in the cell, the waste was pumped to a reservoir situated at a constant height (40cm) above the pumps.

The microcalorimeter was used for both liquid and gas adsorption experiments. In each case, all the connections in the calorimeter, and all external plumbing, consisted of 1mm internal diameter Teflon tubing. The LKB thermostat was placed in a

thermostated room (±1.5°C) and a Churchill chiller was used to cool the air bath's external fans. Under these conditions the minimum detectable heat pulse was about 200μJ, and the minimum detectable continuous heat effect was about 1 μW.

To ensure the fluids used were in thermal equilibrium with the adsorbent, various lengths of Teflon tube were used as heat exchanges in the LKB air bath, depending on the temperature difference between the room and the adsorbent. Several factors had to be considered concerning the length of equilibration tubing and the flow rates necessary to achieve thermal equilibrium. If the pumped fluids had a long residence time in the tubing, then the boundary between solvent and adsorbate solution would not remain sharp. As diffusion occurred the adsorbate and solvent would mix. The initial adsorption would occur at some concentration less than that expected of a perfect plug reactor. This type of reactor is one which is operated such that no axial mixing of reactant 'plug' with the fluid in front (or behind) occurs. Since there is no mixing, there is no dilution to consider. The real reactor obviously lies between this extreme and the other, which corresponds to a perfectly mixed reactor. To minimise sample dispersion, it was found advantageous to use as short a length of tubing as possible, and as high a flow rate consistent with base line noise (see below), while still achieving thermal equilibrium.

For a given flow rate the analysis time could not be reduced significantly by shortening the tubing — the saturation technique is inherently slow. One major reason is the necessity

to use low concentration solutions to minimise heats of dilution in the adsorption cell.

Base line instability consisted of a regular cyclical pulsing on which was superimposed random noise or a short-term background noise. That a frictional heat effect was present was easily shown by stopping the fluid flow and observing a fall in the heat generated (base line shifted endothermically). Switching the flow on again caused heat to be generated and the base line shifted in an exothermic direction. Provided the flow rate was constant, the frictional heating was assumed to be constant. However, all the pumps used caused a slight pulsing in the liquid stream and hence reduced the quality of the base line, by virtue of the cyclical pulsing and the increased background noise generated by this. It was found that the frictional heating effect and pulse effects could be reduced slightly by filling the adsorption cell between one half and one third full. However, the primary factor deciding the extent of filling of the adsorption cell was the expected heat change per unit mass adsorbent/adsorbate reaction.

For a given volume of adsorbent and concentration of adsorbate solution, the flow rate and length of equilibration tubing were thus a compromise between a number of conflicting factors: the rate of delivery of reactant, the rate of attainment of thermal equilibrium, the effect of diffusion and the effect of heats of dilution. To maintain a constant frictional effect, it was necessary to match the flow rates of solvent and solution as closely as possible. Typically between 0.5m and 1.0m of equilibration tubing was used in

conjunction with a liquid flow rate of $0.2cm^3min^{-1}$, and a gas flow rate of about $4cm^3min^{-1}$.

V-3-2 The Liquid Adsorption Experiment.

The experimental arrangement is shown schematically in Figure V-14. The two pumps, one for solvent and one for adsorbate solution, were connected by a four-way LKB PTFE valve to the LKB assembly. The thermostat was set at 25.00°C. The flow of solvent was commenced, and when a steady base line was obtained the sample pump was switched on with the solution going to waste. Once this was operating satisfactorily the valve was switched, causing the solution to interchange with the solvent. The subsequent adsorption peak was recorded, calibrated, and the flow interchanged again, causing desorption to occur.

Initially a peristaltic pump (LKB 10200 Perpex Pump) with a 1.5mm. internal diameter 'Viton' tube in the pump and a 1000 : 1 reduction gearbox was used to pump the solvent. This gave a flow rate of $0.03cm^3min^{-1}$., which was far too slow and impossible to match with the other pumps available (Model A99, Razel Scientific Instruments Ltd.). These Razel pumps gave a wide range of flow rates and were used in conjunction with $50cm^3$ gas-tight Hamilton syringes. Unfortunately, these pumps all gave an undulating pulse effect, even after repeated overhauls. This was found to be largely attributable to the pumps rather than the syringes. Eventually only one pump was retained, and a Harvard Apparatus Compact Infusion

pump was obtained that had a number of flow rates compatible with those of the Razel in the flow range 0.33$cm^3 min.^{-1}$ to 0.02$cm^3 min.^{-1}$. The bulk of the liquid adsorption work was carried out using the Razel and Harvard pumps which only showed a slight pulsing at the highest sensitivity settings, which were not often used.

The solvent used was n-heptane, dried over activated 4Å molecular sieves. All the solutions were made up as weight percentages in n-heptane.

V-3-3 The Water Vapour Adsorption Experiment.

The experiemental arrangement is shown schematically in Figure V-15. The nitrogen was delivered from a B.O.C. 'White Spot' cylinder into the bottom of a 500cm^3 flask fitted with freshly activated molecular sieves. The peristaltic pump, mentioned above, was used to draw nitrogen from this reservoir. Excess gas was vented to atmosphere via an oil bubbler. A needle valve controlled the rate of delivery of nitrogen to the reservoir.

A two-way LKB PTFE valve led from the pump into the calorimeter. One route was straight through about 1m of equilibration tubing in the air bath into the reaction cell. The other was via a water bubbler in the air bath before joining the first straight-through route. About 0.75m of tubing was used as a heat exchanger in the air bath before the water bubbler which was filled with distilled water and connected to the main route by a piece of silicone tube (Figure V-16). To prevent unwanted diffusion of water

along this tube a simple on-off device was provided. This consisted of two aluminium plates either side of the silicone, which could be screwed together through a small hole, packed with cotton wool, in the thermostat lid.

The flow was measured, using a modified 50cm^3 grade 'A' burette and timing the rise of soap bubbles up a known volume. Flow rates could be determined to $\pm 0.1 cm^3 min.^{-1}$ in about $5 cm^3 m^{-1}$. When the nitrogen was switched from the 'dry' to the 'wet' route a reduction of about 10% was noted in the flow rate. The flow rate was dependent on the total hold up volume of the system, and hence the volume of water in the bubbler and the volume of sample present. To reduce the dead volume in the adsorption cell a teflon plug was inserted, thus halving the total volume and virtually eliminating any dead space. The flow rate decreased with time (over several days), presumably as the sample became more packed. A transient reduction in flow was always noted on switching from 'dry' to 'wet' as the water bubbler became slightly pressurised.

Pulsing and frictional effects, although present, were negligible compared to the heats of reaction. Frictional heating effects were less for the gas experiments than for the liquid experiments. The upward flow mode was used for the preliminary experiments, but it was found that the channel inside the teflon plug became blocked. It was therefore decided to use the downward mode to overcome this problem.

V-4. Materials.

The adsorbent ferric oxide 'A' was prepared by the method of Lambert and Clark[187]. An 8wt.% aqueous sodium hydroxide solution was slowly added to a well-stirred 30wt.% aqueous solution of ferric chloride. The reagents were Analar grade and obtained from B.D.H. Chemicals Ltd. The precipitate was allowed to stand overnight and then filtered and washed with distilled water. Drying was carried out in an oven at 100°C for 48 hours and then at 170°C for 24 hours. The material thus produced was found to be hydrated (see Chapter VI) and contained about 4wt.% of chloride ions [186].

Bignall[186], in collaborative work, prepared and characterised the other ferric oxide adsorbents used in this work. These were another batch of ferric oxide prepared by the method of Lambert and Clark (ferric oxide 'B'); α-goethite prepared by the method of Atkinson et al[188], and β-goethite prepared by the method of Weiser et al[189].

Crystallographically, ferric oxide A was found to be predominantly β-goethite and ferric oxide B predominantly α-goethite. Some amorphous material was present in both samples. All the ferric oxide samples were found to be hydrated. A low surface area α-haematite sample was obtained from Johnson Matthey Chemicals Ltd (batch 581377) and used without purification.

Three surface area standards obtained from the National Physical Laboratory were used:

1) Certified Reference Material M11-01, Sterling FT-GI(2700), a graphitised carbon black.

2) Certified Reference Material M11-03, Silica TK800, a non-porous silica.

3) Certified Reference Material M11-05, α-alumina a low surface area non-porous alumina.

In the vacuum adsorption experiments, helium gas was supplied by B.O.C. Ltd., and was used without purification, to measure the "dead" and "free" space volumes. Oxygen free nitrogen (B.O.C. Ltd.) was used as the adsorbate , again without purification.

The solvent for the liquid microcalorimetric experiments was n-heptane (B.D.H. Chemicals Ltd.). It conformed to International Purification specification for normal-heptane, and had a nominal GLC assay of 99.5%. To remove any possible residual polar organic impurities and water, the heptane was successively passed through three columns containing:

1) Aluminium oxide (Basic grade B.D.H. Chemicals Ltd).
2) Silica gel (6-120 mesh, B.D.H. Chemicals Ltd).
3) 4Å molecular sieves (B.D.H. Chemicals Ltd.) activated for 4 hours at 340 °C.

The last column was a pressure compensated closed system to avoid ingress of atmospheric moisture. The purified heptane was stored over activated molecular sieves.

1-butanol, Aristar grade, was obtained from B.D.H. Ltd. It had a nominal GLC assay of 99.9% and was stored over activated 4Å molecular sieves before use.

1,2 -epoxybutane, nominally 99% was obtained from Ralph N. Emanuel Ltd., and stored over activated molecular sieves before use. Volumetric analysis found 98.2% epoxybutane before treatment with molecular sieves. The major impurities were thought to be hydrolysis products and water.

1,2-propandiol with a minimum G.L.C. assay of 99% was obtained from Koch Light Ltd., and used without purification.

FIG. V.1.

The Adsorption Apparatus.

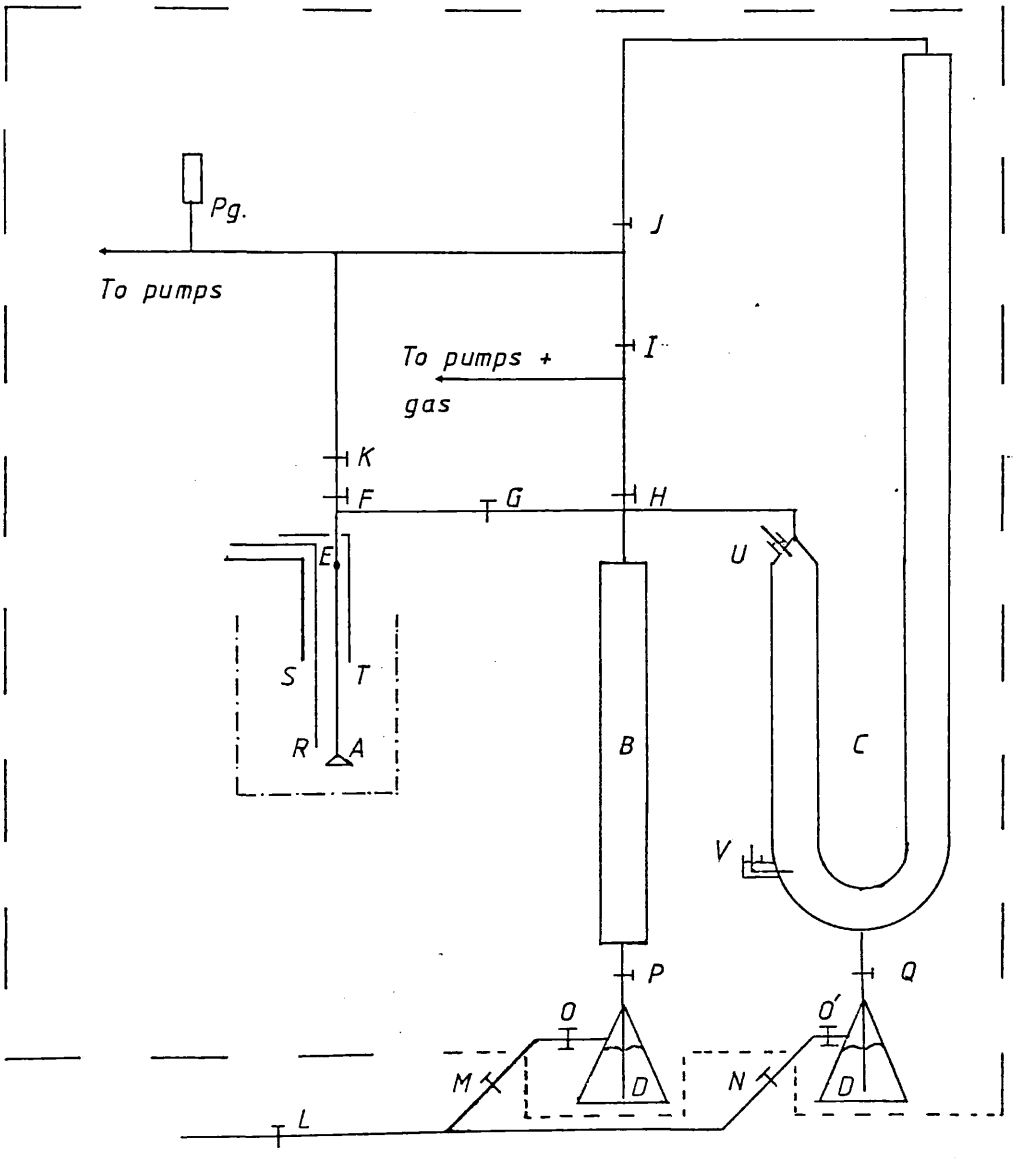

FIG. V.2.

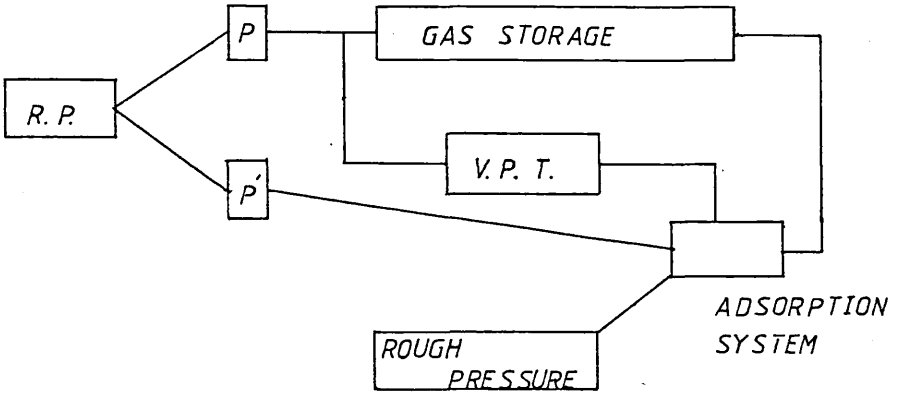

The Vacuum System.

FIG. V.3.

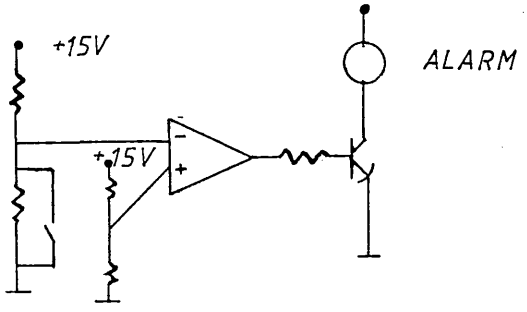

The Circuit Diagram for Maintaining a Constant Height in the Short Arm of the Manometer.

FIG. V.4.

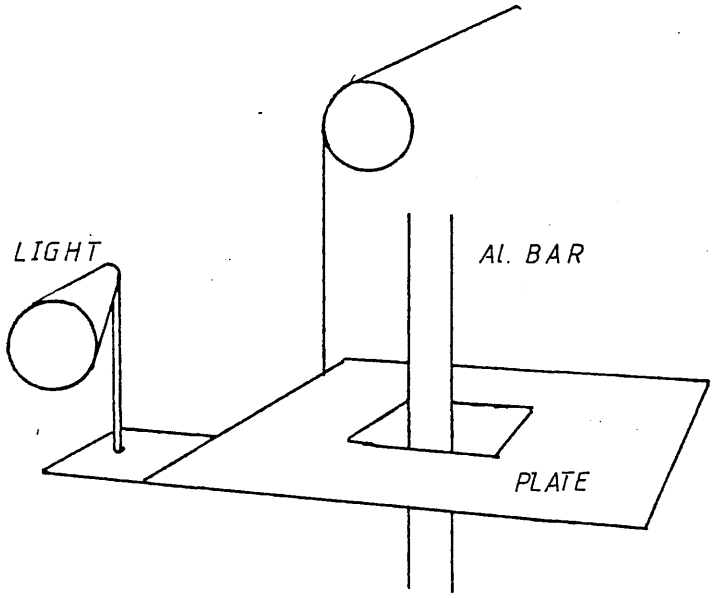

The Lighting Unit for the Long Arm of the Manometer.

FIG. **V.5.**

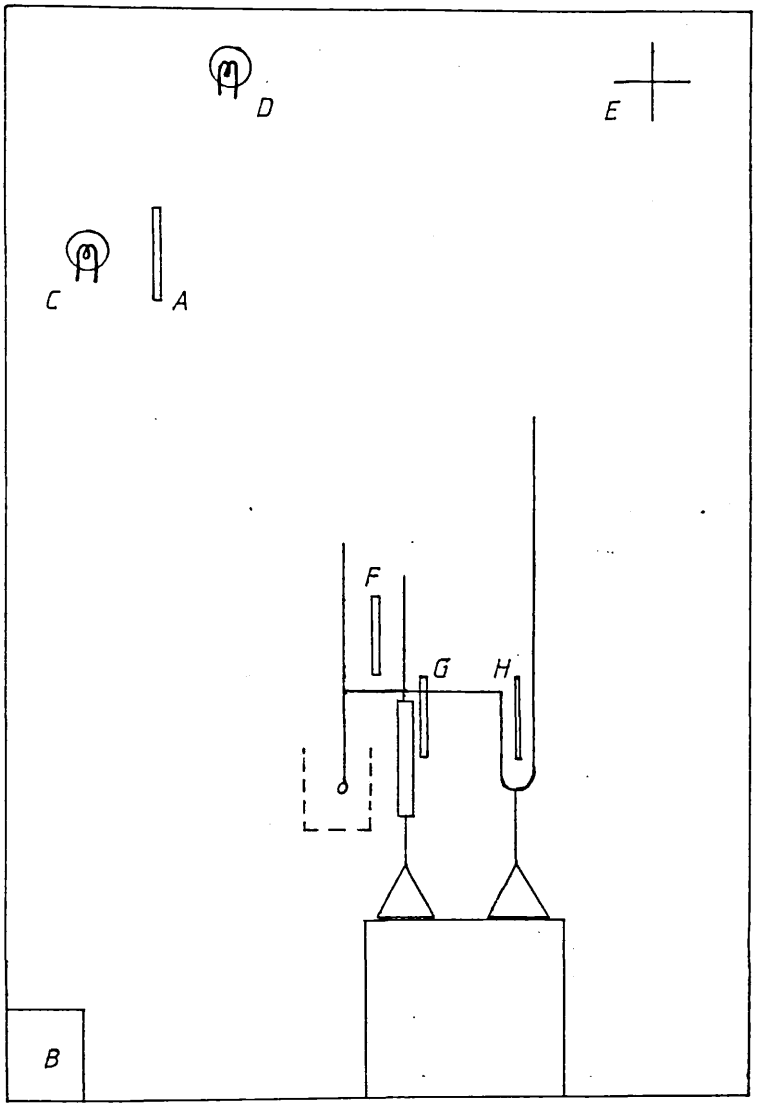

The Air Bath Thermostating System.

FIG. V. 6.

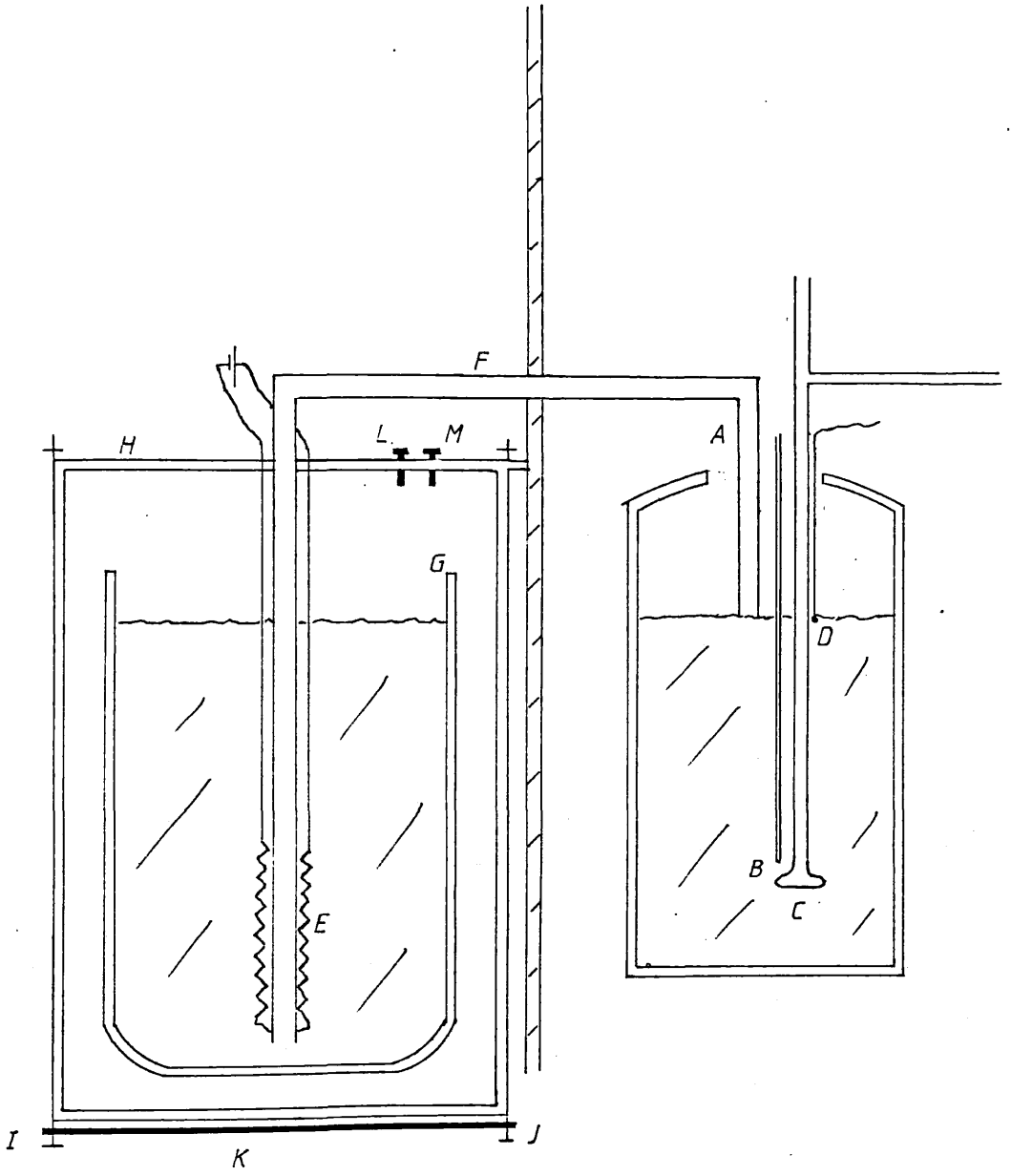

The Liquid Nitrogen Topping Up Device.

FIG. V.7.

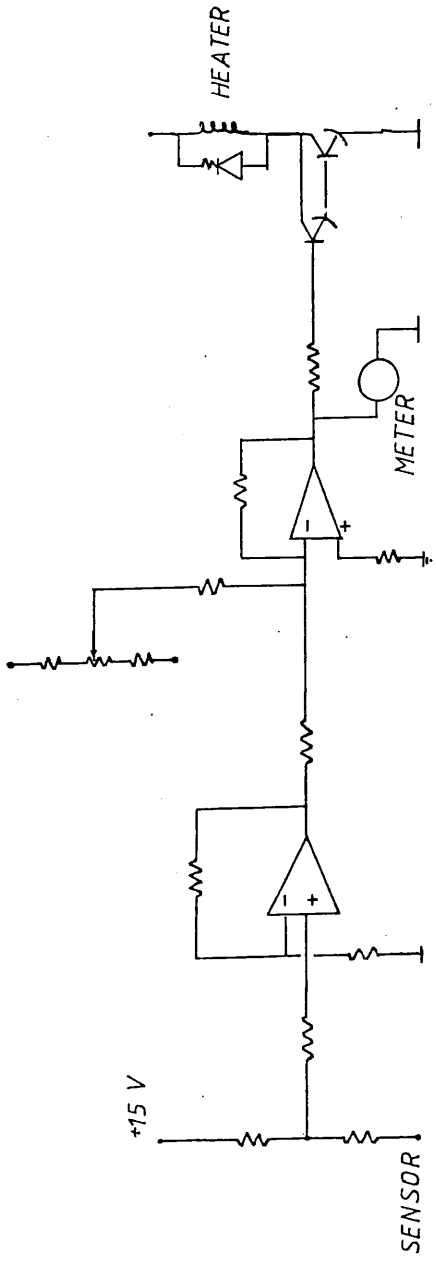

The circuit diagram for the Liquid Nitrogen Topping Up device.

FIG. V.8.

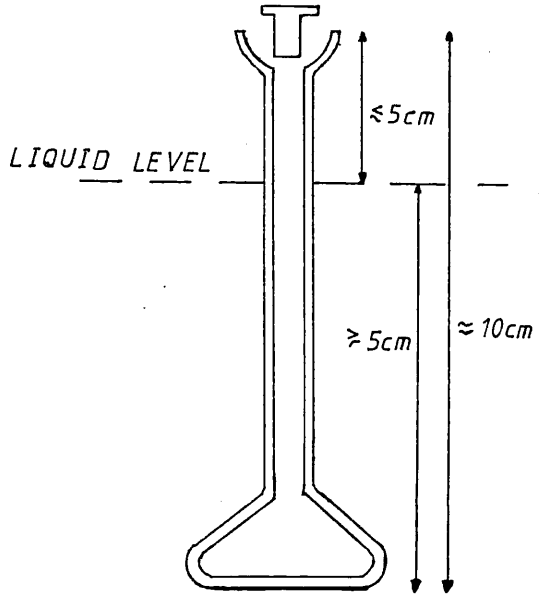

A Typical Adsorption Bulb.

FIG. V.9.

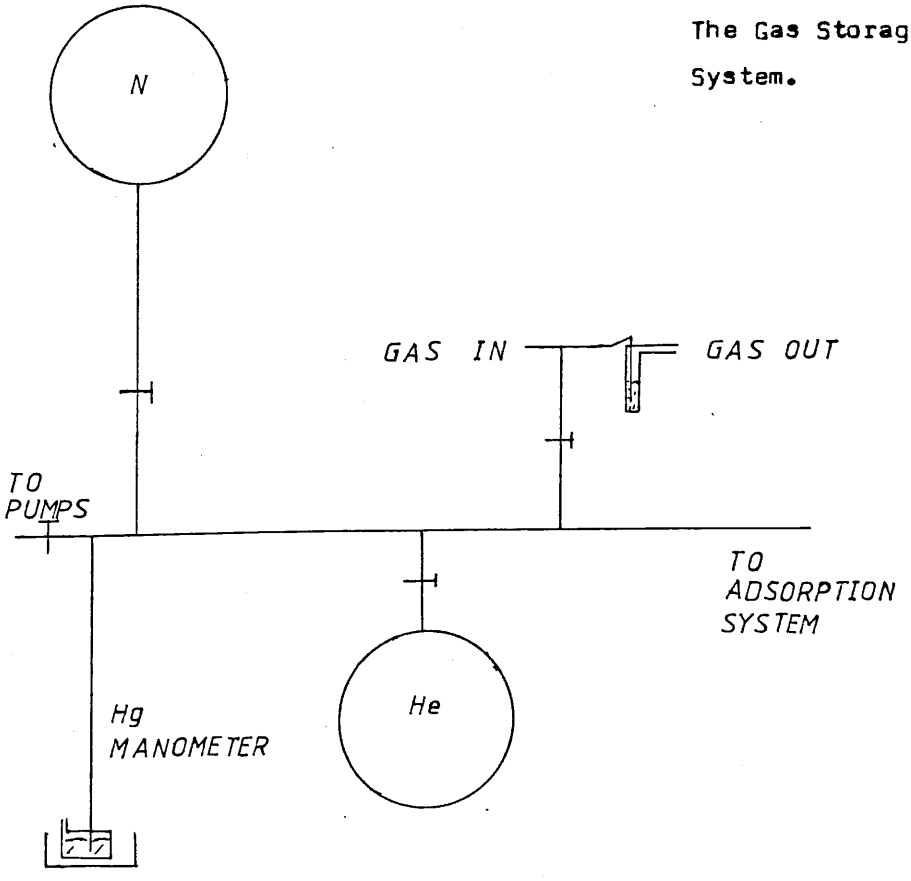

The Gas Storage System.

Fig. V.10.

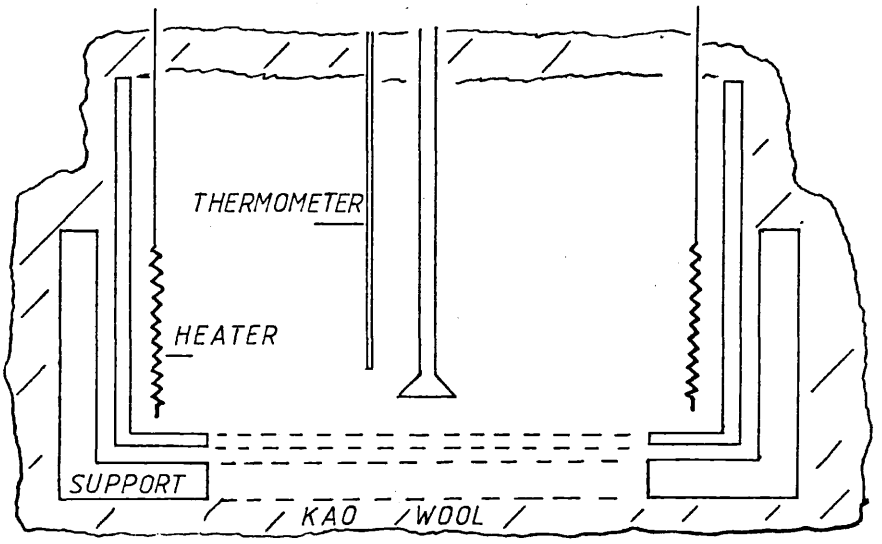

The Furnace Used for Outgassing.

FIG. V.11.

The Microcalorimetric Sorption Cell.

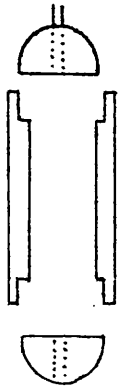

Fig. V.12.

The LKB Microcalorimeter.

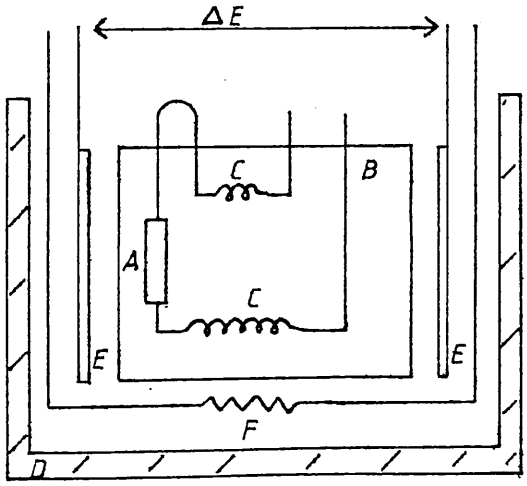

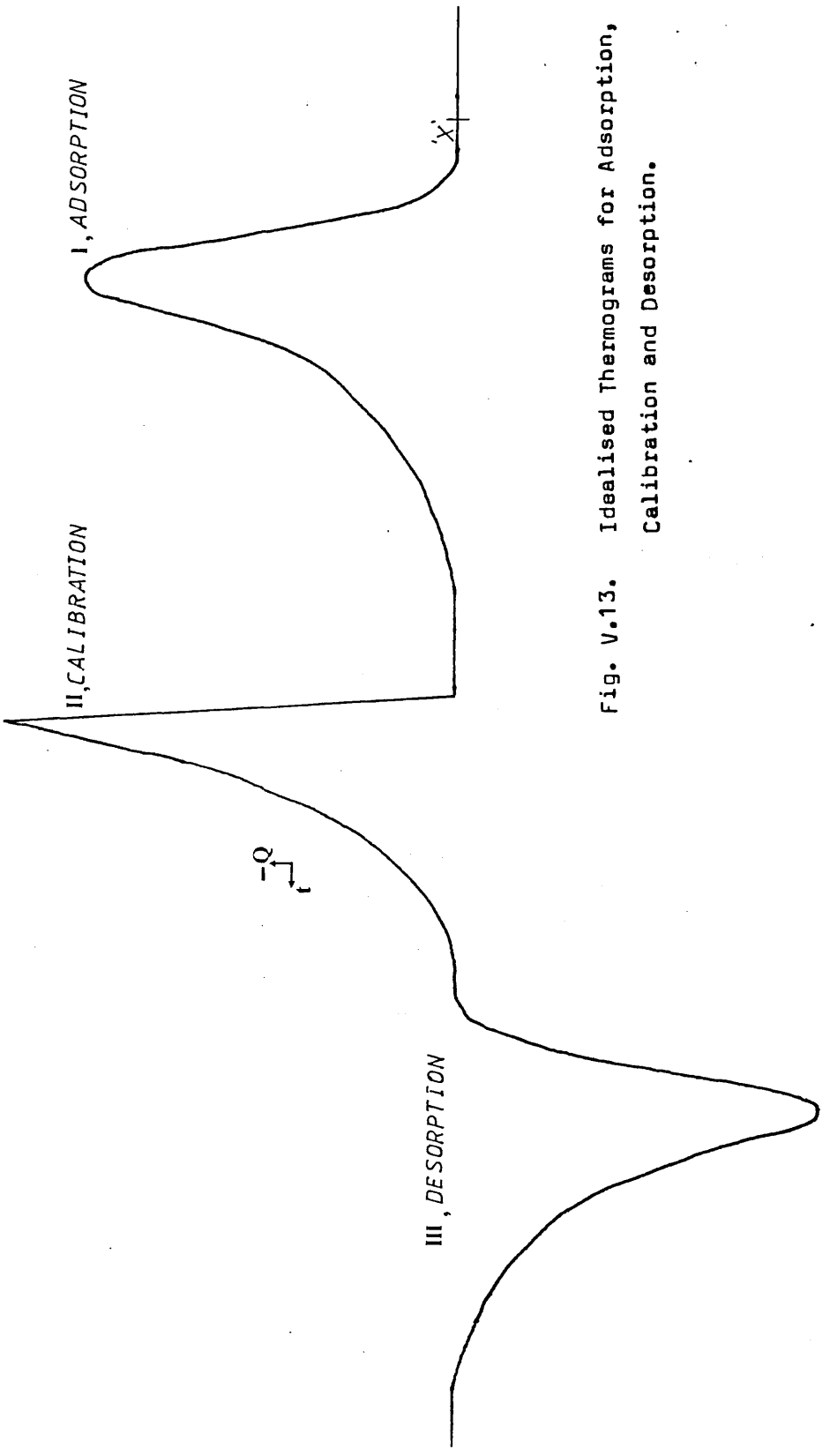

Fig. V.13. Idealised Thermograms for Adsorption, Calibration and Desorption.

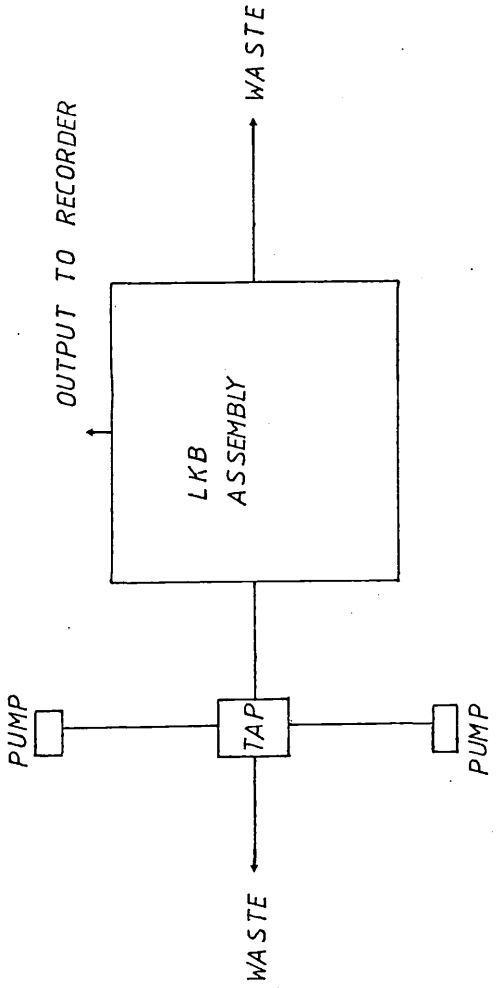

FIG.V.14.

The Experimental Arrangements for the Liquid Adsorption Experiments.

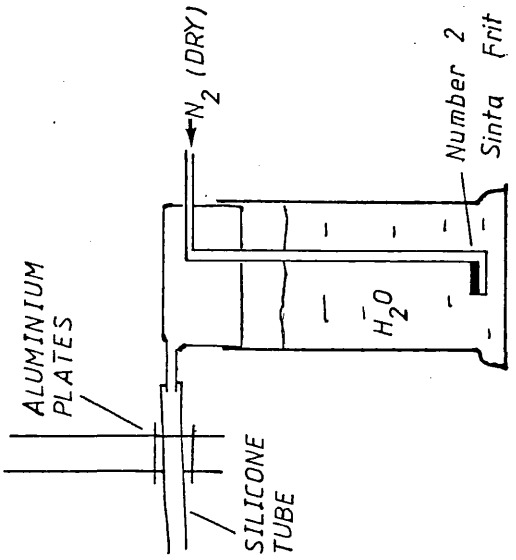

FIG. V.16.
The Water Bubbler.

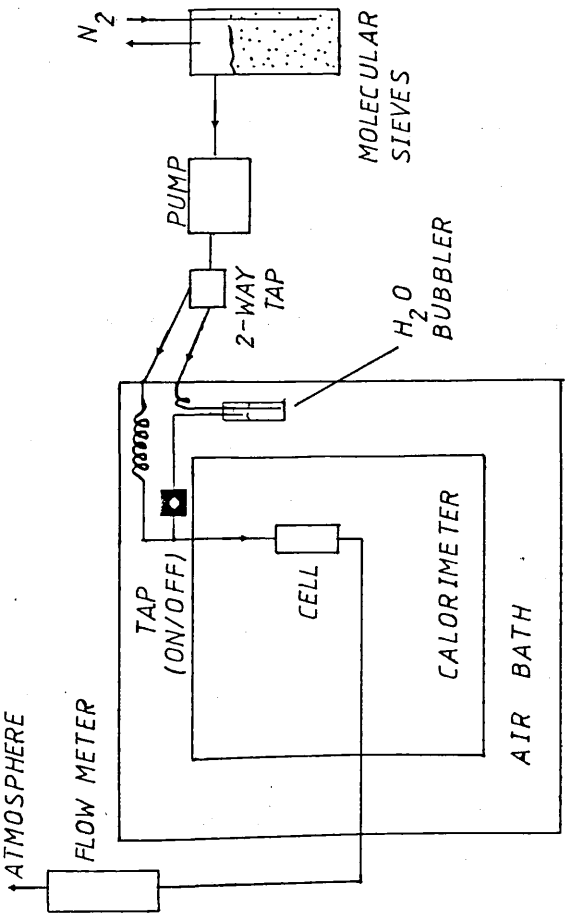

FIG.V.15.
The Experimental Arrangements for the Vapour Adsorption Experiments.

CHAPTER VI.

The Vacuum Adsorption Experiments.

VI-1 Results.

VI-1-1 The Free Space Calibration.

The free space volume was calibrated at 27 °C using helium which was assumed to be inert and ideal. The results of four separate experiments, each starting with different initial pressures, were used to calculate a mean free space volume of 4.207 ± 0.017 cm^3. The error is the standard deviation σ_{N-1} with N = 12.

VI-1-2 Standardisation of the Vacuum Apparatus.

To establish that the adsorption apparatus was capable of giving reliable results, nitrogen adsorption experiments were performed on two well characterised surface area standards, Silica TK800 and Sterling FT-G2700[28].

The silica sample, a fine, non-porous powder with a certified specific surface area of 165.8 ± 2.1 $m^2 g^{-1}$ was used first. Great care was required to evacuate the sample in order to prevent entrainment. Prior to the helium calibration of the dead space volume, the sample was outgassed for 5 hours at room temperature followed by 12 hours at 120 °C and then 5 hours at 143 °C. The final pressure was less than 5×10^{-5} mm Hg. With about 0.3g of silica initially present, the dead space volume was found to be 9.02 cm^3, of which 7.52 cm^3 was at liquid nitrogen temperature, 77K. After the calibration, the sample was evacuated for a further

4 hours to an ultimate pressure of 3×10^{-5} mm Hg before the start of the adsorption experiment. The results are given in Table VI-1. Eleven measurements were made in the N.P.L. specified relative pressure range (0.04 - 0.20) over which the B.E.T. plot is linear. The best fit least squares plot is shown in Figure VI-1, from which the specific surface area was calculated to be $164.1 \pm 1.4 m^2 g^{-1}$. A weight loss of about 1.5% was found compared to an NPL measured weight loss of 2.1% obtained after outgassing at 140°C for 16 hours[28].

The adsorbent Sterling FT-G2700 is a non-porous graphitised carbon black consisting largely of small pellets approximately 1mm in diameter, together with a small quantity of finer material. No inhomogeneity of the sample with respect to surface area ($11.1 \pm 0.8 m^2 g^{-1}$) was found by the SCI/IUPAC/NPL working party on surface area standards[28].

A sample of about 1.8 g was evacuated for 9 hours at room temperature and then for 7 hours at 303°C prior to the helium calibration. This yielded a total dead space volume of 3.42 cm^3 of which 1.49 cm^3 was at 77K. Between the calibration and adsorption experiments the sample was evacuated for 12 hours to an ultimate pressure of 2×10^{-5} mm Hg. Six adsorption measurements were made, of which four fell within the NPL specified relative pressure range (0.04 - 0.15) over which the BET plot is linear. The results are given in Table VI-2. The best fit least squares line of these four points, Figure VI-2, gave a negative intercept and hence a negative 'c' value, which is not uncommon for

this sample[28]. The calculated surface area was $10.92 \pm 0.4 m^2 g^{-1}$. There was no weight loss.

For both of the test samples, the quoted error is twice the standard deviation σ_{N-1} of the monolayer volume Vm calculated from the standard deviation of the intercept and gradient of the least squares BET plot. The small errors introduced by the weight measurements have been neglected.

VI-1-3 The Adsorbent Ferric Oxide A.

About 0.8g of ferric oxide was outgassed first at 27°C and then at 130°C for 14½ hours before the helium dead space calibration. This yielded a total volume of $3.97 cm^3$ of which $2.18 cm^3$ was at 77K. Between the calibration and adsorption experiments, the sample was evacuated for 16 hours to an ultimate pressure of 2×10^{-5} mmHg. The adsorption results are given in Table VI-3, in the first two columns, and the isotherm is drawn as curve I in Figure VI-3. No attempt was made to record the desorption isotherm, because the adsorption measurements had taken too long. Above a relative pressure of about 0.4, sometimes over 30 min. elapsed before equilibrium was established and the pressure could be recorded. The pressure decreased slowly with time.

A further sample of approximately 0.8g was subjected to the same outgassing regime as above. The dead space volume was found to be $3.90 cm^3$ with $2.54 cm^3$ at 77K. Both the adsorption and desorption isotherms were measured and the results given in the last four columns of

Table VI-3. The curves II and III in Figure VI-3 are the adsorption and desorption isotherms respectively. The hysteresis loop closes at a relative pressure of about 0.35, and indicates the presence of mesopores in the sample. The desorption isotherms were accurately plotted on a large sheet of paper, and the gaseous 'volumes adsorbed' read off at convenient relative pressures. Using this data, a pore size distribution was calculated by the method of Pierce[55], as discussed earlier (Chapter II-12). The distribution curve is drawn in Figure VI-4.

From the first run, 11 readings between the relative pressures 0.07 and 0.30 were used to calculate a BET surface area of 240.6 ± 1.4m^2g^{-1}. Only three adsorption measurements were made within this relative pressure range on the second sample. A value of 244.0m^2g^{-1} was calculated for the surface area from these three measurements.

During the outgassing procedure, a sudden increase in pressure was observed when the temperature reached about 100°C. The pressure changed by over an order of magnitude of about 2 x 10^{-3}mmHg. It was assumed that this effect was associated with the loss of water previously adsorbed inside the pores. As a result it was decided to investigate the effect of outgassing on the surface area. A sample was accurately weighed and then outgassed for 12 hours at 126°C to an ultimate pressure of 5 x 10^{-5}mmHg. Nitrogen was then admitted to the vacuum system at room temperature, and the weight redetermined. A

weight loss of 12.7% was found. The same sample was then outgassed again under identical conditions and the helium calibration and nitrogen adsorption experiments conducted as normal. The weight loss as a result of the second outgassing was only 0.5%

The total dead space volume was 4.49 cm^3 of which 3.03 cm^3 was at 77K. Eighteen measurements were taken up to a relative pressure of about 0.55. The results are shown in Table VI-4, and the adsorption isotherm is drawn as curve I in Figure VI-5. The best BET plot was obtained from ten measurements within the relative pressure range 0.06 - 0.31, and yielded a surface area of 249.2 ± 1.4m^2g^{-1}.

A fresh sample was outgassed for 20 hours at 122°C. The dead space volume was found to be 4.31 cm^3 of which 2.94 cm^3 was at 77K. Twenty two nitrogen adsorption measurements were made over the first half of the adsorption isotherm. The results are shown in Table VI-4 and the adsorption isotherm is drawn as curve II in Figure VI-5. The best BET plot was obtained from eleven measurements within the relative pressure range 0.05-0.27. The surface area was calculated as 245.9 ± 1.8 m^2g^{-1}.

To eliminate possible inhomogeneity effects, three subsequent experiments were performed on the same sample which was left open to the atmosphere for about 36 hours between each run. Each outgassing regime was more vigorous than the preceding one. The dead space volumes were calibrated at the start of these experiments, and the

values obtained used for all the calculations. Care was taken to ensure no powder was lost by entrainment. About 1g of ferric oxide was used.

The entire vacuum apparatus was evacuated as usual except for the adsorption bulb and the dead space volume. These volumes, and hence the sample, were evacuated for three hours at 27°C to an ultimate pressure of 5×10^{-5} mmHg. The dead space volume was determined as 4.28 cm^3 of which 3.15 cm^3 was at 77K. After the calibration, the sample was evacuated for a further 3 hours at 27°C. Thirteen adsorption measurements were made in the relative pressure range 0.07-0.29. These are recorded in Table VI-5, and plotted in Figure VI-5 as curve III. Using all the readings, the least square analysis of the BET plot gave a surface area of 222.1 ± 2.0 $m^2 g^{-1}$. After this run the sample was left open to the atmosphere for about 36 hours before being outgassed for 12 hours at 27°C to an ultimate pressure of 5×10^{-5} mmHg. Seven adsorption measurements were made, although only four fell in the BET relative pressure range. The results are given in Table VI-5, and plotted as curve IV in Figure VI-5. The surface area was calculated as 224.7 ± 1.0 $m^2 g^{-1}$. The final outgassing, after the sample had again been left open to the atmosphere, lasted for 20 hours at 50°C. Eight adsorption measurements were made and using six of them, a surface area of 230.3 ± 1.4 $m^2 g^{-1}$ was calculated. The results are given in Table VI-5, and plotted as a curve V in Figure VI-5.

VI-1-4 The Maleic Anhydride Treated Ferric Oxide A.

Collaborative work conducted by Bignall[186] was partly concerned with attempts to modify iron oxide surfaces by the irreversible adsorption of various small organic molecules. Some of the ferric oxide A was treated by refluxing with maleic anhydride in tetrahydrofuran and then washed and dried. The effect of this pretreatment was tested by subjecting two batches of the treated oxide to different outgassing regimes.

About 0.6 g was outgassed at 50°C for 20 hours before the helium calibration, and for a further 11 hours at 27°C afterwards. The dead space was 3.91 cm^3 of which 2.51 cm^3 was 77K. The adsorption and desorption results are given in Table VI-6 and the isotherms drawn in Figure VI-6. The surface area was calculated as 178.1 ± 1.5 m^2g^{-1} from six measurements in the BET region. The treated ferric oxide was analysed for carbon and hydrogen content before and after the adsorption experiment (Butterworth Laboratories Ltd., U.K.), and the results are given in Table VI-7a. A weight loss of 2.5% was measured.

A further sample was outgassed for 18 hours at 130°C before the helium calibration and for a further 1 hour afterwards at 27°C. The dead space volume was 3.89 cm^3 of which 2.53 cm^3 was at 77K. The adsorption and desorption results are given in Table VI-8 and the isotherms drawn in Figure VI-7. The surface area, calculated from five measurements in the BET region, was 202.9 ± 2.0 m^2g^{-1}. A weight loss of 3.5% was recorded. The carbon and hydrogen analyses are given in Table VI-7b. The pore size distribution curves calculated for each of the differently outgassed samples are

plotted in Figure VI-8. Curve I represents the sample outgassed at 50°C and curve II the sample outgassed at 130°C.

Infra-red spectra were recorded of the treated samples before and after outgassing. KBr discs were made of the untreated oxide, the treated oxide and the treated and outgassed oxide in approximately equal proportions. The untreated disc was placed in the reference beam of the spectrometer, and the infra-red spectra of the treated discs were recorded; Figure VI-9. Figure VI-10 compares the spectra of the treated and untreated samples in the region 3500-2500 cm^{-1}.

VI-1-5. Absorbent Ferric Oxide B.

About 0.5 g of ferric oxide B was outgassed for 16 hours at 127°C before the helium calibration and for a further 24 hours at 27°C afterwards. The total dead space volume was 3.95 cm^3 of which 2.59 cm^3 was at 77K. The nitrogen adsorption results are shown in Table VI-9 and the isotherm is drawn as curve I in Figure VI-11. A BET plot, using six measurements in the relative pressure range 0.06 - 0.24 gave a surface area of 158.5 ± 1.6 $m^2 g^{-1}$. A weight loss of 5.7% was recorded. No attempt was made to measure the desorption isotherm because the adsorption measurements took too long. In order to record the desorption isotherm it was decided to make only a few adsorption measurements before recording the desorption, using a fresh sample.

A further sample of about 0.5 g was outgassed for 19 hours at 127°C before the helium calibration and then

evacuated to 5×10^{-5} mm Hg for 1 hour before the experiment. The dead space volume was 3.94 cm^3 of which 2.56 cm^3 was at 77K. Four adsorption measurements were taken before the desorption was started. The results are given in Table VI-9, and plotted as curves II and III for the adsorption and desorption respectively in Figure VI-11. The hysteresis loop suggests that the sample is porous. The pore size distribution curve, obtained from the desorption isotherm is plotted in Figure VI-12.

VI-1-6 The Maleic Anhydride Treated Ferric Oxide B.

A quantity of ferric oxide B was treated with maleic anhydride by Bignall as described for ferric oxide A.

About 0.4 g was outgassed at room temperature for 10 hours and then at 50°C for 9½ hours before the calibration experiment. The dead space volume was 3.97 cm^3 of which 2.54 cm^3 was at 77K. The sample was evacuated for a further 10½ hours at 27°C before the adsorption experiment. The results of both the adsorption and desorption measurements are given in Table VI-10 and the isotherms are plotted in Figure VI-13. A BET plot using 7 measurements in the relative pressure range 0.05 - 0.24 gave a surface area of 135.7 ± 2.2 $m^2 g^{-1}$. The pore size distribution curve, calculated from the desorption isotherm, is given in Figure VI-14. The results of carbon and hydrogen analyses (Butterworth Ltd., U.K.) before and after outgassing the sample are given in Table VI-11. A weight loss of 0.5% was recorded.

VI-1-7 The Adsorbent α-Goethite.

About 0.4 g was outgassed for 14 hours at 125°C before the helium calibration and for two hours afterwards at 27°C. The dead space volume was 3.73 cm^3 of which 2.62 cm^3 was at 77K. The adsorption and desorption results are given in Table VI-12 and plotted in Figure VI-15. The asymptotic behaviour of the adsorption isotherm is indicative of inter-particle condensation. The desorption curve does not rejoin the adsorption curve at low relative pressures. It was assumed that the desorption was dominated by evaporation of adsorbate condensed between particles rather than by evaporation of adsorbed material. Consequently, the pore size distribution was calculated using data extracted from the adsorption isotherm. Distribution obtained by starting the calculation at relative pressures of 0.85,0.81, 0.80 and 0.79 are shown in Figure VI-16. Using six measurements in the relative pressure range 0.07 to 0.28, a least squares BET plot gave a surface area of 112.3 $\pm 1.6 m^2 g^{-1}$.

VI-1-8 The Adsorbent β-Goethite.

About 0.4 g was outgassed for 12 hours at 125°C before the helium calibration, and for a further 1½ hours afterwards at 27°C. The dead space volume was 3.94 cm^3 of which 2.56 cm^3 was at 77K. The adsorption and desorption results are given in Table VI-13 and plotted in Figure VI-17. The BET plot, using five measurements in the relative pressure range 0.09 - 0.31, gave a surface area of 105.1 $\pm$ 1.2 $m^2 g^{-1}$. The pore size distribution curve, calculated from the desorption isotherm, is shown in Figure VI-18.

VI-I-9 The Adsorbent α-Haematite.

About 2.5 g of α-haematite was outgassed for 12 hours at 125°C before the helium calibration and for 4 hours afterwards at 27°C. The total dead space volume was 5.76 cm^3 of which 4.29 cm^3 was at 77K. The adsorption and desorption results are given in Table VI-14 and the isotherms plotted in Figure VI-19. There is no hysteresis loop. A BET plot, using six measurements in the relative pressure range 0.05 - 0.26 gave a surface area of 2.74 ± 0.4 m^2g^{-1}. A weight loss of 0.12% was found.

VI-2. Discussion.

VI-2-1 Apparatus Standardisation.

The specific surface areas calculated for silica, 164.1 ± 1.4 m^2g^{-1}, and graphite, 10.9 ± 0.4 m^2g^{-1}, agree with the relevant NPL certified specific surface areas. The calculated values are both slightly lower than the quoted areas, although within the limits given for the reference materials. The value for silica is within 1% of the actual area and the value for graphite within 2% of the actual area. The apparatus therefore was considered to be capable of giving reliable results.

VI-2-2 α_s - Plots.

The low specific surface area of the α-haematite sample, 2.74 ± 0.4 m^2g^{-1} and the lack of porosity as evidenced by the identical adsorption and desorption isotherms (fig. VI-19) are in agreement with the manufacturer's claims, and an analysis performed at NPL on a similar batch of ferric oxide. It was decided to use the α-haematite as the non-porous reference

in the construction of α_s-plots for the other materials studied (Chapter II-14). These are given in Figures VI-20, VI-21 and VI-22. Figure VI-20 compares the outgassed ferric oxide A result, with those obtained for the maleic anhydride treated samples. In Figure VI-21 the treated and untreated ferric oxide B plots are given together with the untreated ferric oxide A plot. In Figure VI-22 the plots of the untreated ferric oxides A and B and α- and β-goethite are given.

All the plots show an upward deviation from linearity at about $\alpha_s = 1$ indicative of capillary condensation in mesopores. The α_s-plots for the maleic anhydride treated ferric oxides are similar to the untreated plots, except that the amount adsorbed at any given relative pressure is reduced. There is no evidence that the pore structures have been significantly altered in any way by the treatments.

VI-2-3 Ferric Oxide A and β-Goethite.

Ferric oxide A was found to be porous in agreement with the earlier work of Foster[110]. The adsorption isotherms varied uniformly with outgassing temperature (Figure VI-5). The amount adsorbed at any given relative pressure decreased with temperature and duration of outgassing. The surface areas therefore decreased with decreasing thoroughness of outgassing. The results are listed in Table VI-15. The differences between the areas obtained after outgassing above 100°C most probably arise from sample inhomogeneity. These four areas have a mean area of 245 $m^2 g^{-1}$. It is well established that outgassing at 25°C removes all physically adsorbed water from iron oxides (see Chapter IV-2). Thus

the changes in surface area must arise from changes in the surface hydroxyl concentration. It seems unlikely that the material lost by outgassing above 27°C was bulk water held in pores or strongly bound physically adsorbed water. The surface area would be expected to increase very rapidly with increasing outgassing temperature if this was the case.

Before outgassing, elemental analysis showed about 1.5% by weight of hydrogen was present in the sample. Using a hydroxyl concentration of 5.88 OH per 100Å^2, the weight of hydrogen in a monolayer of hydroxyl groups was estimated for 1 g of oxide. Subtraction of this quantity from the total hydrogen content yielded the amount of hydrogen in physically adsorbed water. The sample was calculated to consist of 15.5% by weight of hydroxyl groups and physically adsorbed water. 11.7% was water, corresponding to about 2 monolayers. A weight loss of 12.7% for outgassing above 100°C therefore indicates the removal of about 6.5% of the total hydroxyl coverage. This small hydroxyl loss is in accord with expectations, since the complete desorption of the hydroxyl layer requires prolonged outgassing at temperatures in excess of 100°C for porous iron oxides.

Crystallographically, ferric oxide A is predominantly β-goethite. However, the adsorption isotherm and pore size distribution are different from the reference sample of β-goethite. The distribution curves (Figs. VI-4, VI-18) are sketched in Figure VI-23 for comparison. Ferric oxide A has a narrow distribution of pore radii with a maximum at

about $\bar{r}_p$ = 25Å. The distribution for β-goethite is broad, with a slight maximum in the range $\bar{r}_p$ = 70-80Å. The surface area of β-goethite is less than half of the value for ferric oxide A. The differences in surface properties of two crystallographically similar samples must arise from differences in their preparation and the presence of impurities in the ferric oxide A. This material contains minor quantities of other phases together with some amorphous material and about 4% by weight of chloride ions. It is unclear whether this chloride is inherent in the structure, unreacted ferric chloride or precipitated sodium chloride. Gallagher[125] has found that the structure of β-goethite initially precipitated from the hydrolysis of $Fe(111)Cl_3$ has a molecular formula approximating to $FeO_{1-\frac{1}{4}}.(OH)_{1+\frac{1}{4}}.\frac{1}{4}Cl$, which corresponds to about 9% by weight of chloride. The structure was very sensitive to the thoroughness of washing in distilled water and hence to the degree of hydration. A mean pore radius of about 12Å was found for β-FeO.OH. This is much lower than the mean pore radii found in this work. A value of 1.6% by weight of hydrogen was found by elemental analysis for β-goethite used in this work. Assuming the formula $FeO.OH.\ nH_2O$ this corresponds to n = 0.2. It is probable that the removal of the chloride from the ferric oxide and further drying of both the oxide A and β-goethite might result in better agreement of their surface properties.

VI-2-4 Ferric Oxide B and α-Goethite.

Crystallographically the porous ferric oxide B

is predominantly α-goethite. The surface properties of ferric oxide B and α-goethite are, however, quite different. Ferric oxide B has a surface area of 158 m^2g^{-1} compared to 112 m^2g^{-1} for α-goethite. The pore size distribution curves (Figs, VI-12, VI-16) are sketched in Figure VI-24 for comparison. The curves for α-goethite are similar to that of ferric oxide A, although there is some doubt as to their validity owing to inter-particle condensation. The cumulative internal pore areas obtained in the calculation (using the adsorption isotherm) of the α-goethite distributions are all much higher than the BET surface area. The pore area calculated, using relative pressures in the range 0.79 - 0.30, is the nearest at about 125 m^2g^{-1}. This suggests that inter-particle condensation started at about P/P_o = 0.79. For all the other samples studied, the distribution was calculated using the desorption isotherm, and stopping the calculation at about the point where the hysteresis loop closed, gave a cumulative pore area approximately equal to the BET surface area. Hence, for all the other samples, other than α-goethite, it is reasonable to conclude that the BET surface area consists almost entirely of the interior surface area of pores with little or no contribution from plane surfaces.

Elemental analysis found 2.94% and 1.26% hydrogen by weight for α-goethite and ferric oxide B respectively. Using the same procedures as in VI-2-3, n in $FeO.OHnH_2O$ was calculated as about 1.1 for α-goethite. Ferric oxide B was found to consist of 12.4% by weight of hydroxyl groups and physically adsorbed water, giving about 2.5 monolayers of molecular water.

VI-2-5 The Maleic Anhydride Treated Ferric Oxide A.

The elemental analyses in Tables VI-7a,7b indicate that the bulk composition of ferric oxide A was altered by the maleic anhydride treatment and that outgassing the sample does not remove all the organic material. Assuming uniform adsorption and an occupied area per adsorbed maleic anhydride molecule of 2.6×10^{-19} m^{-2},[186] a coverage of 0.63 of a monolayer was calculated from the carbon content before outgassing. If it is also assumed that the adsorption occurs over the hydroxyl monolayer (which is not displaced), then the amount of physically adsorbed water present is related to the difference between the total hydrogen content (before outgassing) and the hydrogen associated with the organic and hydroxyl layers. This argument shows that the organic treatment removes about half of the previously adsorbed water.

Comparison of the infra-red spectra of the treated and untreated samples in the region 3500-2500 cm^{-1} (Figure VI-10) shows that the broad spectrum is decreased in intensity by the organic treatment. This broad band is attributed to surface hydroxyl groups and adsorbed water. The breadth of the band arises from intermolecular bonding (i.e. H-bonds). The loss of intensity suggests that some of the physically adsorbed water and possibly loosely bound hydroxyl groups have been displaced by the maleic anhydride treatment.

The effect of outgassing is to increase the percentage carbon content and decrease the hydrogen content. Since the samples outgassed at both 50°C and 130°C both lost weight during the outgassing, this suggests that the organic material was preferentially retained relative to

the water content. From the actual weight loss for the sample outgassed at 130 °C, and the carbon contents before and after outgassing, the hydrogen weight loss associated with desorption of maleic anhydride was calculated (< 0.1 mg). This quantity was subtracted from the total weight loss of hydrogen to yield the weight loss due to desorption of water and hydroxyl groups. Assuming no desorption of surface hydroxyls, then the observed weight loss requires only one quarter of the physically adsorbed water to desorb. About 90 times as many water molecules desorbed as did maleic anhydride molecules. A similar calculation for the sample outgassed at 50 °C showed no changes in the numbers of organic molecules desorbing. The reduction in temperature, however, caused the number of water molecules desorbing to drop by half. These calculations are based on the assumption that the maleic anhydride was uniformly distributed throughout the sample. Given this, it appears that increasing the severity of outgassing only effects the water coverage, simply causing more water to desorb.

The specific surface areas of the untreated and treated oxides outgassed at 50 °C and 130 °C are collected in Table VI-15. The surface areas of the treated samples are less than those of the untreated samples irrespective of temperature. The treated sample outgassed at 130 °C has an area of about 91% of the untreated sample outgassed at 27 °C for the minimum length of time (S_w = 222 $m^2 g^{-1}$). Hence the surface area of ferric oxide A has been altered by the maleic anhydride treatment.

From the above, the difference in the surface areas of the treated samples (25 $m^2 g^{-1}$) arises principally from differences in the physically adsorbed water content. The actual

figure is 5.4×10^{20} molecules per gram of sample. The area occupied by a water molecule lies in the range 10.6 - 14.8 $\mathring{A}^2$, from which the observed surface area difference is of the same order of magnitude as the calculated difference. Using $A(H_2O)$ = 12.7 $\mathring{A}^2$, the calculated figure is about 2.5 times the observed difference of 25 m^2.

The pore size distribution curves of the untreated ferric oxide and the maleic anhydride treated samples outgassed at 50°C and 130°C are redrawn in Figure VI-25 for comparison. The minor differences between the treated curves are probably not significant. The maxima for the treated samples are both at lower mean pore radii than the untreated samples maximum. The "untreated" distribution has the smallest range, centred around 25 - 30$\mathring{A}^2$. If the maleic anhydride was adsorbed uniformly over the surface, it would be expected that the "treated" distributions would become sharper than the untreated distribution and that the effect would be more pronounced at small mean pore radii. This is not observed. The only effect of the organic treatment appears to be a reduction in the number of pores in the range $\bar{r}_p$ = 25 - 30Å; this suggests preferential adsorption in or close to those pores. It is possible that, given the small coverage of organic material, the differences in the distribution curves are artificial and independent of the organic treatment.

The infra-red spectra of treated samples before and after outgassing,(Figure VI-10) show a triplet characteristic of anhydrides in the range 1600 - 1300 cm^{-1} which is unchanged by the outgassing.

The treatment of ferric oxide A with maleic anhydride clearly alters the nitrogen adsorption properties of the bulk powder and the infra-red spectra. It is, however, impossible to determine if the maleic anhydride is evenly dispersed throughout the sample (i.e. uniformly adsorbed). It is possible that the organic material is present as solid crystals or adsorbed "non-uniformly" in small clusters on the surface. Some preliminary electron microscopy was inconclusive on this point.

VI-2-6 The Maleic Anhydride Treated Ferric Oxide B.

The elemental analyses in Table VI-11 indicate that the bulk composition of ferric oxide B was altered by the maleic anhydride treatment and that some organic material remained after outgassing. Using the same procedure as before, (VI-2-5) an organic coverage of 0.65 of a monolayer was calculated from the carbon content before outgassing, compared to 0.63 for ferric oxide A. About half of the physically adsorbed water was lost as a result of the treatment. Infra-red spectra of ferric oxide B before and after the organic treatment showed the same effect in the region of 3500 - 2500 cm^{-1} as ferric oxide A (Figure VI-10), again suggesting a reduction in the water content of the sample.

Outgassing has no effect on the proportion of carbon present; however, since a small (0.5%) weight loss was found, it follows that a small amount of organic material was lost. The weight loss is less than that found for ferric oxide A outgassed under the same conditions (2.5% at 50 °C). About ten times as many water molecules (H_2O)

desorbed as did maleic anhydride molecules per unit area of surface, compared with the equivalent ratio of about 40 for ferric oxide A. Both oxides lose more water than maleic anhydride. Ferric oxide A loses about 2.5 times as much organic material and 10 times as much water as feric oxide B, and hence has the larger overall weight loss.

The pore size distribution curves of the treated and untreated (outgassed 127°C) samples are redrawn in Figure VI-26 . There are no significant differences between them. Both curves are broad, with no predominant pore size. The treated ferric oxide B has a surface area of 135.7 m^2g^{-1} compared to 158.5 m^2g^{-1} for the untreated sample. Compared to ferric oxide A, the reduction in surface area is not so great as a result of treatment. Infra-red spectra indicate that organic material is present before and after outgassing.

The maleic anhydride treatment has thus altered certain of the properties of ferric oxide B. It is, however, uncertain if these effects are real surface effects or not. Preliminary electron microscopy experiments failed to provide conclusive evidence.

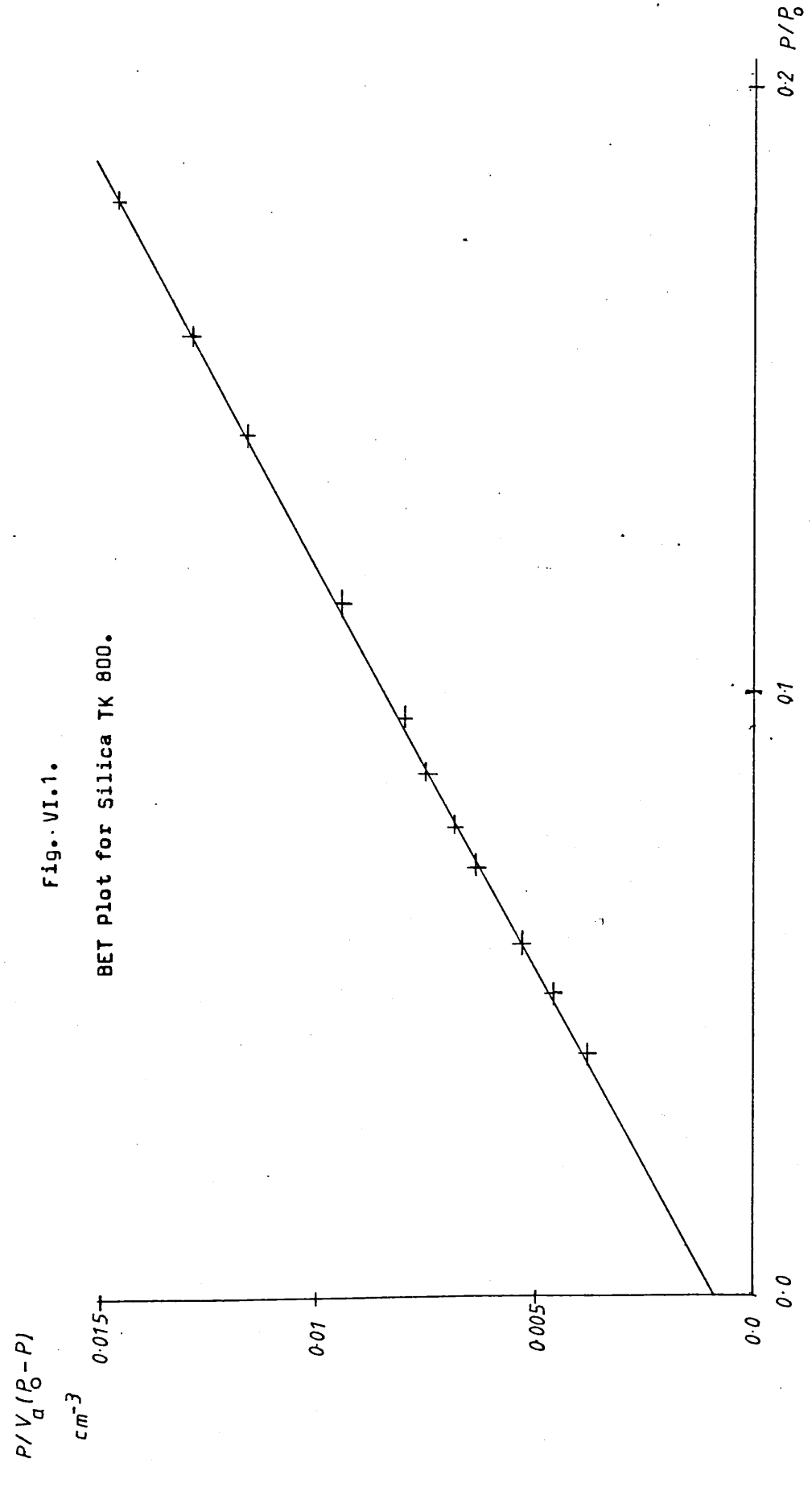

Fig. VI.1.

BET plot for Silica TK 800.

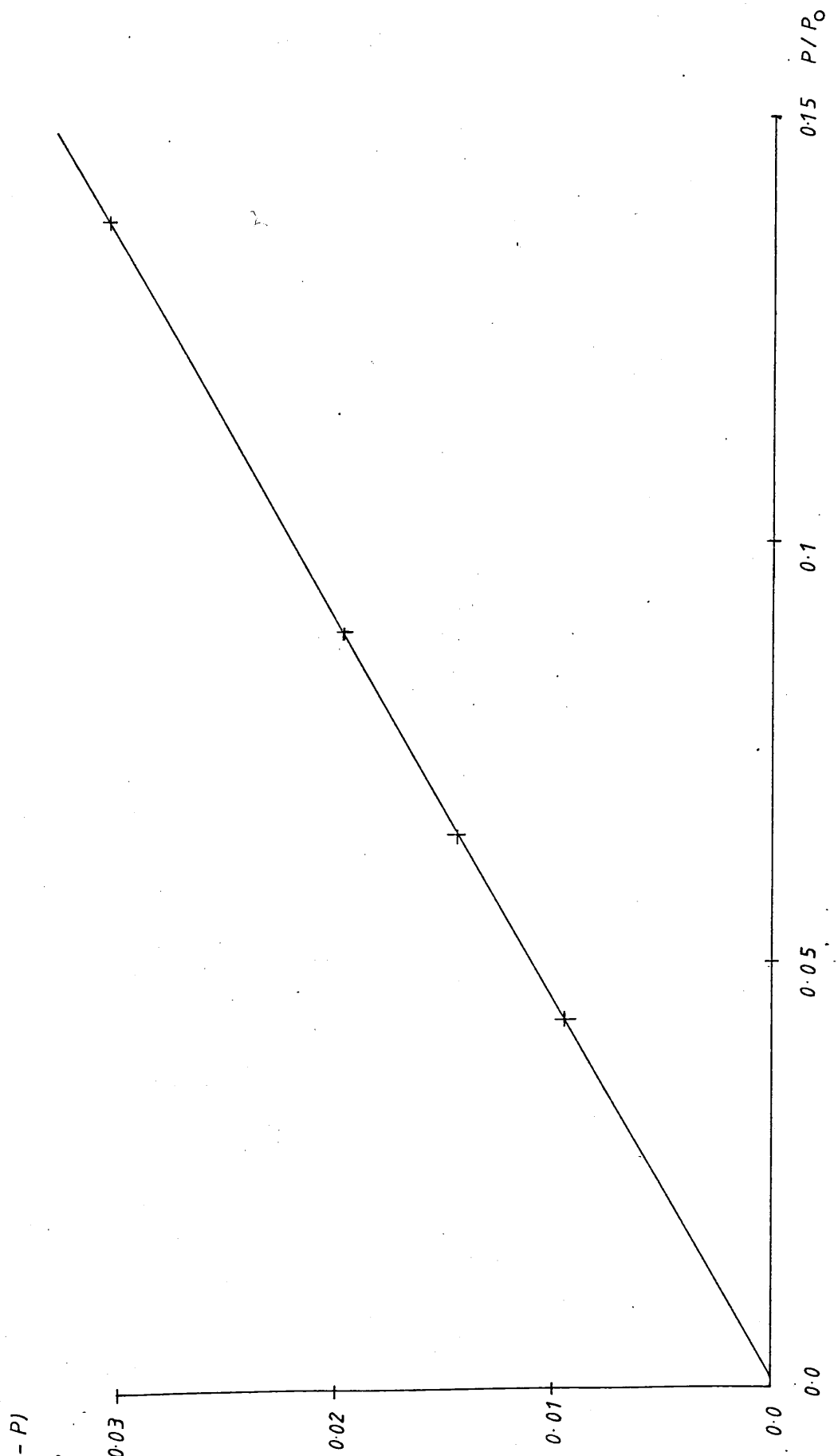

FIG. VI.2. The BET for Sterling FT-G2700.

FIG. VI.3.

Nitrogen adsorption and desorption isotherms on ferric oxide A at 77K.

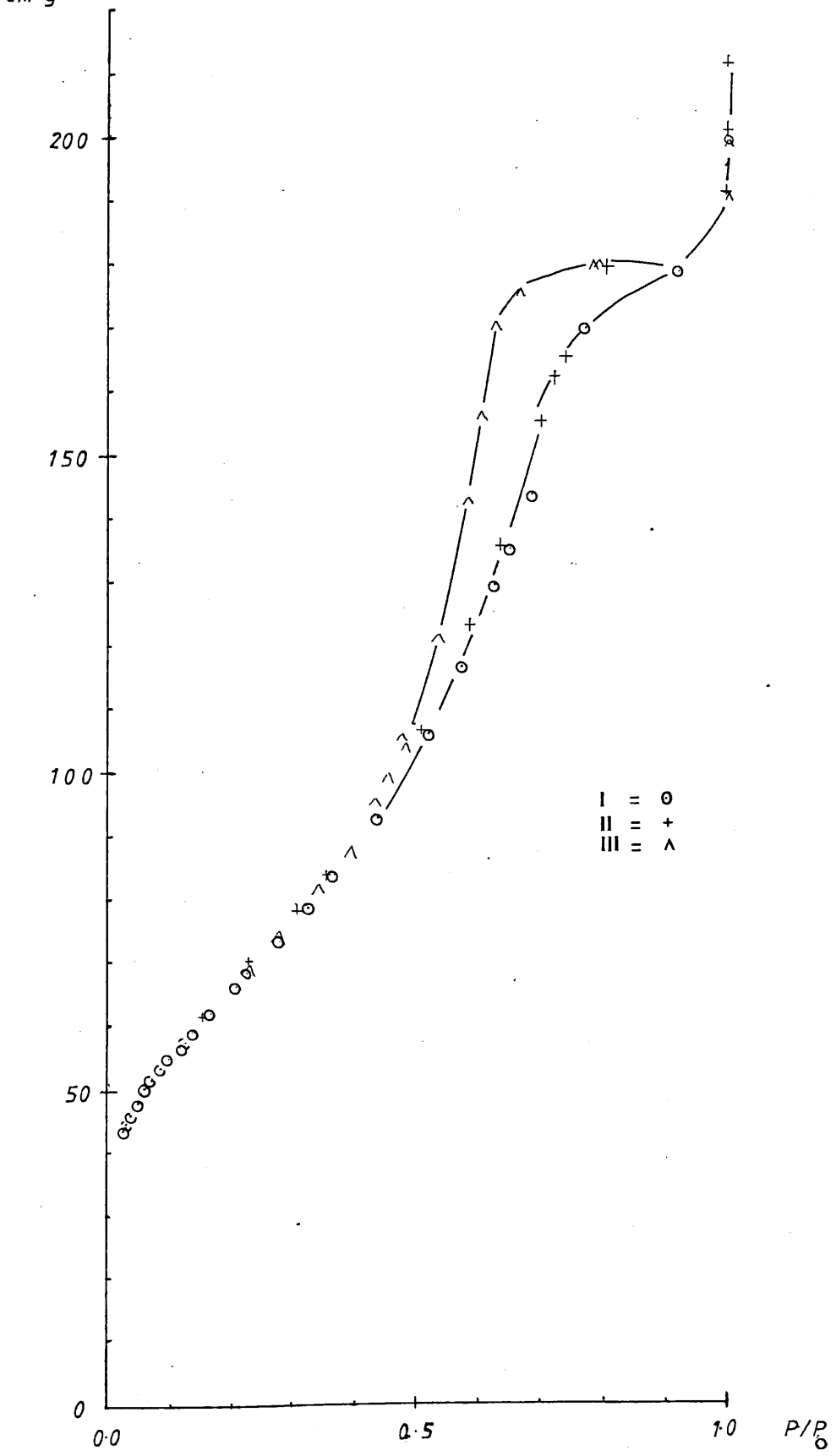

FIG. VI.4.

The pore size distribution plot for ferric oxide A.

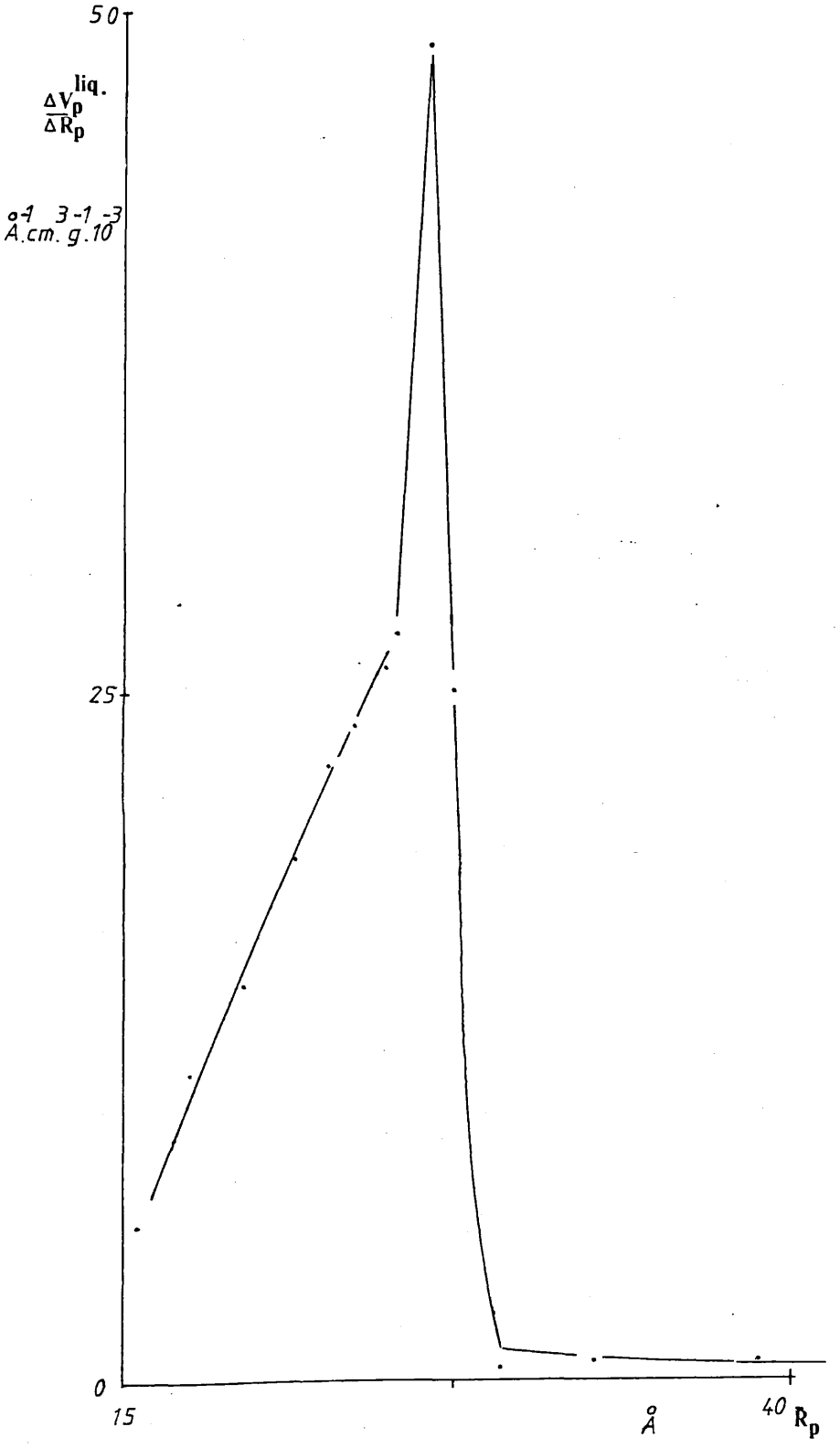

FIG. VI.5.

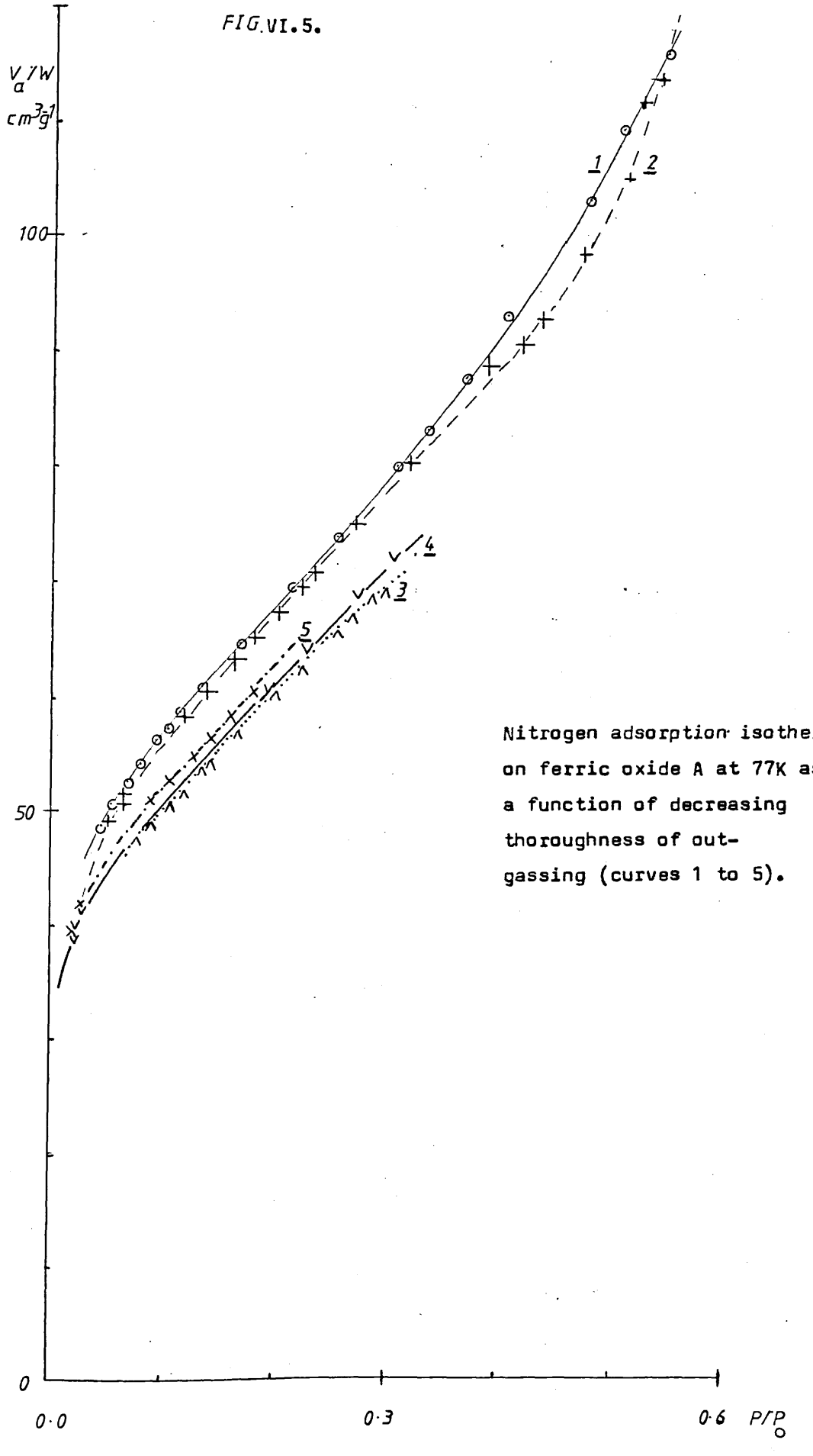

Nitrogen adsorption isotherms on ferric oxide A at 77K as a function of decreasing thoroughness of out-gassing (curves 1 to 5).

FIG. VI.6.

The nitrogen adsorption and desorption isotherms, measured at 77K, on the maleic anhydride treated ferric oxide A, outgassed at 50°C.

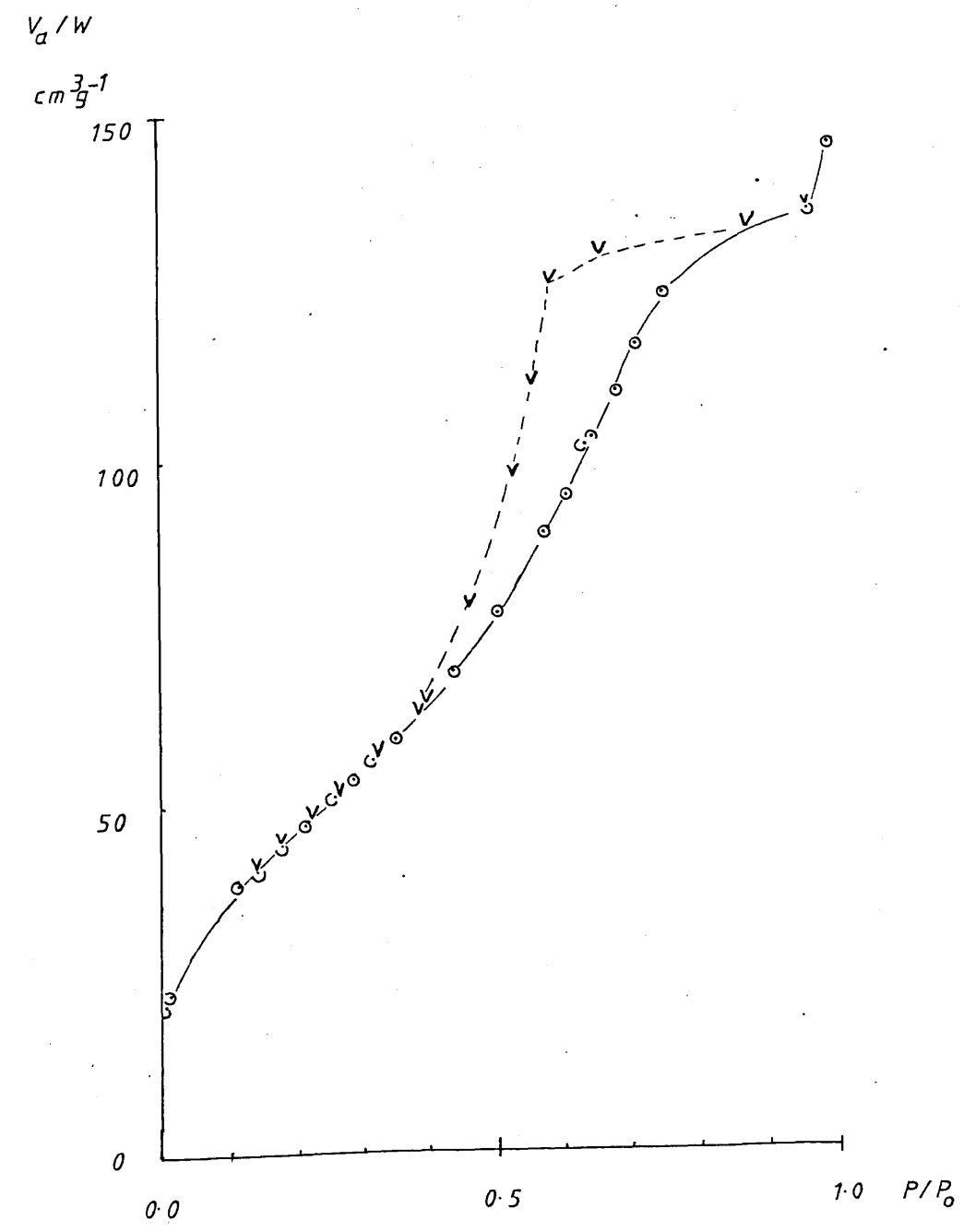

FIG. VI.7.

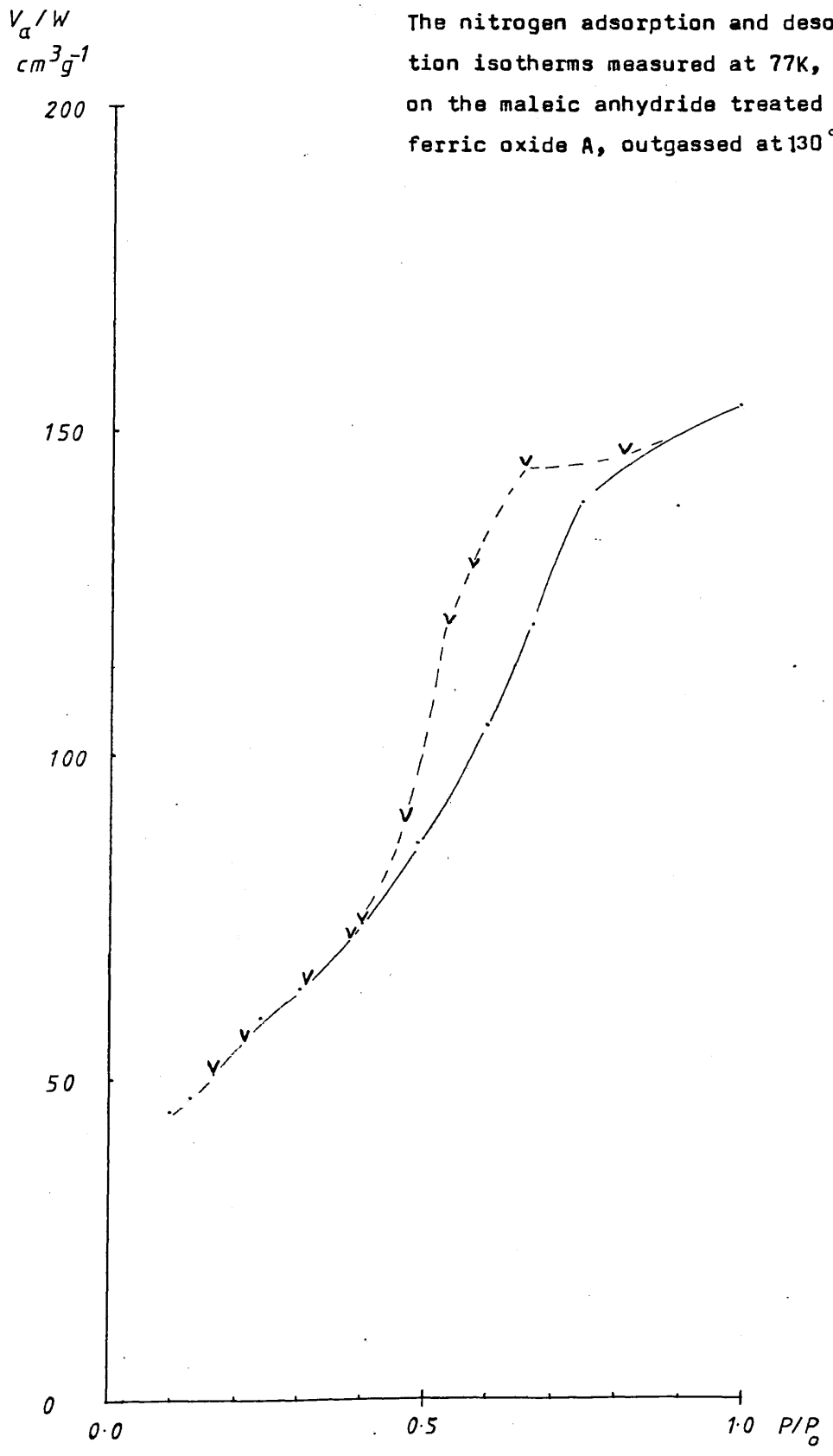

The nitrogen adsorption and desorption isotherms measured at 77K, on the maleic anhydride treated ferric oxide A, outgassed at 130 °C.

FIG. VI.8.

The pore size distribution plots of the maleic anhydride treated ferric oxide A, outgassed at 50°C (I) and outgassed at 130°C (II).

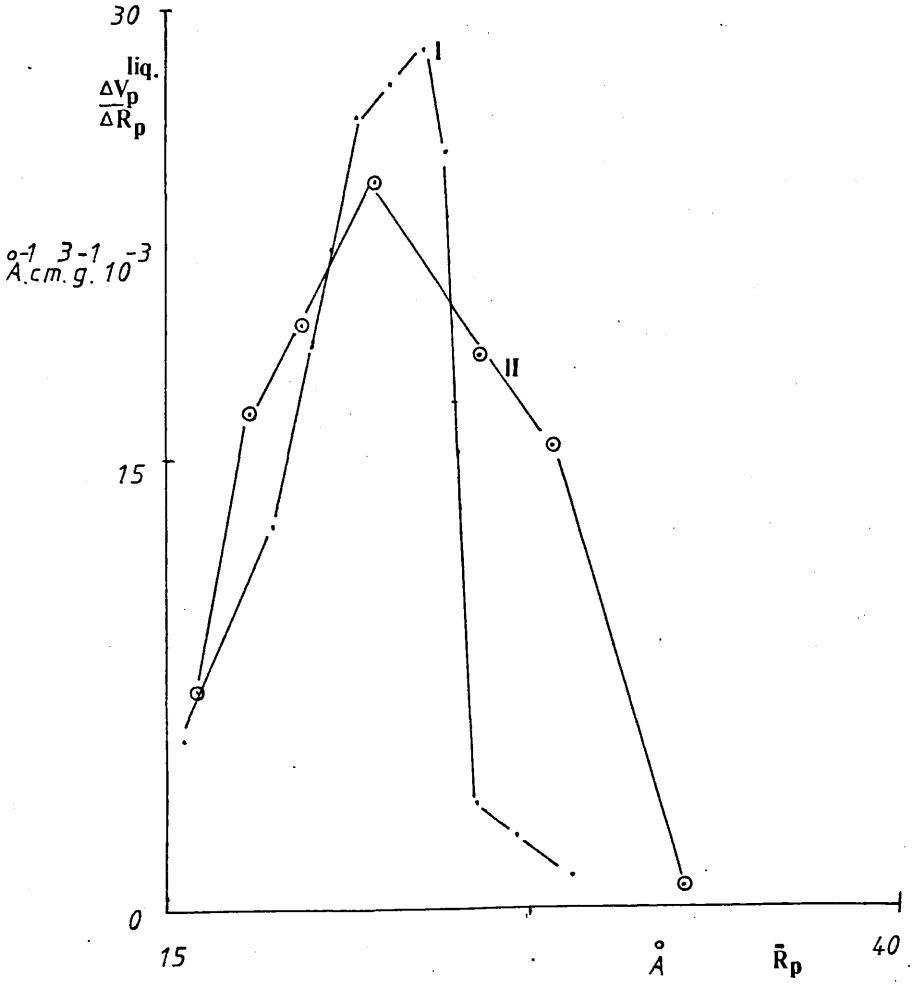

FIG.VI.9.

A comparison of the infra-red spectra of the maleic anhydride treated ferric oxide A before I and II after outgassing using an untreated sample as the reference.

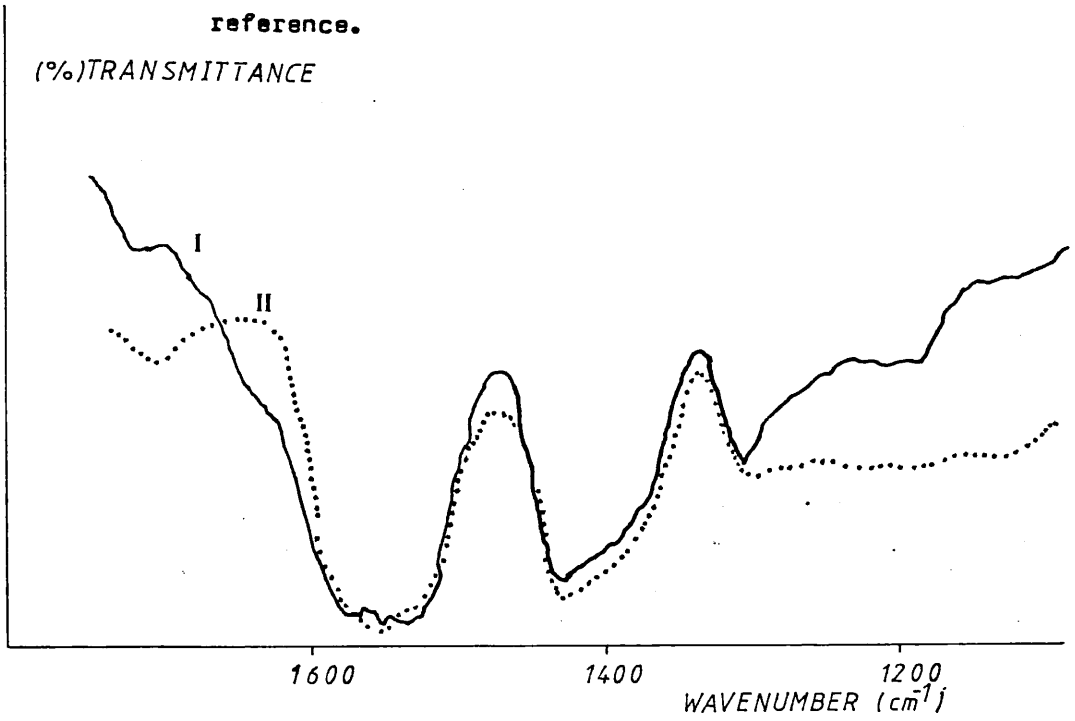

FIG.VI.10.

A comparison of the infra-red spectra of the maleic anhydride treated ferric oxide A (I) and the untreated sample(II) in the region of hydroxyl adsorption.

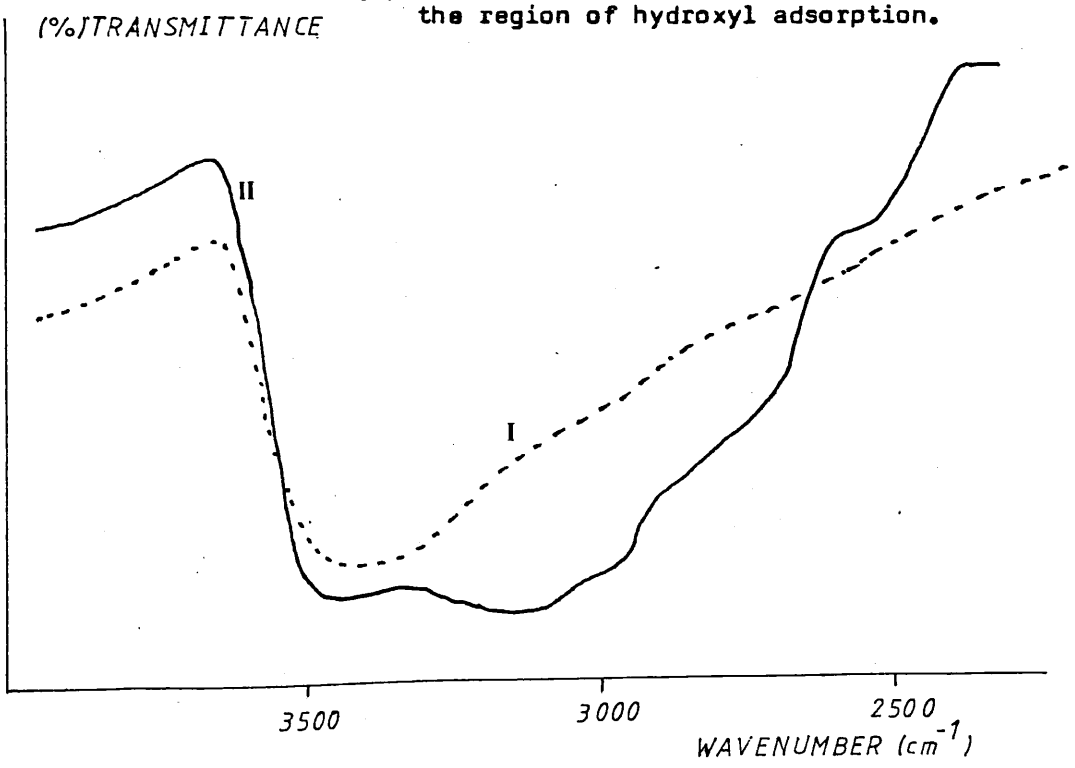

FIG. **VI.11.**

The nitrogen adsorption and desorption isotherms on ferric oxide B at 77K.

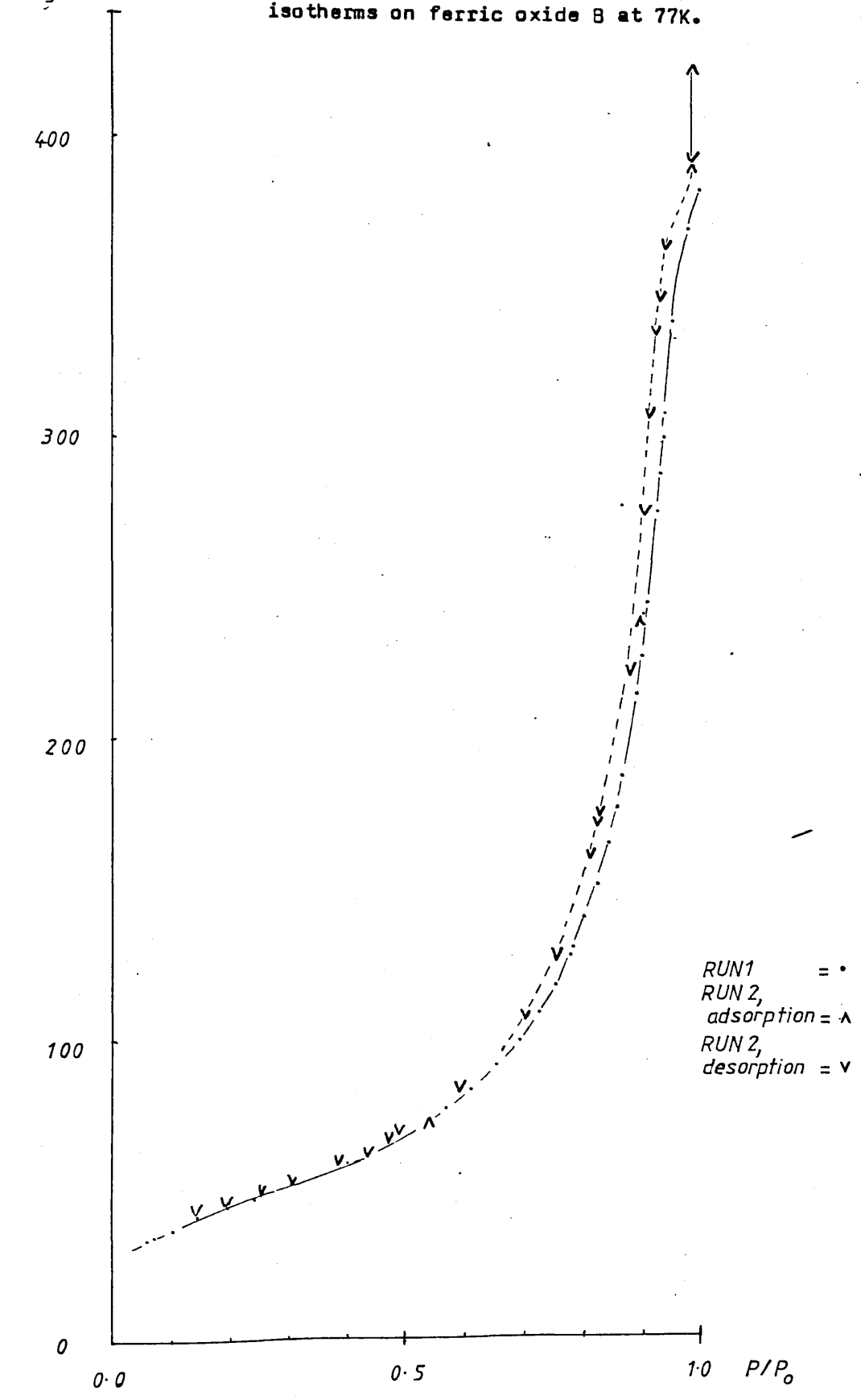

FIG. **VI.12.**

The pore size distribution plot for ferric oxide B.

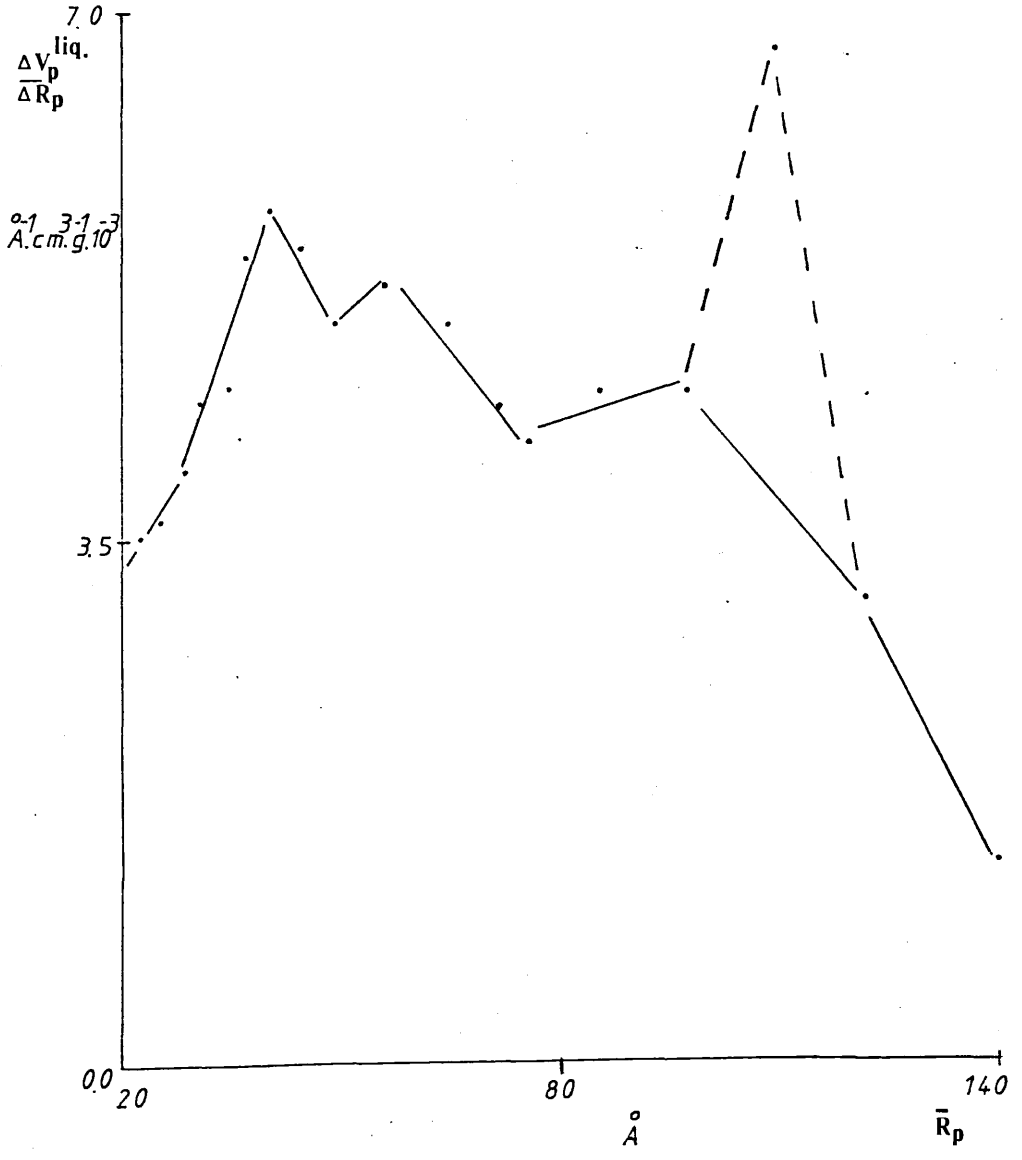

FIG. VI.13.

The adsorption and desorption isotherms measured at 77K, on the maleic anhydride treated ferric oxide B outgassed at 50 °C.

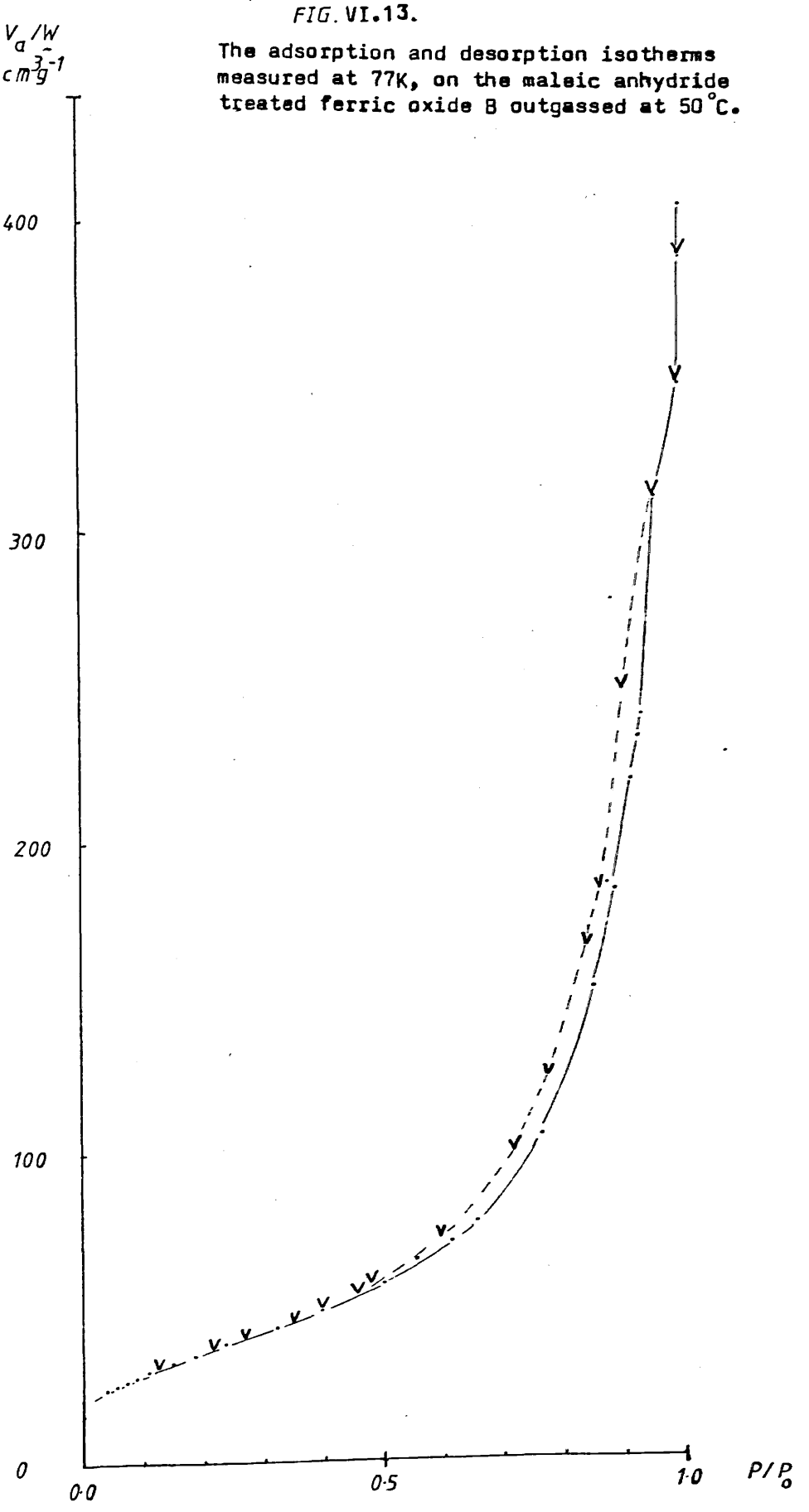

FIG. **VI.14.**

The pore size distribution plot of the maleic anhydride treated ferric oxide B outgassed at 50°C.

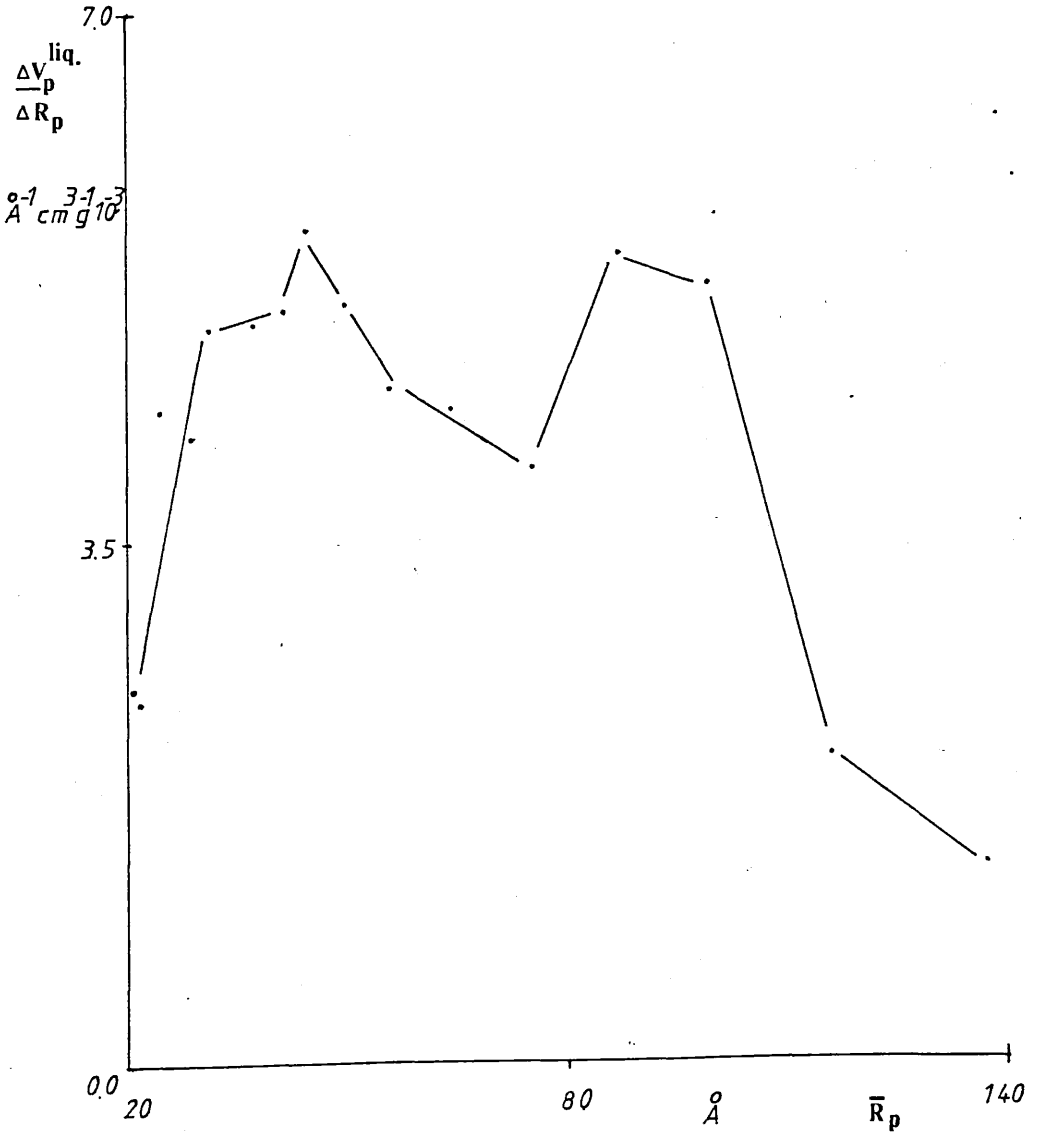

FIG. VI.15.

Nitrogen adsorption and desorption isotherms on α-goethite at 77K.

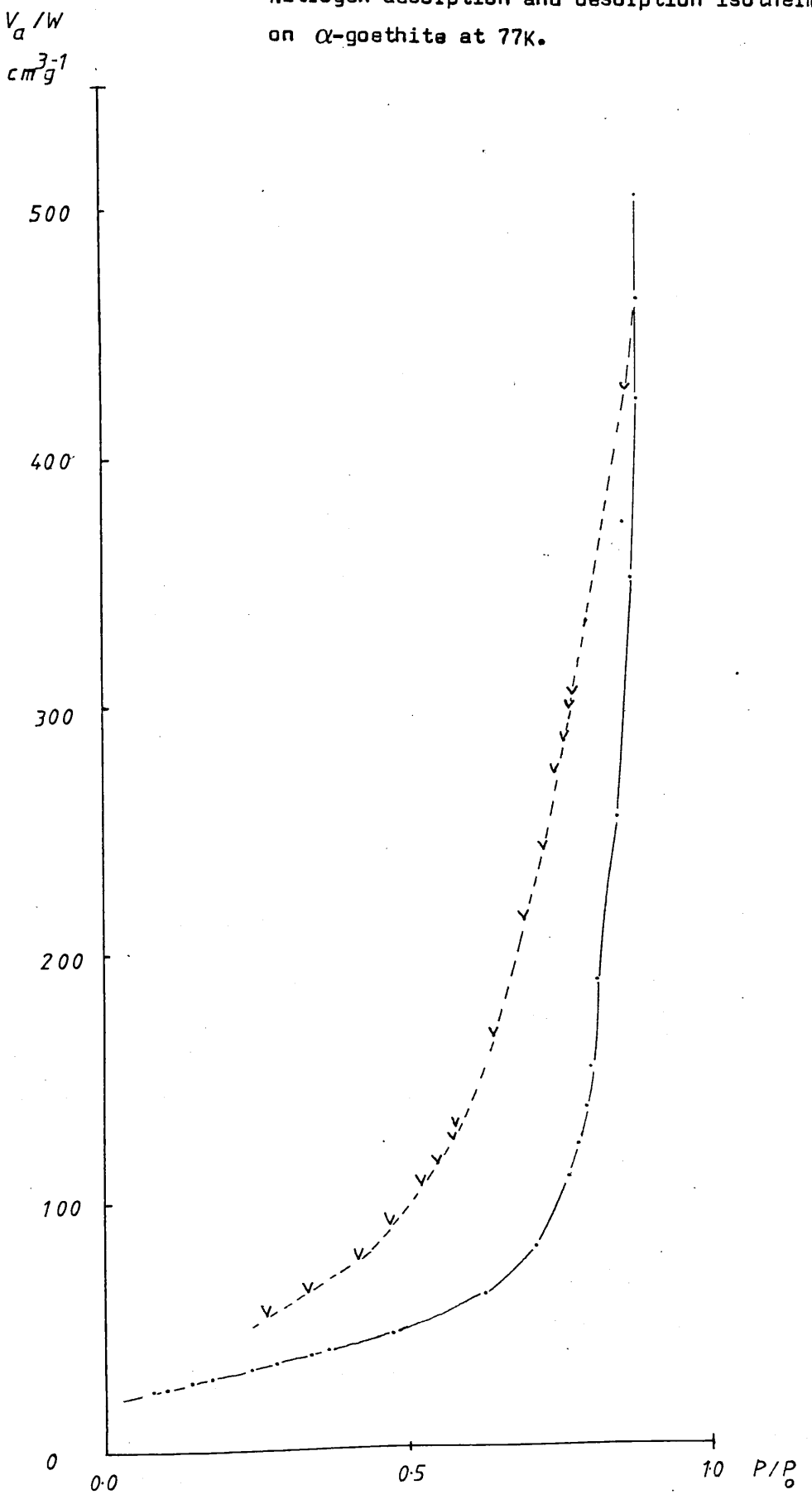

FIG. VI.16.

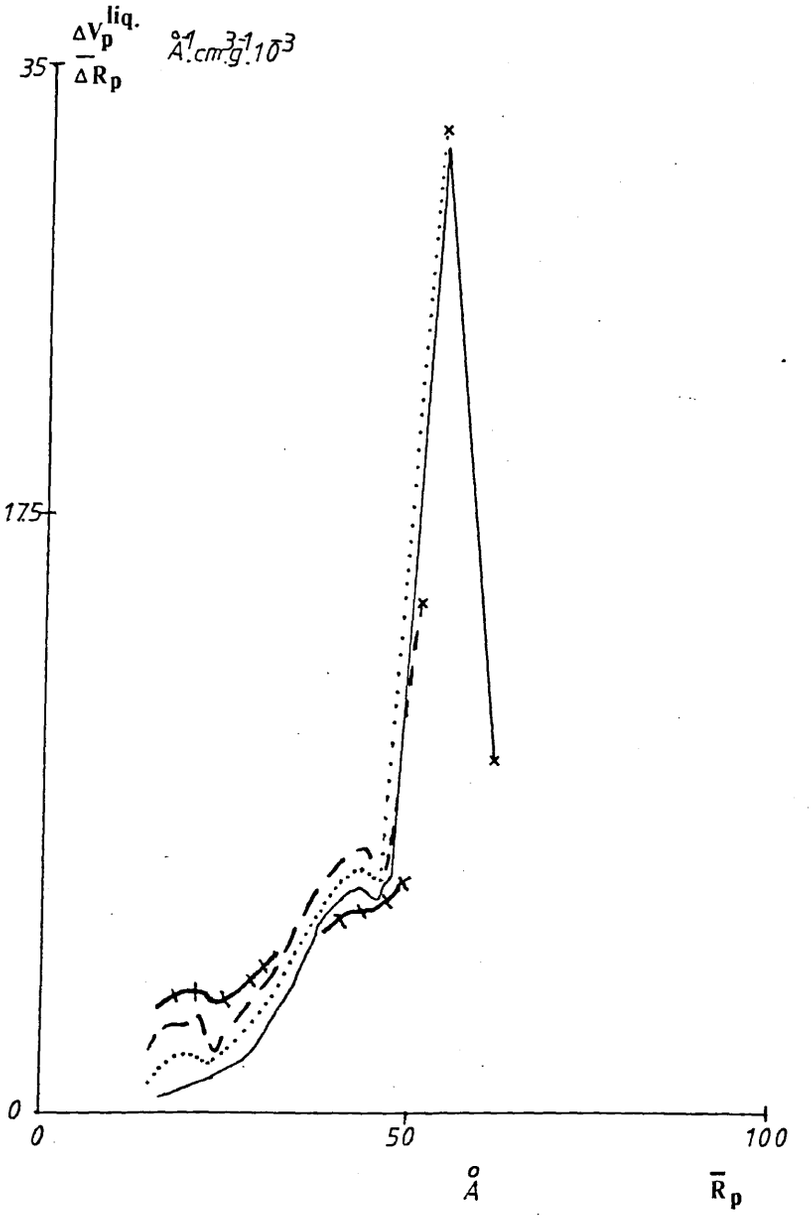

Pore size distribution plots for α-goethite derived from the adsorption isotherm, starting with relative pressures of 0.85, 0.81, 0.8 and 0.79.

FIG. VI.17.

Nitrogen adsorption and desorption isotherms on β-goethite at 77K.

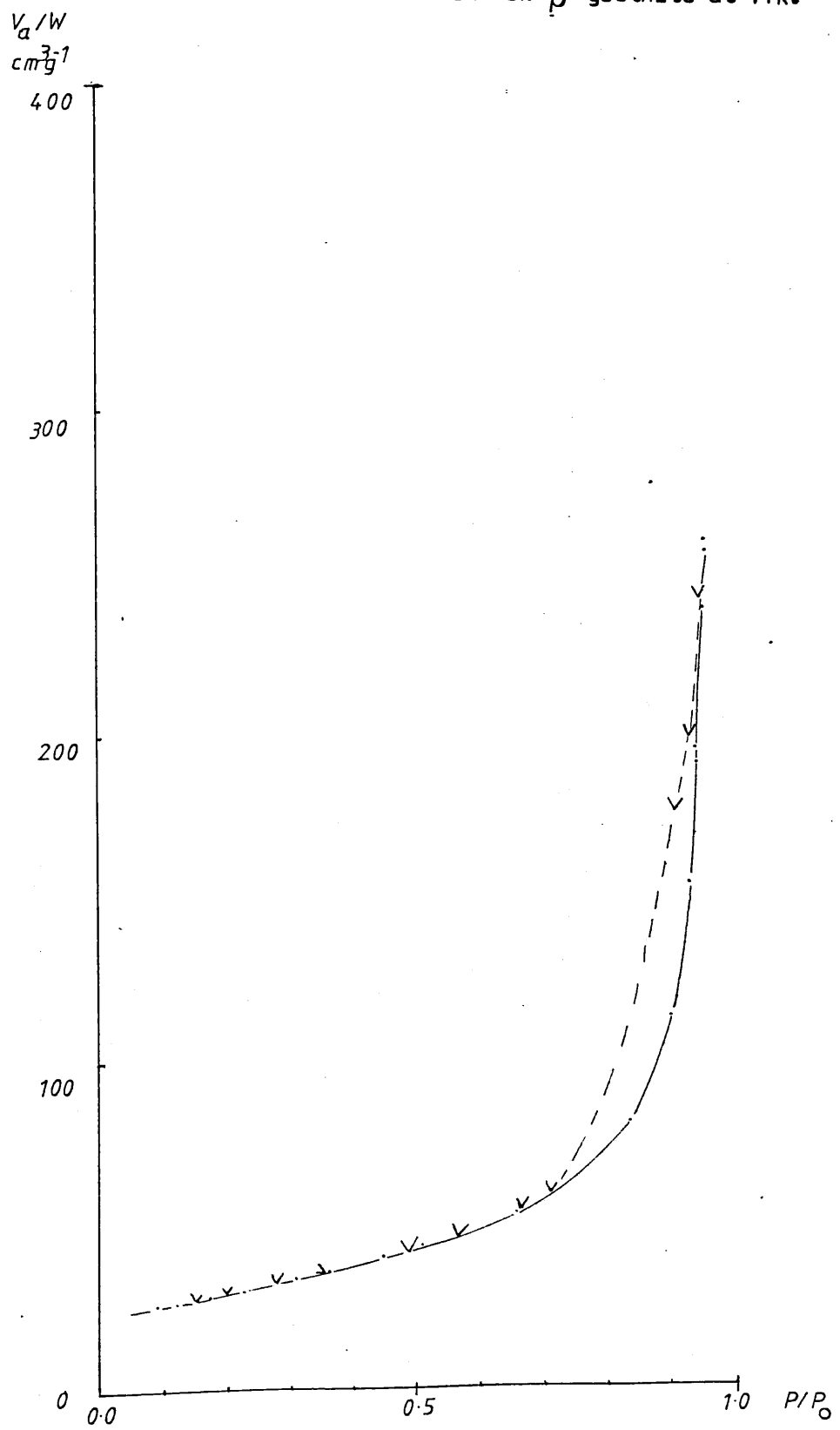

FIG. VI.18.

Pore size distribution plot for β-geothite.

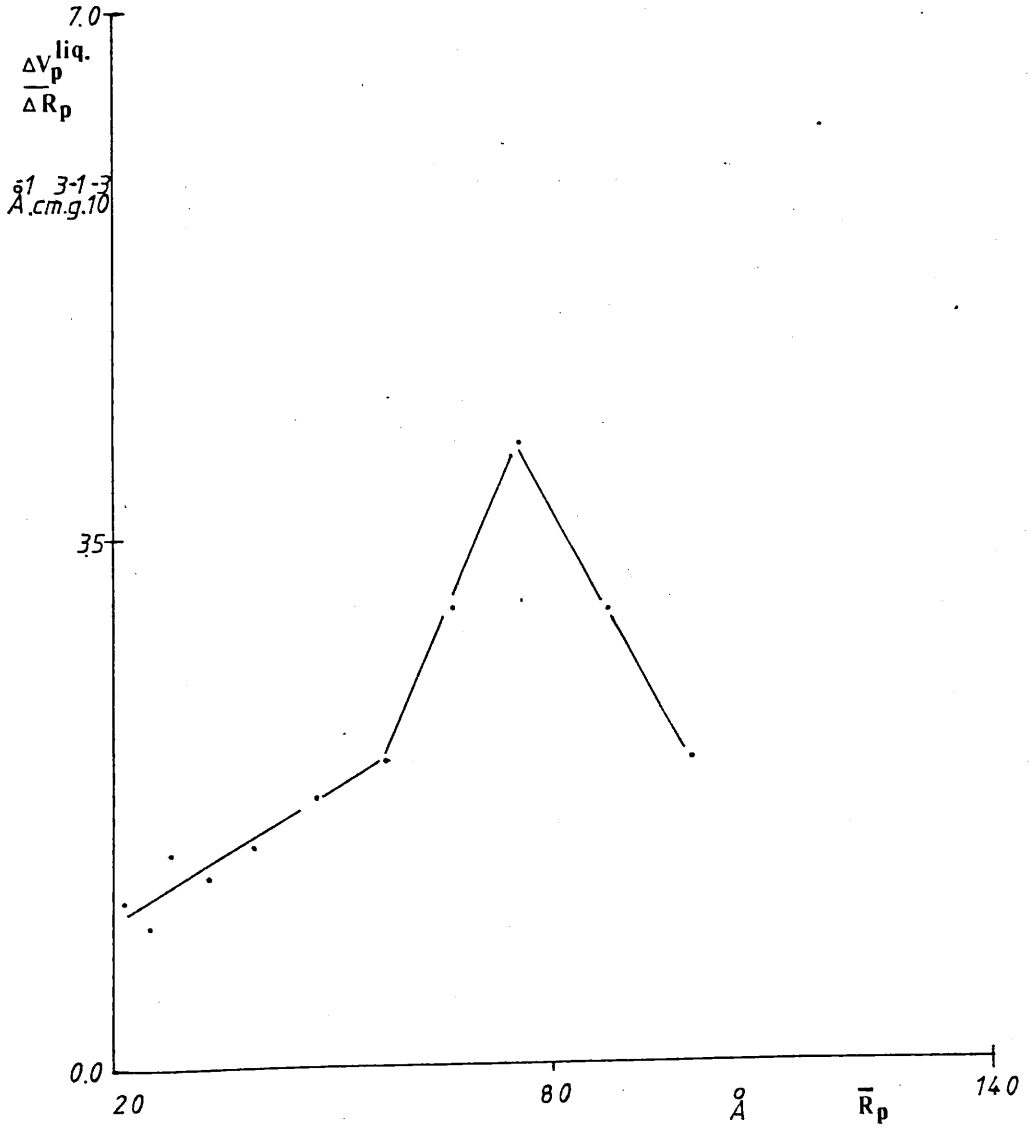

FIG. VI.19.

Adsorption and desorption isotherms

Adsorption (.) and desorption (V) isotherms on α-haematite at 77K.

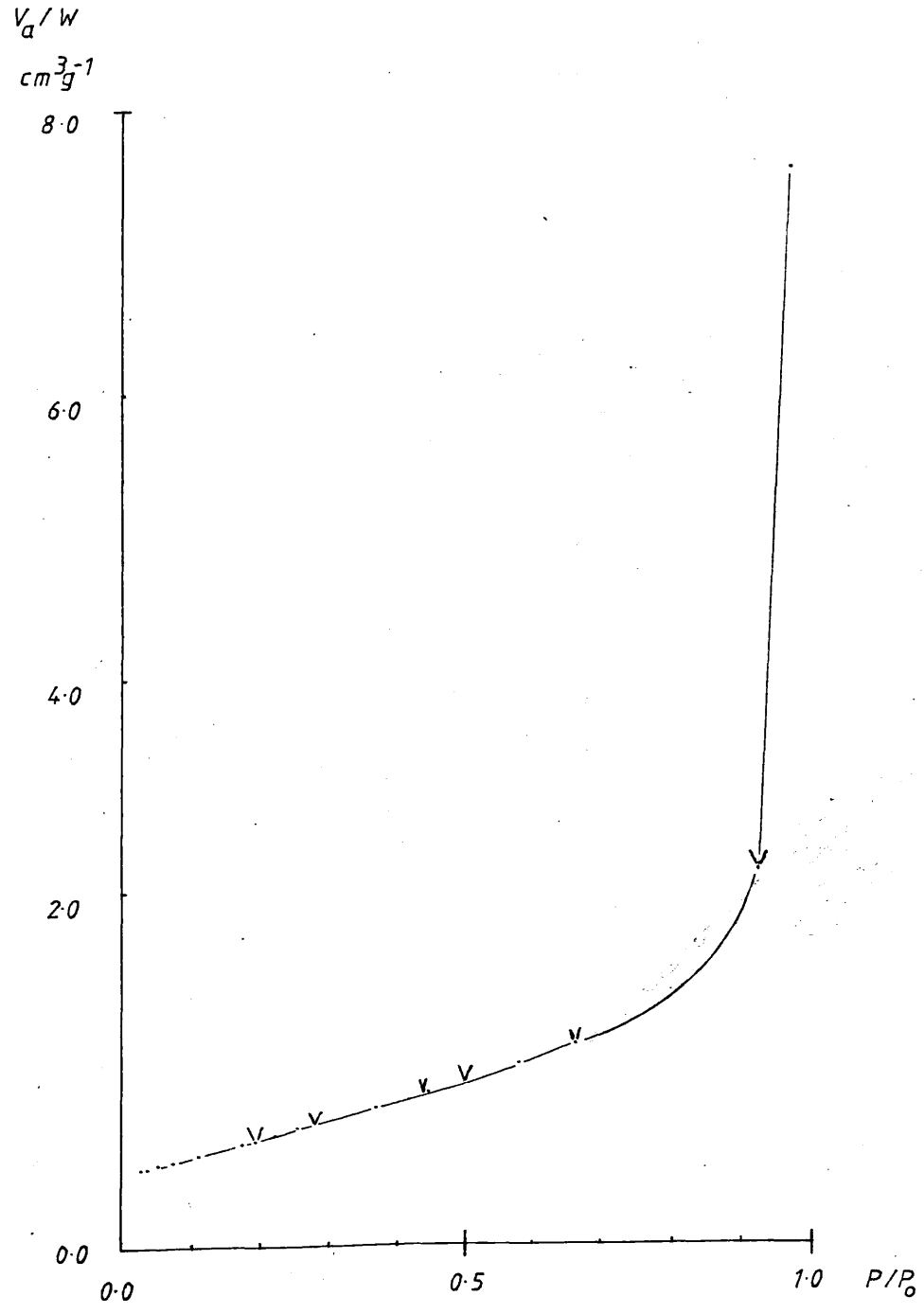

FIG. VI-20.

α_s-plots of ferric oxide A.
Runs 1 and 2 (curves 1) and the
treated samples outgassed at 130°C
(curve 2) and 50°C (curve 3)

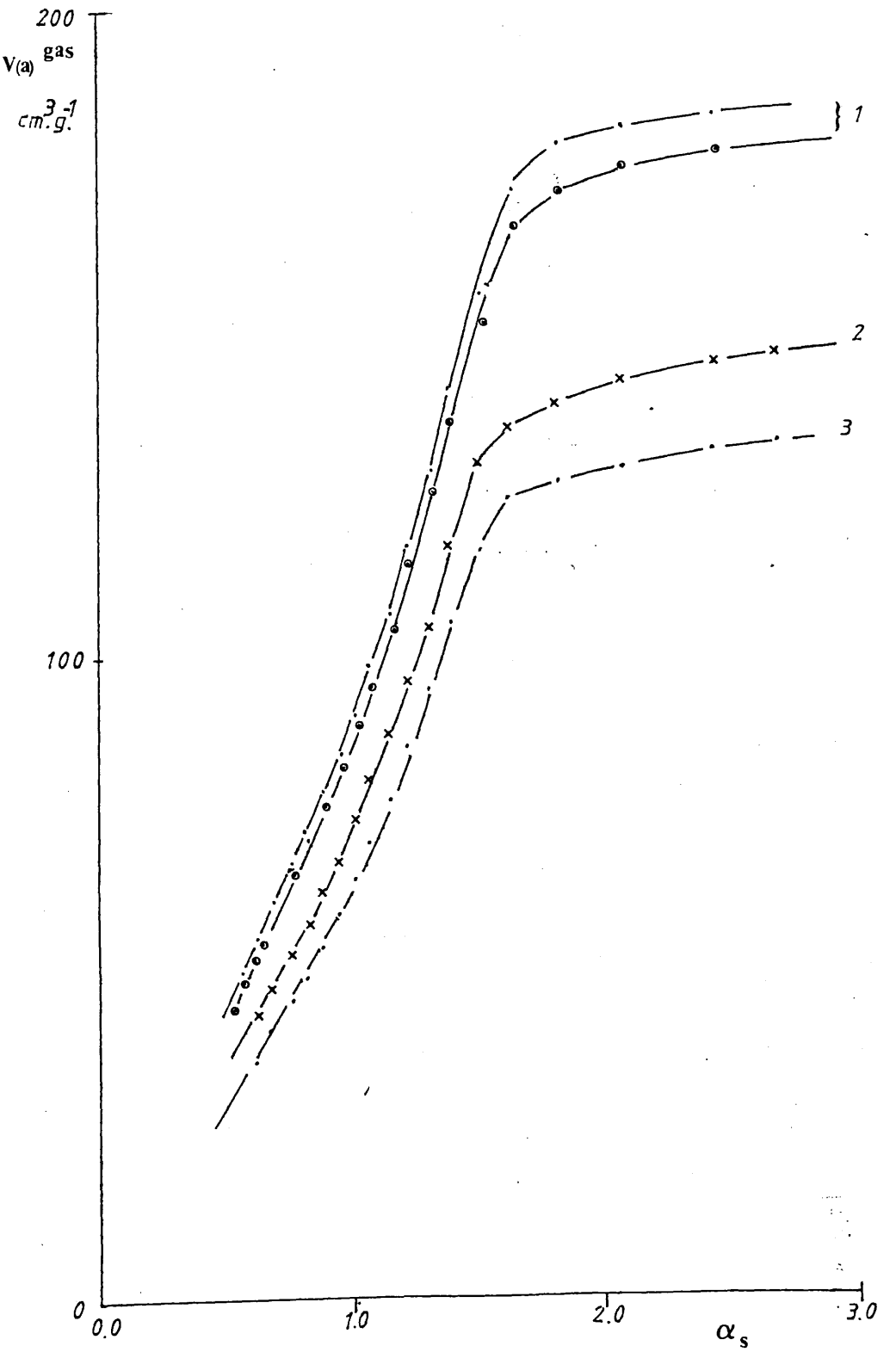

FIG. VI.21.

α_s- plots of ferric oxide B, "treated" (1), "untreated" (2) and ferric oxide A, "untreated" (3).

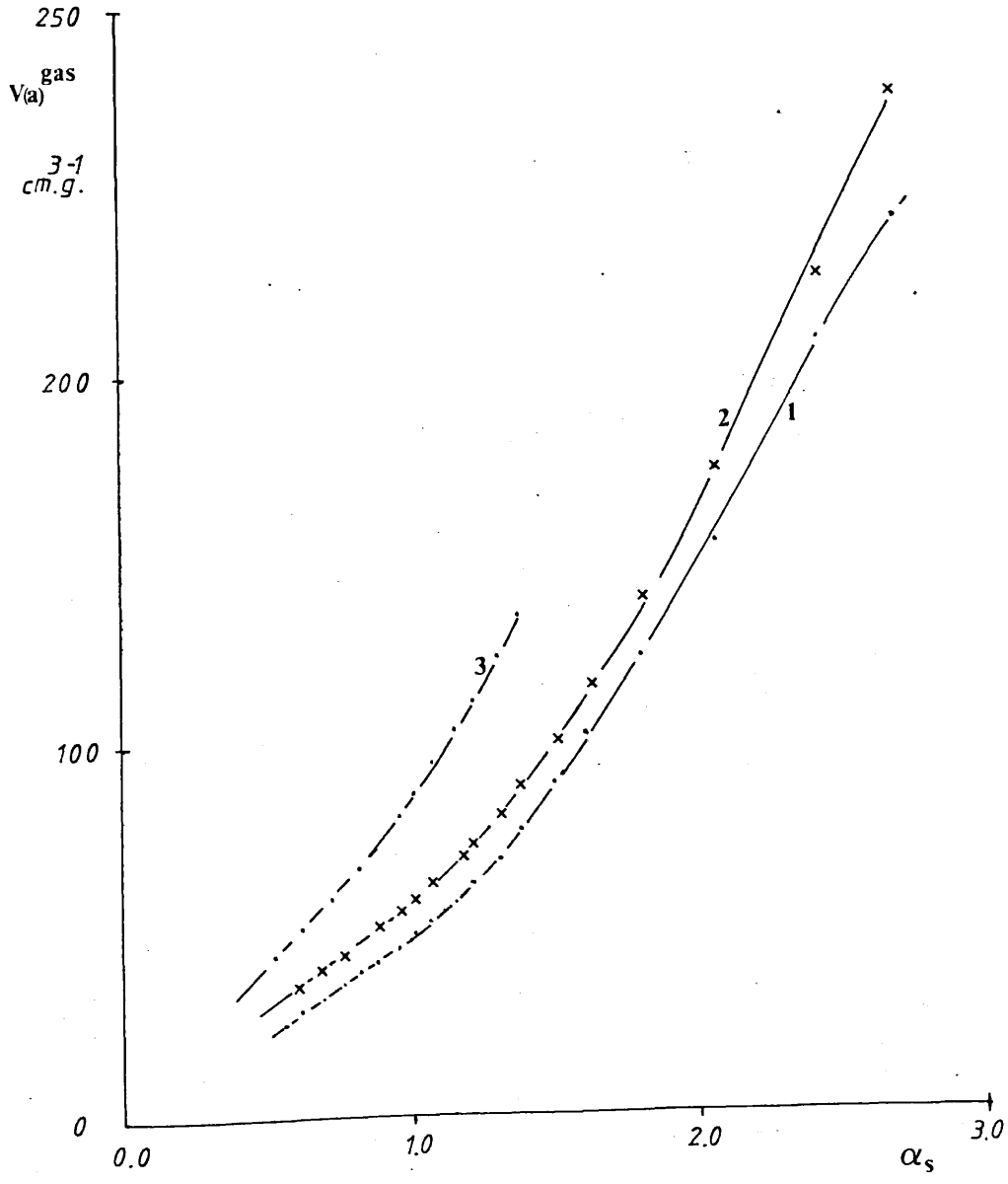

FIG. VI.22.

α_s- plots of ferric oxide A (1), ferric oxide B (2), α-goethite (3), and β-goethite (4).

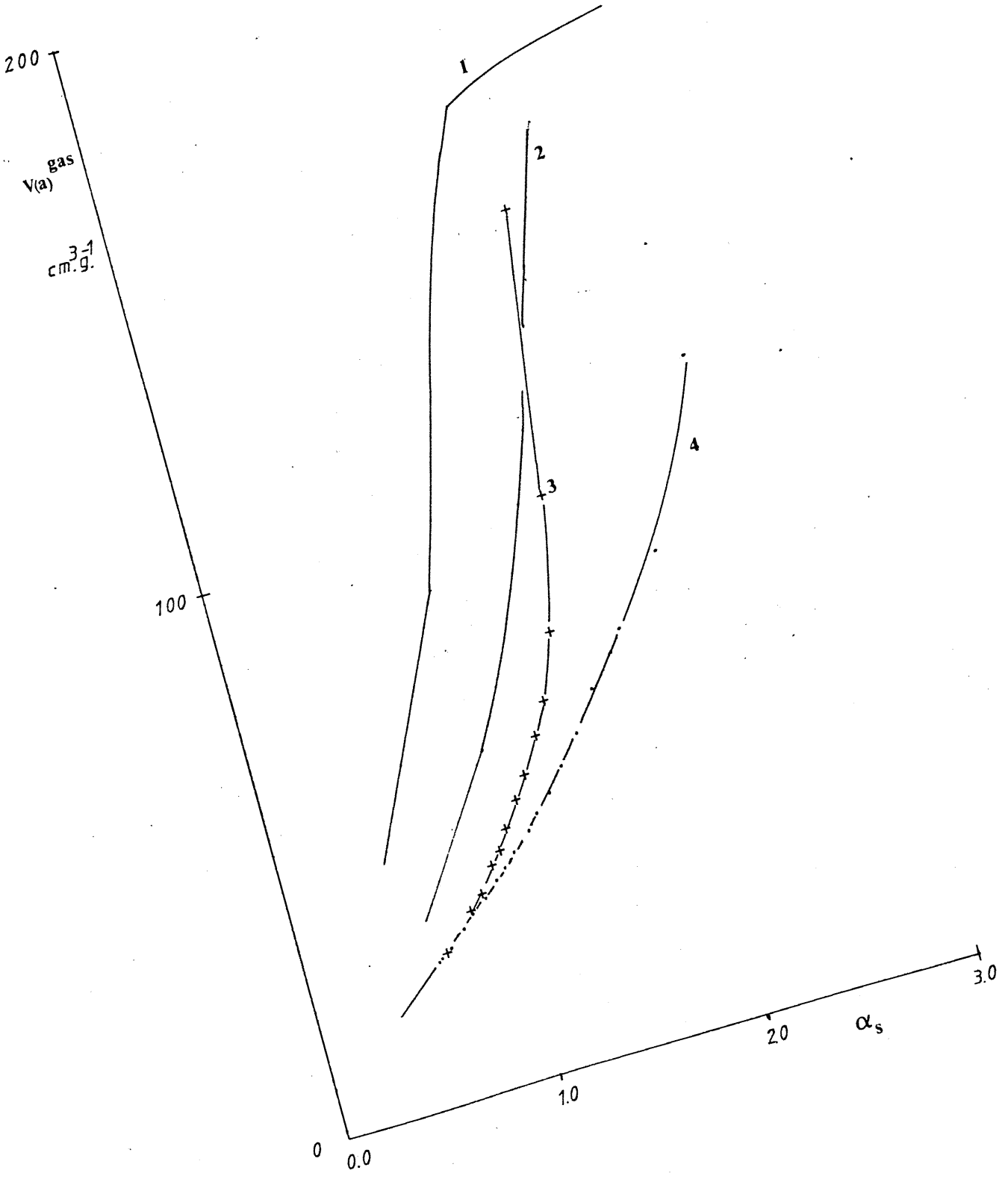

FIG. VI.23.

The pore size distribution plots of ferric oxide A (1) and β-goethite (2)

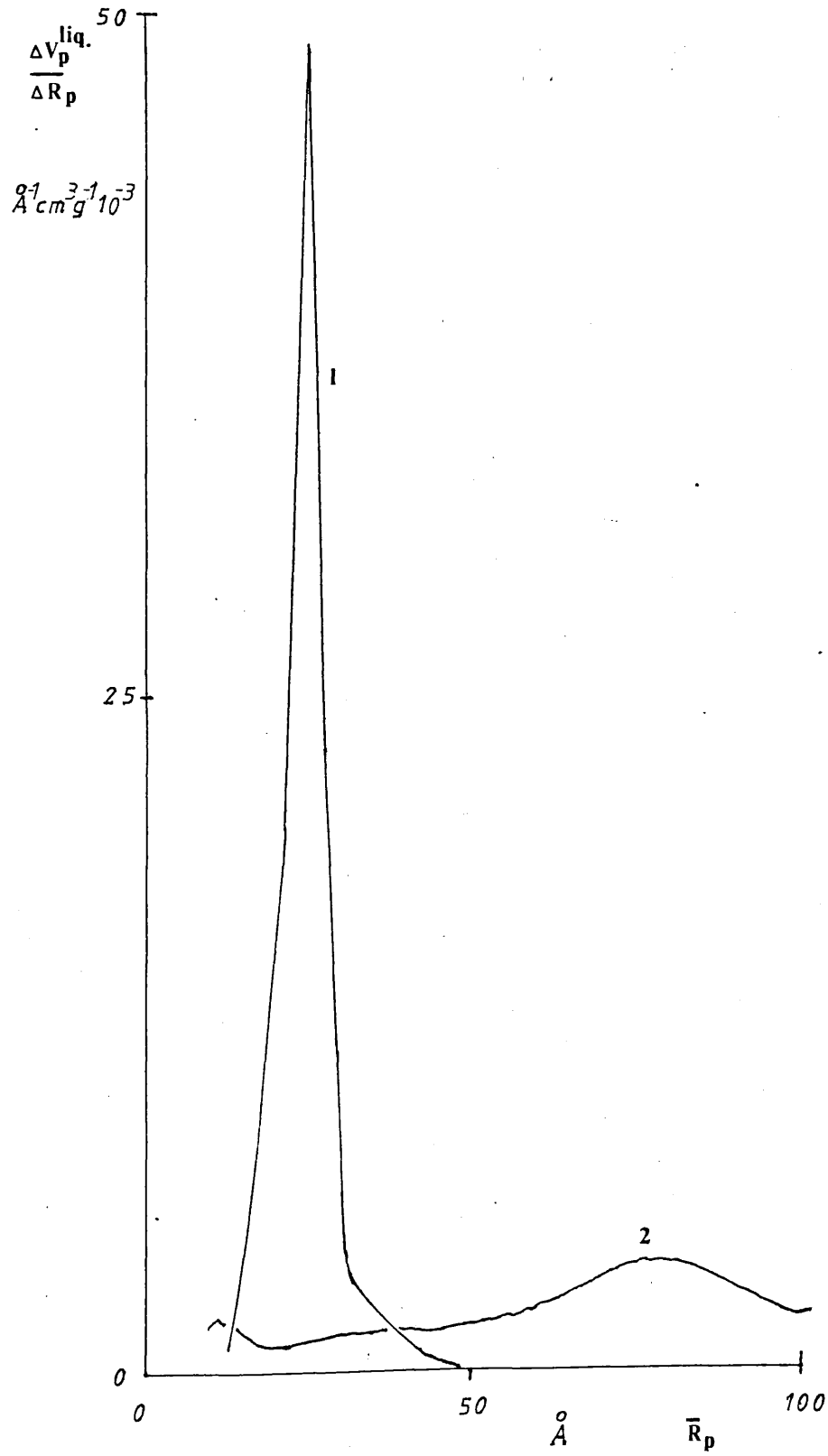

FIG. VI.24.

The pore size distribution plots of α-goethite (1), and ferric oxide B (2).

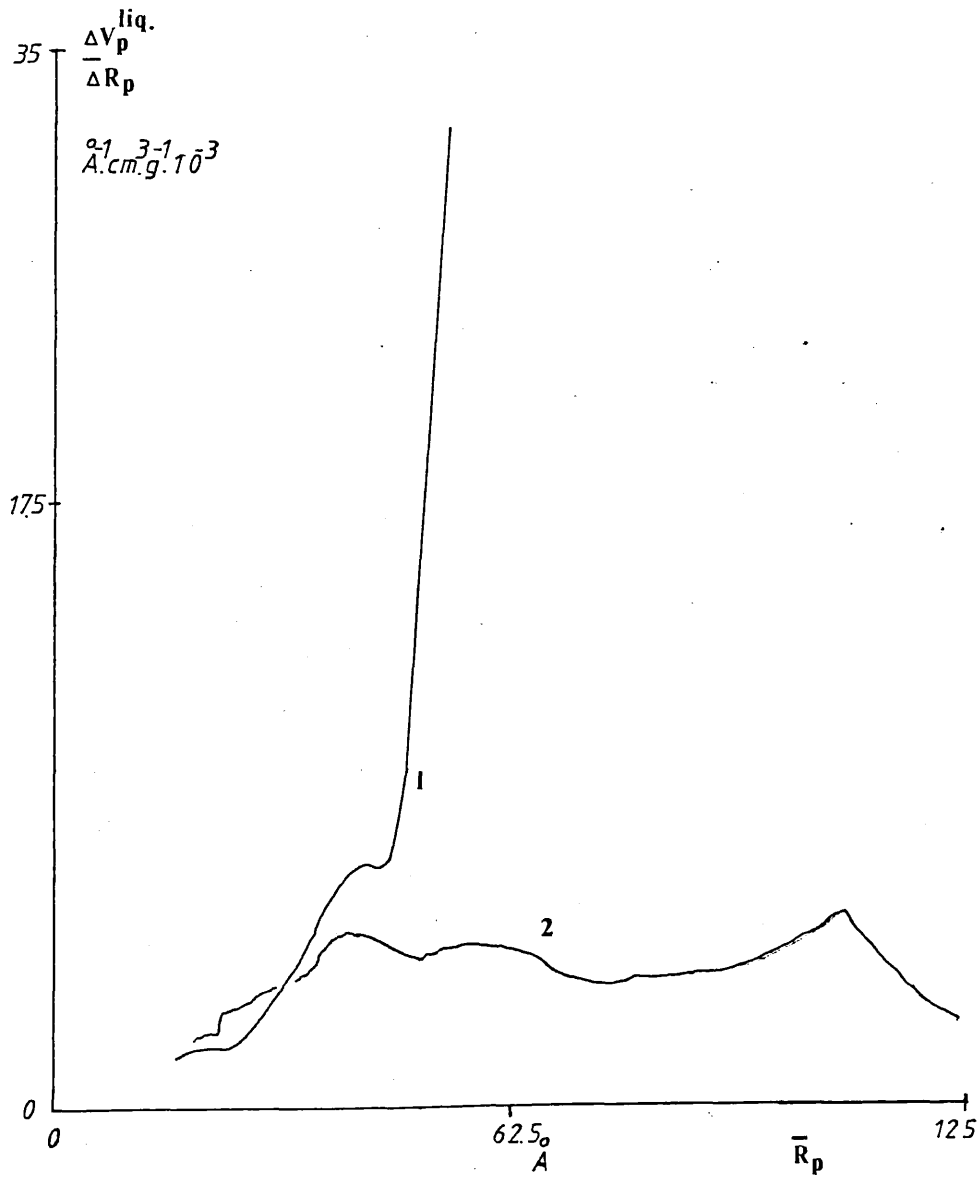

FIG. VI.25.

The pore size distribution plots of ferric oxide A: "untreated" (1), "treated" and outgassed at 50°C (3) and 130°C (2).

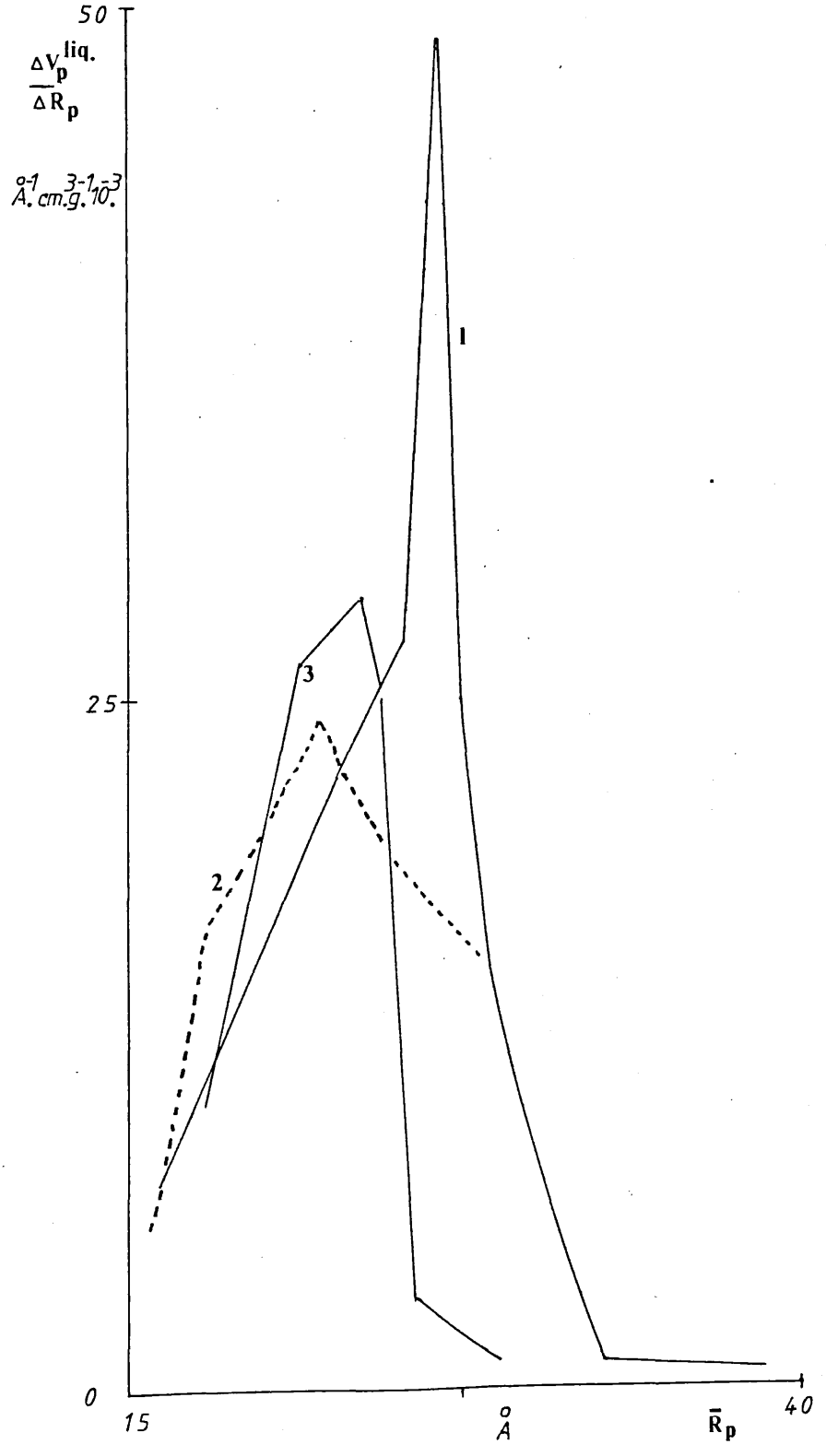

FIG.VI.26.

The pore size distribution plots of ferric oxide
B: "untreated" (1), "treated" (2).

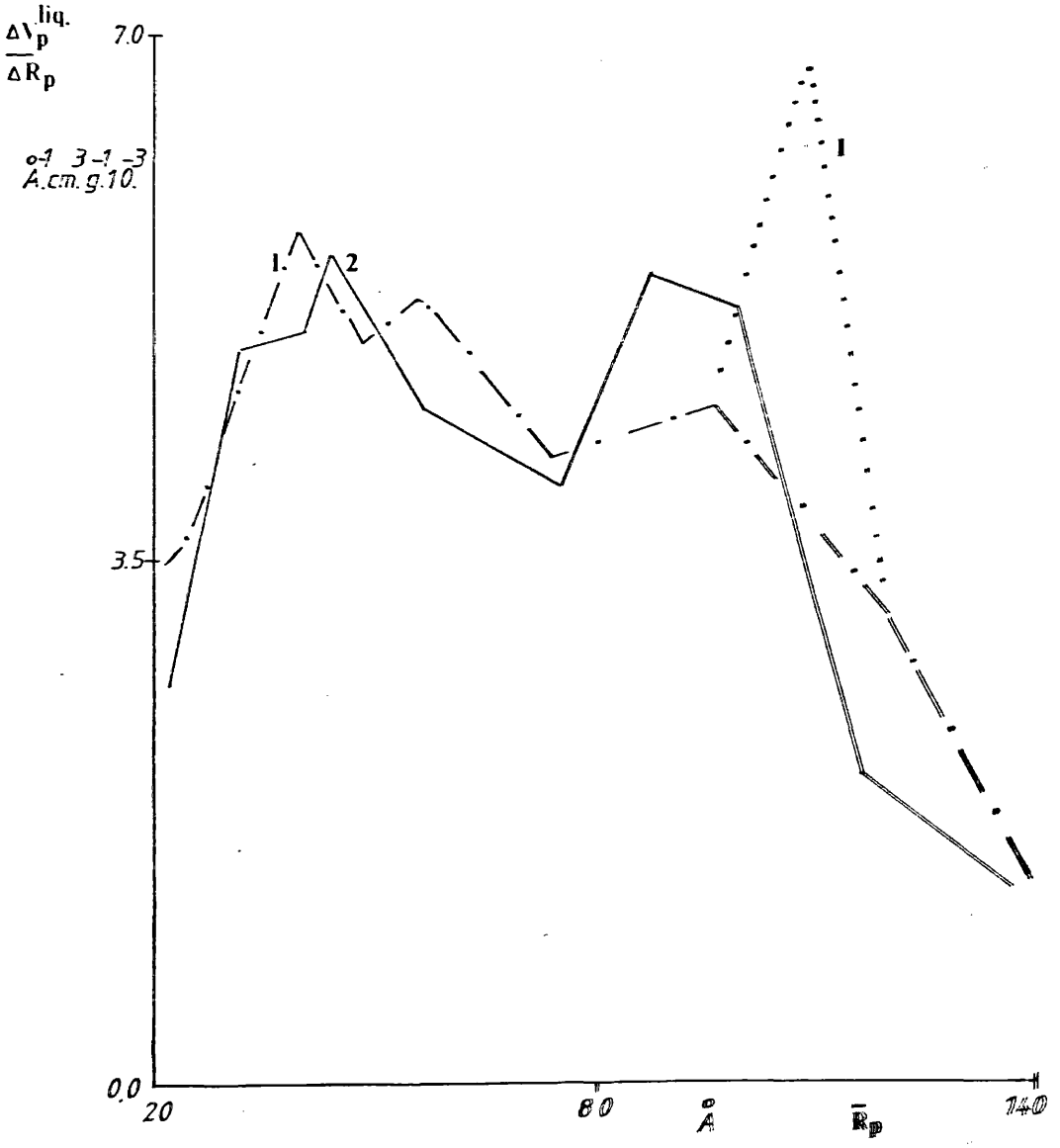

CHAPTER VII.

The Liquid Adsorption Experiments.

VII-1. Results.

VII-1-1 The Adsorption of Butanol on α-Haematite.

Throughout this work, all heats of reaction are quoted as positive quantities. Exothermic and endothermic processes are therefore written as positive, even though exothermic processes liberate heat and strictly have a negative enthalpy change. As stated earlier (Chapter V-3-2), all liquid concentrations are expressed as weight percentages.

The adsorption of 0.2% butanol in n-heptane was measured as a function of flow rate on α-haematite previously equilibrated with atmospheric moisture to give about two physically adsorbed layers of water. The results are given in Table VII-1. Owing to the small surface area ($2.7 m^2 g^{-1}$) and the pulsing effect of the pumps (Chapter V-3-1) the results are not as precise as was originally hoped for. Typical thermograms are shown in Figure VII-1.

It was decided to use a flow rate of 0.21 $ccmin^{-1}$ for all subsequent work, since the heats of adsorption and desorption were reasonably consistent at this flow rate and pumps were available that a) did not generate a large pulse effect, and b) enabled the flow rates for adsorption and desorption to be matched exactly.

In order to estimate the surface area of the haematite, 0.2% butanol was adsorbed onto an alumina surface area standard and the constant E in equation III-3 was evaluated. The alumina had an NPL certified specific surface area of $2.091 \pm 0.009 m^2 g^{-1}$ and was equilibrated such that about 2 physically adsorbed layers of water were present.

Two consecutive heats of adsorption were measured as 0.291 Jg^{-1} and 0.285 Jg^{-1} with a mean of 0.288 Jg^{-1}. The calibration constant E was calculated to be 0.138 Jm^{-2} and, using the heat of adsorption on haematite obtained with a flow rate of 0.21 cc min^{-1} (0.12 Jg^{-1}) a surface area of 0.87 m^2g^{-1} was calculated.

VII-1-2 The Adsorption of 1,2-Epoxybutane on α-Haematite.

The energies of adsorption and desorption for various strength epoxybutane solutions on α-haematite previously equilibrated to have about two physically adsorbed layers of water are given in Table VII-2. The precision is poor because of the small heat effects and the low signal to noise ratio. Typical thermograms are given in Figure VII-2. The signals are small and broad at low concentrations, and became larger and sharper at higher concentrations. The data is plotted in Figure VII-3., the curves I and II represent smoothed adsorption and desorption curves, and the dotted line is the mean of the experimental adsorption and desorption figures.

A 0.2% butanol solution was adsorbed after the epoxybutane experiments were completed. The heat of adsorption being 0.11 Jg^{-1}, which is the heat of adsorption on a surface not subjected to epoxybutane adsorption. The heats of adsorption and desorption of 0.27% 1,2-propandiol, 0.12 Jg^{-1} and 0.11^{-1}, respectively, were measured to see if the additional alcohol group had any effect.

A dilution experiment was performed to investigate the possibility that the divergence of the adsorption and desorption curves in Figures VII-3 and VII-10 could be explained by dilution effects. The experiment consisted of filling the reaction cell

with an inert material to give a known free volume inside the cell and then alternately flowing solvent and solution through the cell. Non-porous 100-mesh glass beads, thought to have a surface area approximating to their geometrical area were chosen as the inert filling. The results, using butanol solutions, are given in Table VII-3 and plotted in Figure VII-4. Typical thermograms are shown in Figure VII-5. The experiment was not repeated using epoxybutane solutions because of doubts as to the "inertness" of the glass beads.

VII-1-3 The Adsorption of Butanol on Ferric Oxide A.

Preliminary adsorptions of 0.2% butanol on ferric oxide A (ca. 0.27g) with between 1 and 2 physically adsorbed water layers initially present showed that the heats effects were large (ca. $20Jg^{-1}$) and inconsistent, and that the rate of desorption was much less than the rate of adsorption. A typical thermogram is shown in Figure VII-6. It was thought that the slow desorption could account for the inconsistent heats of adsorption. This was tested by measuring the heats after washing the surface with a known volume of heptane. A 2% solution was used because the plateau region in the adsorption signal made the areas difficult to measure and was possibly the consequence of not supplying the butanol fast enough. The heats of desorption were not measured because of the difficulty in determining the area under the slowly decaying desorption signals. The results of these experiments are given in Table VII-4 and plotted in Figure VII-7. Clearly the heat of adsorption is a function of the volume of heptane passed over the surface before the adsorption - the "flushing" volume. Typical

thermograms are shown in Figure VII-8.

The slow rates of desorption and the high heats of adsorption found with the 0.2% solution on the fresh surface suggested that some butanol was irreversibly adsorbed. This idea was tested by measuring the heats of adsorption and desorption on a fresh sample of ferric oxide A. Between 1 and 2 physically adsorbed layers of water were initially present. A flushing volume of about $80cm^3$ was used. The results are given in Table VII-5 and plotted in Figure VII-9 as a function of the number of adsorption/desorption cycles. The decrease in the heat of adsorption over the first few cycles suggests that some butanol is irreversibly adsorbed. There is a greater degree of uncertainty in the desorption heats than in the adsorption heats caused by the difficulty in assigning the correct area to the slowly decaying desorption signals.

The ferric oxide was further characterised by determining the relationship between the heats of adsorption and desorption and the concentration of butanol. The sample used above for the "cycling" experiments was used so that the initial surface was saturated in terms of irreversibly adsorbed material. To reduce the time involved for each adsorption/desorption cycle, the flushing volume was reduced to $60cm^3$. Starting with a 2% solution, successively more dilute solutions were adsorbed. The results are given in Table VII-6 and plotted in Figure VII-10. They indicate that the heat of adsorption reaches a maximum in the concentration range 0.2 - 0.4% and that increasing the concentration further causes a decrease in the heat of adsorption. The thermograms sketched in Figure VII-11 illustrate the variation of signal shape and size with concentration.

VII-1-4 The Adsorption of 1,2-Epoxybutane on Ferric Oxide A.

The ferric oxide sample used in the experiment to investigate the relationship between heats of adsorption and butanol concentration, was flushed with 240cm^3 of heptane before 2.0% 1,2-epoxybutane was adsorbed. The adsorption was exothermic and the signal had a significant base-line drift (Figure VII-12, curve I). After 70 min only 90% of the maximum deflection had decayed. The area was measured from the point giving heat of adsorption of 27.1 Jg^{-1}. The heat of desorption was about 3 Jg^{-1}, the signal (Figure VII-12, curve II) being very small. 40 cm^3 of heptane was passed through the cell and epoxybutane readsorbed (Figure VII-12, curve III). The heat of adsorption was about 4 Jg^{-1}. A further 300 cm^3 of heptane were passed through the cell and the epoxybutane readsorbed. The heat of adsorption was again about 4 Jg^{-1}, and the signal (Figure VII-12, curve IV) was not significantly altered. 75 cm^3 of heptane were then passed through the cell and 2.0% butanol adsorbed, the heat change being 6.7 Jg^{-1}. These results indicate that a substantial amount of the epoxybutane is irreversibly adsorbed and that prolonged flushing does not promote desorption.

VII-2. Discussion.

VII-2-1 Butanol Adsorption on α-Haematite.

Previous work in this laboratory[160] on the haematite/butanol system, using the downward flow mode that had revealed a small spurious endothermic peak immediately after the exothermic adsorption. No such signals were positively identified in this work (using the upwards flow mode), although the pulsing of the

pumps may have obscured this effect. Various authors have observed a similar effect for the adsorption of carboxylic acids, but not for butanol adsorption (Chapter IV-3). Heal and McEwan[97], however, have found a spurious desorption signal dependent on the amount of water in the system. They advanced the view that fast flow rates could obscure the effect by building up pressure gradients within the reaction cells that could act as small heat sinks. This could possibly explain the results of the earlier work. The flow rates used in this work could not have compacted the sample but simply ensured that a well mixed suspension was present in the cell. It is unlikely that pressure gradients were present.

If butanol adsorption causes preadsorbed water to be displaced, giving rise to the desorption signal, this effect could only operate until all the water was displaced. It is doubtful that the dried heptane could have delivered enough water in the required time to continually replace the butanol displaced water.

The heat of adsorption was taken to be 0.12 ± 0.01 Jg^{-1} and the heat of desorption to be 0.16 ± 0.01 Jg^{-1}. These quantities should be equal in magnitude and opposite in sign. The discrepancy probably arises from errors in measuring the area of the desorption signal. The desorption signal was always much broader than the adsorption signal (Figure VII-1) and had a pronounced "tail", thereby making it difficult to decide when the signal and base-line merged. Decreasing the flow rate caused both the adsorption and the desorption signals to broaden with a consequent decrease in reproducibility. Discrepancies exist in the literature regarding the value of the heat of

adsorption of 0.2% butanol in ferric oxides[86,88]. The value found here is less than the literature values by a factor of at least two. The heat of adsorption is very sensitive to the surface pretreatment, especially to the amount of water present. Generally the heat of adsorption decreases with increasing water coverage[96]. The low heat of adsorption found here is most readily explained in terms of the water coverage. It is known that less than two physically adsorbed layers of water are enough to completely "screen" an oxide surface from an adsorbate. About two layers of physically adsorbed water were initially present on the haematite surface. Even assuming butanol does displace water, it is unlikely that no physically adsorbed water was present because of the residual moisture on the solvent. Hence the butanol was at least partially "screened" from the full adsorption potential of the surface. A further measurement of the heat of adsorption of butanol on haematite in this laboratory yielded a value of 0.16 Jg^{-1}.[186]

The specific surface area of the haematite is 2.74 m^2g^{-1} compared to the surface area found by the microcalorimetric technique of 0.87 m^2g^{-1}. The discrepancy is almost certainly due to the screening effect of the water present. However, since both the alumina and the haematite initially had approximately the same water coverages, some self-cancelling of the effect should have occurred. If the effective area of the alumina was decreased, the constant E will be increased and the surface area of the haematite will decrease. In general, it has been suggested that the areas found by the microcalorimetric techniques[96] are the effective areas of the surface

and are a measure of the reduction in specific surface area due to preadsorbed water. In this work, however, the calculation was based on an assumed knowledge of the alumina surface area, and so is likely to be in error. The discrepancy between the liquid and gas phase results could also be viewed in terms of a decrease in surface reactivity rather than a simple area effect.

VII-2-2 1,2-Epoxybutane Adsorption on α-Haematite.

The 1,2-epoxybutane/ α-haematite system was considered to be a model for the adsorption of constituents of epoxy adhesives on steel surfaces. The haematite sample was used to ensure the absence of effcts due to porosity. The heats of adsorption at a concentration of 0.2% are less than those found for butanol. The butanol adsorption carried out after the epoxybutane experiment indicated that none of the epoxybutane was irreversibly adsorbed. The propandiol result shows that the additional alcohol group has no effect on the heats of sorption.

It was expected that the heats of adsorption and desorption of epoxybutane would initially increase with increasing concentration and then reach a plateau. This is not observed (Figure VII-3). Two possible explanations for the observed trends were considered. At the higher concentrations, an endothermic dilution effect may become significant. This would depress the exothermic signal and enhance the endothermic signal. Alternatively, it was thought that the adsorption and desorption reactions might be different. If, at some stage during the cycle : adsorption, subsequent residence on the surface, and then desorption, the higly strained epoxy ring was hydrolysed, then the second hypothesis is feasible. However, there is no reason why the proposed hydrolysis should operate only at high

concentrations. Preliminary experiments using gas-liquid chromatography failed to provide any evidence that haematite catalysed ring opening. The propandiol result also suggests that if a diol was produced on the surface the effect might not manifest itself in the heat of desorption. A rough calculation concerning the likely heat effect for the cleavage of the epoxy ring gives a figure well above the observed energy difference between the two curves in Figure VII-3. The most feasible explanation is therefore the dilution effect, since it only becomes operative at higher concentrations where the curves diverge. Assuming this to be true, taking the mean of the adsorption-desorption energies should cancel the dilution effect. The dotted line in Figure VII-3 shows the mean result and does level off tending towards a plateau.

Figure VII-10 shows the effect of butanol concentration on the heats of adsorption and desorption on ferric oxide A. The adsorption curve reaches a maximum and then the heat effect decreases with increasing concentration, while the desoprtion heat shows a gradual increase with increasing concentration. That a completely different system shows a broadly similar trend to that observed for epoxybutane, indicates the underlying cause in both cases is physical rather than chemical. The dilution experiment was unable to furnish quantitative corrections because the glass beads were not inert, so that the measured heat effects included a component arising from a sorption process. Evidence for this is provided by the doublet type structure of the signals in Figure VII-5. However, the general trends suggest that dilution effects are important. All the "desorption" heats are endothermic while the "adsorption" heats undergo a change in sign becoming endothermic

at high concentrations. Qualitative application of these trends to both of the reaction systems considered will have the effect of decreasing the magnitude of the heats of desorption and increasing the magnitude of the heats of adsorption.

VII-2-3 Butanol Adsorption on Ferric Oxide A.

The heats of adsorption of butanol on ferric oxide A are several orders of magnitude larger than those on α-haematite when expressed in Jg^{-1}. However, per unit of surface area (Jm^{-2}) the figures become comparable (of the same order of magnitude). The exact figures depend on the relative effective areas and on the particular heat of adsorption chosen for ferric oxide A. The surfaces are therefore energetically similar. This is reasonable since the mean pore radius is 26Å and the α_s-plot (Figure VI-20) indicates an absence of micropores, so no great increase in the "adsorption" potential would be expected.

The slow desorption (Figure VII-6) is presumably a consequence of the porosity of the sample. It is not clear why the adsorption process is not similarly affected. A similar, but less marked, effect was observed for the desorption of butanol from haematite. This suggests that the effect is kinetic and that it is exaggerated by the porous nature of the surface of ferric oxide A. Although the pore shapes and sizes cannot be the primary factor, (otherwise the adsorption process would be similarly effected) they presumably further hinder the movement of molecules in an already kinetically difficult mechanism.

The plateau in the adsorption signal of 0.2% butanol (Figure VII-6) is simply the consequence of not supplying the butanol sufficiently fast to the reaction cell. Estimations of the time required to supply a monolayer to the surface depend critically on the effective area available for reaction and the area occupied by the butanol molecule on the surface. Several calculations were made, using different assumed figures for these quantities, all of which showed that the butanol was not being delivered fast enough to the reaction cell. Increasing the concentration by a factor of 10 eliminated the plateau region as in Figure VII-8.

Figure VII-7 shows that the heat of adsorption is a function of the volume of heptane passed over the surface prior to the adsorption. Thus the desorption is not only slow relative to the adsorption in the short term, (comparison of adsorption and desorption signals) but also over a much longer period of time. Intuitively diffusion of molecules in and out of a network of pores will not be instantaneous, especially when the molecules are large relative to at least parts of the pores. However, why this effect should only apply to the desorption process is uncertain. It is conceivable that the adsorption was initially fast and then proceeded so slowly that it was undetected, although this does not solve the problem of the different rates of adsorption and desorption.

The slow desorption is complicated by the fact that for a given flushing volume some butanol is "irreversibly" adsorbed (Figure VII-9). For a given flushing volume, the

"irreversibly" adsorbed material almost certainly has a component that is permanently adsorbed irrespective of the flushing volume and a component that is dependent on this volume and which can be desorbed by increasing the flushing volume. More than one adsorption/desorption cycle is required before the heats of adsorption become constant. The first adsorption cycle could result in the permanent component being left on the surface and the second cycle could deposit material less strongly bound. It is possible that some butanol is chemisorbed. In general, the heat of adsorption of the permanently adsorbed butanol will not be equal to the heat of adsorption of the reversibly adsorbed butanol, but will be larger. Estimating the proportion of the surface occupied by permanently adsorbed butanol by comparison of heats of adsorption is therefore subject to errors. A comparison will yield the maximum possible coverage. The difference between the initial heat of adsorption and the equilibrium heat of adsorption in Table VII-5 suggests that a maximum of 25% of the surface is covered by irreversibly adsorbed material. About equal proportions of irreversibly adsorbed butanol are left on the surface as the result of each of the first two adsorption/desorption cycles. Given the relative sizes of the heptane and butanol molecules compared with the mean pore diameter, it is unlikely that the initial adsorption would result in parts of the surface remaining unexposed to adsorbate, thereby requiring more than 1 adsorption/desorption cycle to ensure complete exposure of the surface.

From Figure VII-7 the heat of adsorption after more than two cycles, using 80 cm^3 of heptane to wash the surface

should be 17.5 Jg^{-1}. The actual value, from Figure VII-9, is about 15 Jg^{-1}. The discrepancy arises from the different preparations of the samples used. The sample used in the first experiment was powdered, using a different procedure to that employed for the second sample used in the "cycling" experiment. All other microcalorimetric experiments and all the gas adsorption work used ferric oxide A taken from this second batch of powder. This discrepancy should in no way negate the usefulness of the trend observed in Figure VII-7. The 1.99% butanol adsorption using a flushing volume of 60 cm^3 (Table VII-6) and the mean of the heats of adsorption after 2 cycles using a flushing volume of 80 cm^3 (Table VII-5) lie equidistant below the curve of heat of adsorption versus flushing volume in Figure VII-7. Hence the general trend is maintained.

The data of Table VII-6, plotted in Figure VII-10, shows that the heat of adsorption has a maximum, and that the heat of desorption curve gradually increases with increasing concentration. Below a concentration of 0.2% the desorption signals become so broad and shallow that it was impossible to measure them accurately. The maximum in the adsorption curve occurs in the concentration range 0.2-0.4%. It is known that butanol molecules form a close packed vertically orientated monolayer at a concentration of 0.2%[83-86]. Thereafter increasing the concentration should have no effect on the heat of adsorption. This is observed for concentrations up to about 0.4-0.5%, after which the heat of adsorption decreases sharply with further concentration increases. This effect and the difference between the adsorption and

desorption curves are, at least partially, explained by the dilution effects discussed above (VII-2-2).

The adsorption signals shown in Figure VII-11 become progressively less sharp and much broader as the concentration is decreased. No plateau region was observed. An attempt was made to correlate the changes in the signal shapes to the area of the surface and the area occupied per butanol molecule. However, this was unsuccessful, because of the uncertainty in the surface area available for reaction arising from the presence of unknown quantities of preadsorbed water and irreversibly adsorbed butanol.

Neglecting surface contamination, the possibility of an enhanced heat of adsorption on a porous surface compared to that on a plane surface requires that the estimation of the constant E (Equation III-3), should be carried out, using a porous surface area standard. No such standard was available. However, given the lack of micropores, the error introduced by failing to use a porous standard is likely to be small. Various estimates of the surface area are given in Table VII-7. The first column was obtained using E = 0.138 Jm^{-2} derived from the alumina calibration. The figures in the second column were calculated using E = 0.116 Jm^{-2} obtained by Bignall[186] from the adsorption of 0.2% butanol on silica TK800. This discrepancy in E values is disturbing, since Groszek[83-86] has shown that a wide range of polar metal oxides should give the same E values. The most likely explanation is that different amounts of water were preadsorbed on the surfaces. Irrespective of the E value used, all the areas are less than the BET specific surface area. For the

adsorption of 2% butanol the mean area is 164 m^2g^{-1} for the surface containing only preadsorbed water, and 121 m^2g^{-1} for the surface containing both water and irreversibly adsorbed butanol. This latter figure represents the effective area available for adsorption as a consequence of the presence of both butanol and water. It is possible that the butanol displaced some or all of the water, although these results cannot distinguish this. Assuming the heats of reversible and irreversible adsorption are the same, the surface area obtained from the initial heat of adsorption shows that about 33% of the BET surface is occupied by water. Since the heat of irreversible adsorption is likely to be larger than the heat of reversible adsorption, 33% is a maximum estimate of the water coverage. These surface area estimates are depressed because of the dilution effect found for 2.0% solutions compared with 0.2% solutions. The mean area for a surface containing both water and butanol, taken from the maximum of the curve in Figure VII-10, corresponding to a concentration of about 0.2%, is 155 m^2g^{-1}. An assumed heat of adsorption (20.5 Jg^{-1}) for 0.2% butanol adsorption with a flushing volume of 80 cm^3 gives an effective area of 163 m^2g^{-1}, compared to 121 m^2g^{-1} found for a 2% solution. Using the reduction in the initial heat of adsorption of a 2% solution to its equilibrium value (Figure VII-9), by proportion, the initial heat of adsorption of a 0.2% solution was calculated at about 27.5 Jg^{-1}. This gives a mean effective area of about 220 m^2g^{-1}. The specific surface area of ferric oxide A calculated after outgassing at 27°C for

6 hours is 222 $m^2 g^{-1}$. If the figure of ca. 220mg^{2-1} is correct, this suggests that all the water was displaced by the butanol. This is not observed for the haematite sample, and it is not clear why the porous surface should behave differently in this respect. There is therefore some doubt as to the validity of this approach, possibly related to differences in the heats of reversible and irreversible adsorption of butanol.

VII-2-4 1,2-Epoxybutane Adsorption on Ferric Oxide A.

The initial heat of adsorption is large, considering the surface already contained some irreversibly adsorbed materials. It is possible that the epoxybutane displaced the adsorbed butanol and residual water, although there is no evidence either for, or against this view. The large disparity between the first and second heats of adsorption (27 Jg^{-1} and 4 Jg^{-1}) and the agreement between the first heat of desorption and the second heat of adsorption (3.5 Jg^{-1} and 4 Jg^{-1}) suggest that the epoxybutane was irreversibly adsorbed. Prolonged flushing of the surface had no effect on the heat of adsorption. Thus the epoxybutane is permanently adsorbed.

The haematite /epoxybutane system behaved quite differently. The adsorption and desorption were reversible, and readsorption of butanol onto the epoxybutane treated surface gave the expected heat of adsorption. Readsorption of 2.0% butanol onto the ferric oxide A resulted in a heat of adsorption of 6.7 Jg^{-1}, less than half of the expected value of about 15 Jg^{-1}.

Hence ,the butanol and epoxybutane occupy some common adsorption sites.

The second heat of adsorption was about 75% of the first, so that very approximately a maximum of 75% of the surface originally available to the epoxybutane was covered with irreversibly adsorbed material. Using a mean 'E' value (Table VII-7) of 0.127 Jm^{-2}, the heat of adsorption of butanol gives a residual area of about 53 m^2g^{-1} . The rest of the surface must be occupied by epoxybutane and some butanol and possibly water.

A feature of the adsorption signals in Figure VII-12 is the failure of the signals to return to the preadsorption level. This cannot be the result of changes in the thermal properties of the contents of the cell. No such effect was observed for the haematite epoxybutane system when the recording sensitivity was 100 times greater. Therefore, the effect must be associated with a slow and continuous evolution of heat. This could arise from the slow hydrolysis of the epoxide ring on the surface. It is well known that epoxides readily undergo acid catalysed ring cleavage and can even be cleaved under basic conditions.[190] If the epoxide ring was cleaved, then the possibility exists that the adsorbed molecule could form a second bond with the surface, with the liberation of more heat. It is well known (Chapter IV-3) that molecules that form multiple bonds with a surface are not easily desorbed.

Hence both the slow decay of the adsorption signal and the irreversible nature of the adsorption can be explained. It is, however, not clear why the effect was not observed for the haematite/epoxybutane system. The effect may have been present but, as a result of the low surface area of the haematite, to such a small extent that it was beyond the limits of detection.

FIG. VII.1.

Sorption thermograms of the 0.2% butanol/α-haematite system using a flow rate of 0.21 $cm^3 min^{-1}$.

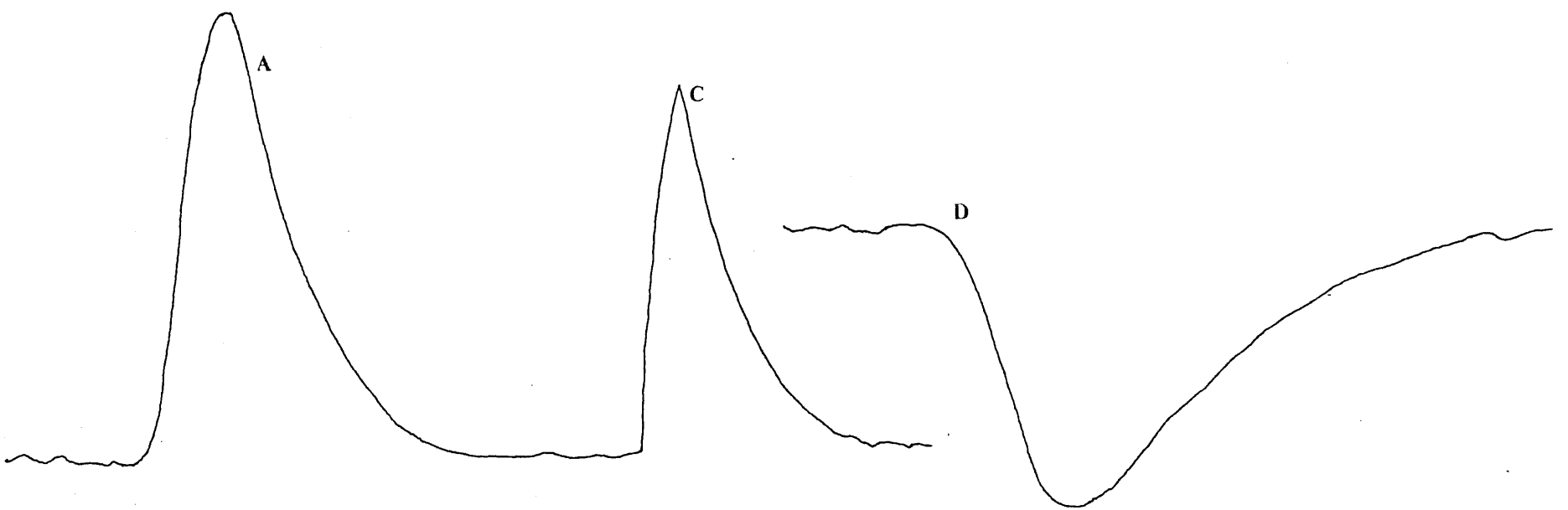

For this and all subsequent figures, the following representations apply: A= adsorption , C=calibration , D=desorption , t=time & Q=heat.

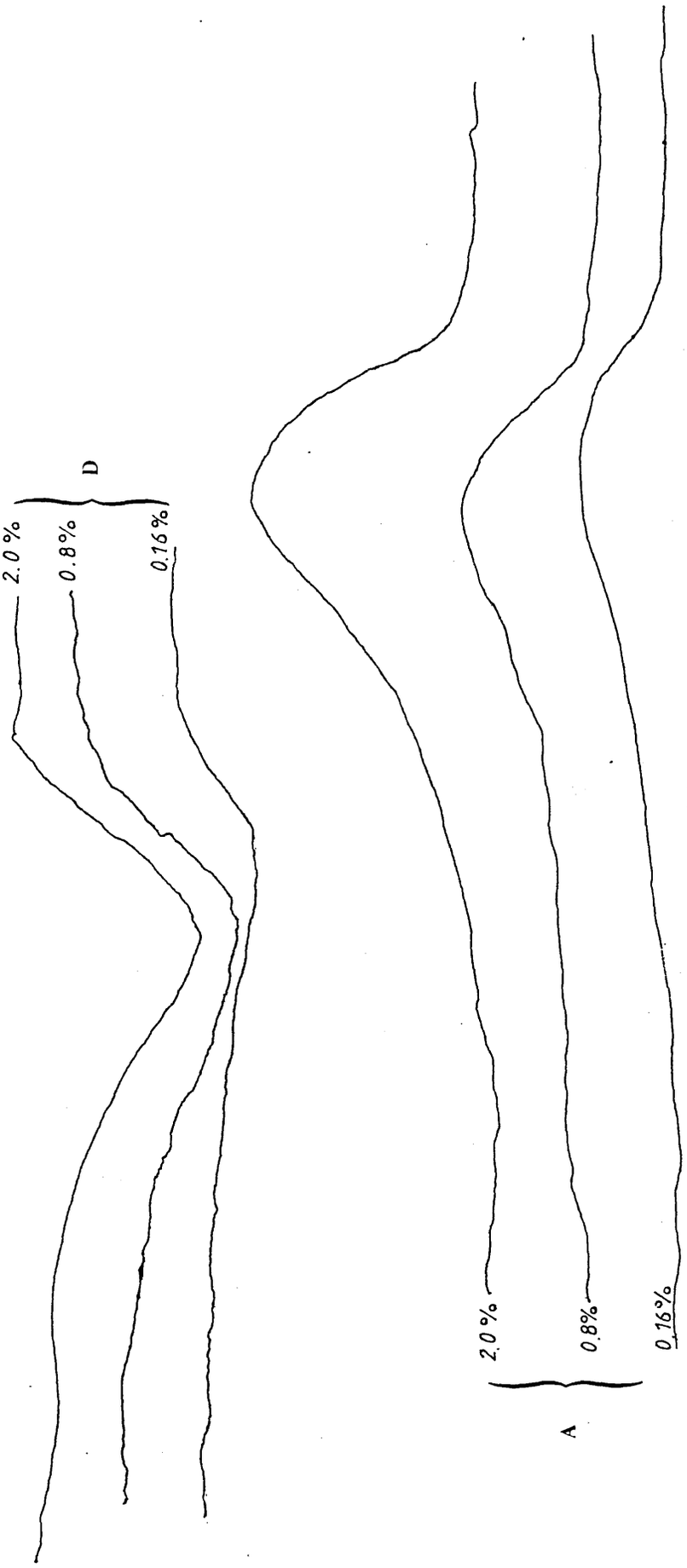

FIG. VII.2. Sorption thermograms of various strength 1,2-epoxybutane solutions with an α-haematite adsorbent.

FIG. **VII.3.** The mean heats of sorption of the 1,2-epoxybutane/α-haematite system as a function of 1,2-epoxybutane concentration.

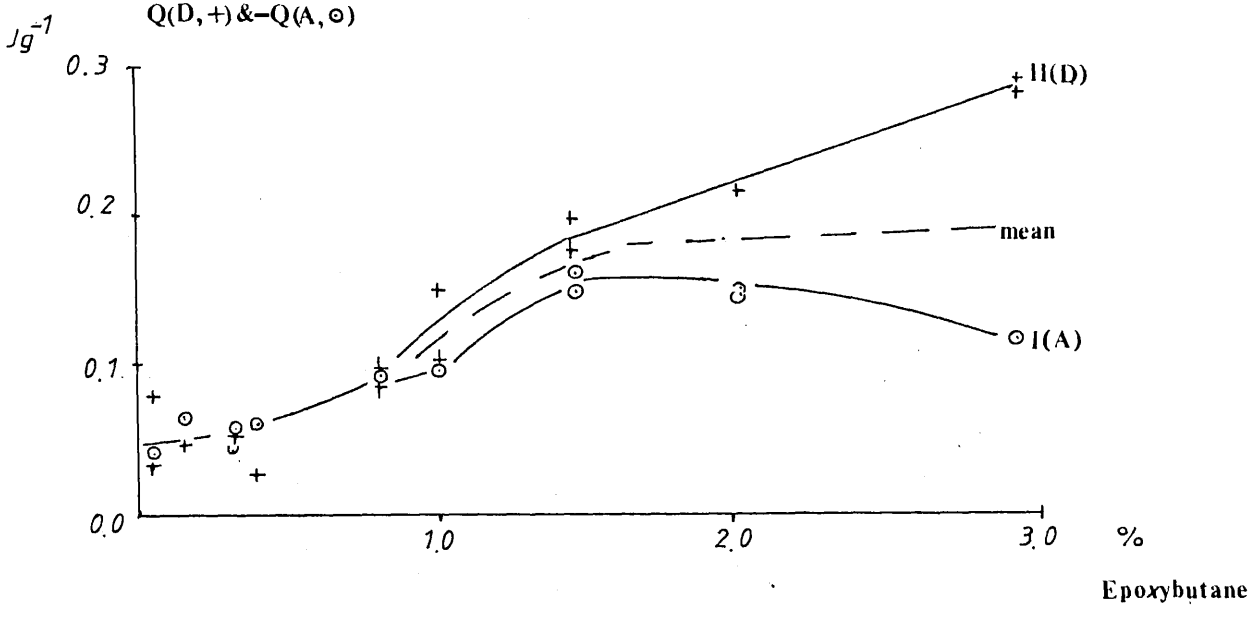

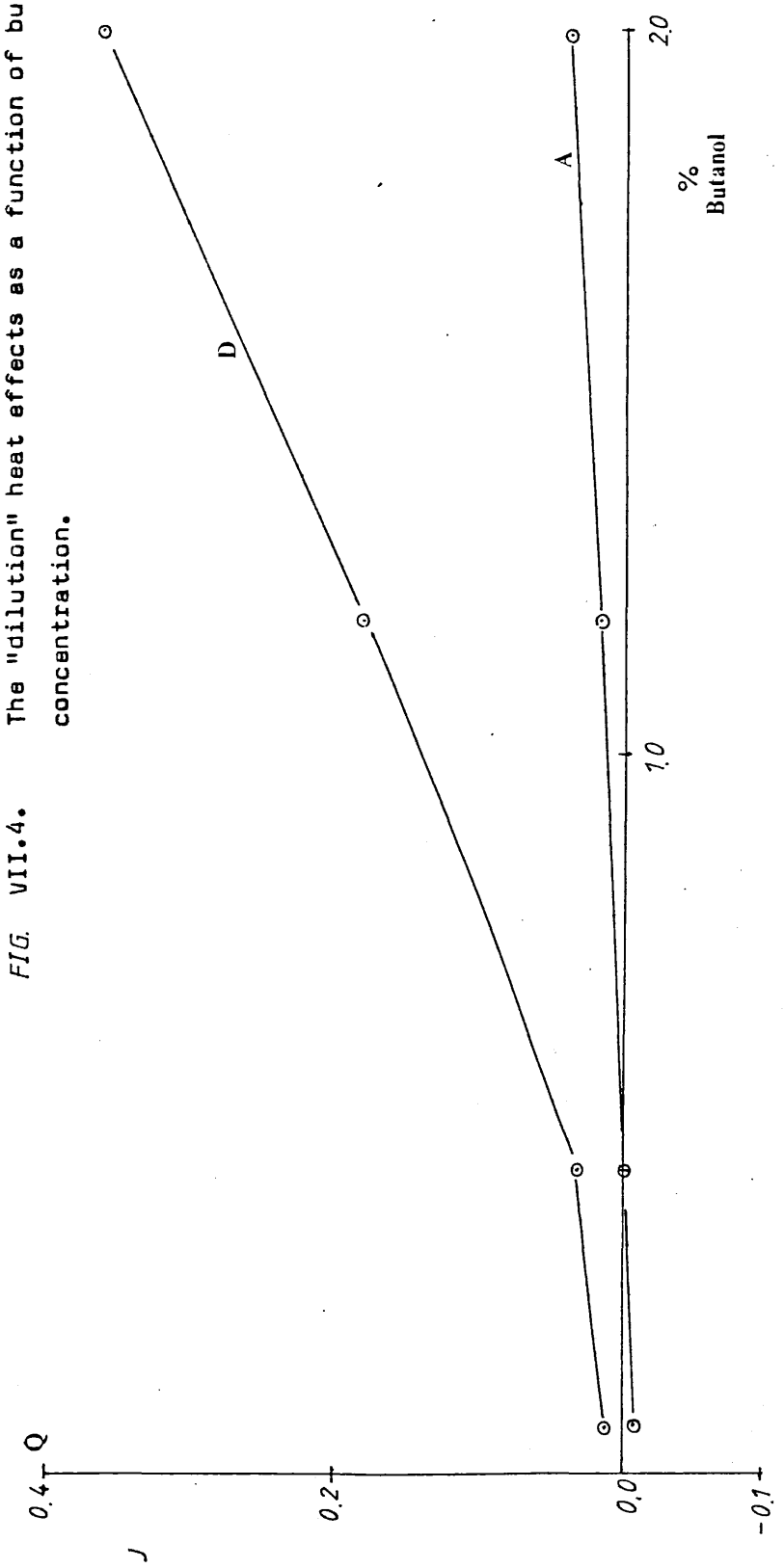

FIG. VII.4. The "dilution" heat effects as a function of butanol concentration.

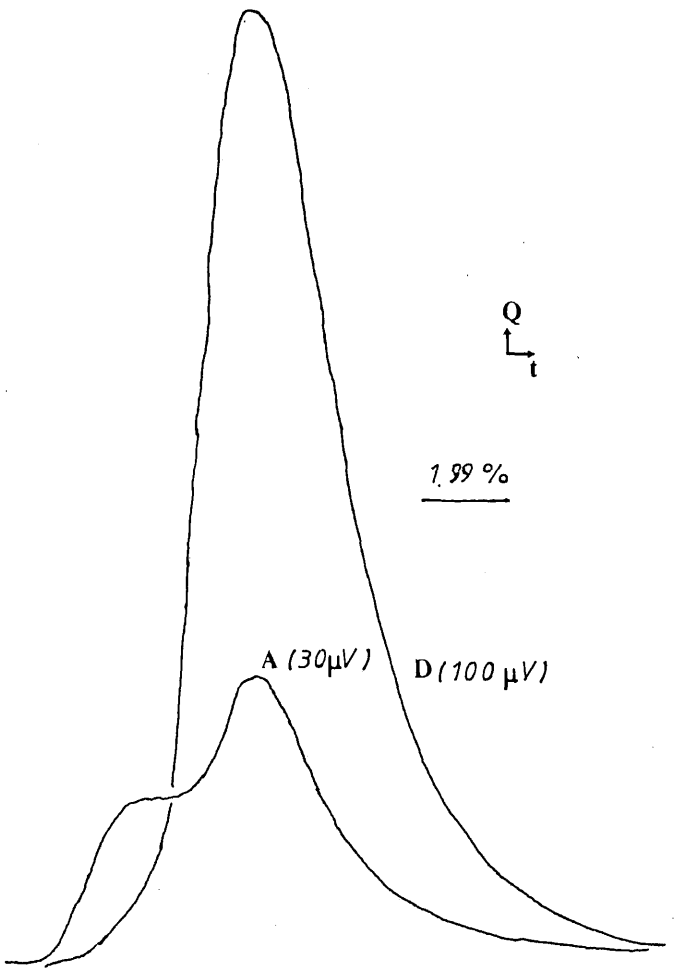

FIG VII.5.

The "dilution" heat signals, with the sensitivity of the recording system given in μV for each signal.

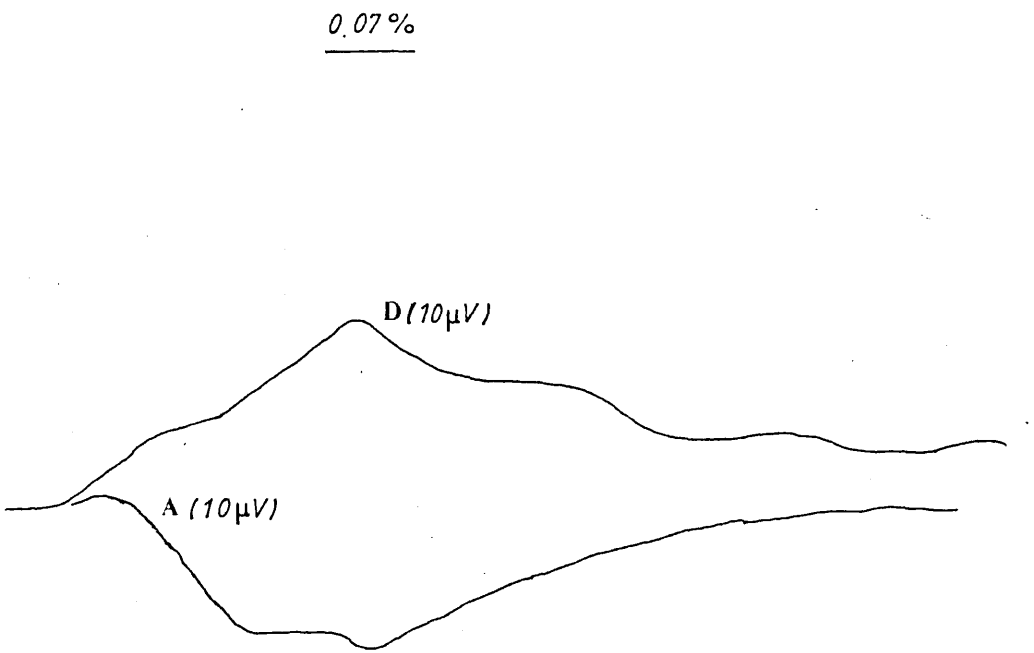

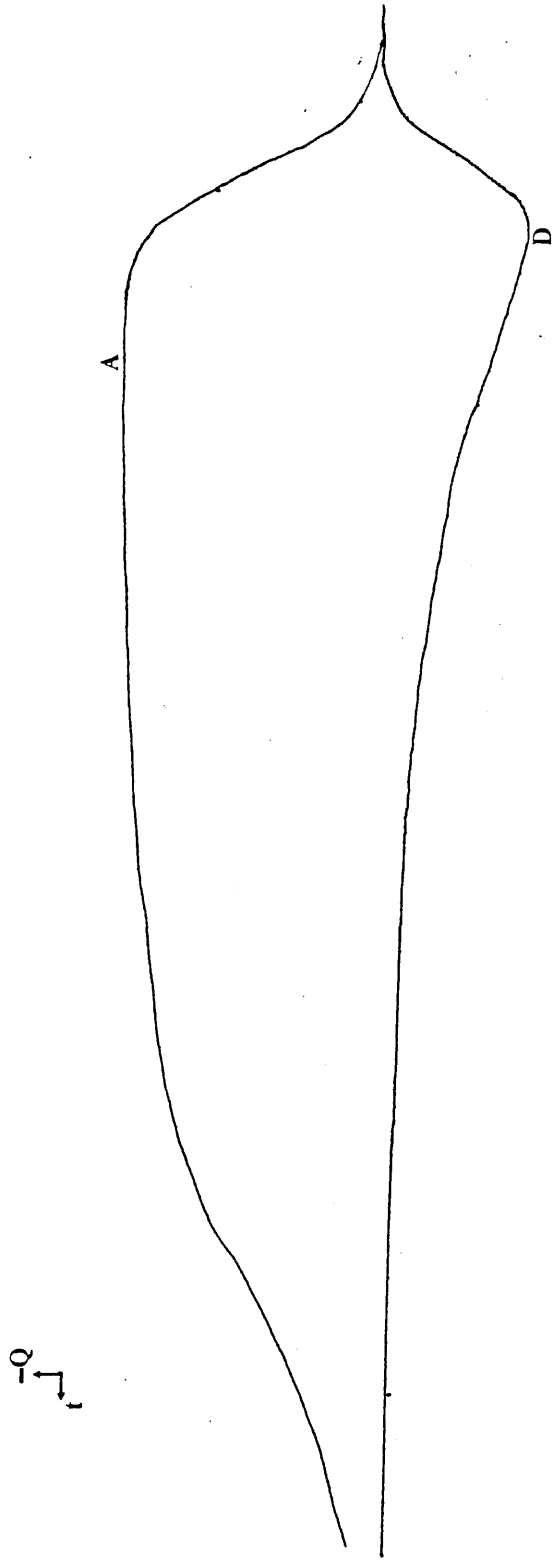

*FIG.*VII.6. Sorption thermograms of the 0.2% butanol/ferric oxide A system.

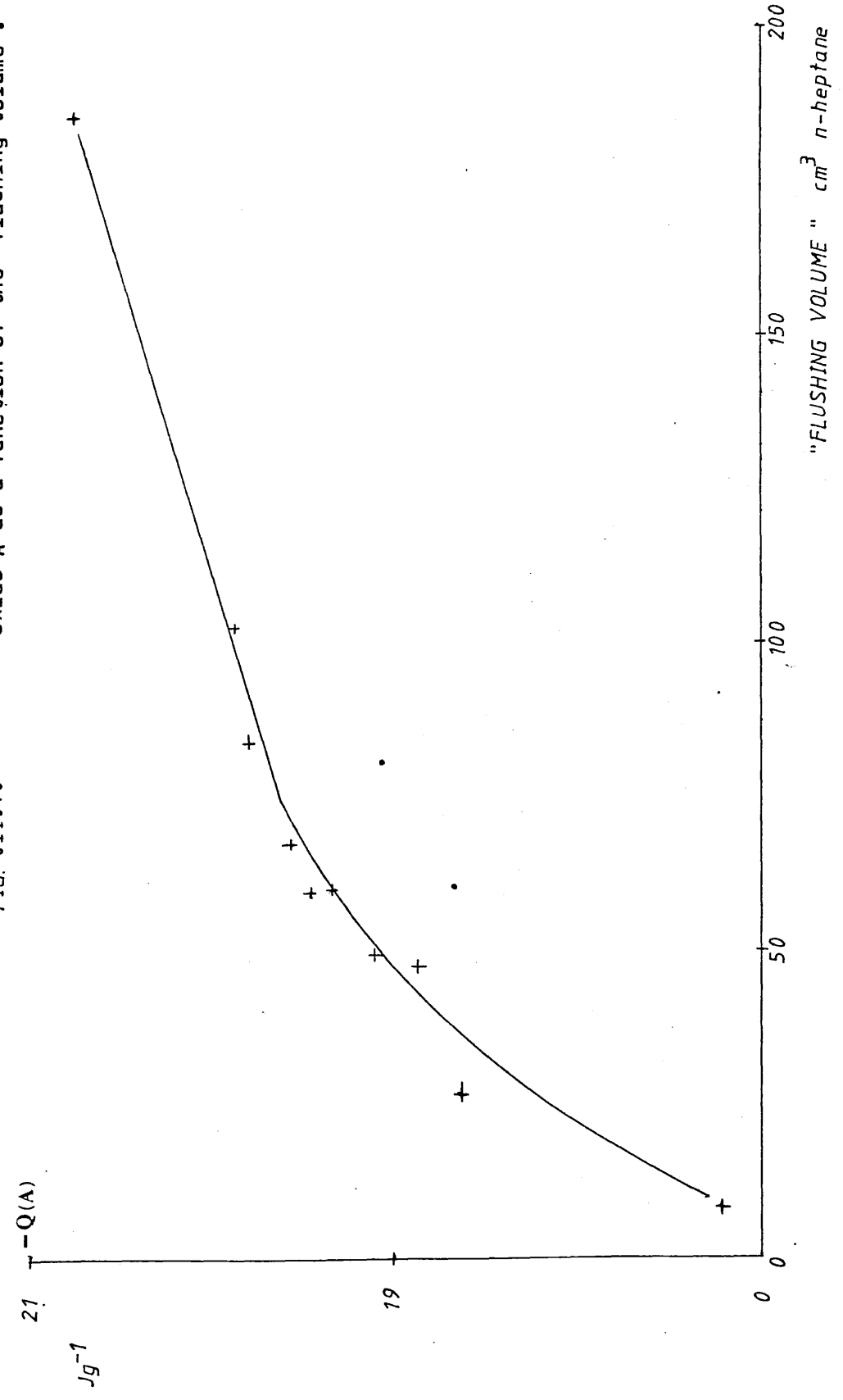

FIG. VII.7. The heat of adsorption of 2.0% butanol on ferric oxide A as a function of the "flushing volume".

FIG. VII.8.

Examples of the adsorption signals for the 2.0% butanol/ferric oxide A system at different flushing volumes.

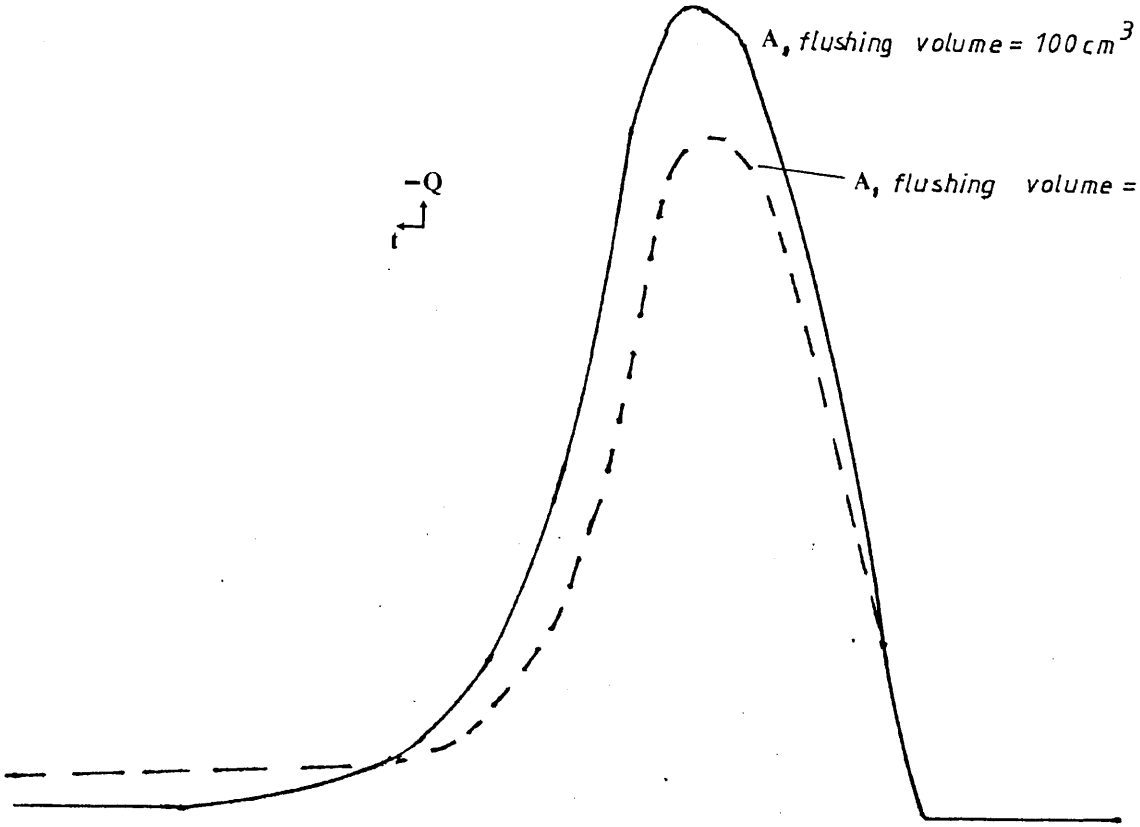

FIG. VII.9.

The heat of sorption of 2.0% butanol on ferric oxide A as a function of the number of previous sorption cycles using a flushing volume of 80 cm^3.

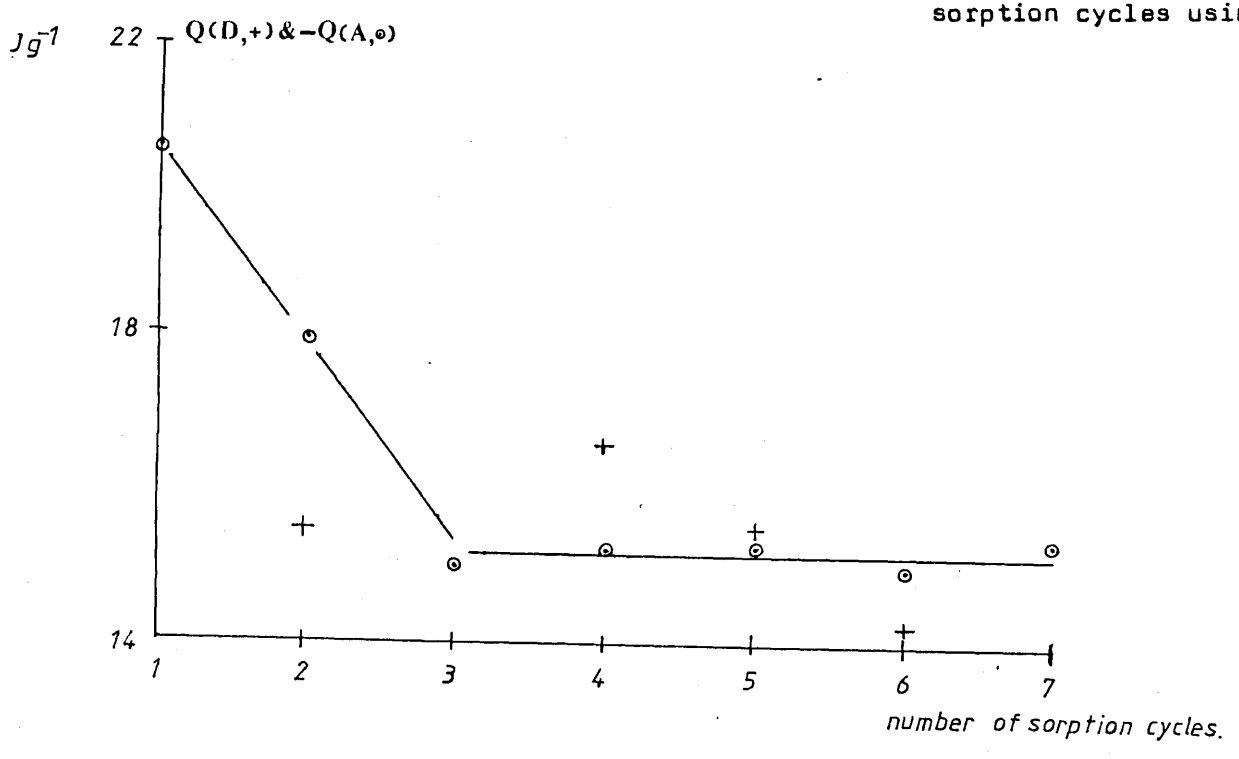

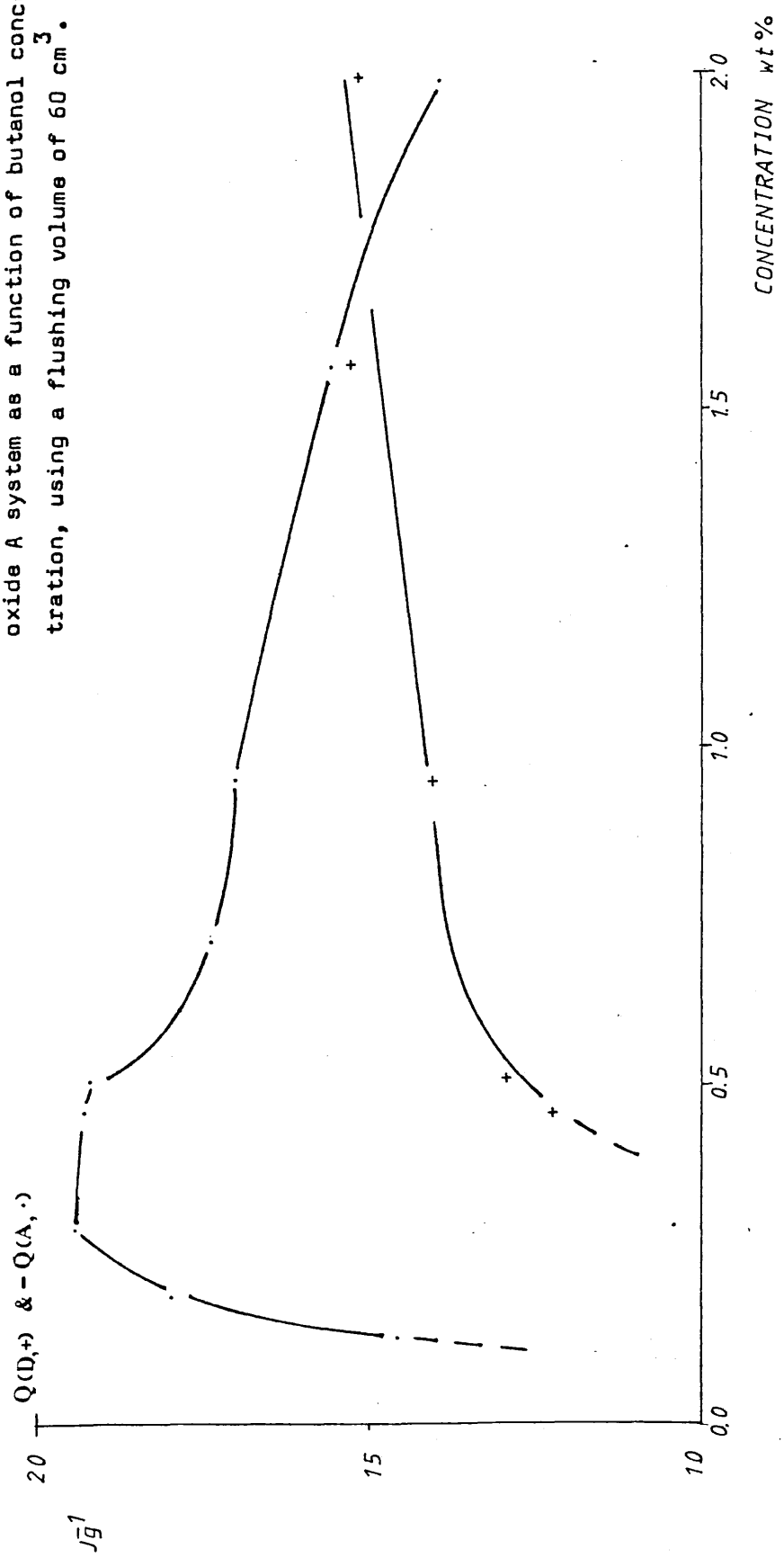

FIG. VII.10. The mean heats of sorption of the butanol/ferric oxide A system as a function of butanol concentration, using a flushing volume of 60 cm^3.

FIG. VII.11.

Adsorption signals for the adsorption of butanol on ferric oxide A at various butanol concentrations using a flushing volume of 60 cm^3.

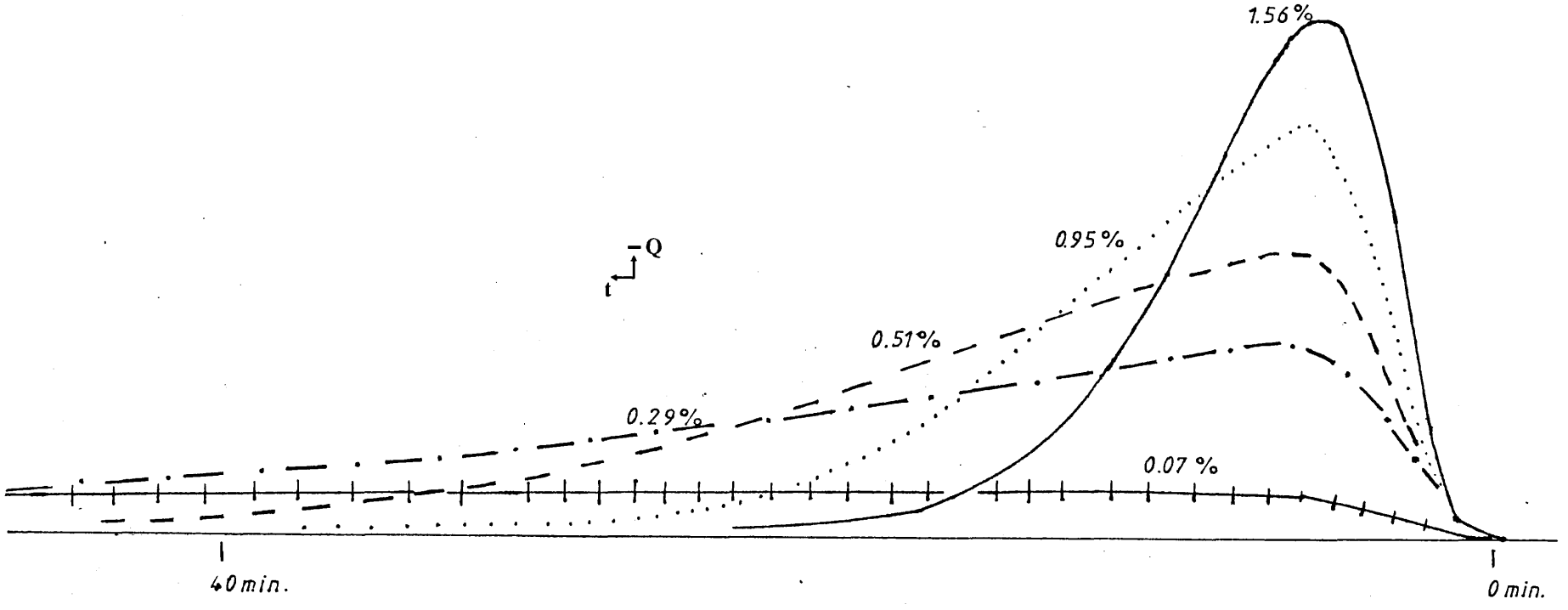

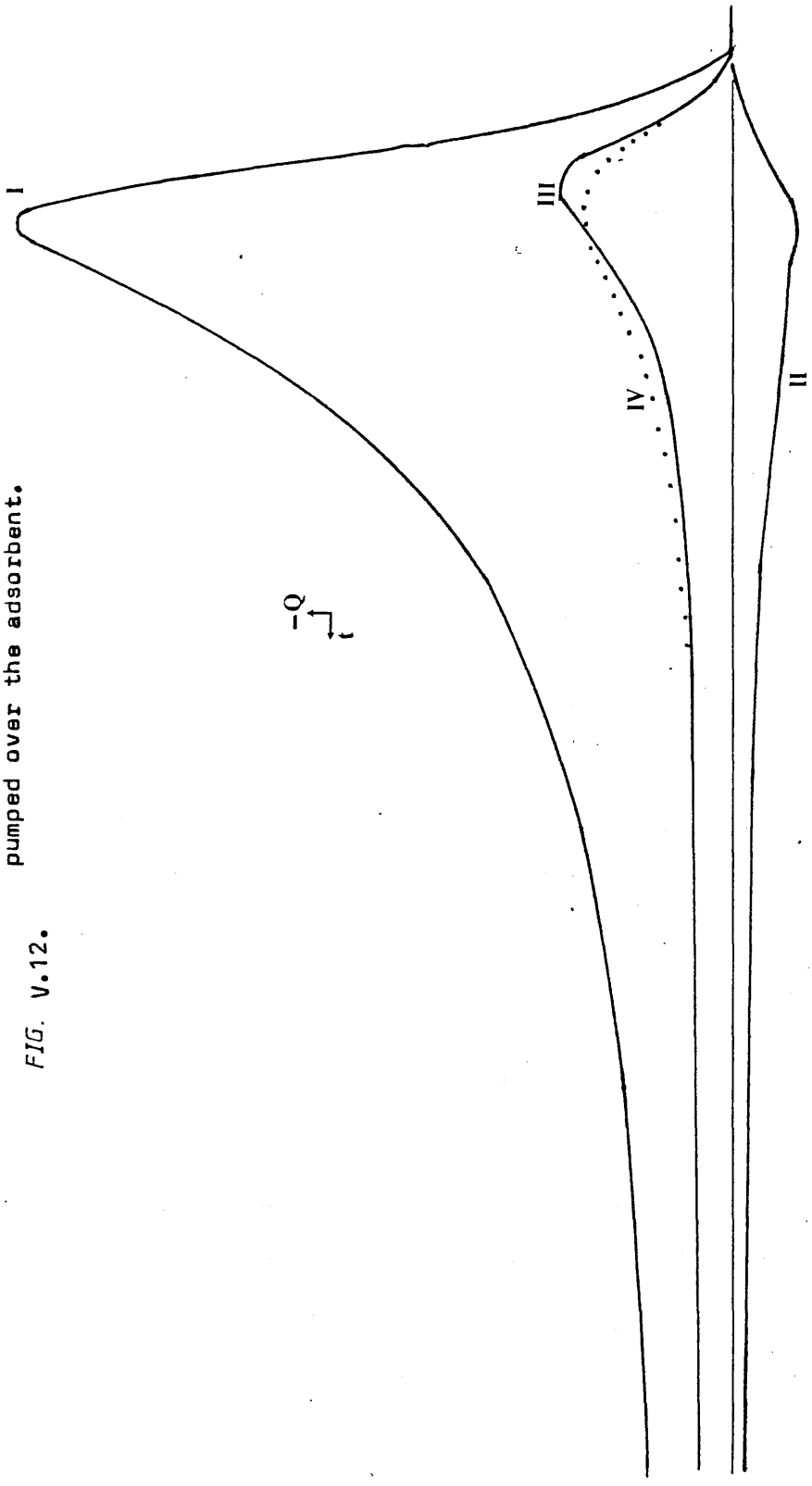

FIG. V.12.

The sorption signals of the 1,2-epoxybutane/ferric oxide A system. Curves I and II are the initial adsorption and desorption respectively. Curves III and IV are the adsorption signals after 40cm^3 and 300cm^3 of n-heptane were pumped over the adsorbent.

Chapter VIII.

The Water Vapour Adsorption Experiment.

VIII-1. Results.

VIII-1-1 The Calibration Experiment.

The water vapour adsorption experiments were carried out using the modified microcalorimeter described earlier (Chapter V-3-3). Dry nitrogen was first passed through the empty reaction cell, and then the flow was switched through the water bubbler. This caused nitrogen, at least initially saturated with water vapour at the temperature of the experiment, to pass through the reaction cell. An exothermic heat change was recorded. Once thermal equilibrium was re-established, the flow was switched back to dry nitrogen and an endothermic signal resulted. This procedure was carried out at 25.00 ± 0.05°C and 37.20 ±0.05°C. In the context of this calibration experiment, adsorption and desorption refer to the effect of changing the flow of nitrogen from "dry" to "wet" and "wet" to "dry" respectively. The results are given in Table VIII-1. Typical thermograms are sketched in Figure VIII-1. These results indicate that, as expected, the effect of changing the moisture content of the nitrogen was complicated and that possibly more than one process was involved. The heat effects for adsorption and desorption were, within experimental error, equal in magnitude but opposite in sign irrespective of the temperature. There was no significant difference between the results obtained at the different temperatures. A mean heat effect of 0.60 J was assumed and applied to all subsequent

measurements. The flow rate was 5 $cm^3 min.^{-1}$ for the "dry" nitrogen and 4.5 $cm^3 min.^{-1}$ for the "wet" nitrogen.

To investigate if adsorption on an iron oxide surface caused an additional, detectable heat effect, the experiment was repeated with about 0.1 g of the high purity α-haematite in the reaction cell, at 37.20 °C. A dry flow rate of 4.8 $cm^3 min.^{-1}$ was used; the wet flow rate was about 10% less. The results are given in Table VIII-2. Typical sorption signals are sketched in Figure VIII-2. These results indicate that the presence of the haematite causes an additional heat effect compared to the blank experiment. This is presumably caused by adsorption. The mean heats of adsorption (32.8 Jg^{-1}) and desorption (30.9 Jg^{-1}) are, within experimental error, the same. Inspection of the signals showed that the rates of desorption was faster than the rates of adsorption.

The experiment was repeated at 19.55 °C. The rates of reaction were reduced compared to those at 37 °C, although the desorption was still faster than the adsorption. The adsorption and desorption signals are sketched in Figure VIII-2. The adsorption signal did not return to the initial base line. Hence the "true" area under the curve is difficult to define, and any heats of reaction become order of magnitude estimates only. The heats of adsorption were approximately of the same order of magnitude as those obtained at the higher temperature. The desorption signal returned closer to its original base line. Two desorption heats were found to be 27.3 and 32.8 Jg^{-1}, the

mean of which is about the same as the heat of desorption obtained at 37°C.

VIII-1-2 Water Adsorption on Ferric Oxides A and B.

The reaction between water vapour and ferric oxide A was investigated at 4 different temperatures. The results for both adsorption and desorption are given in Table VIII-3, in which the figures in brackets are the number of hours for which the sample was treated with dry and wet nitrogen before the adsorptions and desorptions respectively. Typical thermograms are sketched in Figure VIII-3. They are not to scale and only reflect the major structural differences between the observed signals. The structures of the adsorption and desorption signals were related. With reference to the schematic curves in Figure VIII-4, desorbing before the knee(i) in the adsorption signal gave a "structureless" desorption signal without the rounded minimum or the inflexion(2). Desorbing after the knee in the adsorption signal resulted in the "normal" desorption signal. At 37°C more than 9 hours of flushing with dry nitrogen were required to achieve complete desorption. After 9 hours of flushing, the heat of adsorption was 568 Jg^{-1} compared to a mean of 644 Jg^{-1} obtained using flushing times of between 44 and 24 hours. The reaction at 19.5°C was so slow that the heats of reaction can only be considered as order of magnitude estimates. No other work was carried out at this low temperature as a consequence.

Water vapour was adsorbed on about 0.08g ferric oxide B at about 25.50 ±0.05°C and 37.20 ± 0.05 °C. The results are given

in Table VIII-4, and typical thermograms sketched in Figure VIII-5. The structural features found in both the adsorption and desorption and signals for ferric oxide A are absent. At 25°C ferric oxide B showed a greater base line shift after a given period of time than ferric oxide A. The following trends were observed for both samples:

1, Heat of adsorption at 25°C was less than the heat of adsorption at 37°C.;

2, Heat of adsorption at T°C was less than or equal to the heat of desorption at T°C (T = 25 or 37°C);

3, Rate of reaction at 37°C was greater than the rate of reaction at 25°C;

4, Rate of desorption at T°C was greater than the rate of adsorption at T°C (T = 25 or 37°C).

VIII-1-3 Water Adsorption on α- and β-Goethite.

The results of the water vapour adsorption experiment, using α- and β-goethite as the adsorbent in turn are given in Table VIII-5. The adsorption and desorption signals for both samples were simple curves without any of the structural features present in the ferric oxide A signals. Typical signals are shown in Figure VIII-5. The signals tended to return to their original base lines. The qualitative trends observed for the ferric oxides A and B concerning the heats and rates of reaction, stated above (VIII-1-2) were again found to be true.

VIII-2. Discussion.

VIII-2-1 The Calibration Experiments.

It was thought that a better understanding of the iron oxide/water interaction would be useful in interpreting the previous adsorption results. The microcalorimeter was used in the flow mode as described earlier in an attempt to provide qualitative differences between the various iron oxides. Vapour phase adsorption was used in these preliminary experiments to simplify the apparatus required and ease the interpretation of the results. Dry nitrogen was passed over the sample and then the flow interchanged with moist nitrogen and the heat effects recorded. The moisture content of the nitrogen was not measured. As a consequence the state of the adsorbent surfaces was never known exactly. The experiment could thus only furnish qualitative differences between the iron oxides studied. These deficiences could be overcome if the experiment was ever to be exploited further. The remaining problem concerns the finite time required to generate a saturated (or other specified concentration) vapour of water in the reaction cell, owing to diffusion and adsorption of the water in the apparatus. It was assumed that, with the flow rates used, the nitrogen carried an amount of water approximating to the maximum saturated content. The nitrogen carrier gas was considered to be inert, even though it is known that nitrogen can adsorb physically and chemically at ambient temperatures on metal oxides. External diffusion of water into the system was also neglected.

The blank calibration and haematite adsorption and desorption experiments were performed to see if the proposed

experiment was feasible. The haematite sample was chosen because of its high purity, lack of porosity and low surface area, as the compound most likely to give an unambiguous test of the sensitivity of the experiment.

The heat effects found when interchanging the flows of "dry" and "wet" nitrogen in the blank experiment have no simple explanation, and are probably the resultant of several phenomena occurring simultaneously. Effects likely to be involved include: changes in the thermal properties of the cell, changes in the frictional heat effect; heat of dilution effects; adsorption and desorption on the walls of the cell; and condensation and evaporation of the bulk liquid. These last3effects are probably the most significant. No attempt was made to investigate the blank heat effect any further. In absolute terms, the heat effects were of the same order of magnitude as the largest heats obtained during the liquid adsorption measurements. For reversible changes, the heats of reaction in each direction should be equal in magnitude and opposite in sign. This was found to be true at both temperatures within the limits of experimental error. The heats of reaction at 25°C and 37°C were sufficiently close so that a mean of heat of 0.6 J was assumed for the effect. This figure is a negative quantity when referred to an exothermic (adsorption) process. Comparison of the thermograms in Figure VIII-1 show that the figures for both adsorption and desorption are sharper at the lower temperature. This suggests that the rate of heat flow is initially faster at the lower temperature. The reason for this is unclear.

The additional heat effects observed when the experiment was repeated with haematite in the reaction cell

were assumed to result from the adsorption and desorption of water. The base line of the thermal signals (Figure VIII-2) often did not return to their original position after the primary heat change was completed. This "tail" effect was most pronounced at the lower temperature. Generally the adsorption signals were most affected and this was subsequently found to be true for all the oxides studied.

The slow return of the signals presented a problem in defining the area under the curve as in Figure VIII-6. The area is clearly dependent on the choice of the base line, and the hatched area is not included in either estimate. The blank calibration signals did not show this effect, suggesting that it is "real" and not an artefact. Tests of the base stability at several stages throughout the course of the experiments failed to produce base line drifts that could account for the "tail" effect. It was noticed that changes in the flow rate did cause minor shifts in the base line. This effect was small and complicated, apparently linked to transient pressure changes caused by the operation of taps as well as through actual long-term variations in flow rate. The different iron oxides studied had different tail effects associated with them; α- and β-goethite had smaller tail effects than ferric oxide A or B. Ferric oxide A suffered the most from the tail effect and haematite the least. These variations almost certainly mean that the tail effect is real and dependent on the surface chemistry of the iron oxide/water interaction. Guderjahn and co-workers [146] in immersion studies of AL_2O_3 in water have noticed

a slow evolution of heat for several hours after the main heat change had finished. This was attributed to the partial rehydration of surface hydroxyls lost during outgassing. It is also well known that metals and metal oxides react slowly with atmospheric moisture. Collins et al[96] found that rust required up to 20 hours to equilibrate to a set humidity. Hence the equilibrium between free molecular water and physically adsorbed water is attained only slowly. It seems likely that the slow physical adsorption and desorption of water was the main reason for the tail effect, as evacuation and heating to at least above 50°C are normally required to desorb appreciable numbers of surface hydroxyls.

The heats of adsorption and desorption at 37°C (Table VIII-2) were approximately equal, as expected for a reversible process. At ca 20°C the heat of adsorption was of the same order of magnitude, although possibly smaller. The large tail made accurate assessment of the heat effect impossible. The heats of desorption at 20°C and 37°C were about the same. All of these measurements were made neglecting the hatched region shown schematically in Figure VIII-6. This area was estimated as about 5-10% of the measured area at 37°C.

VIII-2-2 Water Adsorption on Ferric Oxide A.

The main heats of adsorption and desorption for the water vapour/ferric oxide A system are given in Table VIII-3, and plotted as a function of temperature in Figure VIII-7. The heats of desorption are greater than the heats of adsorption irrespective of temperature. The apparently anomolous result at ca 25°C corresponds to the only pair of adsorption/desorption reactions with similar flushing times (see Table VIII-3).

The adsorption curve is sigmoidal, although it must be stressed that the data at ca. 19°C can only be regarded as approximate. The curve reflects the balance between the extent of reaction as determined by the total number of molecules reacting and the "average" energy of each molecular reaction. The detailed interpretation of these results hinges on the effect of the surface pretreatment, which is unknown. It is doubtful that chemisorption reactions are significant. It is known that the first physically adsorbed water layer is doubly hydrogen bonded to iron oxide surfaces. Assuming a hydrogen bond strength of 20 $KJmol^{-1}$; half of the difference between the heats of adsorption at ca. 25 and 37°C can be accounted for by assuming that the reaction at 37°C involves the first physically bound water layer, while that at 25°C does not. It is possible that some of the observed trends result predominantly from the differences between the rates of reaction relative to the period of observation and measurement. If it is assumed that the "reactivity" of the surface with respect to either adsorption or desorption can be represented by the maximum signal height, then the plot of height versus temperature will give an indication of the change of reactivity with temperature. The initial reactivity can be considered as a measure of the favourability of the reaction comprising both kinetic and thermodynamic terms. The mean signal heights for adsorption and desorption, measured to at least 1 part in 300, are plotted against temperature in Figure VIII-7. The reactivity is low at the lower temperature and increases steadily with increasing temperature. This adsorption curve does not match the heat of reaction versus temperature curve, suggesting that rate effects are important. The mean heights for desorption

signals are consistently larger than those for adsorption signals, confirming the differences found between the heats of adsorption and desorption.

For reversible changes the heats of reaction in either direction should be the same. This was found for the heats of adsorption and desorption of water vapour on the non-porous haematite sample. The ferric oxide A is porous, and it is likely that the relative pressures of water used were at least above 0.3 - 0.4. This means that the adsorption and desorption reaction occurred in the relative pressure range for which capillary condensation in mesopores is important. The adsorption and desorption reactions are likely to be different and not exactly reversible. Different heats of adsorption and desorption are therefore to be expected. Various authors [191,192,193] have found anomalously high differential heats of adsorption and desorption for different vapour phase adsorption systems in the region of saturation. The effect has generally been found to be greater for desorption than for adsorption. These results lend support to the view that the differences between the heats of adsorption and desorption found in this work are real and not some artefact.

The reactions were slow and the structure of the adsorption and desorption signals were related (Figure VIII-4). The signal structure could be related to the porous structure of the adsorbent. None of the other oxide samples studied showed this effect, and none of them definitely had a narrow pore size distribution. There is some doubt as to the validity of the distribution curve for α-geothite.

VIII-2-3 Comparison Between the Iron Oxides.

The heat effects for ferric oxide B, α- and β-goethite were less than those found for ferric oxide A. For all the samples, the heats of reaction at ca 37°C are greater than those at ca 25°C. The goethite samples had approximately equal heats of adsorption and desorption at ca 37°C. This suggests that they have similar surfaces with respect to water adsorption and desorption. The maximum heats of adsorption of all the samples studied are given in Table VIII-6 in Jg^{-1} and in Jm^{-2}. The goethite samples have approximately the same surface areas and heats of reaction. It is unclear why ferric oxide A and B should have similar heats of adsorption when expressed in Jm^{-2}. The pore size distributions and surface areas of the two oxides are different, which suggests that they have different affinities for water per unit area of surface. The most striking feature of Table VIII-6 is in the high heat of adsorption of water on haematite when expressed in terms of Jm^{-2}. This suggests that the porous nature of the other samples, which are all similar, accounts for the difference. Either, the application of the specific surface areas is incorrect, which suggests that the interior surfaces of the porous samples did not react, or the reactions were so slow that the bulk of the heat effect was not measured.

There was no relevant data in the literature with which to compare these results. It was decided to check that the heats of adsorption were consistent with general expectations by calculating some theoretical heat changes from a hypothetical thermochemical cycle (Figure VIII-8) and comparing the results. Heats of vaporisation of water

are well known, and so the steps 1 and 4 can be calculated. Partyka et al[81] have shown that for many metal oxides, a heat of immersion of a hydroxylated surface in water at 31 °C releases about 450 mJm^{-2}, and that immersion of a surface with 2 or more water layers preadsorbed results in a heat change of about 112.5 mJm^{-2}. Using these values for steps 2 and 5 respectively, and assuming 5 monolayers of water adsorbed, the results in Table VIII-7 were calculated. Considering the assumption involved, the agreement between the calculated and observed values is surprisingly good. The calculation was repeated, using the exact data taken from Partyka's paper, for ZnO and Al_2O_3 for comparison. When expressed in Jm^{-2}, the calculated values are constant, at about 3.7 Jm^{-2}, whereas the observed values differ slightly (see Table VIII-6). It is not clear why the observed heat of adsorption on haematite is so high.

The general trends of increasing rate and heat of reaction with temperature are in accordance with general expectations. The differences between the porous and non-porous iron oxides became apparent in the discrepancies between the heats of adsorption and desorption, and by changes in the rates of reaction. The heat changes associated with ferric oxide A gave thermal signals which were not the simple curves found for the other samples. This is possibly connected with the narrow pore size distribution found for ferric oxide A. The slow rates of reaction make detailed interpretation of these results difficult.

FIG. VIII.1.

The blank calibration thermograms.

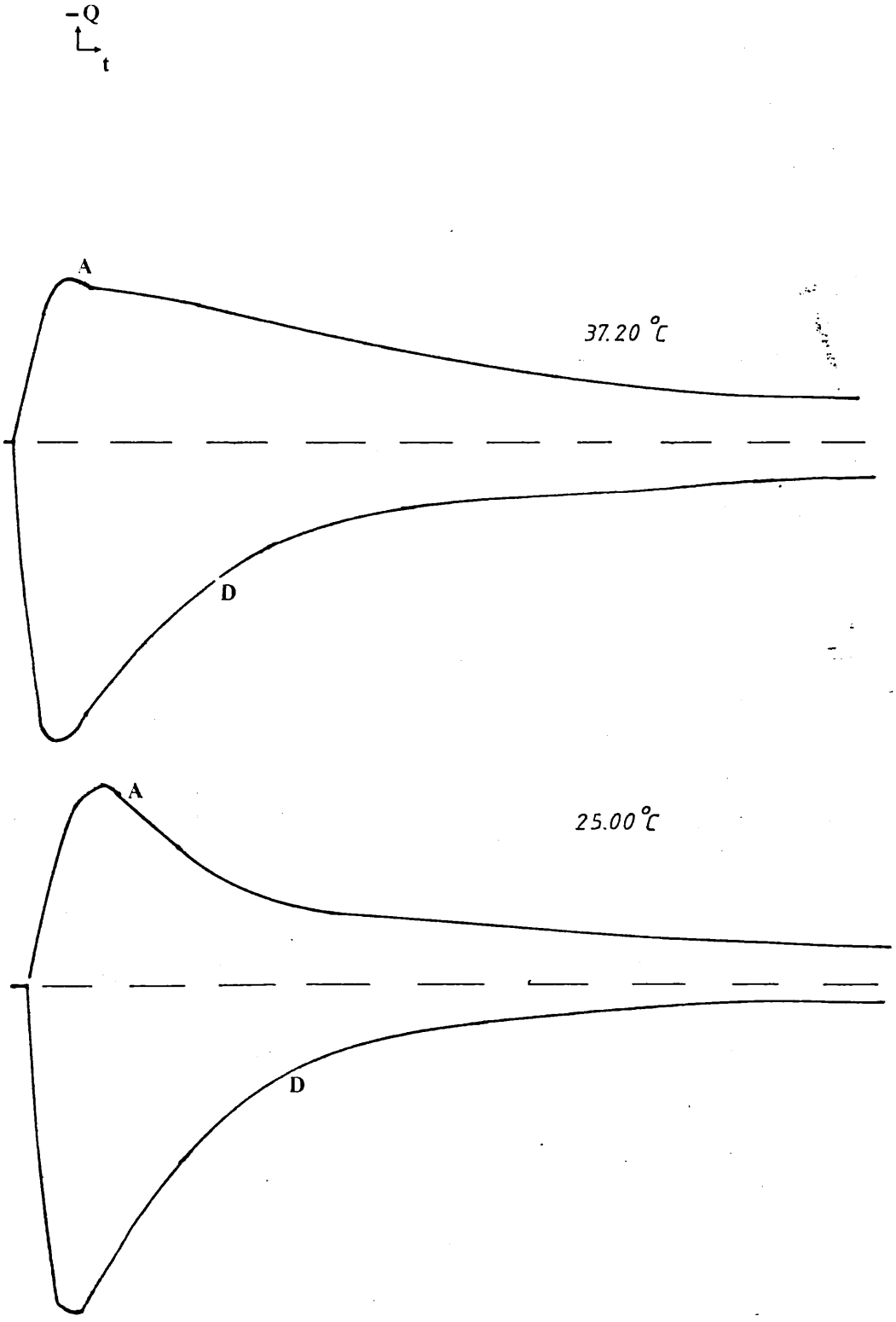

FIG. VIII.2.

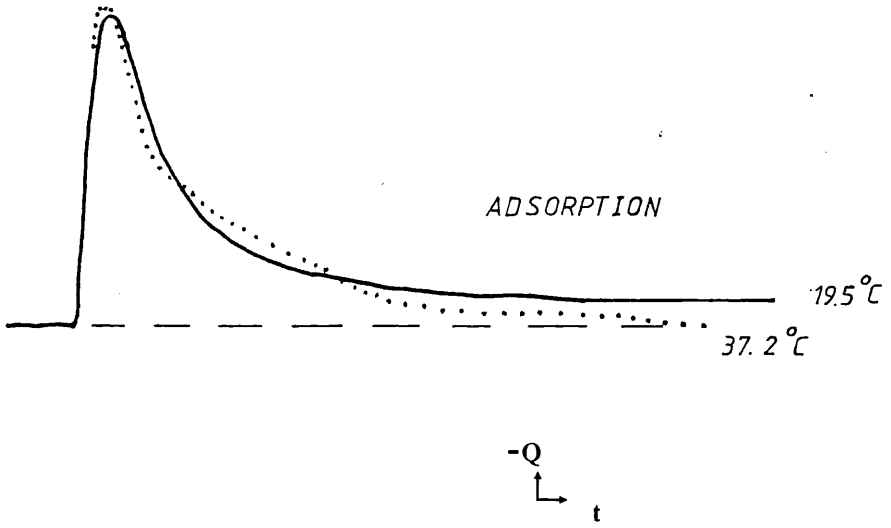

Sorption thermograms of the water vapour/ α-haematite system.

FIG. VIII.3.

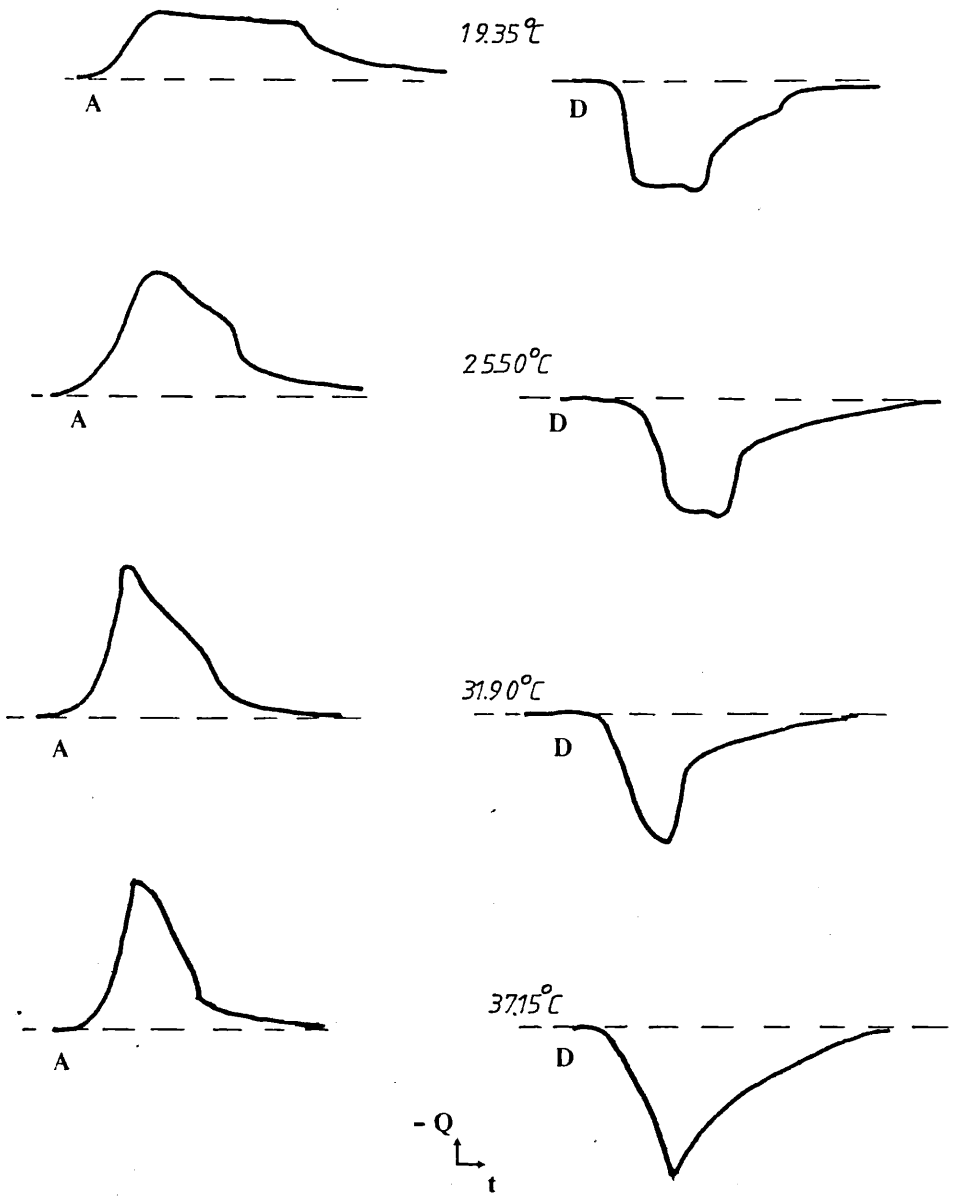

Sketches of the sorption thermograms of the water vapour/ferric oxide A system.

FIG.VIII.4.

The structural features of the sorption signals for the water vapour/ferric oxide A system.

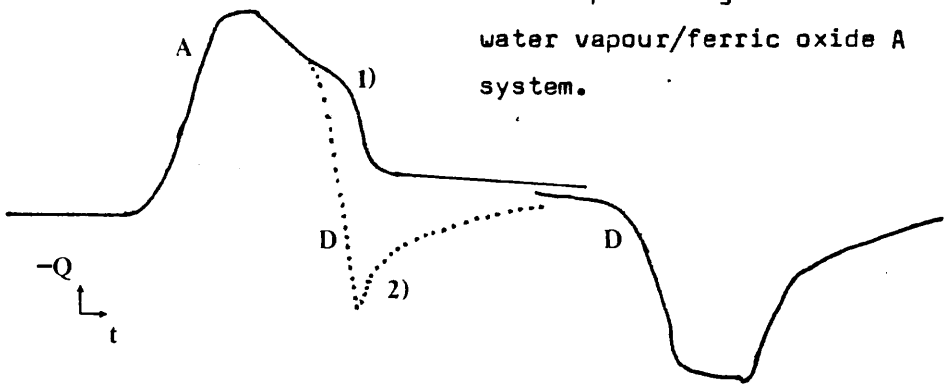

FIG. VIII.5.

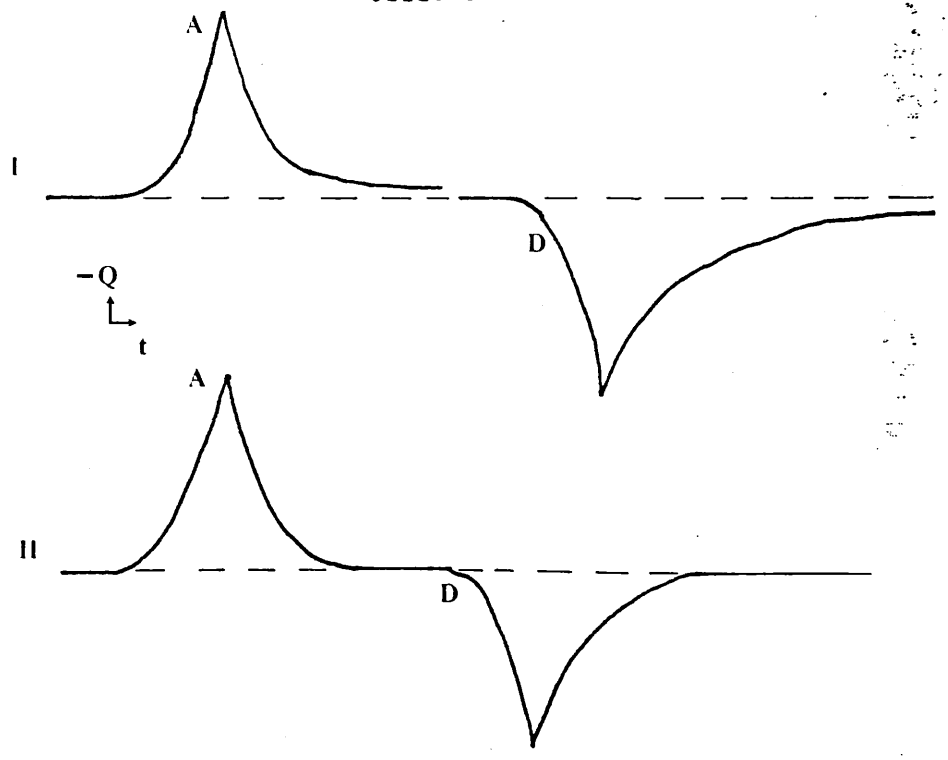

Sketches of the sorption thermograms of the water vapour/ ferric oxide B system I., and the water vapour/ α-and β -goethite sustems III, (not to scale).

FIG. VIII.6.

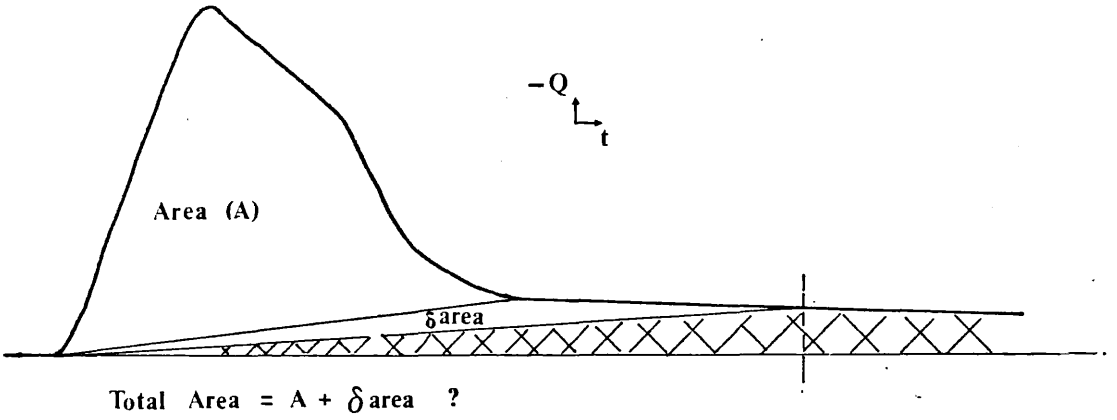

An illustration of the problem of assigning an area to a slowly decaying sorption signal.

FIG. **VIII.7.**

The mean heats of sorption and mean heights of the sorption signals for the water vapour/ferric oxide A system.

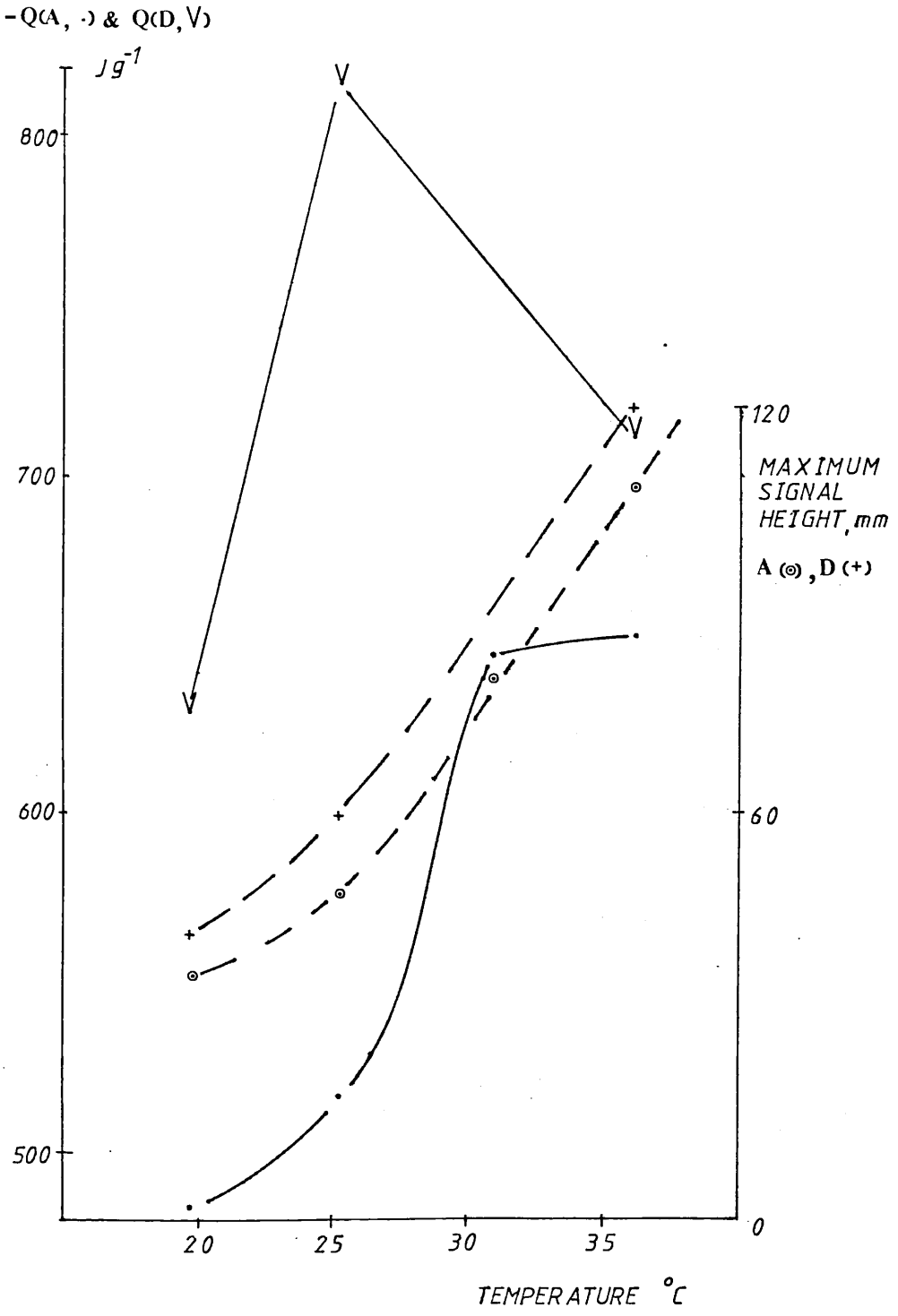

Fig. VIII.8.

A hypothetical thermochemical cycle for the adsorption of water vapour on a hydroxylated surface S.

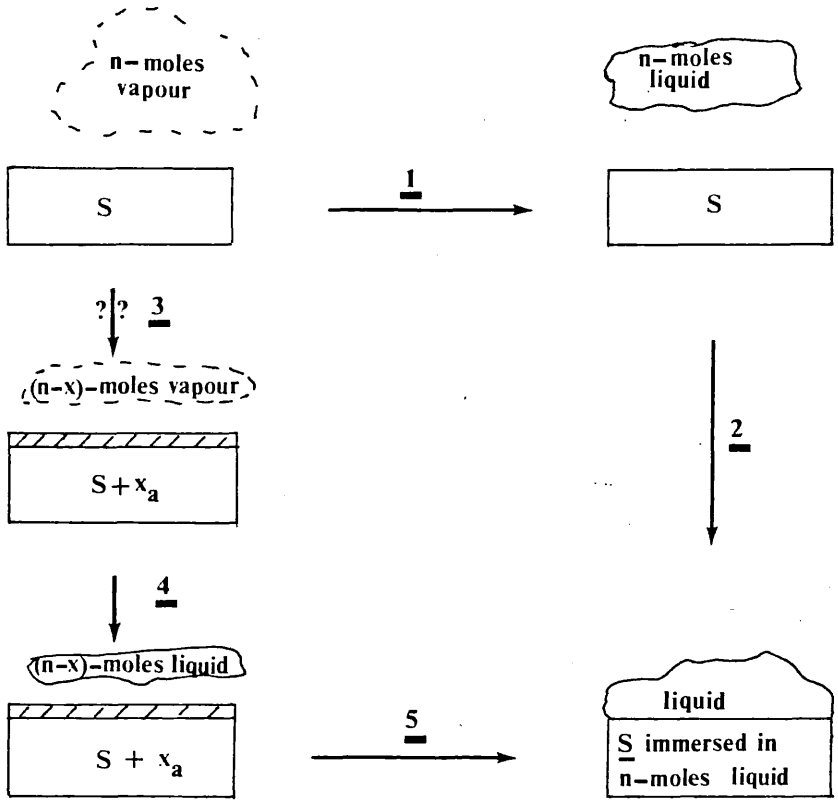

Chapter IX

Summary and Conclusions

A volumetric nitrogen adsorption apparatus was built and tested using the commercially available standards Sterling FT-G(2700) and Silica TK 800; satisfactory results were obtained (see table below). The apparatus was used to characterise five iron (III) oxides, assumed to be model constituents of the surface of mild steel:-

Sample	Isotherm type	Hysteresis Type	S_w /m^2 g^{-1}	c (BET)
Silica TK 800	-	-	164.1 ± 1.4	83
Sterling FT-G(2700)	-	-	10.9 ± 0.4	-949
Ferric oxide A	IV	A	245 ± 2.5	75
Ferric oxide B	IV	B	158.5 ± 1.6	114
α-goethite	IV	low pressure	112.3 ± 1.6	80
β-goethite	IV	B	105.1 ± 1.2	179
α-haematite	II	none	2.7 ± 0.4	79

Except for α-haematite the isotherms for the iron oxides exhibited a hysteresis loop indicative of capillary condensation in mesopores and α_s-plots (Fig. VI-22), constructed using α-haematite as the non-porous reference, confirmed both this and the absence of micropores. The porous samples had similar adsorbent-adsorbate interactions as α-haematite in the relative pressure range of monolayer formation. The isotherm for α-goethite was dominated by interparticle condensation above $P/P_o \simeq 0.8$ and exhibited a low pressure hysteresis loop. This may be caused by swelling of the structure during adsorption trapping some adsorbate thereby hindering desorption. Pore size distributions indicated that oxide A had a narrow distribution with $\bar{r}_p \simeq 25$ Å in contrast with the continuous distributions for the other oxides. However, these calculations are questionable since only the hysteresis loop for oxide A resembled Type A.

In an attempt to improve the weathering characteristics of the adhesive-adherend interface, maleic anhydride has been used to modify the surfaces of oxides A and B. The maleic anhydride displaced some

physisorbed water and could not be removed by outgassing. For oxide A, increasing the outgassing temperature induced desorption of water rather than anhydride:-

Outgassing Conditions	Treated oxide A		Untreated oxide A	
temperature, time, final pressure / (°C, hr, mm Hg)	S_w /m^2 g^{-1}	c (BET)	S_w /m^2 g^{-1}	c (BET)
50, 20, $<10^{-4}$	178	39	230	75
130, 18, $<10^{-4}$	203	58	240, 244	81, 82

For oxides A and B the amount adsorbed at any given relative pressure is less for the treated surface than for the untreated surface. The pore structures were unaffected, as exemplified by the α_s-plots (Figs. VI-20, 21) and the pore size distributions. The effect of the organic treatment is to reduce the surface area of the oxides probably by blocking the most active adsorption sites.

The adsorption of n-butanol from an n-heptane solution onto α-haematite was found to be reversible although the desorption was slower than the adsorption. The heat of adsorption was 44 mJ m^{-2} and the heat of desorption 58 mJ m^{-2} (assuming BET areas). These effects may be interpreted by supposing the adsorption is a nearly-activationless process and probably includes some displacement of surface water whereas desorption, which is accompanied by adsorption of solvent, is activated and produces a surface devoid of water unlike the initial surface. The feasibility of this is demonstrated by assuming a residual 10 ppm water in the dried solvent, of which about 3 dm^3 is required to generate a monolayer equivalent of water per 100 $Å^2$ of surface. Typically 20-25 cm^3 would then be required to generate a monolayer on α-haematite matching the volumes used experimentally. The pore structure of oxide A further hindered the already kinetically unfavourable desorption: the heat of adsorption was a function of the number of previous sorption cycles, the

"flushing volume" and the concentration. These effects cannot be entirely attributable to water contamination of the heptane. To supply the large surface area of oxide A with a monolayer of water the volume of solvent was approximately 10 times more than that actually used. However, a slow surface reorganisation, after the initial adsorption, independent of the presence of moisture would explain the observed effects. Experiments (Fig. VII-9) showed that some butanol was irreversibly adsorbed and occupied about 25% of the available surface. This irreversibility makes comparisons with haematite difficult, although generally the heat of butanol adsorption on oxide A is greater than for α-haematite. The maximum in the heat of adsorption versus concentration curve for oxide A (Fig. VII-10) occurs in the range 0.2-0.4 wt. % butanol which is close to the concentration at which a close packed, hydrogen bonded layer forms on a non-porous surface. This suggests that, for butanol adsorption, much of the porous surface behaves similarly to a non-porous surface and that the remainder has an increased interaction arising from either weak chemisorption or from an enhanced adsorption potential in small pores.

The adsorption of 1,2-epoxybutane on α-haematite was reversible and for a 0.2 wt. % solution the heat of adsorption (ca. 26 mJ m^{-2}) was about half that found for butanol. The heat of adsorption versus concentration curve reached a maximum (55 mJ m^{-2}) in the range 1.0-2.0 wt. %. Assuming this region is associated with the state of maximum packing of adsorbate, it occurs at a higher concentration than for butanol adsorption, suggesting surface orientation effects are important. In contrast the adsorption of 1,2-epoxybutane on oxide A was largely irreversible (Fig. VII-12) and the initial adsorption (Q ads. = 110 mJ m^{-2}) was slow compared to butanol adsorption. Subsequent heats of sorption were much smaller ($\simeq$ 16 mJ m^{-2}), irrespective of the flushing volume, implying that about 15% of the surface is available for

reversible sorption. In view of the high initial heat of adsorption it is possible that, following adsorption a surface hydrolysis occurs resulting in conversion of the adsorbed species to a diol.

The water vapour sorption experiments were speculative but indicated that heats of adsorption on the non-porous haematite (12 Jm^{-2}) were about 5 times larger than those on the other porous oxides (2-3 Jm^{-2}); this could be a kinetic effect. Desorption was faster than adsorption for all the oxides in contrast to the solution phase experiments.

These results are relevant to the mechanism of adhesion, provided the hydrated oxides are a genuine representation of corroded steel surfaces. It is known that these frequently consist of thin, often porous oxide films. Further it is well-established that removal of adventitious water from a surface prior to bonding enhances the joint's characteristics. The qualitative kinetic observations made during the water vapour sorption suggest that a short "drying period" immediately prior to bonding of a surface could desorb more water than would readsorb in a smilar time interval between drying and application of adhesive. The irreversible adsorption of maleic anhydride also displaced some surface water and probably blocked the more active adsorption sites, thereby decreasing the extent of subsequent water adsorption. In both cases the reduction of surface water would increase a joint's life. If suitable substituents (e.g.:- NH_2 , $-\overset{O}{\overset{\frown}{CH-CH_2}}$) could be incorporated into the maleic anhydride, then the possibility exists that primers, acting in a similar mode to silane-based primers, could be developed. Alternatively, if a substituted epoxide could be irreversibly adsorbed on a surface then, either the use of primers becomes unnecessary or the epoxides could be used as the primer. The microcalerimetric results clearly distinguish between the irreversible sorption of butanol and epoxybutane on a porous surface and their reversible sorption on a nonporous surface. Epoxybutane was 80-90% irreversibly adsorbed on the porous surface,

possibly as a result of a surface hydrolysis to a diol after the initial adsorption; in which case the adsorption mechanism would resemble that for dissociative chemisorption. The partly irreversible adsorption of organic material resembles the adsorption behaviour of corroded steels found by Heal[97], supporting the view that the porous oxides at least are a reasonable representation of corroded steel surfaces. The water sorption experiments show that the nonporous surface is more reactive (has a higher heat of water adsorption) than the porous surface, although this is partly a kinetic effect. It might be that the adsorbed water within the pores of oxide A catalyse the hydrolysis of the epoxybutane.

Key to Tables.

1, W is the final weight of adsorbent.

2, $V(a)$ is the gaseous volume adsorbed in cm^3 at a pressure P, corrected to standard temperature and pressure.

3, P/P_o is the relative pressure of nitrogen where P is the saturated vapour pressure of nitrogen at the measured temperature of the liquid nitrogen coolant bath.

4, $P\left[V(a)(P_o - P)\right]^{-1}$ is the BET function.

Table II-1. Classification of pores according to IUPAC.

Micropores:	$\lesssim$ 2nm.
Mesopores:	$\gtrsim$ 2nm. $\lesssim$ 50nm.
Macropores:	$\gtrsim$ 50nm.

Table II–2

1	2	3	4	5	6	7	8	9	10	11	12	13	14	15
P/P_o	V_a^{gas}/W	R_k	t	R_p	$\bar{R}_k$	$\bar{R}_p$	Δt	$\Delta V_a^{gas}/W$	ΔV_f	ΔV_K	ΔV_p^{gas}	ΔS_p	$\sum \Delta S_p$	$-\Delta V_p^{liq.}$
.990	145.5	950.8	28.05	978.9										
					711.9	737.0	5.83	3.8	0	3.8	4.07	.172	.172	.006
.980	141.7	473.0	22.22	495.2										
					393.3	414.2	2.84	3.0	.0313	2.97	3.28	.247	.420	.005
.970	138.7	313.7	19.38	333.1										
					273.9	292.4	1.80	2.2	.048	2.15	2.45	.261	.681	.004
.960	136.5	2341	17.58	251.7										

THE START OF THE CALCULATION OF THE
PORE SIZE DISTRIBUTION FOR
FERRIC OXIDE A, OUTGASSED AT 50°C.
ALL LENGTHS ARE IN Å AND ALL VOLUMES IN $cm^3 g^{-1}$.

Table V-1. The Volumes of the Gas Burette.

Bulb.	Volume at 26.9 ± 0.2 °C (this work) cm^3	Volume at 22.2 °C (found by B.P. Ltd). cm^3	Cumulative Bulb Volume cm^3
A.	7.758	7.753	7.758
B.	7.307	7.303	15.065
C.	18.104	18.102	33.169
D.	18.620	18.620	51.789
E.	34.422	34.408	86.211
F.	36.936	36.923	123.147
Total Volume:	123.147	123.109	

Note: For each bulb volume the error in the quoted value is ± 0.002 cm^3 and is the standard deviation σ_{N-1} of 8 determinations.

Table VI-1. Nitrogen adsorption on Silica TK 800.

P/P_0	$V(a)$ (cm^3)	$P/V(a)(P_0 - P)$ $(cm^{-3}) \ 10^{-3}$
0.0328	10.06	3.38
0.0401	10.42	4.00
0.0501	11.15	4.73
0.0586	11.23	5.54
0.0710	11.66	6.56
0.0777	11.87	7.10
0.0869	12.14	7.84
0.0960	12.77	8.32
0.1147	13.24	9.78
0.1422	13.87	12.0
0.1580	14.21	13.2
0.1796	14.65	14.9

W = 0.3372g.

Table VI-2. Nitrogen adsorption on Sterling FT-G2700.

P/P_0	$V(a)$ (cm^3)	$P/V(a)(P_0 - P)$ $(cm^{-3}).10^{-3}$
0.0321	4.270	---
0.0435	4.770	9.53
0.0652	4.865	14.3
0.0889	4.961	19.7
0.1367	5.210	30.3
0.1717	5.457	---

W = 1.7831g.

Table VI-3. Nitrogen adsorption and desorption on ferric oxide A.

RUN I.

Adsorption.

P/P_0	$V(a)/W.$ $cm^3g^{-1}.$
0.0274	44.0
0.0316	44.9
0.0368	45.9
0.0481	47.9
0.0600	49.8
0.0709	51.4
0.0863	53.4
0.0982	54.9
0.1144	56.7
0.1222	57.7
0.1344	59.0
0.1627	62.1
0.2033	66.2
0.2344	69.5
0.2755	73.8
0.2952	76.0
0.3210	78.8
0.3641	84.0
0.4332	93.1
0.5179	106.7
0.5704	117.0
0.6204	129.9
0.6472	135.7
0.6790	144.5
0.7616	171.0
0.9134	180.0
0.9926	200.8

$W = 0.6427g.$

RUN II.

Adsorption.		Desorption.	
P/P_0	$V(a)/W.$ $cm^3g^{-1}.$	P/P_0	$V(a)/W.$ $cm^3g^{-1}.$
0.1531	61.8	0.9966	202.7
0.2284	70.0	0.9943	192.6
0.3064	78.5	0.7843	181.7
0.3512	84.0	0.7763	181.5
0.4319	95.1	0.6592	176.9
0.5054	107.1	0.6194	171.9
0.5849	123.8	0.5995	157.5
0.6308	135.9	0.5797	143.8
0.6775	149.7	0.5347	122.3
0.6997	155.9	0.4770	105.9
0.7174	163.0	0.4812	104.5
0.7318	166.5	0.4571	100.1
0.7996	180.7	0.4384	96.1
0.9889	192.7	0.3912	88.4
0.9935	202.7	0.3414	82.6
		0.2796	75.2
0.9937	213.5	0.2309	69.9

$W = 0.6377g.$

Table VI-4. Nitrogen adsorption on ferric oxide A after outgassing at various temperatures.

RUN I.
Sample outgassed at 126 °C for 12 hrs.

P/P_o	$V(a)/W.$ $cm^3 g^{-1}.$
0.0458	48.8
0.0551	50.4
0.0686	52.4
0.0795	54.0
0.0954	56.0
0.1035	57.1
0.1144	58.4
0.1350	60.8
0.1671	64.4
0.2151	69.6
0.2545	74.0
0.3077	80.2
0.3357	83.5
0.3679	87.9
0.4049	92.9
0.4767	103.7
0.5064	109.7
0.5459	116.7

W = 0.4330g.

RUN II.
Sample outgassed at 122 °C for 20 hrs.

P/P_o	$V(a)/W.$ $cm^3 g^{-1}.$
0.0002	24.3
0.0515	49.1
0.0606	50.5
0.0656	51.3
0.1184	58.1
0.1369	60.3
0.1617	63.1
0.1796	65.0
0.2011	67.3
0.2232	69.7
0,2324	70.8
0.2706	75.0
0.3185	80.5
0.3869	89.1
0.4195	91.0
0.4353	93.3
0.4722	99.0
0.5110	105.6
0.5257	112.4
0.5411	114.7
0.5725	122.4
0.6358	138.7

W = 1.031g.

Table VI-5. Nitrogen adsorption on ferric oxide A after outgassing at various temperatures.

RUN III. Sample outgassed at 27°C for 6 hrs.		RUN IV. Sample outgassed at 27°C for 12 hrs.		RUN V. Sample outgassed at 50°C for 20 hrs.	
P/P_o	$V(a)/W$ $cm^3 g^{-1}$	P/P_o	$V(a)/W$ $cm^3 g^{-1}$	P/P_o	$V(a)/W$ $cm^3 g^{-1}$
0.0763	47.4	0.0241	38.6	0.0195	39.5
0.0894	48.9	0.0245	39.7	0.0285	41.7
0.1058	50.7	0.0297	40.9	0.0905	50.9
0.1187	51.7	0.1932	60.3	0.1057	52.6
0.1345	53.7	0.2279	63.8	0.1259	54.8
0.1420	54.4	0.2729	68.4	0.1415	56.3
0.1660	56.9	0.3052	71.9	0.1601	58.2
0.1997	60.2			0.1801	60.3
0.2244	62.6				
0.2549	65.6				
0.2694	67.1				
0.2860	68.9				
0.2895	69.3				
W = 0.9509g.		W = 0.9509g.		W =0.9509 g.	

Table VI-6. Nitrogen adsorption and desorption on ferric oxide A after treatment with maleic anhydride and outgassing at 50 °C.

Adsorption.		Desorption.	
P/P_o	$V(a)/W.$ $cm^3 g^{-1}.$	P/P_o	$V(a)/W.$ $cm^3 g^{-1}.$
0.0083	21.4	0.9565	135.9
0.0118	22.9	0.8698	133.5
0.1138	38.6	0.6532	130.1
0.1407	41.1	0.5784	125.9
0.1812	44.6	0.5523	111.2
0.2145	47.5	0.5241	97.8
0.2609	51.6	0.4623	78.9
0.2849	53.8	0.3976	65.5
0.3152	56.7	0.3861	64.0
0.3487	60.0	0.3234	57.5
0.4381	69.8	0.2678	52.3
0.5000	78.2	0.2265	48.7
0.5711	89.4	0.1762	44.3
0.6009	95.1	0.1420	41.3
0.6317	101.8		
0.6433	103.5		
0.6701	110.1		
0.7026	117.7		
0.7392	124.5		
0.9590	135.8		
0.9902	145.9		

$W = 0.5783g.$

Table VI-7a+b a) C and H analyses on ferric oxide A, treated with maleic anhydride, before and after outgassing at 50 °C.

	Wt.%C.	Wt.%H.
Before	5.06	1.30
After	5.12	1.19

Weight loss = 2.5%.

b) C and H analyses on ferric oxide A, treated with maleic anhydride, before and after outgassing at 130 °C.

	Wt.% C.	Wt.% H.
Before	5.06	1.30
	5.10	1.31
After	5.17	1.02
	5.15	1.02

Weight loss = 3.5%

Table VI-8. Nitrogen adsorption and desorption on ferric oxide A after treatment with maleic anhydride and outgassing at 130^{0}C.

Adsorption.		Desorption.	
P/P_0	$V(a)/W.$ $cm^3g^{-1}.$	P/P_0	$V(a)/W.$ $cm^3g^{-1}.$
0.1010	45.2	0.8047	147.7
0.1257	47.6	0.6496	145.5
0.1630	51.3	0.5701	129.7
0.2422	58.5	0.5362	113.0
0.2999	64.0	0.4679	90.0
0.3981	74.7	0.3976	74.8
0.4859	86.3	0.3805	72.8
0.5961	104.9	0.3129	65.5
0.6630	120.7	0.2127	55.9
0.7413	139.9	0.1635	51.2
0.9844	154.8		

$W = 0.4692g.$

Table VI-9. Nitrogen adsorption and desorption on ferric oxide B.

RUN I : Adsorption.		RUN II : Adsorption.		RUN II : Desorption.	
P/P_0	$V(a)/W.$ $cm^3 g^{-1}$	P/P_0	$V(a)W.$ $cm^3 g^{-1}$	P/P_0	$V(a)W.$ $cm^3 g^{-1}$
0.0575	34.1	0.5426	74.0	0.9859	391.0
0.0714	35.4	0.8941	230.0	0.9383	362.7
0.0947	37.1	0.9862	391.0	0.9514	360.4
0.1479	40.6	0.9877	424.4	0.9323	347.4
0.1928	43.5			0.9221	335.3
0.2398	46.7			0.9118	305.1
0.3039	51.1			0.9019	274.6
0.4002	58.6			0.8753	221.7
0.4771	65.6			0.8274	173.8
0.5711	76.5			0.8259	171.0
0.6114	82.6			0.8098	159.8
0.6532	90.4			0,7552	126.3
0.6567	90.9			0.7036	106.6
0.6906	98.5			0.5960	81.8
0.7220	107.7			0.4909	67.9
0.7277	108.8			0.4742	66.2
0.7532	117.6			0.4377	60.9
0.7787	127.9			0.3837	58.0
0.7816	129.9			0.3060	52.1
0.8050	139.6			0.2527	48.1
0.8200	150.9			0.1895	43.9
0.8257	154.3			0.1492	41.3
0.8400	165.0				
0.8527	176.8				
0.8543	177.8				
0.8668	187.3				
0.8890	215.4				
0.8983	227.0				
0,9068	239.8				
0.9082	245.4				
0.9202	275.5				
0.9263	287.8				
0.9352	301.0				
0.9380	308.0				
0.9481	339.7				
0.9783	370.1				
0.9881	383.0				

W = 0.5015g.

Table VI-10. Nitrogen adsorption and desorption on ferric oxide B after treatment with maleic anhydride and outgassing at 50°C.

Adsorption.		Desorption.	
P/P_0	$V(a)/W.$ $cm^3g^{-1}.$	P/P_0	$V(a)/W.$ $cm^3g^{-1}.$
0.0435	24.2	0.9836	390.6
0.0537	25.4	0.9812	349.8
0.0703	27.3	0.9398	314.0
0.0850	28.6	0.8937	250.2
0.1085	30.5	0.8557	186.2
0.1440	33.0	0.8570	181.3
0.1816	35.4	0.8350	167.1
0.2334	38.5	0.7724	125.2
0.3157	43.8	0.7150	100.9
0.3953	49.0	0.5934	72.6
0.5104	58.0	0.4811	58.0
0.5522	63.6	0.4558	55.1
0.6092	71.5	0.3965	50.1
0.6511	78.2	0.3508	46.7
0.7606	106.6	0.2689	41.1
0.8478	153.5	0.2152	37.9
0.8819	185.7	0.1228	32.0
0.9068	220.8		
0.9175	235.4		
0.9209	243.8		
0.9465	313.0		
0.9813	349.7		
0.9831	390.6		
0.9828	407.2		

W = 0.4063 g

Table VI-11. C and H analyses on ferric oxide B, treated with maleic anhydride, before and after outgassing at 50 °C.

	Wt.% C.	Wt.% H.
Before	3.16	1.10
After	3.16	1.02

Weight loss = 0.5%.

Table VI-12. Nitrogen absorption and desorption on α-goethite.

Adsorption.		Desorption.	
P/P_o	$V(a)/W$. cm^3g^{-1}.	P/P_o	$V(a)/W$. cm^3g^{-1}.
0.0763	24.5	0.8546	429.2
0.0991	25.7	0.7707	305.9
0.1386	27.6	0.7650	300.8
0.1763	29.5	0.7545	286.6
0.2401	32.7	0.7423	273.8
0.2801	34.7	0.7217	242.6
0.3387	38.0	0.6916	214.4
0.3689	39.8	0.6408	167.5
0.4752	46.9	0.5792	130.2
0.6271	62.5	0.5765	125.5
0.7117	81.6	0.5485	116.0
0.7638	110.3	0.5233	107.9
0.7817	123.2	0.4692	90.8
0.7963	138.0	0.4121	78.5
0.8010	153.5	0.3287	64.3
0.8102	189.9	0.2681	54.9
0.8463	256.1		
0.8412	280.7		
0.8664	352.1		
0.8747	425.8		
0.8756	466.4		
0.8745	506.0		

$W = 0.3673g.$

Table VI-13. Nitrogen adsorption and desorption on β-goethite.

Adsorption.		Desorption.	
P/P_o	$V(a)/W.$ $cm^3 g^{-1}.$	P/P_o	$V(a)/W.$ $cm^3 g^{-1}.$
0.0922	25.0	0.9400	243.0
0.1207	26.3	0.9254	199.8
0.1700	28.5	0.9053	157.7
0.2195	30.5	0.8423	92.1
0.3047	34.1	0.7070	59.4
0.3605	36.6	0.6622	54.8
0.4463	40.5	0.5629	47.1
0.5084	43.7	0.4846	42.7
0.6567	53.4	0.3531	36.4
0.8343	81.6	0.2741	33.1
0.8970	114.6	0.1940	29.7
0.9232	155.4	0.1477	27.7
0.9339	191.7		
0.9338	196.6		
0.9458	240.4		
0.9490	258.4		
0.9441	260.9		

$W = 0.3467g.$

Table VI-14. Nitrogen adsorption and desorption on α-haematite.

Adsorption.		Desorption.	
P/P_o	$V(a)/W$ $cm^3 g^{-1}$	P/P_o	$V(a)/W$ $cm^3 g^{-1}$
0.0303	0.527	0.9211	2.648
0.0401	0.542	0.6625	1.399
0.0578	0.568	0.4995	1.138
0.0760	0.590	0.4458	1.057
0.1095	0.633	0.2816	0.857
0.1735	0.709	0.1960	0.739
0.1948	0.738		
0.2558	0.821		
0.3689	0.960		
0.4478	1.070		
0.5782	1.264		
0.6621	1.409		
0.9190	2.615		
0.9660	7.624		

$W = 2.6506g.$

Table VI-15. Specific Surface Areas (S_w) of ferric oxide A.

Untreated sample.		Organically treated sample.	
Outgassing conditions (°C, hr.)	S_w /$m^2 g^{-1}$	Outgassing conditions (°C, hr.)	S_w /$m^2 g^{-1}$
130,14.5	240.6	50,20	178.1
130,14.5	244.0	130,18	202.9
126,12	249.2		
122,20	245.9		
27,6	222.1		
27,12	224.7		
50,20	230.3		

Table VII-1.

Energies of adsorption and desorption of 0.2% 1-butanol in n-heptane on α-Fe_2O_3 at different flow rates.

Flow Rate $cm^3 min^{-1}$	Energy of Adsorption Jg^{-1}	Energy of Desorption Jg^{-1}
0.238	0.112	0.128
0.238	0.108	---
0.238	0.114	0.148
0.238	0.110	---
0.238	0.096	0.173
mean ($\pm\sigma_{N-1}$) =	0.108 ± 0.007	0.150
0.210	0.120	0.154
0.210	0.108	0.174
0.210	0.118	0.149
0.210	0.134	
mean ($\pm\sigma_{N-1}$) =	0.120 ± 0.011	0.159
0.108	0.086	0.113
0.108	0.115	0.149
mean =	0.101	0.131
0.15	0.101	0.188
0.047	0.117	--
0.047	0.097	--
mean =	0.107	--
0.024	0.095	--

Table VII-2. Energies of adsorption and desorption of 1,2-epoxybutane in n-heptane on α-Fe_2O_3.

Concentration of epoxybutane in n-heptane.	Energy of Adsorption.	Energy of Desorption.
Wt.%	Jg^{-1}	Jg^{-1}
0.04	0.055	0.078
0.04	---	0.033
0.16	0.065	0.047
0.32	0.042	---
0.32	0.057	0.054
0.40	0.059	0.025
0.80	0.093	0.097
0.80	0.093	0.085
1.00	---	0.104
1.00	0.097	0.151
1.46	0.151	0.197
1.46	0.161	0.176
2.00	0.149	---
2.00	0.147	0.218
2.92	0.118	0.281
2.92	0.118	0.290

Table VII-3. Energies of "Dilution".

Concentration of 1-butanol in n-heptane.	Adsorption Energy Effect.	Desorption Energy Effect.
Wt.%.	10^2J.	10^2J.
0.07	1.05+	1.20
0.07	1.05+	--
0.43	0*	3.10
0.43	0*	2.59
1.18	1.35	18.3
1.18	1.44	17.8
1.18	1.45	--
1.18	1.62	--
1.99	3.90	37.3
1.99	4.12	36.0
1.99	--	36.1
1.99	--	36.1

Note: 'Adsorption' and 'Desorption' in this context imply a change in the fluid flowing over the sample from heptane to solution and solution to heptane respectively.

\+ These figures relate to an exothermic process, all others an endothermic.

* The adsorption was so small it could not be distinguished from the background noise.

Table VII-4. Energies of adsorption and desorption of 1-butanol on ferric oxide A.

Concentration of 1-butanol in n-heptane.	Energy of Adsorption.	Volume of n-heptane passed over sample prior to adsorption.
Wt.%	Jg^{-1}.	cm^3.
0.205	20.1	---
0.205	21.2	---
0.205	18.0	---
1.99	17.5	50.0
1.99	19.1	80.0
2.01	15.3	49.0
2.01	16.0	60.0
2.01	16.4	59.5
2.01	13.9	26.5
2.01	17.6	102.0
2.01	16.3	58.0
2.01	9.6	7.5
2.01	16.7	67.0
2.01	17.4	84.0
2.01	20.2	185.0
2.01	14.6	47.0

Note : These results were obtained in chronological order starting from the top of the Table.

Table VII-5. Energies of adsorption and desorption of 1.99% 1-butanol in n-heptane on ferric oxide A as a function of the number of adsorption/desorption cycles.

Volume of n-heptane passed over sample prior to adsorption of 1.99% 1-butanol. / cm^3	Cycle. (n)	Energy of Adsorption. / Jg^{-1}	Energy of Desorption. / Jg^{-1}
---	1	20.7	---
81.0	2	18.1	15.4
82.5	3	15.0	---
81.5	4	15.3	16.6
81.5	5	15.3	15.6
81.5	6	15.0	14.1
81.5	7	15.4	---
	mean of cycles for which $n \geq 3$:	15.2 ± 0.2	15.4

Table VII-6. Energies of adsorption and desorption of 1-butanol in n-heptane on ferric oxide A as a function of concentration.

Concentration of 1-butanol in n-heptane. Wt.%.	Volume of n-heptane passed over sample prior to adsorption. cm^3	Energy of Adsoprtion. Jg^{-1}	Energy of Desorption. Jg^{-1}
1.99	59.5	14.0	15.2
1.56	59.5	15.3	15.0
1.56	59.5	15.9	15.3
1.56	60.0	15.3	---
0.95	59.5	16.9	14.2
0.95	59.5	17.2	14.0
0.71	60.0	17.4	---
0.71	59.5	17.4	---
0.51	60.5	18.9	12.7
0.51	59.5	19.4	---
0.51	59.5	19.3	13.2
0.46	59.5	19.2	---
0.46	60.0	19.5	12.6
0.46	59.5	19.3	12.0
0.46	59.5	19.2	12.3
0.29	59.5	19.4	---
0.29	60.0	19.6	9.3
0.29	60.0	19.4	10.5
0.19	59.5	17.6	---
0.19	59.5	17.8	---
0.19	59.5	18.6	---
0.13	60.0	15.5	---
0.13	59.5	14.7	---
0.13	59.5	14.5	---
0.07*	59.5	---	---

* The adsorption figures for 2 runs with 0.07% butanol were too broad and shallow to measure.

Table VII-7. Estimation of the surface area of ferric oxide A.

Heat of adsorption of 1.99% 1-butanol in n-heptane.	Surface area using $E = 0.138 Jm^{-2}$.	Surface area using $E = 0.116 Jm^{-2}$.	Surface area using a mean constant $E' = 0.127 Jm^{-2}$.
Jg^{-1}	m^2g^{-1}	m^2g^{-1}	m^2g^{-1}
(n = 1 Table VII-5)			
20.7	150	178	164
(mean heat with n = 3 Table VII-5)			
15.2	110	131	121

Notes : 1) No account has been taken of dilution effects.

2) The BET specific surface area is $245 m^2g^{-1}$.

3) $E' = \frac{1}{2} (0.138 + 0.116) Jm^{-2}$.

Table VIII-1. Energy changes resulting from changing the flow of the dry nitrogen through the flow reaction cell in the microcalorimeter to moist nitrogen ("adsorption") and back again ("desorption").

Temperature. °C.	Energy of Adsorption. J.	Energy of Desorption. J.
25.00	0.592	0.568
37.20	0.613	0.628

Mean change: 0.60 J.

Table VIII-2. Energies of adsorption and desorption of water vapour in a nitrogen gas stream, using an α-Fe_2O_3 substrate, corrected for the blank heat effect.

Temperature. °C.	Energy of Adsorption. Jg^{-1}.	Energy of Desorption. Jg^{-1}.
19.55	18.9	27.3
	24.1	32.8
37.20	34.5	31.5
	31.1	30.2

Table VIII-3. Energies of adsorption and desorption of water vapour in a nitrogen gas stream using a ferric oxide A substrate, corrected for the "blank" heat effect.

Temperature °C		Energy of Adsorption Jg^{-1}	Energy of Desorption Jg^{-1}
19.35		491 (16)	664 (11.8)
		476 (15)	600 (8.1)
	mean:	484	630
25.50		505, 538 (14)	818 (10.8)
		497, 527 (11.7)	814 (10.8)
	mean:	516	816
31.90		628, 666 (14)	---
	mean:	647	
37.15		635, 650 (14.5)	631 (10)
		662, 678 (15.7)	689, 744 (9)
		646, 665 (17)	---
		634, 646 (24)	780 (24)
	mean:	652	711

Notes: 1) Where 2 figures are given, separated by a comma, they are the minimum and maximum estimates of the energy of the major heat signal, neglecting the contribution arising from the slow decay of the heat signals;

2) The figure in brackets is the number of hours for which the sample was treated with dry and wet nitrogen before the adsorptions and desorptions respectively;

3) The mean values are the means of all the results quoted for a given temperature irrespective of the sample pretreatment;

Table VIII-4. Energies of adsorption and desorption of water vapour in a nitrogen gas stream using a ferric oxide B substrate, corrected for the "blank" heat effect.

Temperature °C	Energy of Adsorption Jg^{-1}	Energy of Desorption. Jg^{-1}
25.50	166, 217 (12)	150 (16)
	212, 308 (22)	632, 647 (16)
37.15	301, 411 (10.5)	517 (13.5)
	323, 445 (14)	537 (34)
	301, 403 (17)	540 (18)
	mean 364	531

Notes: 1) Where 2 figures are given, separated by a comma, they are the minimum and maximum estimates of the energy of the major heat signal, neglecting the contribution arising from the slow decay of the signals. The decay was so slow at ca. 25°C that the errors are very large;

2) The figure in brackets is the number of hours for which the sample was treated with dry and wet nitrogen before the adsorption and desorption respectively;

3) The mean values are the mean of all the results quoted for a given temperature irrespective of the sample pretreatment;

Table VIII-5. Energies of adsorption and desorption of water vapour in a nitrogen gas stream using a) α-geothite, and b) β-geothite as substrates and corrected for the "blank" heat effect.

a) α-geothite:

Temperature. °C	Energy of Adsorption. Jg^{-1}	Energy of Desorption. Jg^{-1}
25.10	124, 163 (17)	269 (19)
	126, 174 (19)	285 (23.5)
	126, 169 (9.5)	250 (15.5)
mean:	147	268
37.10	155, 178 (11)	213 (19)
	163, -- (6)	221 (19)
	154, 183 (8)	205 (14.5)
mean:	167	213

b) β-geothite:

Temperature. °C	Energy of Adsorption. Jg^{-1}	Energy of Desorption. Jg^{-1}
25.10	128, 175 (5)	301 (23)
	142, 196 (8.5)	305 (19)
	141, 188 (17)	320 (22)
mean:	162	309
37.10	178, 207 (4)	206 (9)
	164, 191 (22)	201 (13)
	160. 182 (22)	194 (16)
mean:	180	200

Notes: 1) Where 2 figures are given, separated by a comma, they are the minimum and maximum estimates of the energy of the major heat signal, neglecting the contribution arising from the slow decay of the signals.

2) The figure in brackets is the number of hours for which the sample was treated with dry and wet nitrogen before the adsorption and desorption respectively.

3) The mean values are the means of all the results quoted for a given temperature, irrespective of the sample pretreated.

Table VIII-6. The maximum energies of adsorption of water vapour at ca. 37°C on the iron oxide samples in Jg^{-1} and Jm^{-2}.

Sample.	Energy of Adsorption. Jg^{-1}	Energy of Adsorption. Jm^{-2}
α-haematite (2.74)	33	12
ferric oxide A (245)	650	2.7
ferric oxide B (158)	360	2.3
α-goethite (112)	170	1.5
β-goethite (105)	180	1.7

Note: The figures in brackets are the specific surface areas of the adsorbents in m^2g^{-1} and the energies are the mean figures taken from the preceding tables.

Table VIII-7. Estimated energies of vapour phase adsorption on oxide surfaces compared with observed energies, at ca. 30-40 °C.

Sample	Calculated Energy of Adsorption.		Observed Energy of Adsorption.
	Jg^{-1}	Jm^{-2}	Jg^{-1}
α-haematite	10	3.65	33
ferric oxide A	920	3.76	650
ferric oxide B	580	3.66	360
α-goethite	420	3.75	170
β-goethite	400	3.80	180
zinc oxide	10	3.44	-
aluminoxid	300	3.70	-

Note: 1) The calculated energies are derived from the thermochemical cycle shown in Figure VIII-8.

The values calculated for zinc oxide ($S_w = 2.9 m^2 g^{-1}$) and aluminoxid ($S_w = 81 m^2 g^{-1}$) were obtained using the thermodynamic data found by Partyka et al[81] for these two materials.

References.

1) Wake W.C., "Adhesion and the Formulation of Adhesives", Applied Science, London, 1976.

2) Internal Technical Report, Central Dockyard Laboratory, Portsmouth, 1976.

3) Gettings M., Baker F.S. and Kinloch A.J., J. Appl. Polym. Sci., 21, 2375, 1977.

4) Eley D.D and Rudham R., "Adhesion Fundamentals and Practice", Elsevier, 1970.

5) Holiday, L. (Ed), "Ionic Polymers". Applied Science, London, 1975.

6) Gibbs J.W., "Collected Works"; 2nd ed., Longmans, New York, 1928.

7) Guggenheim E.A., "Thermodynamics" 5th ed., North Holland, Amsterdam. 1967.

8) Aveyard R. and Haydon D.A., "An Introduction to the Principles Surface Chemistry", Cambridge University Press, Cambridge, 1973.

9) Fowler R.H. and Guggenheim E.A., "Statistical Thermodynamics", Cambridge University Press, Cambridge, 1939.

10) Hill T.L., Adv. Catalysis, 4, 211, 1952.

11) Langmuir I., J. Amer. Chem. Soc., 40, 1361, 1918.

12) Brunauer S., Emmett, P.H. and Teller E., J. Amer.Chem. Soc., 60, 309, 1938.

13) Jaycock M.J. and Parfitt G.D., "Chemistry of Interfaces", Ellis Horwood, Colchester, 1981.

14) London F., Z. Phys., 63, 245, 1930.

15) London F., Z. Phys., 11, 222, 1930.

16) Kiselev A.V., Disc. Faraday Soc., No.40, 205, 1965.

17) Barrer R.M., J. Colloid Interface Sci., 21, 415, 1966.

18) Dubinin M.M., J. Colloid Interface Sci., 23, 487, 1967.

References (Cont.).

19) Adamson A.W., "Physical Chemistry of Surfaces", 3rd ed. Wiley-Interscience; London, p. 592, 1976.

20) Stone F.E., in "Chemistry of the Solid State". Ed. Garner W.E., Butterworths, London, 1955.

21) Novakova J., Jiru P. and Zavadil V., Collect. Czech. Chem. Commun., 32, 2439, 1967.

22) Chalmers B., King R., and Shuttleworth R; Proc. Roy. Soc. London, A193, 465, 1948.

23) Flood E.A., Ed., "The Solid Gas Interface", Vol. 1., Dekker, New York, 1966.

24) Steele W.A., Adv. Colloid Interface. Sci., 11, 3, 1967.

25) Dollimore D., Spooner P. and Turner A., Surface Technol., 4, 121, 1976.

26) Brunauer S., Deming L.S., Deming W.E. and Teller E., J. Amer. Chem. Soc. 62, 1723, 1940.

27) Gregg S.J. and Sing K.S.W., "Adsorption, Surface Area and Porosity"; Academic Press, London, 1967.

28) Everett D.H., Parfitt G.D., Sing K.S.W. and Wilson, R., J. Appl. Chem. Biotechnol., 24, 199, 1974.

29) Brunauer S., "Solid Surfaces and the Gas Solid Interface", Adv. Chem. Series, No. 33, Amer. Chem. Soc., 1961.

30) Lowell S., Powder Technol., 12, 291. 1975.

31) Anderson, R.B., J. Amer. Chem. Soc., 68, 686. 1946.

32) Brunauer S., "The Adsorption of Gases and Vapours", Oxford University Press, London, 1944.

33) Hüttig G.F., Monatsh. Chem., 78, 177, 1948.

34) Dole, M., J. Chem. Phys., 16, 25, 1948.

References (Cont.).

35) Halsey G., J. Chem. Phys., 16, 931, 1948.

36) Ferguson R.R. and Barrer R.M., Trans. Faraday Soc., 46, 400, 1950.

37) Theimer O., Trans. Faraday Soc., 48, 326, 1952.

38) Frenkel, J., "Kinetic Theory of Liquids", Clarendon Press, Oxford, 1946.

39) Hill T.L., J. Chem. Phys. 17, 590, 1949.

40) Steele W.A., in "The Solid-Gas Interface", Vol.1., Ed. Flood E.A.; Dekker, New York, 1966.

41) McClellan A.L. and Harnsberger H.F., J. Colloid Interface Sci., 23, 577, 1967.

42) Dymond J.H. and Smith E.B., "The Virial Coefficients of Gases - A Critical Compilation", Clarendon Press, Oxford, 1969.

43) Adamson, A.W., "Physical Chemistry of Surfaces", 3rd ed., Wiley-Interscience Ch.14, 1976.

44) Polanyi M., Verh. Dtsch. Phys. Ges. 16, 1012, 1914.

45a) Dubinin M.M. and Radushkevich L.V., Dokl. Akad. Nauk. SSSR. 55, 331, 1947.

45b) Dubinin M.M., Zaverina E.D. and Radushkevich L.V., Zhur. Fiz. Khim, 21, 1351, 1947.

45c) Dubinin M.M., Proc. Conf. Ind. Carbon and Graphite, Soc. Chem. Ind., London, 1958.

46) de Boer J.H., in "The Structure and Properties of Porous Materials", Ed. Everett D.H. and Stone F.S., Butterworths, London, 1858.

47) La Mer V.K. J. Colloid Interface Sci., 23, 297, 1967.

References (Cont.).

48) Karnaukhov A.P., Kinetika i Kataliz, 8, 172, 1967.

49) Brunauer S., Mikhail R.S. and Bodor E.E., J. Colloid Interface Sci., 24, 451, 1967.

50) Cranston R.W. and Inkley F.A., Adv.Catalysis, 9, 143, 1957.

51) Everett D.H., Haynes J.M. and McElroy P.J., Sci. Prog. Oxford, 59, 279, 1971.

52) Defay R., Prigogine I., Bellemans A. and Everett D.H., "Surface Tension and Adsorption", Longmans, London, 1966.

53) Tolman R.C., J. Chem. Phys, 17, 333, 1949.

54) Wheeler A., in "Catalysis", Ed. Emmett P.H., Reinhold, New York, 1955.

55) Pierce C., J. Phys. Chem., 57, 149, 1953.

56) Orr C. and Dalla Valle J.M., "Fine Particle Measurement", Macmillan, London, 1959.

57) Barrett E.P., Joyner L.G. and Halenda P.P., J. Amer. Chem. Soc., 73, 373, 1951.

58) Schull C.G., J. Amer. Chem. Soc., 70, 1405, 1958.

59) Oulton T.D., J. Phys. Colloid. Chem. 52, 1296, 1948.

60) Innes W.B., Anal. Chem., 29, 1069, 1957.

61) Brunauer S., Hagymassy J. Jr., Odler I., Skalny J. and Yudenfreund M., J. Colloid Interface Science, 38, 20, 1972.

62) Harris M.R, and Sing K.S.W., Chem. Ind., London, 11, 1959.

63) Kiselev A.V., Usp. Khim., 14, 367, 1945.

64) Lippens B.C. and de Boer J.H., J. Catalysis, 4, 319, 1965.

References (Cont.).

65) Sing K.S.W., Chem. Ind., 829, 1967.

66) Sing, K.S.W., in "Characterisation of Powder Surfaces", Ed. Parfitt G.D. and Sing K.S.W. Academic Press, London, 1976.

67) Everett D.H., Israeli J. Chem, 14, 267, 1975.

68) Everett D.H., Specialist Periodical Report, Colloid Sci., Vol. 1., Chem. Soc. 1973.

69) Adamson A.W., "Physical Chemistry of Surfaces", 3rd ed., Wiley-Interscience, Ch.9., 1976.

70) Kipling J.J., "Adsorption from Solutions of Non-Electrolytes", Academic Press, London, 1965.

71) Aveyard R and Haydon D.A., "An Introduction to the Principles of Surface Chemistry", Cambridge University Press, Cambridge, p.200, 1973.

72) Schay G., in "Surface and Colloid Science", Ed. Matijevic E. Wiley-Interscience, New York, Vol.2., 1969.

73) Ash S.G., Bown R. and Everett D.H., J. Chem. Soc., Faraday Trans.I, 71, 123, 1975.

74) Brown C.E., Everett D.H. and Morgan C.J., J. Chem. Soc., Faraday Trans. I, 71, 883, 1975.

75) Polanyi M., Verh. Dtsch. Phys. Ges., 18, 55, 1916.

76) Baret J.F., Kolloid-Z., 246, 636, 1971.

77) Eyring H., Ree T. and Hirai N., Proc. Nat. Acad. Sci., U.S.A, 44, 683, 1958.

78) Ash S.G., Everett D.H. and Findenegg G.H., Trans. Faraday Soc., 66, 708, 1970.

References (Cont.).

79) Schay G., in "Proc. Int. Symp. Surface Area Determination 1969", Butterworths, London, 1970.

80) Harkins W.D. and Jura G., J. Amer. Chem. Soc. 66 1362, 1944.

81) Partyka S. Rouquerol F. and Rouquerol J., J. Colloid Interface Sci., 68, 21, 1979.

82) Wedler G., J. Thermal Anal., 14, 15, 1978.

83) Groszek A.J., Chem. Ind. 482, 1965.

84) Groszek A.J., Chem. Ind. 1754, 1966.

85) Groszek A.J., Soc. Chem. Ind. Monograph 28, 174, 1968.

86) Groszek A.J., A.S.L.E. Trans. 13, 278, 1970.

87) Templer C.E., Particle Size Analysis Conf. 1970.

88) Templer C.E., Nature, 235, 158, 1972.

89) Allen T. and Patel R.M., J. Appl. Chem., 20, 165, 1970.

90) Allen T. and Patel R.M., J. Colloid Interface Sci., 35, 647, 1971.

91) Allen T and Patel R.M., Powder Technol., 2, 111, 1968.

92) Jaycock M.J., in "B.P. Symposium on The Significance of Heats of Adsorption at the Solid/Liquid Interface", March 1971; Ed. Groszek M.J.

93) Rahman M.A. and Gosh A.K., J. Appl. Chem. Biotechnol., 27, 529, 1977.

94) Rahman M.A., Bangladesh J. Sci. Ind. Res., 12, 151, 1977.

References (Cont.).

95) Partyka S. and Rouquerol J., J. Calorim Anal. Therm. 9A, 13, 1978.

96) Collins A.H., McEwan I.J. and Heal G.R., in "Third Particle Size Analysis Conf. Salford, 1977." Ed. Grooves M.J., Heyden, 1978.

97) Heal G.R. and McEwan I.J., Powder Technol. 30, 243, 1981.

98) Keisser J.T, Brown C.W. and Heidersbach R.H., International Laboratory, July/August 12, 1982.

99) Horton J.B., Regional Technical Meetings, American Iron Steel Institute, New York, 1966.

100) Keller P., Werkstoffe U. Korr., 10, 865, 1967.

101) Sharma H.P., Singhania G.K. and Pandley S.N., J. Sci. Technol., 62, 210, 1968.

102) Nestler G.G., Fritsche G., Kampfe B. and Lange D., Technik, 31, 47, 1976.

103) Zettlemoyer A.C. and McCafferty E., Z. Phys. Chem. 64, 41, 1969.

104) Buckland A.D. Rochester C.H. and Topham S.A., J. Chem. Soc. Faraday Trans. I, 76, 302, 1980.

105) Wells A.F., "Structural Inorganic Chemistry" 4th ed., Clarendon Press, Oxford. 1975.

References (Cont.).

106) Cotton F.A. and Wilkinson G., "Advanced Inorganic Chemistry" 3rd ed., Wiley-Interscience, New York, 1972.

107) Ben Dor L. and Fischbein E., Acta Cryst., B32, 667, 1976.

108) Butler G. and Ison H.C.K., Chem. Comm., 264, 1965.

109) Baneyeva M.I. and Bendeliani N.A., Geokhimiya, 7, 1106, 1973.

110) Foster A.G., J. Chem. Soc. 360, 1945.

111) Rao K.S., J. Phys. Chem., 45, 500, 1941.

112) Rao, K.S. and Nayar B.C., Indian J. Chem., 11, 910, 1973.

113) Saraswat I.P., Vajpei A.C., Garg V.K., Sharma V.K. and Prakash N., J. Colloid Interface Sci., 73, 373, 1980.

114) Towe K.M. and Bradley W.F., J. Colloid Interface Sci., 24, 384, 1967.

115) Chukhrov, F.V., Zryagin B.B., Gorshkov A.I., Ermilova L.P., Rudnitskaya E.S., and Ezvestia A.N., SSSR Ser. Geol. NI., 1971.

116) Chukhrov F.V., Zryagin B.B., Ermilova L.P. and Gorshkov A.I., in Proc. Int. Clay Conf., Madrid, June, 1972, Ed. Serratsova J.M.: Sociedad Espanola de Arcillas, and Association Internationale pour L'Etude des Argiles, 1972.

117) Van der Giesson A.A., Philips Res. Rep. Suppl., 12, 1968.

118) Mackenzie R.C. and Berggren G., in "Differential Thermal Analysis", Vol I., Ed. Mackenzie R.C., Academic Press, London, 1970.

References (Cont.).

119) Dousma J., Van der Hoven T.J, and de Bruyn P.L. J.Inorg. Nucl. Chem., 40, 1089, 1978.

120) Kaufman K. amd Hazel F., J. Inorg. Nucl. Chem., 37, 1139, 1975.

121) Wefers. K., B. Deut. Kermanischen Gasellschaft, 43, 677, 1966.

122) Wefers K., B. Deut. Kermanischen Gesellschaft, 43, 703, 1966.

123) Tanaka S., Okayam Daigaku Onsen Kenkyusho Hokoku, 20, 42, 1958.

124) Ishikawa T. and Inouge K., Bull. Chem. Soc. Jap., 46, 2665, 1973.

125) Gallagher K.J., Nature, 226, 1225, 1970.

126) Naono H. and Fujiwara R., J. Colloid Interface Sci., 23, 406, 1980.

127) van Oosterhaut G.W., Acta Cryst., 13, 932, 1960.

128) Blyholder G. and Richardson E.A., J. Phys. Chem., 66, 2597, 1962.

129) Berube Y.G., Onoda G.Y. and de Bruyn P.L., Surface Sci., 8, 448, 1967.

130) Asher R.C., Goodman J.F. and Gregg S.J., Proc. Brit. Ceram. Soc., 5, 125, 1965.

131) Morimoto T., Nagao M. and Tokuda F., Bull. Chem. Soc. Jap., 41, 1533, 1968.

132) Morimoto T., Nagao M. and Tokuda F., J. Phys. Chem., 73, 243, 1969.

133) McCafferty E. and Zettlemoyer A.C., Trans. Faraday Soc., 66, 1720, 1970.

134) McCafferty E. and Zettlemoyer A.C., Trans. Faraday Soc., 66, 1732, 1970.

References (Cont.).

135) McCafferty E. and Zettlemoyer A.C., J. Colloid Interface Sci., 34, 452, 1970.

136) Healey F.H., Chessick J.J. and Fraioli A.V., J. Phys. Chem. 60, 1001, 1856.

137) McCafferty E and Zettlemoyer A.C., Disc. Faraday Soc., 52, 239, 1971.

138) Jurinak J., Proc. Soil Sci. Amer., 30, 559, 1966.

139) Boehm H.P., Disc. Faraday Soc., 52, 264, 1971.

140) Zettlemoyer A.C. and McCafferty E., Croat. Chem. Acta., 45, 173, 1973.

141) Griffiths D.W.L., Hallam H.E. and Thomas W.J., J. Catalysis, 17, 18, 1970.

142) Rochester C.H. and Topham S.A., J. Chem. Soc. Faraday Trans. I., 75, 1073, 1979.

143) Rochester C,H. and Topham S.A., J. Chem. Soc. Faraday Trans. I, 75, 591, 1979.

144) Blyholder G. and Richardson E.A., J. Phys. Chem., 68, 3882, 1964.

145) Morimoto T., Yokota Y. and NagaoM., J. Colloid Interface Sci., 64, 188, 1978.

146) Guderjahn C.A., Paynter D.A., Berghaust P.E. and Good J.D., J. Phys. Chem., 63, 2066, 1959.

147) Holmes H.F., Fuller Jnr. E.L. and Beh R.A., J. Colloid Interface Sci., 47, 365, 1974.

148) Kittaka S., Kanemoto S. and Morimoto T., J. Chem. Soc., Faraday Trans. I, 24, 676, 1978.

149) Schinder P.W., Walti E. and Furst B., Chimia, 30, 107, 1976.

150) Jurinak J.J., J. Colloid Interface Sci., 19, 477, 1964.

References (Cont.).

151) Rossi P.F., Mater. Chem., 3, 7, 1978.

152) Gast R.G., Landa E.R. and Meyer G.W., Clays Clay Min., 22, 31, 1974.

153) Hagane T.T., Iguchi Yoshiaki Inouye Micho, 57, 15, 1971.

154) Kusano K., Nelander B. and Wädso I., Chemica Scripta, 1, 211, 1971.

155) Parfitt R.L., Russel J.D. and Farmer V.C., J. Chem. Soc. Faraday Trans. I., 72, 1082, 1976.

156) Russel J.D., Parfitt R.L., Fraser A.R. and Farmer V.C., Nature, 248, 220, 1974.

157) Paterson E. and Swaffield R., J. Therm. Anal., 18, 11, 1980.

158) Husbands D.I., Tallis W., Waldsax J.C.R., Woodings C.R. and Jaycock M.J., Powder Technol., 5, 31, 1971.

159) Jaycock M.J., Disc. Faraday Soc., 52, 261, 1971.

160) Gardner P.J. and Linton R.W., unpublished work.

161) Horner L., Werkstoffe U. Korr., 15, 466, 1972.

162) Funke W. and Hammann K., Korrosion, 16, 193, 1963.

163) Hughes R.I., Corrosion Sci., 9, 535, 1968.

164) Hingston F.J., Posner A.M. and Quirk J.P., J. Soil Sci., 25, 16, 1974.

165) Kavanagh B.V., Posner A.M. and Quirk J.P., J. Colloid Interface Sci., 61, 545, 1977.

References (Cont.).

166) Watson J.R., Posner A.M. and Quirk J.P., J. Soil Sci., 24, 503, 1973.

167) Raghavan S. and Fuerstenau D.W., J. Colloid Interface Sci., 50, 319, 1975.

168) Pope C.G., Matijevic E and Patel R.C., J. Colloid Sci., 80, 74, 1981.

169) Lucas J., Vandervell D. and Waugh K.C., J. Chem. Soc. Faraday Trans. I, 77, 15, 1981.

170) Parfitt R.L., Farmer V.C, and Russel J.D., J. Soil Sci., 28, 29, 1977.

171) Parfitt R.L. Fraser A.R. and Farmer V.C., J. Soil Sci., 28, 289, 1977.

172) Parfitt R.L. and Russel J.D., J. Soil Sci., 28, 297, 1977.

173) Rochester C.H. and Topham S.A., J. Chem. Soc., Faraday Trans. I., 75, 1259, 1979.

174) Rochester C.H. and Topham S.A., J. Chem. Soc., Faraday Trans. I, 75, 872, 1979.

175) Joy A.S., Vacuum, 3, 254, 1953.

176) Ross S. and Olivier J.P., "On Physical Adsorption"; Interscience, New York, 1964.

177) Emmett P.H. in "12th Report Committee Catalysis", Physical Adsorption in the Study of the Catalysis Surface, J. Wiley, 1940.

178) Collins C. and Blaisdell B.E., Rev. Sci. Inst., 7, 213, 1936.

References (Cont.).

179) Thomson G.W., in "Physical Methods of Organic Chemistry", 3rd ed. Vol.1., Ed. Weisberger A, Interscience, New York. 1959.

180) C.R.C., Handbook of Chemistry and Physics, 54th ed. 1973-74.

181) Blaisdell B.E., J. Math. Phys. (M.I.T.), 19, 186, 1940.

182) Kistemaker J., Physica 11, 270, 1945.

183) Emmett P.H. and Brunauer S., J. Amer. Chem. Soc., 58, 1553, 1937.

184) Redhead P.A., Hobson J.P. and Kornelsen E.V., "The Physical Basis of Ultra High Vacuum", Chapman and Hall, 1968.

185) B.S., 4359, Part One, 1969. H.M.S.O.

186) Bignall J., Internal Report Chemistry Department, Royal Holloway College, 1980.

187) Lambert B. and Clark A.M., Proc. Roy. Soc., A117, 184, 1929.

188) Atkinson R.J., Posner A.M. and Quirk J.P., J. Inorg. Nucl. Chem., 30, 2371, 1968.

189) Weiser M.B., Milligan W.O. and Cook E.L., Inorg. Syn. 2, 215, 1946.

190) Morrison R.T. and Boyd R.N., "Organic Chemistry" 3rd ed., Allyn and Bacon Inc., Boston, 1973.

191) Kington G.L. and Smith P.S., Trans. Faraday Soc., 60, 705, 1964.

192) Beebe R.A., Millard B., and Cynarski J., J. Amer. Chem, Soc. 75, 839, 1953.

193) Kiselev A.V., in "2nd. Int. Cong. Surface Activity", Vol.2., Butterworths, London, 1957.

194) LKB., Operation Manual, Sorption Microcalorimeter 2107-030.

ERRATA

Page 18	lines 24-26	to read "exothermic heats of adsorption (<20 kJ mol^{-1} of adsorbate) usually of the same order of magnitude as the heat of liquefaction; is substantially non-specific, reversible and has a small or zero activation energy." not "exothermic heats of adsorption (<20 kJ mol^{-1} of adsorbate) of the same order of magnitude as the heat of liquefaction, is non-specific, reversible and has no activation energy."
Page 44	line 10	to read "about ten minutes. If narrow pores or pores with narrow constrictions are" not "about ten minutes. If narrow pores are"
Page 47	line 19	to read "is completed. Up to point C the adsorption is" not "is completed. In the absence of microporosity the adsorption is"
Page 54	lines 23-24	to read "II isotherm, which at high relative pressures is described by" not "isotherm. This curve is closely described by"
Page 92	line 6	to read "volumetric apparatus, similar to that of Emmett[177]" not "volumetric apparatus, originally described by Emmett[177]"
Page 108	line 17	to read "the total dead space volume that volume" not "the total space volume that volume"
Page 109	line 25	to read "The detailed procedure for measuring the pressure described above", not "The detailed procedure described above,"
Page 185	line 23	to read "flow mode had revealed a" not "flow mode that had revealed a"